Chiral gadolinium complexes as potential contrast agents

Woods, Mark

Chiral Gadolinium Complexes as Potential Contrast Agents

Mark Woods

Department of Chemistry
University of Durham

A thesis submitted for the degree of Doctor of Philosophy

1998

Abstract

The long electronic relaxation time and the high paramagnetism of the gadolinium(III) ion makes it ideal for use as a contrast agent in Magnetic Resonance Imaging. As a result of its toxicity, gadolinium must be administered in the form of a kinetically inert complex. By coupling a gadolinium(III) chelate to a macromolecule, substantial gains in relaxivity (the efficacy of a contrast agent) may be obtained. To this end the synthesis of three types of ligand, substituted with amino- or carboxylate bearing groups, was undertaken. A derivative of 1,4,7,10-tetraazacyclododecane with three amino bearing chains substituted at carbon was synthesised as a single enantiomer. An effective route to acetate substituted derivatives of DO3A was developed. The lanthanide complexes of these ligands do not exhibit the expected properties of a $q = 2$ complex, and therefore do not represent useful chelates for application in a slowly tumbling system.

A study of the lanthanide(III) complexes of all four stereoisomers of tetra(carboxyethyl) DOTA derivatives has been performed. The rate of water exchange has been found to be dependent upon the proportion of a complex adopting a twisted square antiprism in solution. This is ascribed to the steric crowding of the water binding site in this isomer. 2-D EXSY NMR experiments show that the [Ln.(*RRRR*-)] and [Ln.(*RRRS*-)] isomers do not undergo rapid arm rotation at room temperature, showing that ring motion is decoupled from arm rotation. This rigidity increases the stability of these complexes with respect to metal ion dissociation. A selective synthesis of the [Ln.(*RRRR*-)] diastereoisomeric complex is described. Crystal structures of the [Eu.(*RRRR*-)], [Gd.(*RRRR*-)] and [Tb.(*RRRR*-)] complexes each reveal a monocapped square antiprismatic co-ordination geometry at the metal centre in which there is one bound water molecule.

Declaration

The work described herein was carried out in the Department of Chemistry, University of Durham and the Dipartimento di Chimica Inorganica, Chimica Fisica e Chimica dei Materiali, Università degli Studi di Torino, between October 1995 and September 1998. All the work is my own unless otherwise stated, and no part of it has been submitted for a degree at this or any other university.

Statement of Copyright

Acknowledgements

I would like to express my sincerest thanks to:

Prof. David Parker for all his help and support with this work. His enthusiasm has made all this possible.

Prof. Silvio Aime, Dr. Mauro Botta, Allesandro Bargo and **Gabriella Bobba** and all the rest of the group in Torino for a very enjoyable and productive visit, as well as all their invaluable advice and expertise.

Dr Marc Port, Dr. Domonic Meyer and **Olivier Rousseau**, at Guerbet s.a., Paris, for the contribution of samples, ideas and financial assistance.

Janet Moloney for her help, patience and hard work with all the crystallographic studies.

Dr Alan Kenwright, Ian McKeag and **Julia Say**, for their help and patience in devising, setting up and running NMR experiments.

Dr. Andy Beeby, Claire, Allison and **Allison**, for all their help with all the luminescence work.

Dr. Mike Jones and **Lara Turner**, for their help and sympathy in the mass spectrometry lab.

Ray Hart and **Gordon Haswell**, for providing a friendly and unsurpassable glassblowing service.

Members of the Wolfson Laboratory (CG27) whose help, expertise and patience has been invaluable. In particular, **Dr. Stephen Faulkner, Dr. Gareth Williams, Dr. Matt Wilkinson** and **Dr. Linda Govenlock**.

My parents without whom I should have achieved nothing.

The **EPSRC** for funding this work.

Finally, various other members of the Chemistry Department over the years for their suppport and friendship.

"Hasten slowly."

Gaius Suetonius Tranquillus
'Divus Augustus' AD 120

Abbreviations

Chemical

Boc	*tert*-Butoxycarbonyl
Bn	benzyl
Bz	benzoyl
DCC	*N,N*-Dicyclohexylcarbodiimide
DO3A	1,4,7,10-tetraazacyclododecane-1,4,7-triacetate
DOTA	1,4,7,10-tetraazacyclododecane-1,4,7,10-tetraacetate
DOTMA	1,4,7,10-tetraazacyclododecane-1,4,7,10-tetra(α-methyl acetate)
DMF	*N,N*-Dimethylformamide
DMSO	Methylsulfoxide
DTPA	Diethylenetriamine-*N,N,N',N'',N''*-pentaacetate
EDC	1-(3-Dimethylaminopropane)-3-carbodiimide hydrochloride
EDTA	Ethylenediamine-*N,N,N',N'*-tetraacetate
HP-DO3A	1-(*S*)-Hydroxypropyl-1,4,7,10-tetraazacyclododecane-4,7,10-triacetate
Ln	Generic symbol for any lanthanide(III) ion
NOTA	1,4,7-Triazacyclononane-*N,N',N''*-triacetic acid
Np	*p*-Nitrophenol
py	Pyridine
Su	*N*-Hydroxysuccinimide
TFA	Trifluoroacetic acid
THF	Tetrahydrofuran
TETA	1,4,8,11-tetraazacyclotetradecane-1,4,8,11-tetraacetate
Tf	trifluoromethansulfonato
Ts	*p*-toluenesulfenyl

Practical

COSY	Correlation Spectroscopy
ESMS	Electrospray Mass Spectrometry
EXSY	Exchange Spectroscopy
IR	Infrared
Mp	Melting Point
MRI	Magnetic Resonance Imaging
NMR	Nuclear Magnetic Resonance
NMRD	Nuclear Magnetic Relaxation Dispersion
R_f	Retention function
t.l.c.	Thin Layer Chromatography

Contents

Chapter 1. Introduction

1.1. Magnetic Resonance Imaging and Contrast Agents 2
1.2. Relaxivity and Paramagnetic Ions 10
1.3. Lanthanide(III) Ions 17
1.4. Improving the Efficacy of Contrast Agents 33
1.5. The Scope of this Work 41
1.6. References 43

Chapter 2. Structural and Dynamic Studies of Substituted DOTA Derivatives

2.1. Introduction 50
2.2. Synthesis of Substituted DOTA Derivatives 51
2.3. Structural and Dynamic Studies of Europium(III) Complexes 62
2.4. Lanthanide(III) Complexes of Tetra(carboxyethyl) DOTA 79
2.5. Relaxation Measurements of Gadolinium(III) Complexes 87
2.6. Conclusions 101
2.7. References 103

Chapter 3. Substituted DO3A Derivatives

3.1. Introduction 106
3.2. Synthesis of Tri(carboxyethyl) DO3A 107
3.3. The Properties of Lanthanide(III) DO3A Derivatives 111
3.4. A Tri-acetate substituted DOTA Derivative 119
3.5. Conclusions 121
3.6. References 122

Chapter 4. Iron(III) Templated Aza-crown Syntheses

4.1. A Brief History of the Synthesis of Cyclens 125
4.2. Iron(III) Templated Synthesis of 2-Aryl Cyclen Derivatives 127
4.3. The Properties of Lanthanide 2-Aryl DOTA Derivatives 130
4.4. Extending the Use of Iron(III) Templated Cyclen Syntheses 136
4.5. Conclusions 138
4.6. References 139

Chapter 5.

5.1. Introduction 142
5.2. An Iron(III) Templated Synthesis 142
5.3. A Richman-Atkins Type Synthesis 145
5.4. References 150

Chapter 6. Experimental

6.1. Experimental Methods 152
6.2. Chapter 2 Experimental 153
6.3. Chapter 3 Experimental 162
6.4. Chapter 4 Experimental 170
6.5. Chapter 5 Experimental 175
6.6. References 187

Appendices

Appendix I. NMRD Profile Best Fitting Parameters 191
Appendix II. Crystallographic Data 194
Appendix III. Synthesis and Crystallisation of DOTA 237
Appendix IV. Research Colloquia, Lectures and Conferences 244

Chapter One

Introduction

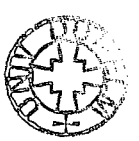

1.1. Magnetic Resonance Imaging and Contrast Agents

The use of low energy radiofrequency radiation to probe the magnetic moments in electrons and nuclei has become commonplace. To date no adverse effects from exposure to this radiation have been reported making it a safe, non-destructive analytical tool. The technique has found a diverse range of applications from the chemistry laboratory to the hospital.

A New Imaging Technique is Born

The history of magnetic resonance begins in 1938[1] when Rabi published a paper entitled "A New Method of Measuring Nuclear Magnetic Moment."[2] Six years later he would be awarded the Nobel Prize for Physics for his work measuring the magnetic properties of atomic nuclei. These experiments involved the application of a magnetic field to a beam of atoms in a vacuum,[3] allowing the magnetic moment of the proton to be determined.[4] The use of the rotating frame for the discussion of magnetogyric motion was already commonplace.[5]

It was not until 1945 that Nuclear Magnetic Resonance (NMR) was discovered in the condensed phase. The discovery was made simultaneously by Bloch,[6] working on aqueous ferric nitrate solutions, and Purcell,[7] working on solid paraffin. Despite the advances that had already been made, the spin-lattice relaxation time of the proton in the condensed phase was unknown. If it were as long as early estimates predicted, then saturation effects would frustrate or preclude detection. Hence when Purcell used a sensitive radiofrequency bridge to observe changes in the dissipation in paraffin at 30 MHz, the bridge was supplied with a weak source, in anticipation of a relaxation time of the order of hours. The experiments performed by Bloch were very different in nature. Iron(III) was used to reduce relaxation times when the transverse component of the proton signal was followed in the 7-11 MHz range. Bloch and Purcell were jointly awarded the Nobel Prize for Physics in 1952. The implications of this new technique in the fields of chemistry, and later, biochemistry and clinical medicine remained unrealised for some time. After all, in these early stages of the development of NMR, experiments were restricted to observing the effects of solutes upon the solvent signal. Even so, the first signals arising from biological samples were recorded very early on. Bloch told how a signal was obtained when he inserted his finger into his magnet.[8] Purcell and Hahn both reputedly observed the signals that could be obtained when their heads were placed in the magnetic field.[9]

Following the development of the double helical model for the structure of DNA by Watson and Crick in 1953, a resurgence of interest in biological macromolecules began. For many years this research had focused on diffraction studies such as those pioneered by Perutz on the wet crystals of proteins. Whilst such studies enabled the structure of proteins such as myoglobin and haemoglobin to be calculated, no information on structural or conformational changes could be obtained. Increasingly NMR was employed to observe the hydration states of DNA,[10] proteins and other biological tissues.[11] By 1958 the relationship of water concentration in these samples upon the observed signal were under investigation.[12] The importance of the effect of increased motion upon both the "spin-lattice" relaxation time (T_1) and the "spin-spin" relaxation time (T_2) as well as that of anisotropy upon line width was realised. In 1963 the non-linear dependence of the solvent proton relaxation rate upon the oxidation state of the copper centre of the protein ceruloplasmin was shown.[13] This suggested that conformational changes within individual protein molecules could be studied in this way, stimulating further research. This, and subsequent work in this field, would eventually underpin a new imaging technique.

Still more research into magnetic resonance was undertaken in physics laboratories and some very important advances made. Amongst these were the discovery of spin echoes by Hahn[14] in 1950 and Gabillard's observation that a field gradient could yield spatial information about an object.[15] The year 1959 saw the first crude imaging by NMR[8] when Kudravecev managed to obtain a Mercator projection of a quail's egg on a television screen. Sadly his work was regarded as a novelty and his results were never published.

By the early 1970's NMR had begun to establish its place as a powerful tool in the chemistry laboratory. Not until 1973, however, did it become clear how an imaging experiment could be performed. Lauterbur's seminal paper[16] detailed how images should be obtained using "projection-reconstruction" methods when a linear gradient field was employed. In the same year Mansfield and Grannell demonstrated the relationship between spin density and signal intensity.[9] The combination of these ideas allowed the spatial differentiation of nuclear magnetic signals in a distributed system, thus the mapping of spin densities could be achieved. The potential scope of these developments only became clear when a patent filed by Damadian in the previous year was published.[17] Central to the patent was the discovery that certain cancerous tissues gave rise to unexpectedly long values of T_1. With clear applications in the generation of anatomical and morphological images

and the diagnosis of tumors, the potential of this new imaging technique became clear.

Surprisingly little interest in imaging with NMR was shown by the manufacturers of other imaging equipment, the only exception being the British company EMI. As a result most, of the development of the techniques[18] and instrumentation[19] throughout the 1970's took place in universities. During this period the technique was also extended to the study of ^{31}P and ^{13}C in biological systems. Eventually in 1978, EMI announced that the projection-reconstruction techniques conceived by Lauterbur, had produced the first image of a head. Shortly afterwards a 0.15T superconducting imager, installed in London's Hammersmith Hospital, went into clinical trials. NMR imaging had been born. The word 'nuclear' was soon dropped to avoid unwanted associations in the public mind with another branch of the physical sciences, and the technique became known as Magnetic Resonance Imaging (MRI).

Clinical MRI

The high water content of biological systems means that protons are both the most NMR sensitive and the most abundant nuclei *in vivo*. Different tissue types vary substantially in the amount of water present (Table 1.1). The relaxation times of protons also vary according to their chemical and physical environment. These differences allow spatially encoded NMR experiments to be carried out which provide tomographical information.

Tissue Type	Water Content	Tissue Type	Water Content
Brain	71 -84 %	Myelin	40%
Muscle	79%	Teeth	10%
Liver	71%	Femur	12%
Kidney	81%		

Table 1.1 Water content of some selected tissue types[20]

In many respects magnetic resonance imaging resembles any other magnetic resonance experiment. The equipment required is basically the same. However, the sample size is substantially larger so the magnet must be physically much larger. In addition a set of gradient coils, for the application of a variable field gradient are added. It is these coils that allow spatial information to be gathered from the experiment.

The aim of the imaging technique is to measure the spatial relationship between spin density and the relaxation times of protons in the sample. This is achieved through the application of a linear gradient field across the sample. Since the precessional Larmor frequency of a nucleus (ω_o) is field dependent, (Eqn. 1.1) protons with different spatial co-ordinates will resonate at different frequencies when a gradient field is applied. This, in effect, spatially encodes the resulting free induction decay (FID).

$$\omega_o = \gamma B_o \qquad (1.1)$$

It is not possible to generate an image from this information alone. Reconstruction of the image is achieved by the repetition of the scan. After each scan, the field gradient (but not the field!) is rotated slightly in the plane of interest. In this way a series of one-dimensional images is built up. These images can be "back projected" to form a map of spin intensities (Figure 1.1).

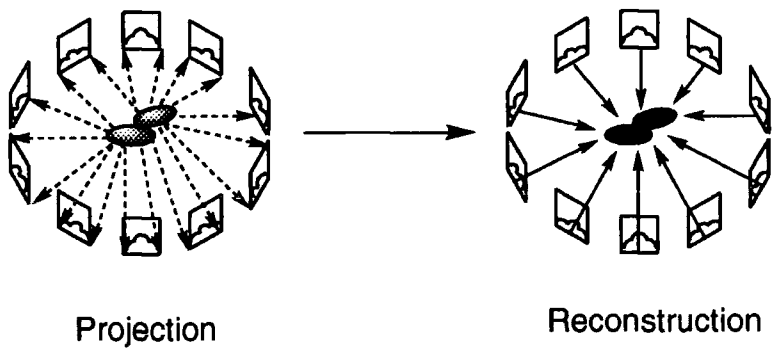

Figure 1.1 A schematic representation of the "Projection-Reconstruction" method devised by Lauterbur.

In practice, this reconstruction is achieved by the use of an operator which returns a particular point in the sample to resonance once the gradient field has knocked it off resonance. The size of this operator changes as the gradient field rotates. The operator is then summed over all the scans and applied to all the FIDs acquired. This back-projects the spin density of the point under consideration. This procedure is then applied to subsequent points until a map of spin densities is obtained.

The use of "spin echo pulse sequences" in MRI allows the dispersive components of an FID, arising from the motion of nuclei, to be removed. This technique, developed by Hahn,[14] applies a 180° pulse at a given time after the initial 90° pulse of the experiment. This second pulse causes an inversion of the precession of the decaying magnetic moment. The result of this inversion is an echo arising from an increase followed by commensurate loss of coherence in

the magnetic moment. Under this regime the signal intensity in a given voxel (volume element) is given by Equation (1.2),[21] in which T_E is the echo delay time, T_R is the pulse repetition time and H_V the motion factor of the water protons.

$$Intensity = [H_2O]H_V\left\{\exp\left(\frac{-T_E}{T_2}\right)\right\}\left\{1-\exp\left(\frac{-T_R}{T_1}\right)\right\} \qquad (1.2)$$

The relaxation times of water in different environments are different, (Table 1.2), and hence it is also possible to discriminate between tissue types on the basis of their relaxation characteristics.

Tissue	T_1 Cancerous (s)	T_1 Normal (s)
Skin	1.047	0.616
Bone	1.027	0.554
Muscle	1.413	1.023
Breast	1.080	0.367
Liver	0.832	0.570

Table 1.2 The values of T_1 for water in a variety of selected tissues[22]

Depending upon the type of information sought, the image can be weighted in favour of T_1, T_2 or the spin density. In practice this is achieved by the careful selection of an appropriate pulse sequence by the radiographer.

In contrast to other imaging techniques, such as CT scanning, to date no side effects from radio-frequency radiation employed in clinical applications have been reported.

The Introduction of Contrast Agents

The use of paramagnetic metal ions to enhance the proton relaxation rate in magnetic resonance experiments dates back to the very first condensed phase NMR experiments conducted by Bloch in 1945. The effects of paramagnetic solutes in NMR formed a substantial area of research in the following decades. Resulting theories, in particular those of Solomon, Bloembergen and Morgan (Section 1.2), underpin current understanding of such systems.

It was Lauterbur again, along with Mendoca-Dias and Rudin, who first showed the potential of paramagnetic agents as *in vivo* contrast agents.[23]

Normal tissues were distinguished from infarcted tissue in a study involving the injection of manganese(II) salts into dogs with occluded coronary arteries. The longitudinal relaxation times of protons where the manganese had accumulated (the normal tissue) differed from those where it had not (the infarcted tissue). Hence the tissue types could be discriminated on the basis of relaxation rates. These findings were soon confirmed in similar studies.[24]

The first paramagnetic compound to see clinical use in humans was iron(III) chloride. It was administered orally by Young *et al.* in order to enhance the images of the gastrointestinal tract.[25] The first diagnostic imaging agent to see clinical use was $[Gd.DTPA]^{2-}$ in 1983. Injected intravenously, it was used to enhance images of the lesions caused by cerebral tumours.[26]

Since then numerous contrast agents have been developed, mostly based around iron(III),[27] manganese(II)[28] and particularly gadolinium(III).[29,30] Although a number of different types of contrast agents exist, such as those for perfusion studies[27] and some tumour localising agents,[31,32] this thesis is restricted to the discussion of extra-cellular contrast agents.

Extra-cellular contrast agents are non-specific in their biodistribution and as such they can be relatively simple paramagnetic metal complexes. The only significant restrictions are the toxicity of the complex and its *relaxivity*. The *relaxivity* of a complex is defined as the increase in the rate of water relaxation rate per unit concentration of the complex. The action of these agents arises from their diffusion through the extracellular fluid. To avoid detrimental associative interactions with cell membranes, plasma proteins and other lipophilic biological macromolecules these contrast agents tend to lack hydrophobic groups, preferring rather polar and hydrogen bonding groups.

The catalysis of water proton relaxation by a paramagnetic centre takes place through dipole-dipole interactions between the spins of unpaired electrons and that of the proton. The effect of a contrast agent is to reduce both the longitudinal relaxation time (T_1) and transverse relaxation time (T_2) of the extracellular fluid. From Equation (1.2), it can be seen that while a reduction of T_1 will lead to an increase in the signal intensity, decreasing T_2 also decreases the signal intensity. In consequence, when contrast agents are employed in MRI, the pulse sequence is weighted towards T_1. As a result, it is the longitudinal relaxivity rather than the transverse which is more important in MRI, and so relaxivity is often used to refer to R_1, the *longitudinal relaxivity*.

Gadolinium Complexes as Contrast Agents

Gadolinium(III) has the electronic configuration [Xe] $4f^7$. With seven unpaired electrons, it has the highest spin quantum number of any stable element in the periodic table. It is not surprising to find that it forms the basis of the most popular contrast agents in clinical use today. Gadolinium(III) itself is toxic (LD_{50} = 1.4 mmol kg^{-1}),[33] and it must therefore be administered in the form of a kinetically and thermodynamically stable complex. Four extracellular contrast agents are in widespread use today; the gadopentate dimeglumine injection (Magnevist; $[Gd.DTPA]^{2-}$) marketed by Schering, gadoterate meglumine injection (Dotarem; $Gd[DOTA]^-$) marketed by Guerbet, gadoteridol injection (ProHance; [Gd.HP-DO3A]) marketed by Squibb Diagnostics (Bracco), and gadodiamide injection (Omniscan; [Gd.DTPA.BMA]) from Nycomed-Amersham (Figure 1.3).[34]

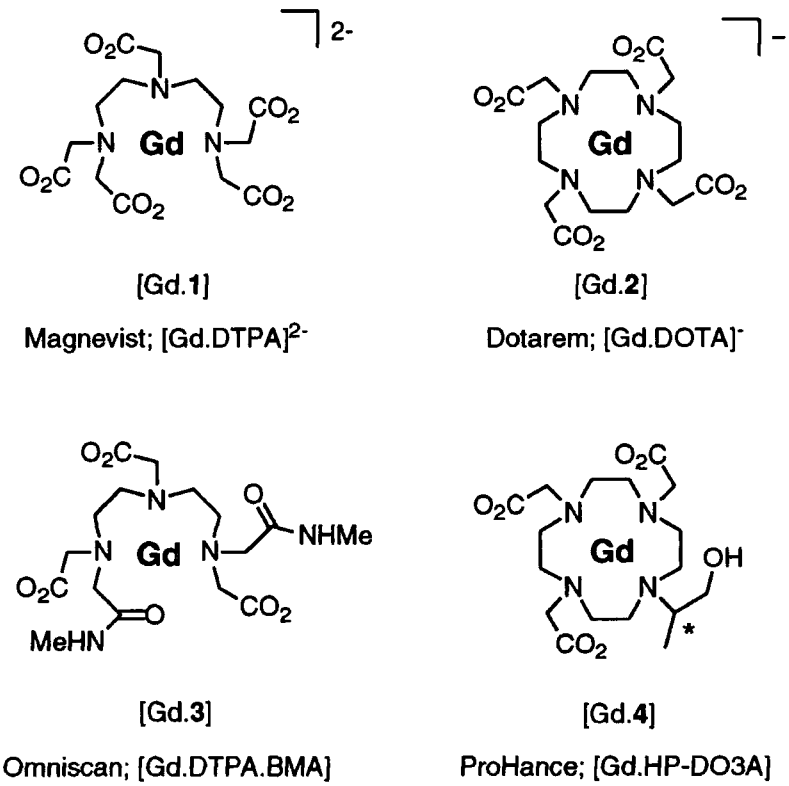

Figure 1.3 The four extracellular contrast agents currently in clinical use

The introduction of multidentate chelating agents reduces the number of water molecules bound to the gadolinium(III) ion. Because this reduces the efficiency of the gadolinium ion as a contrast centre, very high doses of these contrast agents are required typically of the order of 0.1 - 0.2 mmol kg^{-1}. The four major contrast agents all have one bound water molecule.

Magnevist was introduced into clinical use in 1983, shortly followed by Dotarem. The ligands DTPA and DOTA form kinetically inert complexes with respect to metal ion disociation with all the lanthanide(III) ions rendering them safe for *in vivo* applications.[35] The renal excretion of these two contrast agents shows >90% clearance in one hour with >99% clearance after one week.[36] However, both complexes are anionic and hence have relatively high osmolalities which lead to severe osmotic shocks in patients receiving the multigram doses required.

Contrast Agent	Osmolality / osmol $(kg\text{-}H_2O)^{-1}$	log K_a
Magnevist	2.0[37]	22.5[38]
Dotarem	1.1[21]	24.7[39]
ProHance	0.63[40]	23.8[41]
Omniscan	0.79[40]	16.9[42]
Blood	0.3[21]	/

Table 1.3 Stability constants, K_a, and osmolalities for the most popular contrast agents. The osmolality of blood is significantly lower than that of the charged contrast agents

In an attempt to avoid these problems, the charge neutral complexes [Gd.HP-DO3A] and [Gd.DTPA.BMA] have been introduced for use in applications where particularly high dosages are necessary. These complexes are substantially less inert than their ionic counterparts. At pH 7, Omniscan dissociates at a rate three orders of magnitude faster than Magnevist.[35] In view of the high doses which are administered the stability constants are on the borderline of the minimum acceptable for clinical application. The rate of renal clearance for both ProHance and Omniscan is very fast, in fact >94% clearance is observed for both complexes within 24 hours.[43,44] It is this rapid rate of clearance which has allowed their use as contrast agents.

Dotarem is generally considered to be the best contrast agent currently available. Based around the macrocyclic aza-crown 1,4,7,10-tetraazacyclododecane (cyclen), **5**, the ligand forms a very rigid chelate with gadolinium(III) and hence a kinetically inert complex. The rate of dissociation of Dotarem is slow, $3.2 \times 10^{-6}\ s^{-1}$ at pH 1.[41] One major disadvantage of all currently available contrast agents for MRI is that they require high effective

doses. The development of more effective types of contrast agent would represent a significant advance in patient care.

1.2. Relaxivity and Paramagnetic Ions

The relaxation of an excited nucleus occurs *via* two distinct processes. The first, where the energy is dissipated into the surroundings (the lattice), is "spin-lattice" relaxation, represented by the longitudinal relaxation time T_1. The second is "spin-spin" relaxation, which can be thought of as a loss of coherence in the precession of the magnetic moment, represented by the transverse relaxation time T_2. Although T_1 must always be longer than T_2, for most systems T_1 and T_2 are approximately the same. When a paramagnetic centre is added to the system this relationship is perturbed by the dipolar interaction of the unpaired electrons and the nuclei.

A paramagnetic solute provides both a paramagnetic and a diamagnetic contribution to both the longitudinal and transverse relaxation times of the solvent molecules. These terms are additive such that:

$$\frac{1}{T_{obs}} = \frac{1}{T_{dia}} + \frac{1}{T_{para}} \qquad (1.3)$$

and in the absence of any interaction between solvent molecules, a linear relationship between the relaxation rate and the concentration of the paramagnetic solute exists. The relaxivity, R_1 of a complex is defined as the slope of this dependence. It is best thought of as "the increment of the water proton relaxation rate per unit concentration of contrast agent".[45] The relative contributions to the overall relaxation rate of the longitudinal and transverse relaxation are dependent upon the nature of the paramagnetic centre, for example $T_1/T_2 = 2.5$ for the Gd(III) aquo ion[46] and 7.1 for the Mn(II) aquo ion.[47]

Broadly speaking two mechanisms exist for the catalysis of water proton relaxation by a paramagnetic centre. The first is termed the *outer sphere* mechanism and arises through the diffusion of the paramagnetic agent through the bulk solvent. The second occurs only where water molecules are directly coordinated to the paramagnetic metal centre. Exchange of these bound water molecules with the bulk solvent leads to relaxation of the bulk through an *inner sphere* mechanism. The overall longitudinal relaxivity of a complex is given by Equation 1.4: namely the sum of the water relaxation rate, plus the relaxivity arising from the inner sphere mechanism and that arising from the outer sphere mechanism.

$$R_1^{obs} = R_1^{water} + R_1^{inner-sphere} + R_1^{outer-sphere} \quad (1.4)$$

Outer Sphere Relaxation

The outer sphere contribution to relaxivity has been shown to depend upon two features of the paramagnetic ion, the electronic relaxation time (T_{1e}) and the spin state (S).[33] Comparison of paramagnetic complexes in which no bound water is present (q = 0) reveals that longer values of T_{1e} result in enhanced relaxivities. The value of T_{1e} for gadolinium(III) has been estimated to be 0.1 - 1.0 ns, whereas for terbium and dysprosium it is of the order of 0.1 - 1.0 ps. The observed relaxivity for q = 0 complexes of gadolinium is three orders of magnitude higher than for terbium or dysprosium.

The outer sphere contribution to the overall relaxivity of a paramagnetic complex is difficult to quantify. For complexes with long electronic relaxation times, its contribution has been estimated to be equivalent to one bound water molecule.[48] The study of gadolinium(III) chelates with no bound water molecules such as the phosphinate, [Gd.**6**]$^-$ synthesised by Parker *et al.* reveals that significant relaxivities may be obtained.[45] At 20 MHz and 25°C the relaxivity value obtained for [Gd.**6**]$^-$ was 1.8 mM^{-1} s^{-1}. Indeed this value is around half that obtained for [Gd.DOTA]$^-$ 4.2 mM^{-1} s^{-1} at the same temperature and field.[62]

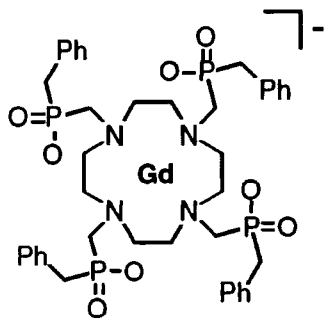

[Gd.**6**]

Although it is generally accepted that the outer sphere relaxivity is related to the diffusional correlation time of the complex, attempts to apply the Pfiefer equations,[49] describing the diffusion of stable free radicals, directly to calculate the magnitude of this effect in iron(III)[50] and manganese(II)[51] complexes, proved inappropriate. The equations modified by Freed[52] to take account of the boundary conditions arising from the distance of closest

approach, are more normally applied. These equations are adapted to give (Equation 1.5).

$$R_1^{o.s.} = \left(\frac{32\pi}{405}\right)\gamma_H^2 g^2 \mu_B^2 S(S+1)\left(\frac{N_A}{1000}\right)\left(\frac{C}{aD}\right) f(\tau_S \tau_D \omega_I \omega_S) \qquad (1.5)$$

where N_A is Avagadro's number, C is the concentration of the paramagnetic solute. The outer sphere relaxivity is therefore dependent upon the translational diffusion correlation time (τ_D), the distance of closest approach of the water, a, and the electronic relaxation time of the paramagnetic centre.

The participation of a second coordination sphere to the outer sphere relaxivity cannot be discounted. Indeed Oakes and Smith proposed that a second coordination sphere of eight water molecules bound to the four carboxylates of manganese(II) EDTA and EGTA was responsible for the relaxivity of these complexes.[53] Despite the application of some inner sphere conditions to these water molecules, a plausible 3.7 Å was obtained for the proton manganese distance. In reality, this model is only likely to account for a proportion of the outer sphere contribution which will vary with complex hydrophobicity.

Inner Sphere Relaxation

For paramagnetic complexes with directly bound water molecules (typically with a gadolinium-oxygen bond distance (r) of 2.9Å in solution) much higher relaxivities are observed. The protons on the coordinated water molecule will relax very quickly since they are very close to the paramagnetic ion. If the coordinated water molecule then dissociates from the complex and is replaced by another, which in turn experiences rapid relaxation, then the bulk water would also experience a degree of relaxation. Clearly this process is most effective if the water molecule resides on the paramagnetic ion no longer than is required for its protons to relax. The more coordinated water molecules there are per paramagnetic ion then the greater the relaxation per paramagnetic ion. The effect of this mechanism on the relaxation of solvent molecules by a paramagnetic solute was studied in depth throughout the late 1940's and 50's. A quantitative description of this contribution to the overall relaxivity of a complex lies in the equations developed by Solomon, Bloembergen and Morgan.

In addition to the exchange of the entire water molecule, proton exchange in the coordinated water molecule will also result in relaxation of the bulk solvent. This mechanism becomes more significant at extremes of pH. In

cationic complexes at high pH the removal of a proton from the bound water molecule reduces the overall charge by one. The hydroxyl group must be reprotonated before water exchange can occur, but since the rate of proton exchange can be extremely rapid (typically ~10^{10} $M^{-1}s^{-1}$) both mechanisms can contribute significantly to the inner sphere relaxivity.[54]

Solomon - Bloembergen - Morgan Theory

Solomon - Bloembergen - Morgan theory was developed to describe the relaxation of nuclei following excitation by radiofrequency radiation.[55] It takes as its basis a model in which the equilibrium of spins in a system of non-interacting nuclei is disturbed. The equilibrium is restored as a result of two interactions. The first interaction is that of the spin of the nuclei with their surroundings. This is characterised by T_1, the longitudinal or "spin-lattice" relaxation time. The second is the interaction of the dipoles of neighbouring nuclei. These interactions cause a fluctuation in the local field experienced by a given nucleus and are characterised by T_2, the transverse or "spin-spin" relaxation time. Both interactions are modulated by diffusional motion, which may be considered to be Brownian in nature. It should be noted that whilst the longitudinal relaxation interaction is dependent upon this diffusional motion for its origin, the transverse relaxation interaction is not, although its magnitude may be. However, this thesis is not concerned with the effects which impinge upon the transverse relaxation rate, and henceforth only the longitudinal relaxation processes will be considered.

Before the perturbation of equilibrium the nuclei are aligned in a homogeneous field. Each individual spin is quantised, and the macroscopic z-component of the spin is the sum of these quanta over all spins. These quanta may then be used to describe the system after perturbation. The interaction of neighbouring spins may be now be expressed in terms of the co-ordinates and orientation of the spins. The diffusion of nuclei will clearly alter these relationships. A Fourier treatment of the positional terms in the expression for interacting spins reveals that transitions in the quanta of ± 1 or ± 2 are possible in which energy transfer occurs through the fluctuations in field caused by the motion. In terms of the model of non-interacting spins, this means that if a neighbouring nucleus moves relative to another such that either; the z-component of the magnetic moment fluctuates with motion such that a frequency synchronous to the precessional frequency of the other is produced ($J \pm 1\nu_0$) or if one nucleus moves such that both circularly polarised components of its precessing frequency interact with the second ($J \pm 2\nu_0$), then an energy

transition may occur. This treatment suggests that transitions increasing in energy are as likely as those decreasing in energy. However the final states must be weighted by Boltzmann factors and the probability of a transition of decreasing energy becomes slightly more favourable.

The model obtained was applied to the relaxation of water protons. It was assumed that the Debye model for dielectric dispersion in polar liquids[56] provides a good estimate of the characteristic time τ_C. In order to take account of diffusion of molecules through the sample, the Stokes relationship for diffusion was incorporated. This relates the T_1 to the correlation time of water molecules and the diffusion of the water as a function of viscosity. The longitudinal relaxation time of water, predicted in this way, showed good agreement with experiment.

The model can now be extended to the interaction of different spins. The interaction of the spins of water protons with those of unpaired electrons is of interest here. The study of aqueous solutions of Fe(III), Co(II), Cu(II) and Ni(II) showed that the relaxation rate was proportional to the concentration of the paramagnetic ion. The relationship of the longitudinal and transverse relaxation times could also be accounted for.[57,58] The anomalous relaxation behaviour of manganese and gadolinium required the addition of a hydration sphere to the paramagnetic ion. This hydration sphere was said to be modulated by three characteristic times; the residence lifetime of a water molecule, the dipolar correlation time which was related to the rotation of the ion, and the spin-lattice relaxation time of the electron spin.[59]

The model thus described accounts for the interaction of any paramagnetic solute in a polar solvent. A quantitative description of the model was finally published in 1961.[60] The equations are normally expressed, in the laboratory frame, in the form shown (Eqns 1.6 - 1.8).

$$R_1 = \frac{[C]q}{55.6}\left(\frac{1}{T_{1M} + \tau_M}\right) \tag{1.6}$$

$$T_{1M} = \frac{2/15\, S(S+1)g^2\beta^2\gamma_I^2}{r^6}\left\{\frac{7\tau_C}{\left(1+\omega_S^2\tau_C^2\right)} + \frac{3\tau_C}{\left(1+\omega_I^2\tau_C^2\right)}\right\} + \frac{2}{3}\frac{A^2}{\hbar^2}S(S+1)\left\{\frac{\tau_S}{\left(1+\omega_S^2\tau_S^2\right)}\right\} \tag{1.7}$$

$$\frac{1}{\tau_C} = \frac{1}{\tau_S} + \frac{1}{\tau_R} + \frac{1}{\tau_M} \tag{1.8}$$

In which:

R_1 = the logitudinal relaxivity

[C] = the concentration of the paramagnetic agent

q = the number of coordinated water molecules
r = metal-proton distance
A = the electronic hyperfine coupling constant
T_{1M} = the longitudinal proton relaxation time
τ_M = the residence lifetime of a bound water molecule
τ_C = the characteristic correlation time
τ_S = the electron spin relaxation time
τ_R = the reorientational correlation time
ω_I = the proton Larmor frequency
ω_S =the electron Larmor frequency.

All other symbols take their usual meaning. Additionally the electron spin relaxation time is modulated by the electronic relaxation time at zero field, τ_{S0}, and the correlation time which characterises the time dependence of the proton relaxation process τ_V, according to Eqn (1.9).

$$\frac{1}{\tau_s} = \frac{1}{5\tau_{s0}}\left[\frac{1}{1+\omega_S^2\tau_V^2} + \frac{4}{1+4\omega_S^2\tau_V^2}\right] \qquad (1.9)$$

It is from this relationship that τ_S derives its field dependent behaviour.

Nuclear Magnetic Relaxation Dispersion Profiles

Due to the strong temperature and field dependence of the proton relaxation rate, relaxivity measurements made at a single field and temperature yield little information about the behaviour of a paramagnetic complex. It is now common practice to study the relaxation rate at variable field over four orders of magnitude. In order to do this a field-cycling relaxometer of the type developed by Koenig and Brown,[61] is employed. These are not commercially available machines: at the time of writing six such instruments are in operation world-wide situated in Illinois, Dartmouth and New York, U.S.A., one in Mons, Belgium, and in Firenze and Torino, Italy. The proton relaxation rate is measured at a variety of fields, set by the operator, to obtain a nuclear magnetic relaxation dispersion (NMRD) profile.

A typical NMRD profile for a small paramagnetic solute, $[GdDOTA]^-$ with one coordinated water molecule is shown, (Figure 1.3). These profiles can be measured at a number of temperatures to build up a picture of the behaviour of the complex in solution.

The experimental profile is fitted to a calculated set of structural and dynamic parameters. This process is most effective if the simultaneous fitting

of profiles at a variety of temperatures is undertaken. However, it is possible that several parameter sets will satisfy the experimental data, some of which may be unrealistic. An evaluation of the experimental profile enables a judicious choice of certain parameters to be made from the outset.

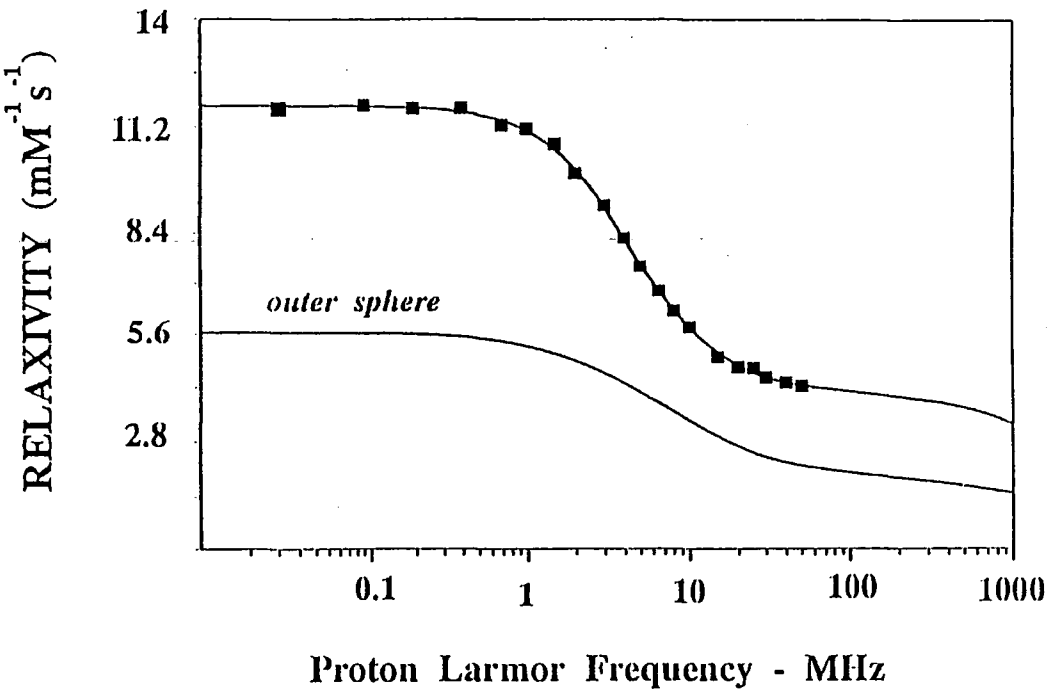

Figure 1.3 An NMRD profile of [GdDOTA]$^-$ recorded at 25°C.[62]

For example, in the profile above the presence of a $q = 0$ complex can be ruled out by the magnitude of the relaxation rate across the profile and the weak inflection at ~20 MHz, both characteristic of a hydrated species. In fact it has been shown both by X-ray crystallography and luminescence that [Ln.DOTA]$^-$ complexes are coordinated to one water molecule. Additionally, parameters such as the water exchange rate may be obtained using ^{17}O NMR studies. Hence a number of parameters can be predicted with some accuracy. Over recent years, a large amount of data has been acquired for the fitting of such profiles allowing this procedure to be undertaken with confidence.

The profile shown (Figure 1.3) separates into two clearly different regions. The profile at low field is characterised by a high proton relaxation rate (in excess of 10 $mM^{-1} s^{-1}$). In this region the effective correlation time, τ_C, is determined primarily by τ_S. The value of τ_S is field-dependent, but at low field it is of the order of nanoseconds, giving rise to high relaxivities. At higher fields (5 MHz and above) the relaxation rate is much lower, only about 5 mM^{-1}

s^{-1}. Here the contribution of the field dependent τ_S to τ_C is reduced. Thus τ_C is increasingly determined by the rotational correlation time, τ_R, and the water exchange rate, τ_M, (Eqn 1.8). For a small paramagnetic complex in which fast exchange conditions hold, such as DOTA, τ_C is dominated by the contribution from τ_R. Because τ_R is short, typically 80 - 100 ps, so is τ_C, hence lower relaxivities are observed in this region. An outer sphere contribution to the relaxivity is estimated and plotted. In this way a picture of the behaviour of a paramagnetic species in solution can be built up.

1.3. Lanthanide(III) Ions

The development of ion-exchange methods in the 1950's allowed the isolation of individual lanthanides.[63] Originally referred to as the "rare earth" elements, they were so called because they occur naturally as their oxide. The lanthanides are, however, by no means rare, being more abundant than elements such as mercury and arsenic.

Early research into the chemistry of the lanthanides revealed that they all share similar chemical and physical properties. The first three ionisation enthalpies of the lanthanides are relatively low, hence the tripositive oxidation state is favoured for each lanthanide. Indeed this is the only oxidation state observed other than Ce^{IV}, Sm^{II}, Eu^{II}, Tb^{IV} and Yb^{II}. A steady contraction in ionic radius is observed upon passing from the lighter to the heavier lanthanide(III) ions. This contraction is ascribed to an increased electrostatic attraction with increasing nuclear charge leading to a change in coordination number across the series. Although coordination numbers of up to 12 have been reported for the early lanthanides, coordination numbers of 8 or 9 are more normally observed.

The 4f orbitals show little or no directionality to their bonding interactions, thus lanthanide ions can adopt a wide range of coordination geometries. Generally a capped square antiprismatic structure is preferred since this allows the distances between ligands to be maximised. These highly electropositive ions are strong, hard acids and favour bonding with hard donors such as nitrogen and oxygen. However, complexes with monodentate ligands are prone to dissociation, hence the most stable complexes involve rigid multidentate chelating agents.

The more strongly luminescent lanthanides quickly found applications in diverse situations such as television screens and fluorescent lighting. The advent of inert lanthanide-chelate complexes has rapidly increased the scope of lanthanide chemistry. Europium and terbium complexes are used as

luminescent probes,[64] whilst dysprosium has been used as a probe in positron emission tomography (PET).[65] As well as its application in MRI, gadolinium has been used as a probe in ESR.[66]

Lanthanide Luminescence

The emission of light falls into two broad categories. "Hot light" or "incandescence" is light emitted from matter due to an increase in temperature. Initially this light is in the red region of the spectrum but as the temperature is increased visible light is observed. "Cold light" was described as "all those phenomena of light which are not solely conditioned by the rise in temperature" by Eilhardt Wiedemann who devised the word "luminescence" for these phenomena in 1888.[67]

Luminescence encompasses a wide range of processes such as bioluminescence, chemiluminescence, and photoluminescence. In the context of this thesis the word is used to refer solely to photoluminescence: light emission resulting from the excitation of matter following the absorption of light.

In principle all lanthanide(III) ions can exhibit luminescence. The luminescence of lanthanide(III) ions occurs through transitions between 4f states. For the electric dipole transitions such transitions are Laporte (or parity) forbidden. The mixing of electronic states of different parity, arising from interactions with the ligand field, with the 4f wavefunctions enables such transitions to occur. Consequently these are referred to as induced electric dipole transitions and their origin accounts for their low intensities in absorption. Magnetic dipole transitions between 4f states are Laporte allowed, although their oscillator strength is low. The magnetic dipole and induced electric dipole transitions obey different selection rules and so a mixture of each transition may be observed in a spectrum. Extinction coefficients greater than 1 $M^{-1}cm^{-1}$ are rarely observed for lanthanide(III) ions.

It is normal to invoke the Russell-Saunders coupling scheme to describe the energy levels of the lanthanides. This scheme represents a reasonable approximation to the relatively large spin-orbit coupling present in the lanthanides. The energy levels for the luminescent lanthanides pertinent to this thesis are shown (Figure 1.4). The ground states are predicted according to Hund's rules.

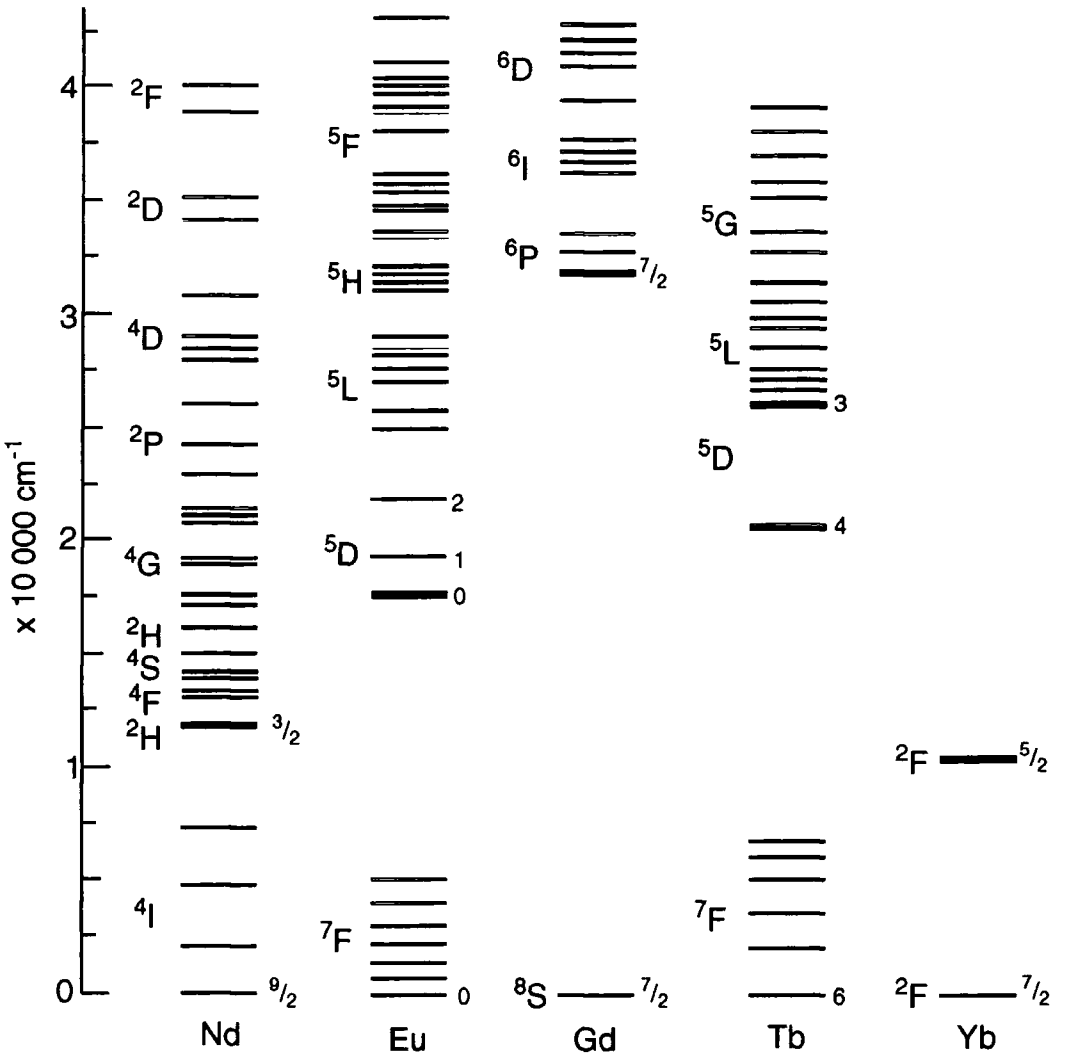

Figure 1.4 The energy levels of selected lanthanide(III) ions. The excited levels from which luminescence is frequently observed are indicated by the bold lines.[68]

The luminescence spectra (emission and absorption) of lanthanide(III) ions are characterised by extremely sharp lines. The sharpness of these bands is due to the small ligand field effects experienced by the 4f electrons. Indeed the maximum value of the 4f eigenfunction lies below that of the closed $5s^25p^6$ subshells. Hence the 4f wavefunctions experience a shielding effect from the ligand field. As a result the observed ligand field splittings are of the order of only 10^2 cm^{-1}.

The long luminescent lifetimes exhibited by lanthanide(III) ions (arising from the forbidden nature of the transitions) combined with the sharp well defined nature of their spectra makes the lanthanides ideal probes for localised chemical environments. To date, most reports of lanthanide(III) probes have utilised europium or terbium ions. In the europium emission spectrum it is the $^5D_0$ - ^7F_J (where J = 0-4, or sometimes 0-6) transitions which are most commonly

observed. The characteristics of these transitions are very different, (Table 1.4), and by observing the changes in these transitions, deductions about the local environment of the lanthanide(III) ion can be made.

ΔJ	Dipole	Range/nm	Intensity	Comments
0	Electric	577 - 581	Weak	Nondegenerate
1	Magnetic	585 - 600	Strong	Insensitive to environment
2	Electric	610 - 625	Strong	Hypersensitive
3	Electric	640 - 655	Weak	Forbidden; always weak
4	Electric	680 - 710	Medium	Sensitive to environment
5	Electric	740 - 770	Very Weak	Forbidden: seldom observed
6	Electric	810 - 840	Very Weak	Seldom measured

Table 1.4 Typical features of the $^5D_0$ - ^7F_J luminescent transitions for europium(III) complexes in solution.[67]

The emission spectrum of [Eu.DOTA]$^-$ showing the $^5D_0$ - $^7F_{0\text{-}4}$ transitions is shown, (Figure 1.5).

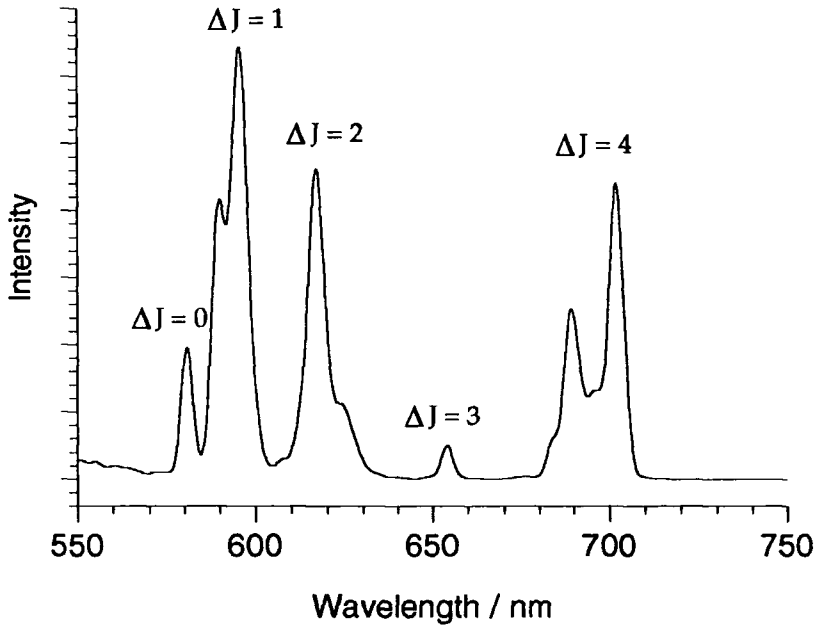

Figure 1.5 Emission spectrum of [Eu.DOTA]- recorded *via* direct metal excitation in H_2O at 397 nm. The $^5D_0$ -> ^7F_J bands for ΔJ = 0,1,2,3 and 4 are assigned.

Two transitions in particular contain some very important information upon the environment of the lanthanide(III) ion. The ΔJ = 0 band is

non-degenerate, hence in principle one line can be observed for each europium species in solution. In practice this degeneracy is not usually observed since an instrument with a resolution better than 0.1 nm must be used to record the spectrum. The $\Delta J = 2$ band is hypersensitive to the coordination environment of the lanthanide. It is absent when the ion lies on an inversion centre.

Paramagnetism and NMR of Lanthanide(III) Complexes

Any NMR active nucleus may experience a magnetic moment arising from the interaction with a lanthanide(III) ion. This magnetic moment arises from the unpaired 4f electrons of the lanthanide and results in the relaxation of the nucleus and often the shifting of the resonance of the nucleus to a different NMR frequency. Such an interaction may only occur for systems in which an anisotropic distribution of the 4f electrons occurs, that is to say for all the lanthanides other than gadolinium. This interaction is termed the dipolar or pseudo-contact shift.

For interactions between a ligand and a lanthanide(III) ion in which some covalent character is present then a second interaction may be observed. This is known as the contact shift. In a covalent interaction, a small amount of the unpaired 4f electron density may reach atoms within the ligand. This electron density also affects the relaxation rate and chemical shift of NMR active nuclei within the molecule.

Indeed a third term must be considered when examining the chemical shift of resonances in the NMR spectra of lanthanide(III) complexes. This is the diamagnetic contribution. These three contributions are related such that the observed shift, δ_{obs}, is the sum of the three contributions (Eqn. 1.10)

$$\delta_{obs} = \delta_{dia} + \delta_{dip} + \delta_{con} \qquad (1.10)$$

δ_{dia} is the diamagnetic contribution and δ_{dip} and δ_{con} are the dipolar and contact contributions respectively. The diamagnetic contribution may be determined from the diamagnetic ions lanthanum(III), yttrium(III) and lutetium(III). It is however the paramagnetic contributions which have the most significant effect for most of the lanthanide series and all those considered in this thesis.

For ions with a $4f^5$ and $4f^6$ electronic configuration, excited states are significantly populated at room temperature and this complicates the quantitative analysis of the contribution of both the dipolar and contact shifts. However, suitable treatments of both effects were devised in the early 1970's. Each is considered in turn.

Contact Shift

The contact contribution to the lanthanide induced shift is a function of the hyperfine coupling constant, A, such that the change in field experienced by a nucleus, ΔH is given by Eqn (1.11).

$$\Delta H = \frac{A\langle S_z \rangle}{g_N \beta_N} \tag{1.11}$$

Where $\langle S_Z \rangle$ is the average lanthanide electron spin of the z- component, which may be calculated from the individual $\langle S_Z \rangle_J$ values for $^{2S+1}L_J$ states. When an orbital reduction factor is included to take account of the bonding interactions then Eqn (1.12) is obtained.

$$\langle S_z \rangle_J = \left(\frac{-\beta H}{3kT}\right)\left[g(g-\gamma)\frac{J(J+1)}{(2-\gamma)} + \left(\frac{2kT}{\lambda}\right)\frac{(g-\gamma)(g-2)}{(2-\gamma)}\right] \tag{1.12}$$

where $\lambda = \pm\frac{\zeta}{2S}$

Ln(III)	$4f^n$	$^{2S+1}L_J$	(g_J-1)	$\langle S_Z \rangle$[69]
Ce	f^1	$^2F_{5/2}$	-1/7	-0.98
Pr	f^2	$^3H_4$	-1/5	-2.97
Nd	f^3	$^4I_{9/2}$	-3/11	-4.49
Pm	f^4	$^5I_4$	-2/5	4.01
Sm	f^5	$^6H_{5/2}$	-5/7	0.06
Eu	f^6	$^7F_0$	-1	10.68
Gd	f^7	$^8S_{7/2}$	1	31.50
Tb	f^8	$^7F_6$	1/2	31.82
Dy	f^9	$^6H_{15/2}$	1/3	28.55
Ho	f^{10}	$^5I_8$	1/4	22.63
Er	f^{11}	$^4I_{15/2}$	1/5	15.37
Tm	f^{12}	$^3H_6$	1/6	8.21
Yb	f^{13}	$^2F_{7/2}$	1/7	2.59

Table 1.5 Parameters affecting the contact contribution to the lanthanide induced shift.

Values of $\langle S_Z \rangle$ were determined for each lanthanide by Golding and Halton.[69] This was achieved by mixing the excited states, as obtained from the Russell-Saunders coupling model, with those of the ground state. The values obtained are collated in Table 1.5.

These values were found to account for the observed ^{17}O shifts in hydrated lanthanide(III) ions measured by Taube *et al.*[70] Because the hyperfine coupling constant A is virtually identical for each lanthanide, the field experienced by a nucleus will be proportional to the value of $\langle S_Z \rangle$. Since the shift experienced by a nucleus is dependent upon the field it experiences it is clear that:

$$\delta_{con} \alpha \langle S_Z \rangle \tag{1.13}$$

Dipolar Shift

A quantitative analysis of the dipolar shift was undertaken by Bleaney.[71] For an axially symmetric complex the dipolar shift, δ_{dip}, of a nucleus with polar co-ordinates θ and r is given by Eqn (1.14).

$$\delta_{dip} = C_J \frac{\beta^2}{60(kT)^2}\left(\frac{3\cos^2\theta - 1}{r^3}\right) \times P \tag{1.14}$$

$$\text{where } C_J = 2A_2^0\langle r^2 \rangle g^2 J(J+1)(2J-1)(2J+3)\langle J \| \alpha \| J \rangle$$

P is a crystal field splitting coefficient, which should adopt the same value for an isostructural series of lanthanide(III) complexes.

The calculated shifts (normalised to -100 for dysprosium(III)) were compared to those obtained experimentally for the complexes of 2,6-dipicolinate (dpa), (Table 1.6).[71]

The degree to which the calculated and experimental values correlate shows that the major contribution to the lanthanide induced shift is from the dipolar shift. The strong relationship between the dipolar shift and the polar co-ordinates, θ and r, of the observed nucleus allows a good deal of structural information to be obtained from analysis of the observed shifts.

In addition to shifting the resonance frequency of an NMR active nucleus, unpaired 4f electrons of the lanthanide(III) ion will catalyse the relaxation of the nucleus. Indeed, this is the central tenet of this thesis. Since this reduces both T_1 and T_2, a considerable degree of line broadening is observed in the NMR spectra of lanthanide complexes. The extent of this catalysis is determined by T_{1e}, the electron-spin relaxation time. For the lanthanides T_{1e} is short enough (~ 10^{-13} s) that relatively sharp lines are

observed. The short values of T_{1e} exhibited for the early lanthanides favours their application in shift reagents.[72] However, theory predicts that the effect of line-broadening is greater in the presence of stronger magnetic fields.[57] For this reason it is often best to record the NMR spectra of lanthanide complexes at lower fields. The remarkably long electronic relaxation time of gadolinium(III) ions, which make them applicable to use as contrast agents, has the effect of broadening lines to such an extent that NMR spectra of gadolinium(III) complexes may not be recorded. An indication of the line broadening effect of each lanthanide(III) ion is shown in column 7 of Table 1.6.

Ln(III)	$4f^n$	C_J[73]	δ_O $(H_2O)_9$[71]	δ_H $(dpa)_3$[74]	$\delta_H(H_2O)_9$[75]	$\Delta\nu_{1/2}$[a]
Ce	f^1	-6.3	-28	/	/	/
Pr	f^2	-11.0	-58	-13	0.27	5.6
Nd	f^3	-4.2	-77	-7.6	0.32	4.0
Pm	f^4	2.0	/	/	/	/
Sm	f^5	-0.7	-2	-1.3	/	4.4
Eu	f^6	4.0	144	12	/	5.0
Gd	f^7	0.0	424	/	3.01	/
Tb	f^8	-86	411	-92	-10.53	96
Dy	f^9	-100	363	-100	-6.95	200
Ho	f^{10}	-39	300	-51	4.88	50
Er	f^{11}	33	244	31	3.83	50
Tm	f^{12}	53	123	64	9.29	65
Yb	f^{13}	22	33	23	2.52	12

Table 1.6 Some parameters affecting the dipolar contribution to the lanthanide induced shift. a) Half peak height line width resonance of the methyl of 2-picoline in the presence of the tris(dipivaloylmethane) complexes of the Ln(III) ion, values in Hz.[76]

The Hydration State, q.

In the late 1970's Horrocks developed a method for determining the hydration state, *q*, of the luminescent lanthanides europium and terbium.

Lanthanide luminescence is known to be quenched by the vibrational oscillators of water. The greater the number of water molecules that are co-

ordinated to the lanthanide the more efficient is the quenching. Comparison of the vibrational levels of H_2O and D_2O with the energy levels of europium(III), reveals substantially more effective overlap in H_2O. (Figure 1.6).[77]

The quenching effect of D_2O is therefore expected to be significantly less than that for H_2O. It is in fact some 200 times less effective[78] and this results in the observation of much longer luminescent lifetimes for lanthanide aqua ions in D_2O as compared to H_2O.

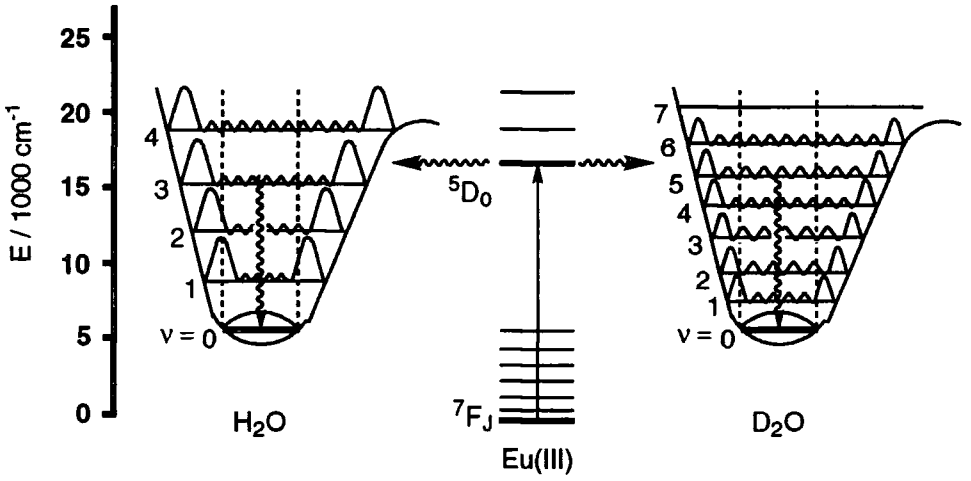

Figure 1.6 The non-radiative de-excitation of europium(III) ions by OH and OD oscillators. The larger overlap in successive vibronic levels in OH oscillators gives rise to more effective luminescent quenching.

Horrocks' exploited this difference in lifetime. The luminescent lifetimes (in either the solid or solution state) for both the hydrogen and deuterium isotopomers were measured for a series of europium and terbium complexes with a known number of bound water molecules. When q (the hydration state) was plotted against Δk (the difference in the rate of lanthanide luminescence quenching) a straight line was obtained. Horrocks called the gradient of this line the A factor, the value of which reflects the sensitivity of a given lanthanide to vibrational deactivation by OH oscillators, (Table 1.7).

Lanthanide(III) Ion	A_{Ln} factor
Neodymium	0.36 μs
Europium	1.05 ms
Terbium	4.2 ms
Ytterbium	1.0 μs

Table 1.7 The A factors of Nd(III)[79], Eu(III), Tb(III),[80] and Yb(III)[81] for determination of q by luminesence.

The value of q for a complex can be determined by application of Eqn (1.15).[80]

$$q = A_{Ln}.(k_{H_2O} - k_{D_2O}) \qquad (1.15)$$

Recently this technique has been extended to the study of neodymium[79] and ytterbium.[81] Problems associated with the measurement of their short luminescent lifetimes at longer wavelengths have been overcome by the development of a deconvolution method for the measured response. The A factors have been estimated (Table 1.7), the smaller values obtained are consistent with the short luminescence lifetimes of these ions.

Horrocks quoted an error of ± 0.5 water molecules in hydration states measured in this manner. Although in reality the values obtained by this method are somewhat more accurate than this, a number of errors are inherent in the method. The integrity of the solvent is an inevitable source of error since isotopic contamination of both H_2O and D_2O is inevitable. Shorter luminescent lifetimes may also be expected to be more inherently inaccurate because a smaller data set is available to determine their value.

An additional source of error is expected to arise from an outer sphere quenching effect. The measurements made by Horrocks were performed in both the solid and solution states. In this way an accurate value for the hydration state could be obtained. The measurements made upon crystalline lanthanide complexes will not experience any outer sphere quenching effects. Since both sets of data were used to calculate the A factor for both terbium and europium, any outer sphere quenching effects are not compensated for in this treatment. It is illuminating to examine the values of q determined by Horrocks' method for a complex which is known to have no directly coordinated water molecules, such as [Ln.**6**]$^-$ complexes (Table 1.8).

Complex	Eu.**6**	Tb.**6**	Yb.**6**
q	0.15	0.07	0.11

Table 1.8 Values of q as determined by Horrocks' method for [Ln.**6**]$^-$, a complex known to have a hydration state of zero.[45,67]

For each complex a residual difference between the two quenching effects is observed. This may be ascribed to the effect of quenching by outer sphere oscillators.[82] Since the magnitude of this effect is likely to be heavily dependent upon the size and shape of the complex it is difficult precisely to quantify this contribution to the quenching. It is not within the remit of this

thesis to account for, or to correct q values to account for this contribution, except in the case of ytterbium where the method described[81] subtracts an outer sphere quenching effect of 0.25 water molecules. However, the reader should note that a contribution, typically 0.1 water molecules for europium(III) and 0.06 water molecules for terbium(III), from outer sphere oscillators is present in the values of q quoted.

^{17}O NMR has also been used to establish the hydration state of dysprosium(III) complexes.[83] The technique is largely limited to dysprosium(III) since the contact shift is the dominant contribution (>85%) to the overall paramagnetic shift, (Table 1.5), although in principle it could be extended to terbium(III). The dipolar contribution may therefore be neglected, avoiding the need for dissection of the relative contributions.

Because the exchange of water molecules bound to lanthanides is fast on the NMR timescale, addition of a lanthanide complex will affect the ^{17}O signal obtained for the bulk water. The water signal shifts to lower frequency in the presence of a dysprosium complex. The observed shift ($\Delta\nu_{obs}$) may be related to the complex concentration and hydration state (q) by equation (1.16), where $\Delta\nu$ is the ^{17}O shift caused by one bound water molecule.

$$\Delta\nu_{obs} = q.\Delta\nu[Dy.L.H_2O_q] \qquad (1.16)$$

By measuring the shift of the ^{17}O signal over a range of dysprosium(III) aqua ion concentrations (20 - 100 mmol dm^{-3}) it was possible to determine the shift arising from a single water molecule (assuming that the dysprosium aqua ion is nine co-ordinate at these concentrations). This was found to be -40 ppm (27.12 MHz). Thus by plotting the ^{17}O shifts as a function of dysprosium complex concentration and applying equation (1.16) the value of q can be determined. The q values obtained by this method were compared to those obtained by Horrocks' method and are generally in reasonable agreement. Several significant deviations were reported, however, (e.g. for DOTA q = 1.5), and a rather equivocal maximum error of one water molecule was quoted.[83]

Lanthanide(III) Complexes of DOTA

The lanthanide complexes of the octadentate ligand DOTA have generated a substantial amount of interest. DOTA was first synthesised in 1976 by Stetter *via* the condensation of chloroacetic acid with cyclen in aqueous solution at pH 9.[84] Since then a number of synthetic methods have employed ester protection of the carboxylate followed by saponification. The study of the corresponding lanthanide and transition metal complexes ensued. In 1988 the

gadolinium complex of DOTA entered commercial use as a contrast agent in MRI. An X-ray quality crystal was grown by the author from acidified aqueous solution by slow evaporation of the solvents. The first crystal structure of the ligand DOTA **2** is shown (Figure 1.7), revealing the preorganised nature of the ligand.

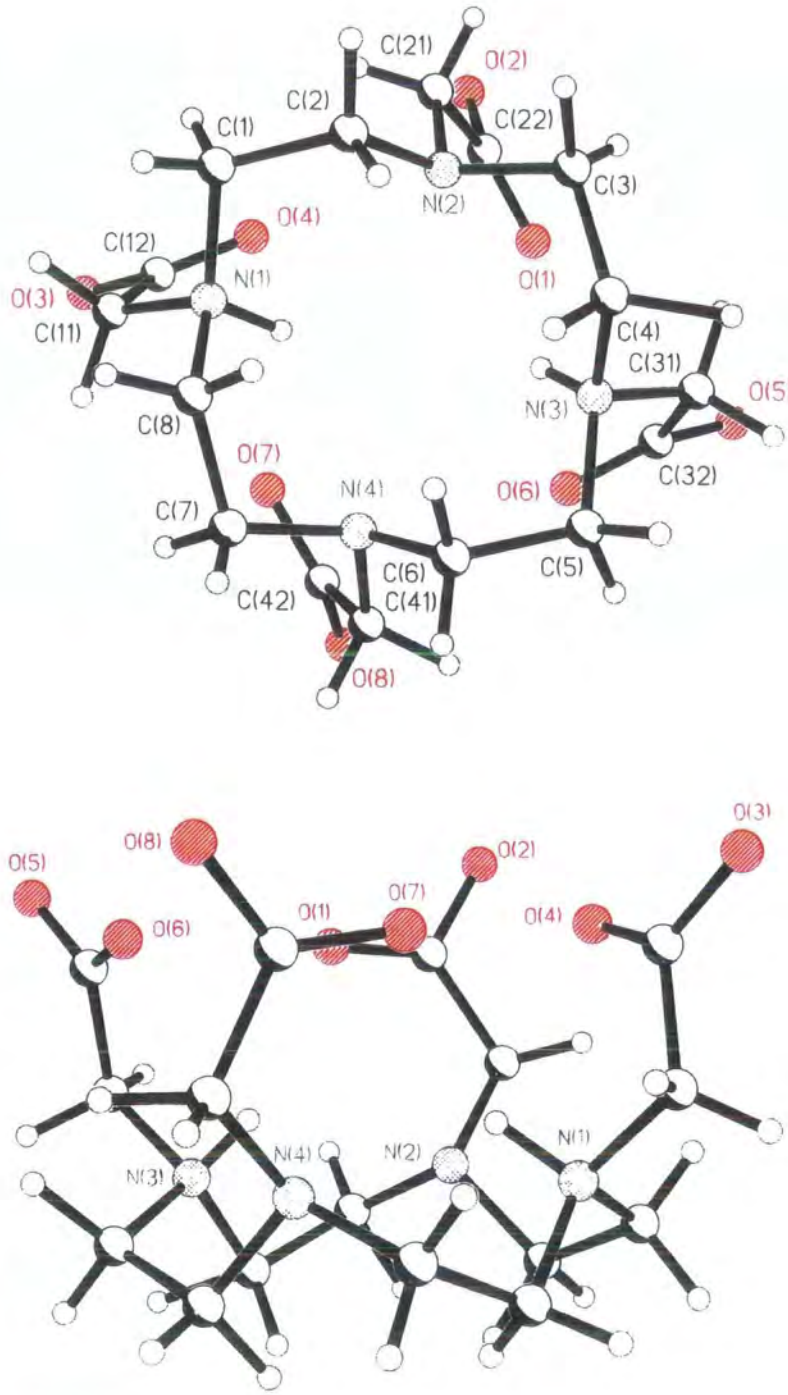

Figure 1.7 The crystal structure of DOTA obtained by the author. Details are provided in Appendix III

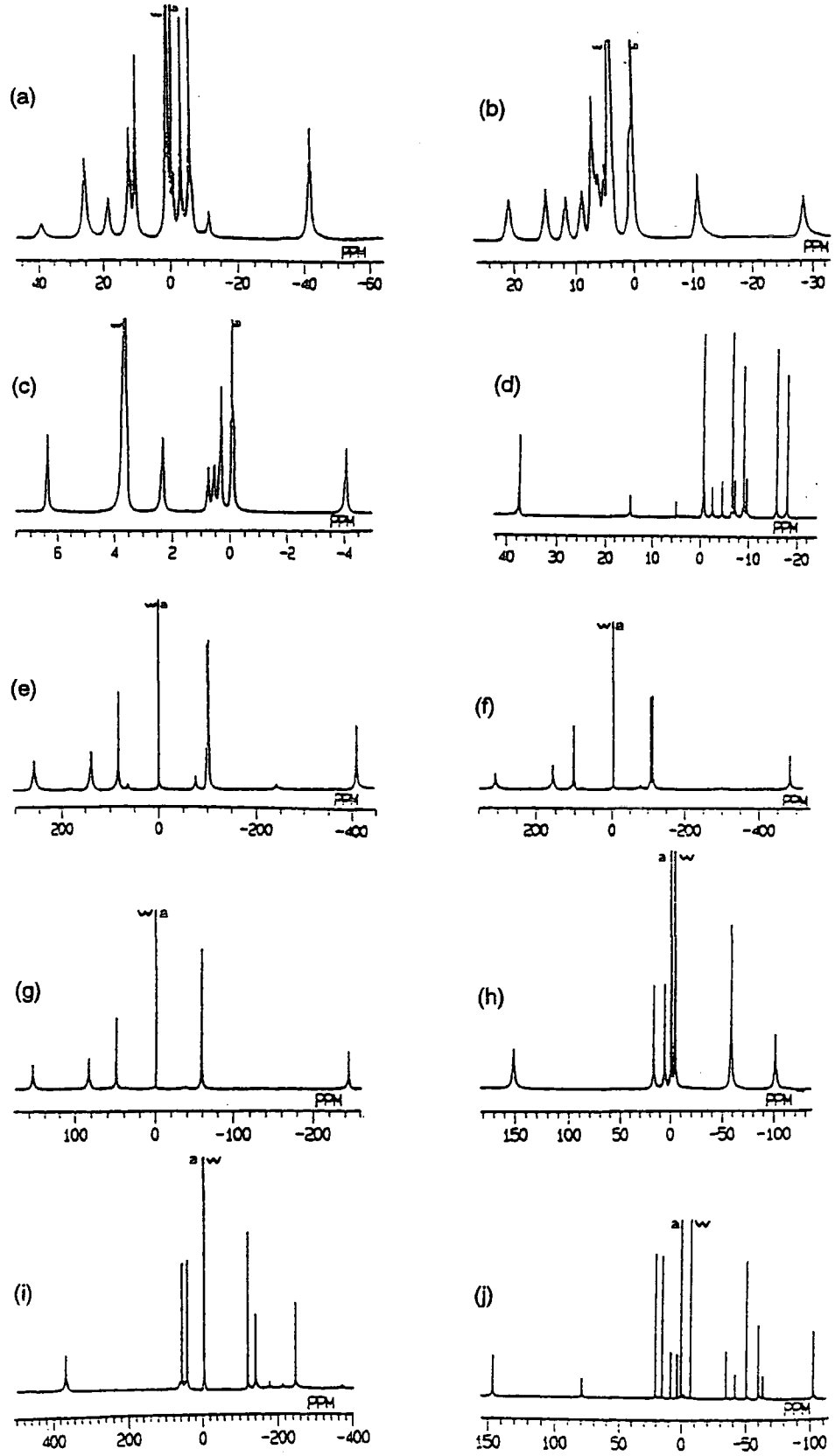

Figure 1.8 The ^{1}H NMR spectra of (a) [Pr.DOTA]$^{-}$, -3°C, (b) [Nd.DOTA]$^{-}$, -5°C, (c) [Sm.DOTA]$^{-}$, -7°C, (d) [Eu.DOTA]$^{-}$, -3°C, (e) [Tb.DOTA]$^{-}$, 28°C, (f) [Dy.DOTA]$^{-}$, 28°C, (g) [Ho.DOTA]$^{-}$, 25°C, (h) [Er.DOTA]$^{-}$, 30°C, (i) [Tm.DOTA]$^{-}$, 30°C, (j) [Yb.DOTA]$^{-}$, 2.5°C. Reproduced with permission.[85]

The ligand DOTA forms complexes of high kinetic and thermodynamic stablilty with all the lanthanide(III) ions. Published crystallographic studies of $[LnDOTA]^-$ complexes show one bound water molecule giving a lanthanide coordination number of nine.[86,87,88] The macrocyle adopts a [3333] conformation, allowing the nitrogen donors to adopt a co-planar arrangement with the four carboxylate oxygens defining a similar co-planar arrangement below. This effectively sandwiches the lanthanide, with the water molecule capping the bottom face generating a mono-capped square antiprismatic coordination geometry.

^1H NMR studies on the $[LnDOTA]^-$ complexes have shown that there are two species present in solution (Figure 1.8). The relative ratio of these species is dependent upon the identity of the lanthanide(III) ion (Figure 1.8).

Towards the beginning of the lanthanide series, one species predominates in the ^1H NMR spectrum. Crystallographic studies of $[La.DOTA]^-$ and $[Ce.DOTA]^-$ show that the lanthanide does not adopt a square antiprismatic co-ordination geometry.[62] The angle of twist between the N_4 plane and the O_4 plane (typically ~40° in a square antiprismatic geometry) is much smaller for these complexes ~29°. In fact they adopt what is often referred to as an "inverted square antiprism", however, the term "twisted square antiprism" more accurately describes the observed co-ordination geometry. In these crystals, the structure is again capped by one bound water molecule.

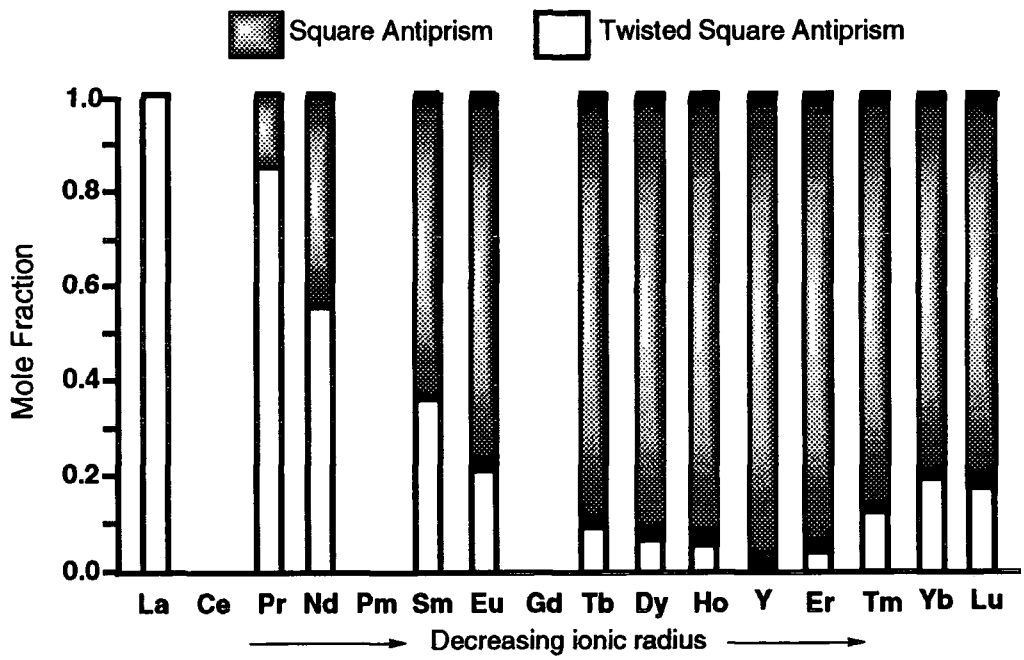

Figure 1.9 The mole fraction of twisted square antiprimatic versus square antiprismatic geometry across the lanthanide series.[89,90]

On passing along the lanthanide series the lanthanides contract with increasing atomic number and the square antiprismatic co-ordination geometry becomes increasingly favoured, reaching a maximum after holmium (Figure 1.9). [Y.DOTA]$^-$ (the ionic radius of yttrium is similar to those observed for the lanthanides although it is not a lanthanide) is believed to exist solely in the square antiprismatic geometry.

On passing to even heavier lanthanides, the twisted square antiprismatic geometry becomes more favoured again. From erbium onwards the reversal in this trend is associated with the twisted square antiprismatic structure becoming eight co-ordinate i.e. it has no bound water molecule.

[Ln.DOTA]$^-$ complexes are chiral, regardless of which co-ordination geometry the complex adopts. This chirality is described by two elements of helicity present in each complex. When the macrocycle cyclen adopts the [3333] ring conformation, two enantiomeric conformers are possible. These are distinguished, according to Corey's nomenclature[91] by considering the conformation of each ethylene bridge when looking along the nitrogen - nitrogen axis, (Figure 1.10). Each conformation has four ethylene bridges so the N-C-C-N torsion angles are denoted (δδδδ) and (λλλλ) for the clockwise and anticlockwise conformers respectively, (Figure 1.10).

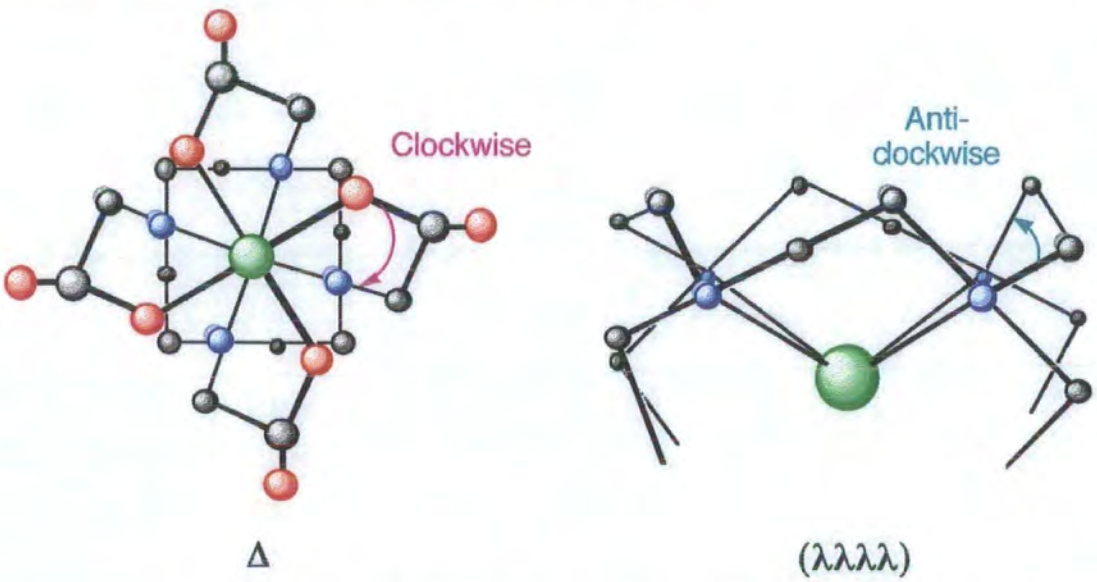

Figure 1.10 The N-C-C-O (left) and N-C-C-N (right) torsion angles define the chiralty of [Ln.DOTA]$^-$ complexes

In addition to the conformation of the macrocyclic ring, the orientation of the pendant arms also defines an element of chiralty. The pendant arms may adopt a clockwise or an anticlockwise orientation. These may be differentiated by the examination of the N-C-C-O torsion angle. The orientation of the arms is

denoted, Δ for a clockwise orientation of the arms and by Λ for an anticlockwise orientation.

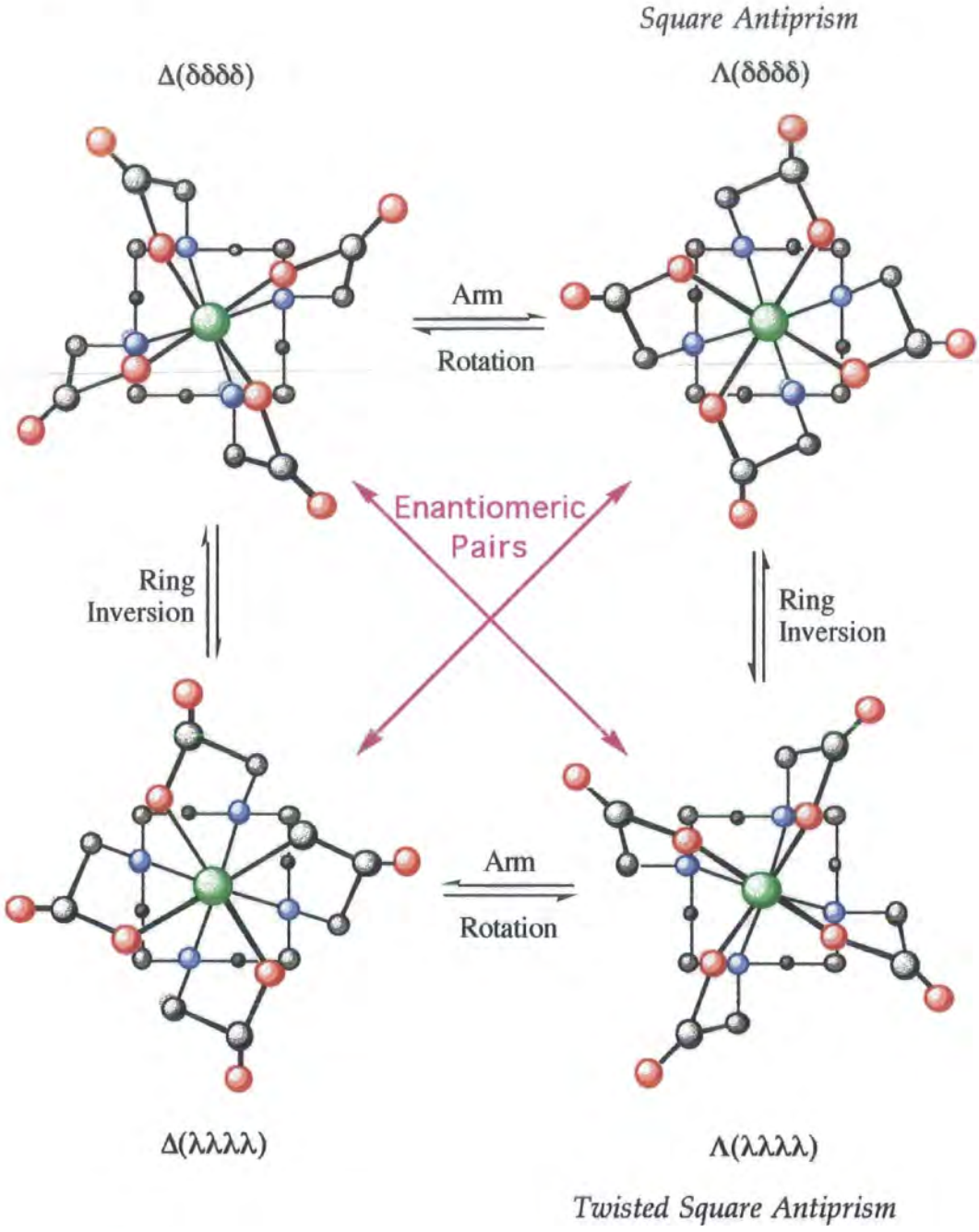

Figure 1.11 A schematic representation of the interconversion of the four structural isomers of [Ln.DOTA]$^-$ complexes.

The combination of these two elements of chirality gives rise to a total of four stereoisomers, although these are related as two enantiomeric pairs. The Δ(λλλλ) and the Λ(δδδδ) which correspond to a square antiprismatic coordination geometry, and Δ(δδδδ) and Λ(λλλλ) which correspond to a twisted square antiprismatic geometry (Figure 1.11).

Exchange spectroscopy (EXSY)[89,92] and variable temperature NMR[85,86] experiments have shown that these four isomers are in dynamic exchange in solution. This interconversion can occur through two possible processes, an inversion of the ring conformation or a rotation of the arm orientation (Figure 1.11). Sequential arm rotation and ring inversion will interconvert enantiomers. ^{1}H EXSY studies on [Eu.DOTA]$^-$ have been used to measure the relative rates of arm rotation and ring inversion which were found to be 78 s^{-1} and 35 s^{-1}, respectively.[89] These figures are susceptible to a fairly large error.

The quantitative EXSY study of Desreux *et al.* has shown that a negative entropy term is associated with the interconversion of the two isomeric forms of [Yb.DOTA]$^-$.[92] This is corroborated by the results of a variable pressure ^{17}O study on [Yb.DOTA]$^-$ by Merbach *et al.* which revealed a positive volume of activation for the isomerisation process.[90] Clearly then the interconversion of the two coordination isomers for the later [Ln.DOTA]$^-$ complexes is associated with loss of a water molecule. These findings are not mirrored for the earlier lanthanides and hence the interconversion of the two isomeric forms of early [Ln.DOTA]$^-$ complexes occurs by means of a simple ring flip or arm rotation.

1.4. Improving the Efficacy of Contrast Agents

The development of improved contrast agents offers several potential benefits to patient care. Firstly, the amount of contrast agent required may be reduced. Consequently the pain arising from osmotic shock upon injection of the contrast agents, particularly when high dosages are required, may be reduced. Secondly, the implications in shortening the acquisition time of an image are dramatic. Furthermore, contrast agents are comparatively expensive, so by reducing the amount required, their application in MRI could be widened.

$$R_1^{o.s.} = \left(\frac{32\pi}{405}\right)\gamma_H^2 g^2 \mu_B^2 S(S+1)\left(\frac{N_A}{1000}\right)\left(\frac{C}{aD}\right) f(\tau_S \tau_D \omega_I \omega_S) \qquad (1.5)$$

The outer sphere contribution to the overall longitudinal relaxivity of a contrast agent by diffusion through the bulk solvent is approximately described by the equation (1.5). Even though a clear description of the parameters affecting this contribution is currently unavailable, it is unlikely that such a model will facilitate the design of contrast agents with high outer sphere relaxivities. The factors which govern the extent of this contribution, such as the diffusional correlation time, τ_D, and distance of closest approach, a, are intrinsic features of a given complex and are not amenable to optimisation.

$$R_1 = \frac{[C]q}{55.6}\left(\frac{1}{T_{1M} + \tau_M}\right) \tag{1.6}$$

$$T_{1M} = \frac{2/15 S(S+1)g^2\beta^2\gamma_I^2}{r^6}\left\{\frac{7\tau_C}{\left(1+\omega_S^2\tau_C^2\right)} + \frac{3\tau_C}{\left(1+\omega_I^2\tau_C^2\right)}\right\} + \frac{2}{3}\frac{A^2}{\hbar^2}S(S+1)\left\{\frac{\tau_S}{\left(1+\omega_S^2\tau_S^2\right)}\right\} \tag{1.7}$$

$$\frac{1}{\tau_C} = \frac{1}{\tau_S} + \frac{1}{\tau_R} + \frac{1}{\tau_M} \tag{1.8}$$

In contrast, the contribution to the overall longitudinal relaxivity made by the inner sphere water relaxation mechanism may be optimised. Inspection of the Solomon, Bloembergen and Morgan equations, (Eqns 1.6 - 1.8), shows that in addition to the concentration of the contrast agent, the number of bound water molecules and a series of correlation times determine the inner sphere relaxivity of a paramagnetic complex. Although optimal values for some of these correlation times exist, to date it is beyond the ability of the chemist to design complexes with these properties. For example, τ_M, relating to the water exchange rate would ideally be no longer than necessary to allow the water protons to be relaxed. In a slowly tumbling system, an ideal value of 30 ns has been estimated.[42] However, the factors governing the water exchange rate are rather crudely understood. Cationic complexes exhibit much slower exchange rates than analogous neutral or anionic complexes. This may be explained in terms of a coulombic attraction between the lone pairs of the water and the positive complex. Clearly then an anionic complex is more likely to satisfy the conditions of fast exchange, however, the value of τ_M measured for [Gd.DOTA]$^-$ is 244 ns,[62] significantly longer than the estimated optimum value.

Two variables over which the chemist may have more control, which also have an effect upon relaxivity are q, the hydration state and τ_R, the rotational correlation time.

Increasing the Hydration State

The coordination number of a paramagnetic ion is determined to a large extent by the size of the ion. Since free gadolinium(III) ion is toxic it must be administered in the form of a stable complex. The majority of the coordination sites are occupied by the donor atoms of a chelating agent. This in turn limits the number of directly coordinated water molecules in the complex. In general, gadolinium(III) adopts nine coordinate complexes. The contrast agents currently in clinical use utilise octadentate ligands, leaving only one vacant coordination site. By lowering the denticity of the chelating agent, it should be

possible to open up more vacant coordination sites to which water molecules may bind. However, a concurrent reduction in the stability of the complex may also be expected. Consideration of the stability constants of the gadolinium complexes of some acyclic and macrocyclic chelating agents, (Table 1.9), reveals that this is indeed the case.

Gd^{III} Chelate	Denticity	Ligand Type	log K_a (298K)
DOTA	8	Macrocyclic	24.7[39]
DTPA	8	Acyclic	22.5[38]
DO3A	7	Macrocyclic	21.0[93]
DO3MA	7	Macrocyclic	25.3[94]
NOTA	6	Macrocyclic	13.7[95]
EDTA	6	Acyclic	17.3[38]

Table 1.9 The thermodynamic stability of gadolinium(III) chelates is reduced with lowering denticity of the ligand.

In general the gadolinium(III) complexes of hexadentate ligands are not sufficiently stable for use *in vivo*. Clearly then a practical maximum value for q is 2, when a heptadentate ligand is used to chelate the gadolinium(III) ion.

Inspection of the the stability constants, (Table 1.9), suggests that macrocyclic ligands tend to exhibit higher stability constants than their acyclic counterparts. This increased stability has been ascribed to an increase in the rigidity of the complex, imparted by the macrocycle. The observation that the gadolinium(III) complex of NOTA has a lower stability constant than that of EDTA may be explained in terms both of ionic charge and geometric factors. The EDTA complex has an overall charge of -1 whereas the NOTA complex is neutral, thus stronger electrostatic attraction to the ion may be expected. The $9N_3$ ring of NOTA is not predisposed to binding large ions such as gadolinium, this results in a poor bite angle and thus a less stable chelate.

With this in mind, the gadolinium(III) chelate of DO3A might have been expected to provide an ideal contrast agent. The complex possesses two bound water molecules, and so should exhibit improved relaxivity over the contrast agents in current use. The complex is charge neutral and a correspondingly low osmolality may be expected. Whilst the stability constant of the complex is some four orders of magnitude lower than that observed for the DOTA

complex, it is still higher than those of some contrast agents currently in clinical use.

However, the thermodynamic stability of a complex alone does not imply that a complex is safe for *in vivo* application. The dissociation kinetics must also be considered. The observed rate of dissociation, k_d, for [Gd.DO3A] is 5 x 10^{-4} s^{-1} at pH 2.[96] Such a rate is too fast for this complex to represent a viable contrast agent.

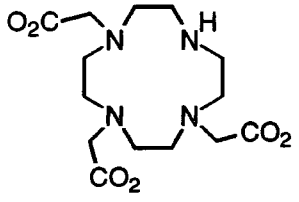

7

DO3A

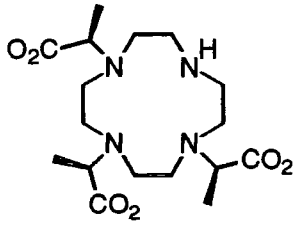

8

DO3MA

The work of Tweedle has shown that the substitution of pendant arms with methyl groups renders the complex more conformationally rigid.[94] The enantioselective synthesis of a DO3A derivative with chiral propionate substituents has been reported.[97] The gadolinium complex of this ligand is much more stable (Table 1.9). It is also less prone to acid catalysed dissociation, k_d = 3.7 x 10^{-5} s^{-1} at pH 1. The gadolinium(III) chelate of DO3MA then represents a stable complex which may, in principle, adopt a hydration state of two.

One potential problem exists with this approach to the problem of increasing relaxivity. This is highlighted by the crystal structure of [Gd.DO3A] in which the two vacant coordination sites are not occupied by water molecules. Rather they are occupied by a carbonate dianion, which acts as a bidentate ligand.[98] Such binding has also been observed at heptacoordinate lanthanide(III) centres in solution by luminescence.[99] Indeed a number of anions and polyanions can act as bidentate ligands for heptadentate lanthanide complexes. Although this effect is reversible, the concentration of lactate (~ 2.3 mM) and in particular HCO_3^- (~ 25 mM) *in vivo* is not inconsiderable and may reduce the relaxivities observed *in vivo*.

Macromolecular Contrast Agents

For contrast agents based around metal ions with long electronic relaxation times, the most substantial increases in relaxivity are to be gained from maximising τ_R, the rotational correlation time.[33] Indeed, much of the

research into contrast agents conducted over recent years has centred around this idea. In theory τ_R may be increased in two ways, either by increasing the mass of the complex or by increasing the viscosity of the medium. In practice, the viscosity of the medium (extracellular fluid) cannot be changed and therefore consideration must be given to increasing the size of the complex, since larger molecules tumble more slowly in solution than smaller ones.

The first example of a macromolecular contrast agent was reported by Lauffer and Brady in 1985.[100] Twenty equivalents of the cyclic dianhydride of DTPA, **9**, and EDTA were condensed with bovine serum albumin (BSA) or immunoglobin G (IgG) at pH 8.2 in aqueous sodium hydrogen carbonate solution, Scheme 1.1. It was expected that the ε amino groups on the protein lysine residues would react with one anhydride the other undergoing hydrolysis.

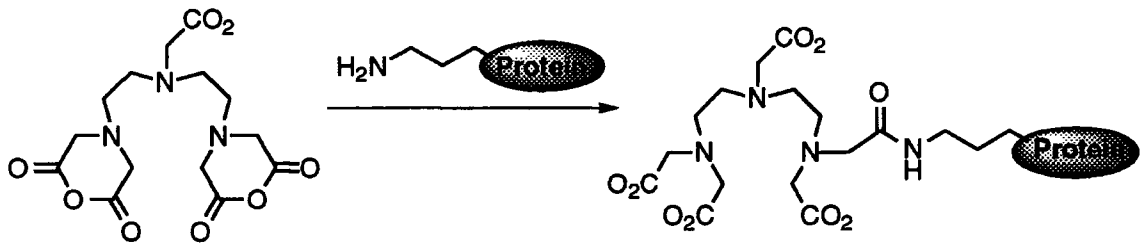

9 **10**

Scheme 1.1 The synthesis of the BSA-DTPA conjugate, **10**.

Both gadolinium(III) and manganese(II) complexes of these conjugates were synthesised. The thermodynamic stability constants of the gadolinium(III) chelates were measured to be 10^{23} for the DTPA conjugates and 10^{17} for the EDTA conjugates. This suggests that only the DTPA conjugates would represent viable clinical contrast agents. The assumption of the authors that such gadolinium(III) DTPA-protein conjugates would be $q = 2$ complexes is in fact erroneous. The high stability constants observed for these complexes preclude the possibility that the acetamide of the DTPA-protein conjugate only forms a heptadentate ligand. The carbonyl of the peptide linkage to the protein must also bind the gadolinium(III), as is observed in a number of other systems[101] and the conjugate will possess only one bound water molecule. Thus the DTPA-protein conjugate and the DTPA complexes of gadolinium(III) can be directly compared as $q = 1$ complexes.

These protein-complex conjugates exhibited dramatically different behaviour to their respective parent complexes at 20 MHz and 38°C. The

NMRD profiles obtained for the two gadolinium conjugates are shown (Figure 1.12), with those of the DTPA and EDTA complexes.

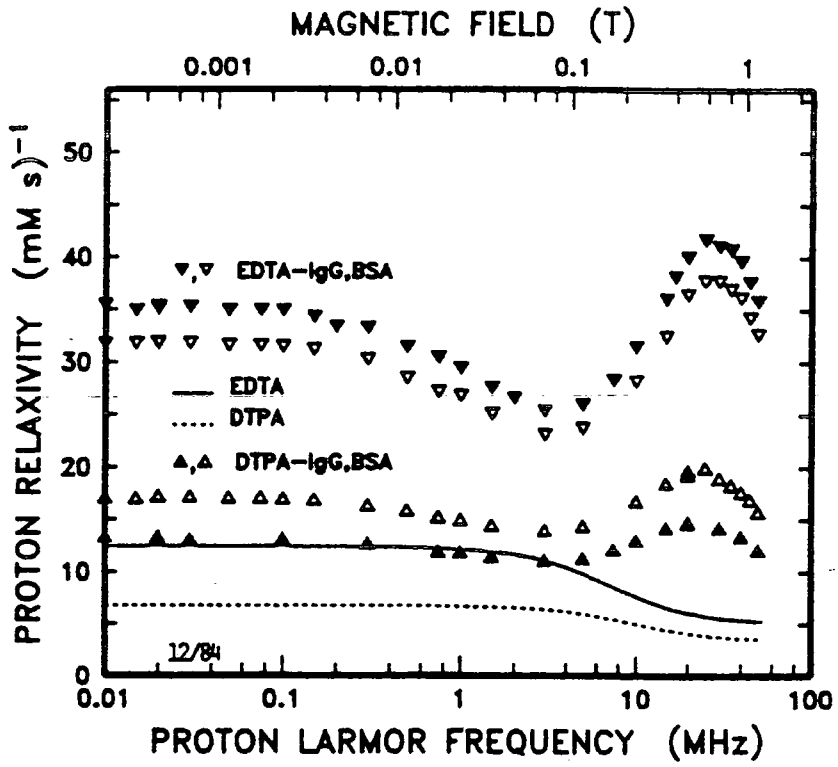

Figure 1.12 The NMRD profiles of the gadolinium EDTA and DTPA - BSA conjugates show significant enhancement of the water proton relaxation rate. Reproduced from reference (33).

The gadolinium(III) DTPA-protein conjugates give rise to a five-fold enhancement in the water proton relaxation rate in the imaging field range (~0.15 - 0.5 T).

It has been shown[102] that an increase in the number of paramagnetic centres per molecule has an additive effect upon the relaxivity of the complex. An average of 3.7 of gadolinium(III) chelates per DTPA-BSA conjugate was determined by competitive titration of gadolinium(III) chloride with EDTA.[103] The presence of three or four gadolinium(III) ions per protein can therefore be expected to result in an increase in relaxivity of the same order.

This scalar effect accounts for some of the observed increase in relaxivity. Inspection of the high field region of the NMRD profile (Figure 1.12) reveals a "hump" in the relaxation rate beyond the inflection point around 5 MHz. Since the relaxivity in this region of the profile is limited by τ_R (Chapter 1.2), it can be concluded that the increased rotational correlation time arising from the

increase in molecular mass is primarily responsible for the remaining increase in relaxivity.

For the EDTA-protein conjugates, however, the increased water proton relaxation rate is the result of an increase in both mass and hydration state (q = 3) for these complexes.

One of the major advantages with this method of increasing the reorientational correlation time is that the issue of biocompatibility does not arise. If proteins which are naturally occurring in the human body are used, then the question of tolerance of the contrast agent can be avoided. For this reason much of the subsequent research in this area has centred around the use of proteins as the macromolecules to increase molecular size. The use of non-covalently conjugated systems has also been addressed. Small discrete paramagnetic complexes bearing a hydrophobic residue, such as the gadolinium chelates **11-14**, bind strongly to a hydrophobic surface of the protein.[104,105,106]

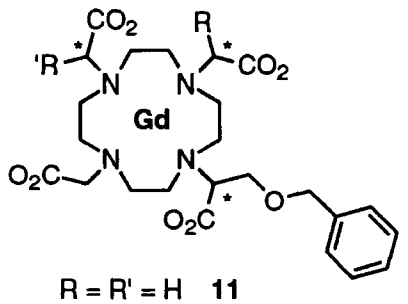

R = R' = H **11**

R = H R =  **12**

R = R' =  **13**

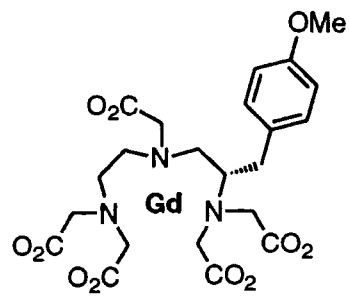

14

A study involving an anionic q = 0 gadolinium(III) chelate and its association to the surface of the BSA, showed a somewhat unexpected increase in relaxivity at high fields.[45] The NMRD profile reveals the characteristic hump, albeit a small one, between 10 and 30 MHz. This increase cannot be explained in terms of an effect on the inner sphere mechanism, since the complex only operates through a nominally outer sphere mechanism. However, the outer sphere contribution is also made up of a contribution arising from a second coordination sphere of water molecules. The relaxivity of these molecules must be affected by rotation in the same manner as an inner sphere water because they are orientationally aligned. For a q = 1 gadolinium(III) chelate an increase in relaxivity by a factor of four is generally observed.

Whilst a proton relaxation rate of close to 20 $mM^{-1}s^{-1}$ at imaging fields represents a significant improvement over that obtained by commercially

available 'small' paramagnetic complexes, it does not represent an optimised set of conditions for a paramagnetic contrast agent. For a gadolinium(III) chelate with q=1, it has been calculated that longitudinal relaxivities of the order of 50 $mM^{-1}s^{-1}$ are theoretically obtainable,[107] indeed relaxivities in excess of 100 $mM^{-1}s^{-1}$ should be obtained if all the parameters are optimised.[42]

By considering the freedom of such a bound chelate to reorientate, an explanation for the difference between the observed and theoretical enhancement in relaxivity at higher fields may be seen. A chelate attached to a macromolecule at one point may rotate about this linkage. The complex is also free to vibrate, (Figure 1.13). Likewise if two points of attachment are utilised, the complex is free to rotate about the axis of the linkers.

Figure 1.13 Description of the motion possible when the paramagnetic complex is linked to one or two macromolecules.

These motions will reduce the value of τ_R, at the paramagnetic centre giving rise to a lower value of relaxivity in that region of the NMRD profile in which τ_R is limiting. Clearly then, to maximise τ_R and thereby the relaxivity these degrees of freedom of motion must be removed.

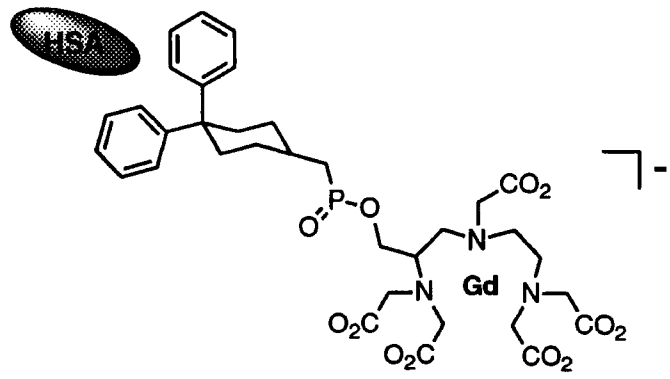

MS 325, **15**

Recently, one potential contrast agent has attempted to overcome the problem of rotational and vibrational reorientation. MS 325, is a substituted DTPA chelate of gadolinium(III) developed by Nycomed.[108]

The substituent bears two phenyl rings for intercalation with human serum albumin (HSA). The connection between these intercalators and the complex is made up of a cyclohexyl ring attached to a phosphate ester. The

idea behind this elaborate system of joining macromolecule and paramagnetic complex is that both the cyclohexane and the phosphate ester restrict the rotation of the complex. In this way a longer reorientational correlation time than can be obtained simply by attachment to HSA can be achieved. This is born out by the NMRD profiles obtained for the HSA conjugate. Relaxivities of 24 $mM^{-1}s^{-1}$ at imaging fields have been reported for this conjugate, which entered phase 1 clinical trials in 1996.

1.5. The Scope of this Work

In the light of the work undertaken so far, it is clear that the optimisation of the effective correlation time τ_C is paramount in the design of new contrast agents. At the relatively high fields at which imaging is performed τ_R, the reorientational correlation time, is limiting for small chelates, (Eqns. 1.6-1.8). By reducing the rate at which the complex tumbles this correlation time becomes longer. As τ_R becomes longer its contribution to τ_C dimishes, and the water exchange rate τ_M begins to limit the relaxivity. Clearly then an ideal contrast agent would have a water exchange rate no longer than is necessary to allow the relaxation of the water protons. This rate has been calculated to be around 30 ns.[42] The complex should also be tumbling at a rate that makes this water exchange rate limiting in terms of the relaxivity obtained.

$$R_1 = \frac{[C]q}{55.6}\left(\frac{1}{T_{1M} + \tau_M}\right) \tag{1.6}$$

$$T_{1M} = \frac{2/15 S(S+1)g^2\beta^2\gamma_I^2}{r^6}\left\{\frac{7\tau_C}{(1+\omega_S^2\tau_C^2)} + \frac{3\tau_C}{(1+\omega_I^2\tau_C^2)}\right\} + \frac{2}{3}\frac{A^2}{\hbar^2}S(S+1)\left\{\frac{\tau_S}{(1+\omega_S^2\tau_S^2)}\right\} \tag{1.7}$$

$$\frac{1}{\tau_C} = \frac{1}{\tau_S} + \frac{1}{\tau_R} + \frac{1}{\tau_M} \tag{1.8}$$

As discussed previously (Chapter 1.4) the association of a paramagnetic complex with a macromolecule results in a longer value of τ_R. However, reorientational motion of the complex by rotation and vibration limit the values of τ_R which may be obtained in this way. It is therefore necessary to remove these degrees of freedom from the paramagnetic complex. If the paramagnetic ion is situated at the *centre* of a macromolecular structure, it may then lie upon the axis of any reorientational motion, and its reorientational correlation time would become correspondingly longer. In this way it may be possible to lengthen τ_R sufficiently such that τ_M becomes limiting.

The structural or dynamic characteristics of a paramagnetic complex which give rise to faster water exchange rates are not fully understood. The design of a complex with the appropriate τ_M value is therefore not possible. The gadolinium complexes of DOTA and DTPA are known to exhibit relatively fast water exchange rates and would therefore provide a suitable basis for the chelating structure of a macromolecular contrast agent.

The success of [Gd.DOTA]$^-$ (Dotarem) as a contrast agent arises from its slow dissociation kinetics *in vivo* and its relatively fast water exchange rate (τ_R = 244 ns).[62] It is possible to envisage a derivative of DOTA in which the complex is held at the centre of a biocompatible macromolecular or dentritic structure by three or four linkages (Figure 1.13). Such a complex would be expected to be sufficiently stable for use *in vivo*. It would tumble slowly enough that the overall relaxivity of the complex was determined by the water exchange rate.

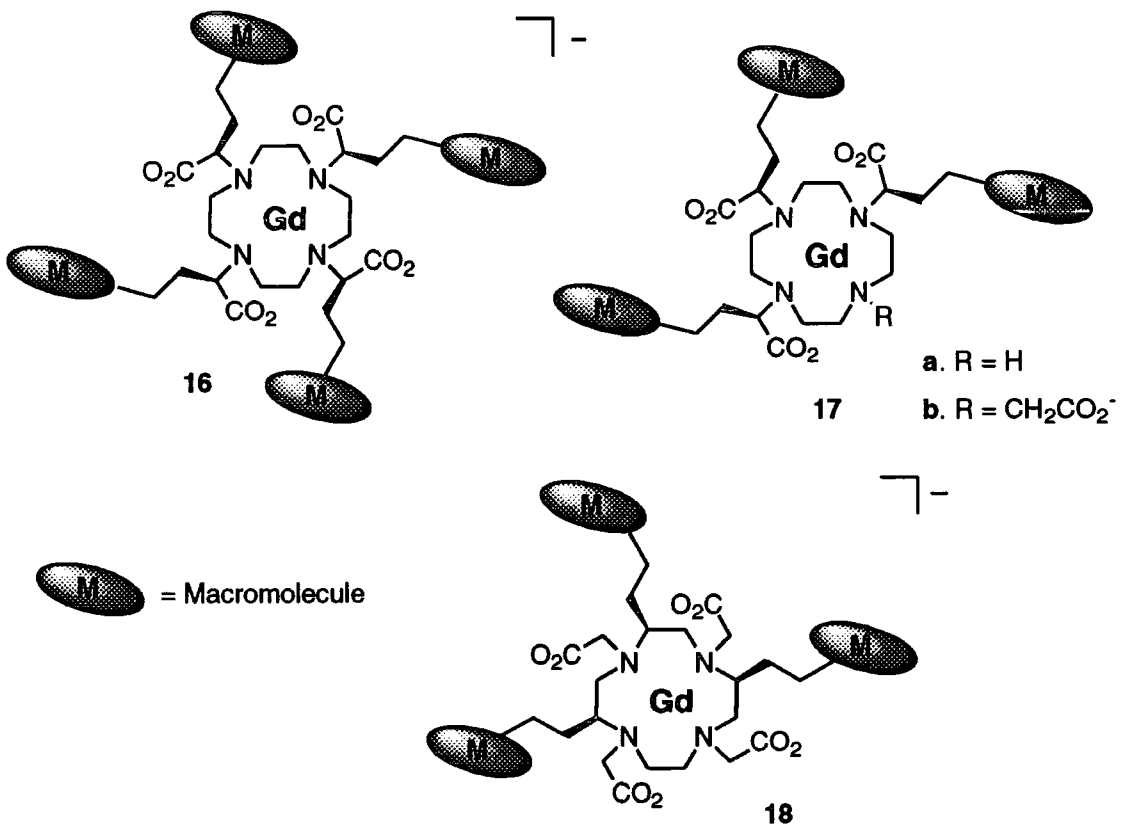

Figure 1.13 Three potentially optimised paramagnetic contrast agents.

The complex may be covalently secured at the centre of the macromolecular structure in one of two ways. Either through substitution of the acetate arms or by substitution of the macrocyclic ring. A minimum of three linkages to the macromolecular structure is required to reduce reorientation of the complex in all directions. Thus the synthesis and study of

three types of complex were undertaken. Chapter 2 deals with complexes derived from tetra acetate substituted DOTA derivatives, of the type **16**. A similar type of acetate substituted complex with only three linkages such as **17**, is discussed in Chapter 3. Complexes in which the fourth acetate arm is omitted, to vacate a second potential coordination site for water are included in this discussion. The final group of compounds are those derived from ring substituted cyclen derivatives, of the type **18**, the synthesis of complexes of this type is examined in Chapter 5.

1.6. References

1 Koenig, S.H.; In *"Encyclopedia of Nuclear Magnetic Resonance" Vol. 1 "Historical Perspectives"*, Eds. Grant, D.M.; Harris, R.K.; Wiley, New York, (1996), 437.

2 Rabi, I.I.; Zacharias, J.R.; Millman, S.; Kusch, P.; *Phys. Rev.*, (1938), **53**, 318.

3 Rabi, I.I.; Zacharias, J.R.; Millman, S.; Kusch, P.; *Phys. Rev.*, (1939), **55**, 526.

4 Kellogg, J.M.B.; Rabi, I.I., Ramsey, N.F. Jr.; Zacharias, J.R.; *Phys. Rev.*, (1939), **56**, 728.

5 Schwinger, J.; *Phys. Rev.*, (1937), **51**, 648.
Rabi, I.I.; *Phys. Rev.*, (1937), **51**, 652.
Bloch, F.; Rabi, I.I.; *Rev. Mod. Phys.*, (1945), **17**, 237.

6 Bloch, F.; Hansen, W.W.; Packard, M.; *Phys. Rev.* (1946), **69**, 127.
Bloch, F.; Hansen, W.W.; Packard, M.; *Phys. Rev.* (1946), **70**, 474.

7 Purcell, E.M.; Torrey, H.C.; Pound, R.V.; *Phys. Rev.*, (1946), **69**, 37.

8 Chen, C-N.; Hoult, D.I.; In *"Biomedical Magnetic Resonance Technology"*, Higler, Bristol, (1989).

9 Mansfield, P.; Morris, P.G.; In *"NMR Imaging in Biomedicine"*, Academic, New York, (1982).

10 Jacobson, B.; Anderson, W.A.; Arnold, J.T.; *Nature*, (1954), **173**, 772.

11 Odeblad, E.; *Acta. Obst. Gyn. Scand. Suppl. 8*, (1968), **47**, 39.

12 Odeblad, E.; *Med. Isotopenforsch*, (1956), **1**, 25.

13 Blumberg, W.E.; Eisinger, J.; Aisen, P.; Morell, A.G.; Scheinberg, I.H.; *J. Biol. Chem.*, (1963), **238**, 1675.

14 Hahn, E.; *Phys. Rev.*, (1950), **80**, 580.

15 Gabillard, R.; *C. R. Acad. Sci. Paris*, (1951), **232**, 1551.
Gabillard, R.; *Phys. Rev.*, (1952), **85**, 694.

16 Lauterbur, P.C.; *Nature*, (1973), **242**, 190.

17 Damadian, R.; US Patent 3,789,832, 5 February 1974.

18 Kumar, A.; Welti, D.; Ernst, R.R.; *J. Magn. Reson.*, (1975), **18**, 69.

Hoult, D.I.; *J. Magn. Reson.*, (1977), **26**, 165.

19 Garroway, A.N.; Grannell, P.K.; Mansfield, P.; *J. Phys. C.: Solid State Phys.*, (1974), **7**, L457.
Lauterbur, P.C.; Kramer, D.M.; House, W.V.; Chen, C-N.; *J. Am. Chem. Soc.*, (1975), **97**, 6866.

20 Diem, K.; Leutner, C.; *"Documenta Geigy Scientific Tables"*, p 517, Gregory, Basel, (1970).

21 Tweedle, M.F.; In *"Lanthanide Probes in Life, Chemical and Earth Sciences"*, Eds. Bunzli, J-C.G.; Choppin, G.R., Elsevier, Amsterdam, (1989), Chapter 5.

22 Damadian, R.; *et al.*; *Proc. Natl. Acad. Sci. USA.*, (1974), **71**, 1471.

23 Lauterbur, P.C.; Mendoca-Dias, M.H.; Rudin, A.M.; In *"Frontier of Biological Energetics"*, Eds. Dutton, P.L.; Leigh, L.S.; Scarpa, A., Academic, New York, (1978), 752.

24 Brady, T.J.; Goldman, M.R.; Pykett, I.L.; Buonanno, F.S.; Kistler, J.P.; Newhouse, J.H.; Burt, C.T.; Hinshaw, W.S.; Pohost, G.M.; *Radiology*, (1982), **144**, 343.
Brady, T.J.; Goldman, M.R.; Pykett, I.L.; Burt, C.T.; Buonanno, F.S.; Kistler, J.P.; Newhouse, J.H.; Hinshaw, W.S.; Pohost, G.M.; *Circulation*, (1982), **66**, 1012.

25 Young, I.R.; Clarke, G.J.; Gailes, D.R.; *et al.*; *Computed Tomography*, (1981), **5**, 534.

26 Carr, D.H.; Brown, J.; Bydder, G.M.; Weinmann, H.J.; Speck, U.; Thomas, D.J.; Young, I.R.; *Lancet*, (1984), **1**, 484.

27 Bjørnerud, A.; Øksendal, A.N.; *Abstracts from the COST D1 Meeting, Bergen*, 9-10th September 1997.

28 Elizondo, G.; Fretz, C.J.; Stark, D.D.; Rocklage, S.M.; Quay, S.C.; Worah, D.; Tsang, Y-M,; Chen, M.C-M.; Ferrucci, J.T.; *Radiology*, (1991), 73.

29 Schaeffer, M.; Meyer, D.; Beaute, S.; Douchet, D.; *Magn. Res. Med.*, (1991), **22**, 238.

30 Weinmann, H-J.; Schuhmann-Giampieri, G.; Schmitt-Willich, H.; Vogler, H.; Frenzel, T.; Gries, H.; *Magn. Res. Med.*, (1991), **22**, 233.
Platzek, J.; Blaszkiewicz, P.; Gries, H.; Luger, P.; Michl, G.; Müller-Fahrnow, A.; Radüchel, B.; Sülzle, D; *Inorg. Chem.*, (1997), **36**, 6086.

31 Hindré, F.; le Plouzennec, M.; de Certaines, J.D.; Foultier, M.T.; Patrice, T.; Simonneaux, G.; *J. Magn. Reson. Imag.*, (1993), **3**, 59.

32 Weissleder, R.; *Magn. Res. Med.*, (1991), **22**, 209.

33 Lauffer, R.B.; *Chem. Rev.*, (1987), **87**, 901.

34 Hasso, A.N.; Stark, D.D.; *J. Mag. Res. Imag.*, (1993), 135.

35 Rocklage, S.M.; Worah, D.; Kim, S-H.; *Magn. Reson. Med.*, (1991), **22**, 216.

36 Wedeking, P.W.; Tweedle, M.F.; *Nucl. Med. Biol.*, (1988), **15**, 395.

37 Niendorf, H.P.; *et al.*; *Radiation Medicine*, (1985), **3**, 7.

38 Martell, A.E.; Smith, R.M.; *Critical Stability Constants*, Plenum, New York, Vol 1, (1974), 204.

39 Cacheris, W.P.; Nickle, S.K.; Sherry, A.D.; *Inorg. Chem.*, (1987), **26**, 958.

40 http://www.rxmed.com/monographs/prohance.html.
Harper, E.S.; Worah, D.; Hals, P-A.; Holtz, E.; Furuhama, K.; Noruma, H.; *Investigative Radiology*, (1993), **28**, Suppl 1, 28.

41 Norman, T.J.; *PhD Thesis*, University of Durham, (1994) and references cited therein.

42 Aime, S.; Botta, M.; Fasano, M.; Terreno, E.; *Chem. Soc. Rev.*, (1998), **27**, 19.

43 McLachlan, S.J.; Eaton, S.; Desimone, D.N.; *Investigative Radiology*, (1992), **27**, S12.

44 Harpur E.S.; Worah, D.; Hals, P.A.; Holtz, E.; Furuhama, K.; Nomura, H.; *Investigative Radiology*, (1993), **28**, S28.

45 Aime, S.; Batsanov, A.S.; Botta, M.; Howard, J.A.K.; Parker, D.; Senanayake, K.; Williams, J.A.G.; *Inorg. Chem.*, (1994), **33**, 4696.

46 Laukien, G.; Schlüter, J.; *Z. Physik*, (1956), **146**, 113.

47 Zimmerman, J.A.; *J. Chem Phys.*, (1954), **22**, 950.

48 Koenig. S.H.; Epstien, M.; *J. Chem. Phys.*, (1975), **63**, 2279.

49 Pfeifer, J.H.; *Ann. Physik*, (1961), **8**, 1.
Pfeifer, J.H.; *Z. Naturforsch*, (1962), **17**, 279.

50 Bloch. J.; Navon. G.; *J. Inorg. Nucl. Chem.*, (1980), **42**, 693.
Oakes, J.; van Kralingen, C.G.; *J. Chem. Soc. Dalton Trans.*, (1984), 1133.

51 Koenig, S.H.; Brown, R.D.; In *Magnetic Resonance Annual 1987*, Eds. Kressel, H.Y., Raven, New York, (1987).
Alsaadi, B.M.; Rossotti, F.J.C.; Williams, R.J.P.; *J. Chem. Soc. Dalton. Trans.*, (1980), 813.

52 Freed, J.H.; *J. Chem. Phys.*, (1978), **68**, 4034.

53 Oakes, J.; Smith, E.G.; *J. Chem. Soc. Faraday Trans. 2*, (1981), **77**, 299.

54 Aime, S.; Barge, A.; Botta, M.; Parker, D.; de Sousa, A.S.; *J. Am. Chem. Soc.*, (1997), **119**, 4767.

55 Bloembergen, N.; Purcell, E.M.; Pound, R.V.; *Phys. Rev.*, (1948), **73**, 697.

56 Debye, P.; In *Polar Molecules*, Dover Publications, New York, (1945), Chapter V.

57 Solomon, I.; *Phys. Rev.*, (1955), **99**, 559.

58 Solomon, I.; Bloembergen, N.; *J. Chem. Phys.*, (1956), **25**, 261.

59 Bloembergen, N.; *J. Chem. Phys.*, (1957), **27**, 572.

60 Bloembergen, N.; Morgan, L.O.; *J. Chem. Phys.*, (1961), **34**, 842.

61 Koenig, S.H.; Brown, R.D.; *"Relaxometry of Tissue in NMR Spectroscopy of Cells and Organisms", Vol II*, Eds. Gupta, R.M.; CRC Press, Boca Raton, FL., (1987), 75.

62 Aime, S.; Botta, M.; *Personal Communication.*

63 Cotton, F.A.; Wilkinson, G.; In *"Advanced Inorganic Chemistry" 5th Ed.*, Wiley, New York, (1988).

64 Chaudhur, D.; Horrocks, W. DeW. Jr.; Amburgey, J.C.; Wber, D.J..; *Biochemistry*, (1997), **36**, 9674.
Frey, M.W.; Frey, S.T.; Horrocks, W.de W.Jr.; Kaboord, B.F.; Benkovic, S.J.; *Chem. and Boil.*, (1996), **68**, 394.

65 Foster, C.E.; *PhD Thesis*, University of Durham, (1996) and references therein.

66 Stephens, E.M.; In *"Lanthanide Probes in Life, Chemical and Earth Sciences"*, Eds. Bunzli, J-C.G.; Choppin, G.R., Elsevier, Amsterdam, (1989), Chapter 6.

67 Bunzli, J-C.G.; In *"Lanthanide Probes in Life, Chemical and Earth Sciences"*, Eds. Bunzli, J-C.G.; Choppin, G.R., Elsevier, Amsterdam, (1989), Chapter 7.

68 Reisfeld, R.; Jørgensen, C.K.; In *"Lasers and Excited States of Rare Earths"*, Springer Verlag, Berlin, (1977).

69 Golding, R.M.; Halton, M.P.; *Aust. J. Chem.*, (1972), **25**, 2577.

70 Lewis,W.B.; Jackson, J.A.; Lemons, J.F.; Taube, H.; *J. Chem. Phys.*, (1962), **36**, 694.

71 Bleaney, B.; *J. Magn. Res.*, (1972), **8**, 91.

72 Sherry, A.D.; In *"Lanthanide Probes in Life, Chemical and Earth Sciences"*, Eds. Bunzli, J-C.G.; Choppin, G.R., Elsevier, Amsterdam, (1989), Chapter 4.

73 Bleaney, B.; Dobson, C.M.; Levine, B.A.; Martin, R.B.; Williams, R.J.P.; Xavier, A.V.; *J. Chem. Soc., Chem Commun.*, (1972), 791.

74 Donato, H.Jr.; Martin, R.B.; *J. Am. Chem. Soc.*, (1972), **94**, 4129.

75 Reuben, J.; Fiat, D.; *J. Chem. Phys.*, (1969), **51**, 4909.

76 Horrocks, W.de W. Jr.; Sipe, J.P.; *Science*, (1972), **177**, 994.

77 Kropp, J.L.; Windsor, M.W.; *J. Chem. Phys.*, (1963), **39**, 2769.

78 Parker, D.; Williams, J.A.G.; *J. Chem. Soc., Dalton Trans.*, (1996), 3613.

79 Beeby, A.; Faulkner, S.; *Chem. Phys. Lett.*, (1997), **266**, 116.

80 Horrocks, W.de W.Jr.; Sudnick, D.R.; *J. Am. Chem. Soc.*, (1979), **101**, 334.
Horrocks, W.de W.Jr.; Sudnick, D.R.; *Acc. Chem. Res.*, (1981), **14**, 384.

81 Beeby, A.; Dickins, R.S.; Faulkner, S.; Parker, D.; Williams, J.A.G.; *J. Chem. Soc. Chem. Commun.*, (1997), **37**, 1401.

82 Dickins, R.S.; Parker, D.; de Sousa, A.S.; Williams, J.A.G.; *J. Chem. Soc., Chem Commun.* (1996), 697.

83 Alpoim, M.C.; Urbano, A.M.; Geraldes, C.F.G.C.; Peters, J.A.; *J. Chem. Soc. Dalton Trans.*, (1992), , 463.

84 Stetter, F.; *Angew. Chem.*, (1976), **88**, 760.

85 Aime, S.; Botta, M.; Ermondi, G.; *Inrog. Chem.*, (1992), **32**, 4291.

86 Aime, S. Barge, A.; Botta, M.; Fasano, M.; Ayala, J.D.; Bombieri, G.; *Inorg. Chim. Acta*, (1996), **246**, 423.

87 Spirlet, M-R.; Rebizant, J.; Desreux, J-F.; Loncin, M-F.; *Inorg. Chem.*, (1984), **23**, 359

88 Dubost, J-P.; Leger, M.; Langlois, M-H.; Meyer, D.; Schaefer, M.; *C. R. Acad. Sci. Paris Ser. 2*, (1991), **312**, 349.

89 Hoeft, S.; Roth, K.; *Chem. Ber.*, (1993), **126**, 869

90 Aime, S.; Botta, M.; Fasano, M.; Marques, M.P.M.; Geraldes, C.F.G.C.; Pubanz, D.; Merbach, A.E.; *Inorg. Chem.*, (1997), **36**, 2059.

91 Corey, E.J.; Bailar, J.C.Jr.; *J.Am. Chem. Soc.*, (1959), **81**, 2620.

92 Jaques, V.; Desreux, J-F.; *Inorg. Chem.*, (1994), **33**, 4048.

93 Kumar, K.; Jin, T.; Wang, X.; Desreux, J.F.; Tweedle, M.F.; *Inorg. Chem.*, (1994), **33**, 3823.

94 Kumar, K.; Tweedle, M.F.; *Inorg. Chem.*, (1993), **32**, 4193.

95 Brucher, E.; Cortes, S.; Chavez, F.; Sherry, A.D.; *Inorg. Chem.*, (1991), **30**, 2092.

96 Kumar, K.; Chang, C.A.; Tweedle, M.F.; *Inorg. Chem.* (1993), **32**, 587.

97 Kang, S.I.; Ranaganathan, R.S.; Emswiler, J.E.; Kumar, K.; Gougoutas, J.Z.; Malley, M.F.; Tweedle, M.F.; *Inorg. Chem.*, (1993), **32**, 2912.

98 Chang, C.A.; Francesconi, L.C.; Malley, M.F.; Kumar, K.; Gougoutas, J.Z.; Tweedle, M.F.; *Inorg. Chem.*, (1993), **32**, 3501.

99 Dickins, R.S.; *PhD Thesis*, University of Durham, (1997).

100 Lauffer, R.B.; Brady, T.J.; *Magn. Reson. Imaging*, (1985), **3**, 11.

101 Murru, M.; Parker, D.; Williams, J.A.G.; Beeby, A.; *J. Chem. Soc. Chem. Commun.*, (1993), 2259.
Aime, S.; Botta, M.; Parker, D.; Williams, J.A.G.; *J. Chem. Soc. Dalton Trans.*, (1995), 2259.
Parker, D.; Williams, J.A.G.; *J. Chem. Soc. Perkin Trans.*, (1995), 1305.

Aime, S.; Botta, M.; Parker, D.; Williams, J.A.G.; *J. Chem. Soc. Dalton Trans.*, (1996), 17.

102 Powell, D.H.; Dhubhghaill, O.M.N.; Pubanz, D.; Helm, L.; Lebedev, Y.S.; Schlaefer, W.; Merbach, A.E.; *J. Am. Chem. Soc.*, (1996), **118**, 9333.

103 Lauffer, R.B.; Brady, T.J.; Brown, R.D.; Baglin, C.; Koenig, S.H.; *Magn. Reson. Med.*, (1986), **3**, 541.

104 Muller, R.N.; Elst, L.V.; Chapelle, F.; *Abstracts from then COST D1 Meeting, Bergen*, 9-10th September 1997.

105 Aime, S.; Botta, M.; Ermondi, G.; Redeli, F.; Uggeri, F.; *Inorg. Chem.*, (1992), **31**, 1100.

Aime, S.; Botta, M.; Fasano, M.; Crich, S.G.; Terreno, E.; *J. Biol. Inorg. Chem.*, (1996), 312.

106 Aime, S.; Botta, M.; Terreno, E.; *Abstracts from then COST D1 Meeting, Bergen*, 9-10th September 1997.

107 Keonig, S.H.; *Investigative Radiology*, (1994), **29**, S128.

108 Dunham, S.U.; Tyeklár, Z.; Midelfort, K.S.; McDermid, S.A.; McMurray, T.J.; Lauffer, R.B.; *Oral Presentation at the COST D1 Meeting, The Hague*, 17th-20th October 1996.

Chapter Two

Structural and Dynamic Studies of Substituted DOTA Derivatives

2.1. Introduction

In 1984 Desreux reported the synthesis of the first substituted derivative of DOTA.[1] The alkylation of cyclen **5** with (*S*)-2-chloropropanoic acid **19** in water at pH 9 yielded a DOTA derivative substituted with a methyl group on each acetate. After purification by crystallisation (*RRRR*-) DOTMA **20** was obtained as a single enantiomer (Scheme 2.1).

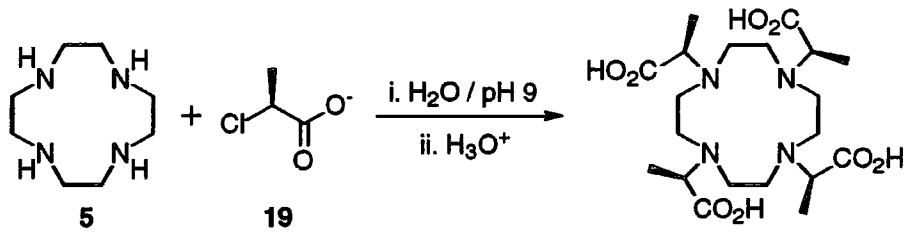

5 **19** **20**

Scheme 2.1 The synthesis of DOTMA **20**

The europium, terbium and ytterbium complexes of DOTMA were studied. These lanthanide complexes are similar in nature to the corresponding DOTA complexes. High resolution luminescence studies focusing on the $^5D_0$ -> $^7F_0$ transition in the emission spectrum of [Eu.DOTMA]$^-$ and NMR studies of [Yb.DOTMA]$^-$ showed that two species were present in solution. Luminescence measurements on crystalline [Eu.DOTMA]$^-$ however suggested the presence of only one species, although a convincing assignment was not put forward. The methods of Horrocks were used to determine the hydration states of [Eu.DOTMA]$^-$ and [Tb.DOTMA]$^-$.[2] Both complexes were found to possess one bound water molecule in solution.

Since then DOTMA has made surprisingly few appearances in the literature.[3,4] An improved synthesis was devised by Tweedle *et al.* in 1993[5] using the triflate derived from benzyl lactate, to effect complete inversion of configuration, thus avoiding the need for purification by fractional crystallisation.

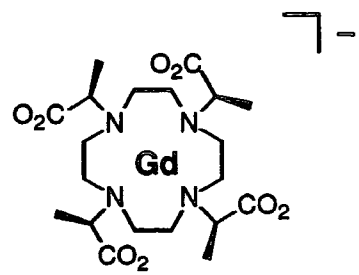

[Gd.DOTMA]$^-$

Later studies on the gadolinium complex of DOTMA[6] have shown similar relaxation behaviour to that observed for [Gd.DOTA]$^-$, (Table 2.1). The complex was described as "a more rigid chelate" than DOTA. It was suggested that this may have led to a longer electronic relaxation time and hence a small increase in relaxivity.

Complex	R_1 / $mM^{-1}s^{-1}$ (37°C)	Complex	q
[Gd.DOTA]$^-$	3.5 ± 0.1	[Tb.DOTA]$^-$	1.0 ± 0.1
[Gd.DOTMA]$^-$	3.8 ± 0.1	[Tb.DOTMA]$^-$	0.71 ± 0.1

Table 2.1. Comparison of the gadolinium and terbium complexes of DOTA and DOTMA taken from reference [6].

Although Horrocks' method was employed, in both cases, the value of q obtained for the terbium complex is significantly lower than that obtained by Desreux. Despite the potential implications of this significantly lower q value upon the relaxivity of the complex, the authors do not discuss its origins further.

The substitution of pendant acetate arms has been shown to have favourable effects upon both the stability and the relaxivity of gadolinium chelates.[7,8] This class of compound therefore represents a logical point at which to begin the investigation of linking 'DOTA like' gadolinium chelates to macromolecules.

2.2. The Synthesis of Substituted DOTA Derivatives

A racemic synthesis of a substituted DOTA derivative leads to a mixture of diastereoisomeric complexes. These diastereoisomers could potentially exhibit very different properties. For this reason a stereoselective synthesis of these isomers was required.

Synthesis of Tetra(carboxymethyl) DOTA Derivatives

The triflate of diethyl malate **21** has been reported[9] to react with secondary amines *via* a purely S_N2 mechanism. It was anticipated that this triflate could be reacted with cyclen with complete inversion of configuration to give an enantiopure compound. Acid catalysed esterification of malic acid **22** gave quantitative conversion to the diethyl ester **23**. The corresponding triflate

21 was synthesised according to the procedure set out by Effenberger (Scheme 2.2).[10] The triflate **21** was separated from the by-products by filtration of a solution in hexane. Although the triflate was handled and used under argon it proved to be remarkably stable to moisture.

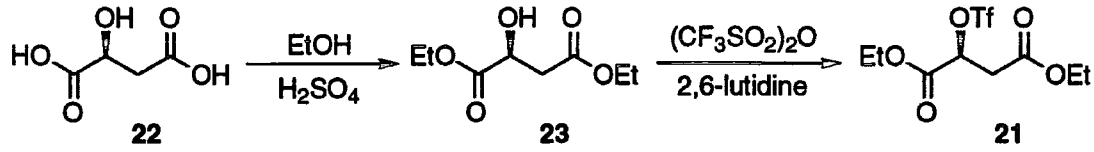

Scheme 2.2 The synthesis of the triflate of diethyl malate

The nucleophilic substitution of cyclen with the triflate **21** was then undertaken in acetonitrile. Triethylamine was employed as the base and the reaction followed by electrospray mass spectrometry. After one week at room temperature no evidence for the tetraalkylation of cyclen was found. When the reaction was heated in an attempt to drive the reaction to completion, competing elimination was found to be a problem and substantial quantities of diethyl fumarate were recovered from the reaction mixture.

When caesium carbonate was employed as the base, the rate of reaction was found to increase substantially. After several days the desired tetraalkylated product **24** was observed in the mass spectrum, (Scheme 2.3).

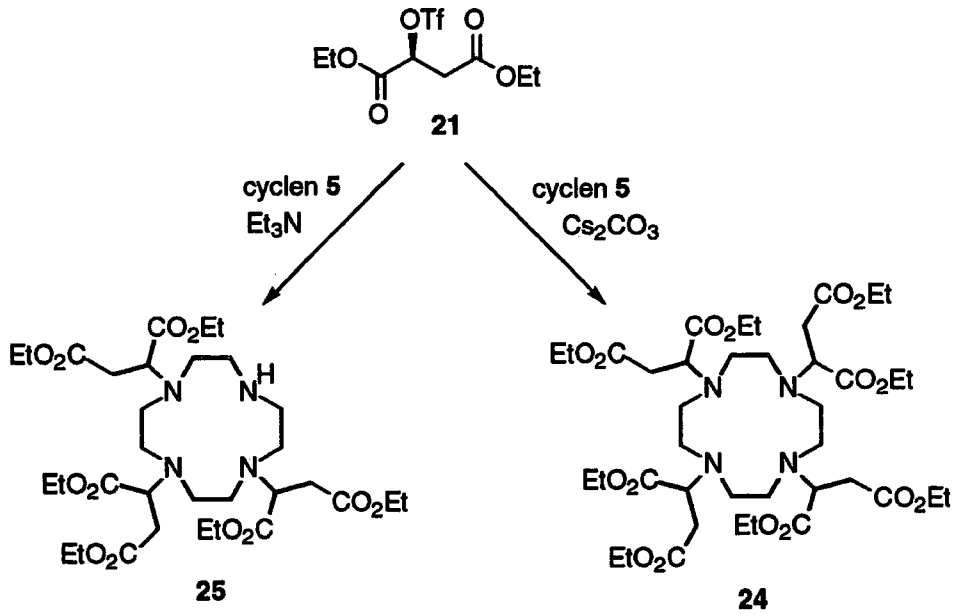

Scheme 2.3 The reaction of cyclen **5** with the triflate **21**.

Each nitrogen in the macrocycle cyclen exhibits a very different pK_a. Although the exact values depend upon the *N*-substituent they are typically around 3, 5, 10 and 13.[11] The reactivity of the four nitrogens is consequently

very different and may be modulated by the choice of base. Caesium carbonate is a relatively powerful base in aprotic solvents and may facilitate the activation of the fourth nitrogen. The pK_a of triethylamine is only 11 and so as the reaction proceeds cyclen rather than triethylamine acts as the base. The resulting monoprotonated cyclen is not a good nucleophile. Reaction with the triflate does not occur until a suitably strong inorganic base is employed.

The trialkylated cyclen derivative **25** was isolated, but ^{13}C analysis revealed the presence of a mixture of diastereoisomers. The integrity of the triflate **21** was re-examined and a strong rotation of plane polarised light observed (-53.3° c, 3 in dichloromethane). Since the triflate **21** is certainly not racemic, it may be inferred that the reaction does not proceed *via* a purely S_N2 mechanism. The observation of competitive elimination and the slow rate of reaction tend to support this conclusion. An alternative synthesis had to be sought.

Synthesis of Tetra(carboxyethyl) DOTA Derivatives

An analogous substituted DOTA derivative **26** was synthesised in France by Guerbet, based around a glutaric acid motif rather than butyric acid motif discussed previously. Alkylation of cyclen with racemic dimethyl α-bromoglutarate **27** (Scheme 2.4) leads to formation of a mixture of isomers.

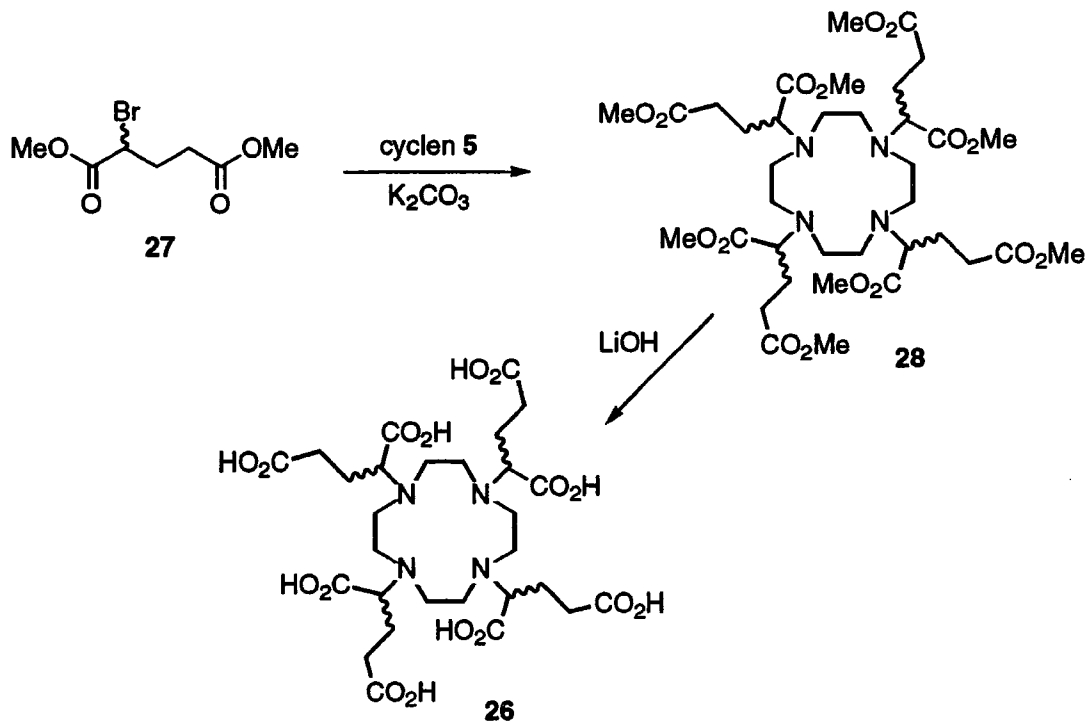

Scheme 2.4 The synthesis of tetra(carboxyethyl) DOTA **26**.

This synthesis had two significant advantages, firstly the reaction is much faster reaching completion overnight, and secondly there is little or no evidence of elimination.

To simplify the procedure, stereoselective routes were also investigated. Attempts at Guerbet s.a. to synthesise an enantiopure bromoglutarate **27** proved unsuccessful. The corresponding triflate **29** was also synthesised but was found to undergo rapid intramolecular cyclisation to yield a five membered lactone **30** (Scheme 2.5).

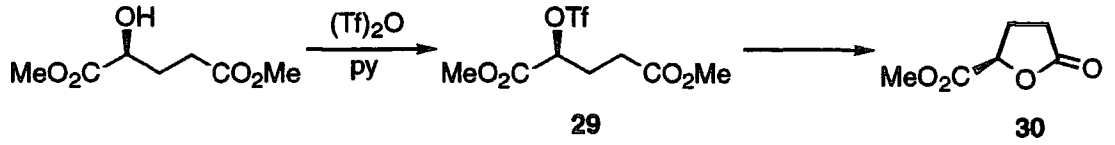

29 **30**

Scheme 2.5 The lactonisation of a 2-substituted dimethyl glutarate

To avoid this problem the synthesis of analogous triflates, **31 - 33** employing different protecting groups for the carboxylates was undertaken by the author. The appropriate alcohol was condensed with triflic anhydride in dichloromethane with a base according to Scheme 2.2.

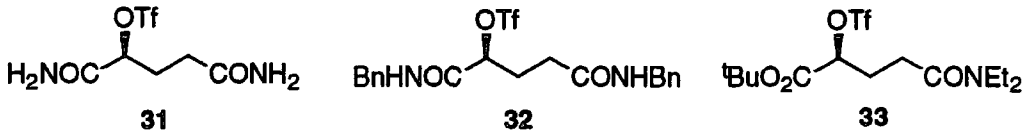

31 **32** **33**

In each case the triflate was not isolated. In the case of **31** the insolublilty of the alcohol in any suitable reaction solvent prevented the synthesis of the triflate. A benzoyl amide was employed to increase the solubility of the alcohol. However, neither **31** and **32** could be converted to the triflate, and only starting materials could be recovered from these reactions. The alternative compound that was considered, **33**, was generated under the reaction conditions, with the proton at the chiral centre exhibiting a shift from 4.3 to 5.3 ppm. The desired triflate could not be isolated from the reaction mixture, however, because of its sensitivity to silica and solubility properties being similar to that of the salts generated in the reaction.

Owing to the difficulties experienced in synthesising a suitable chiral substituent, an enantioselective synthesis of tetra(carboxyethyl) DOTA **26** was not achieved and the compound was only obtained as a mixture of diastereoisomers. It remained important to separate the individual isomers if the properties of each were to be determined. Two approaches to this isolation were undertaken; interconversion of the complex isomers and resolution of the diastereoisomeric mixture of the free acids.

Epimerisation of Europium(III) Complexes

Previous work done in the group has shown that the acetate protons in the lanthanide(III) complexes of DOTA were sufficiently acidic that they could undergo hydrogen-deuterium exchange at pD 11 without compromising complex stability.[12] Hydrogen-deuterium exchange experiments performed on [Eu.DOTA]$^-$ showed 92% incorporation of deuterium in 24 hours, pD 11, 100°C, (Figure 2.1). It can be reasoned then that the methine hydrogen in analogous substituted complexes may also exhibit high acidity. It was anticipated that the substitution of acetate arms would give rise to substantial increase in steric demand.[1] Thus enolisation at this centre may be expected to lead to epimerisation of the complex to whichever diastereoisomer minimised these steric interactions. Intuitively, this was expected to be the (*RRRR-/SSSS-*)-isomer.

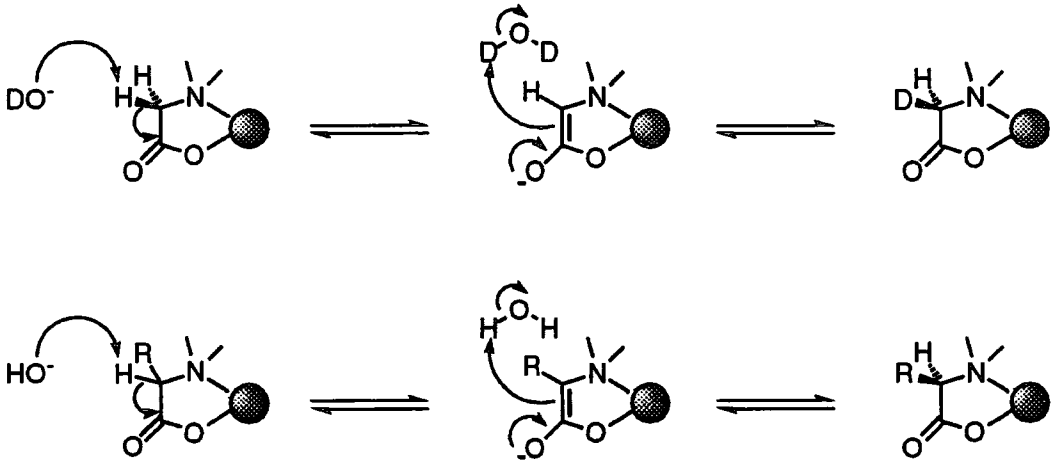

Figure 2.1 An enolisation mechanism facilitating both H/D exchange and the epimerisation of stereoisomers

A mixture of isomers of [Eu.**26**] in sodium hydroxide solution was heated at pH 11 and 110°C. The progress of the epimerisation was followed by ^{1}H NMR. After one week no changes were observed in the spectrum. Accordingly the pH was raised to 12.5 and heating continued. After a further week, the proton spectrum showed significant simplification (Figure 2.2b). Within four weeks one isomer predominated in the proton NMR spectrum (Figure 2.2c), although there did seem to be an associated increase in signal intensity in the region 1 - 5 ppm. It is clear that after a month only one complex was present in solution, and from the form of the ^{1}H NMR spectrum, this complex appeared to be axially symmetric, and therefore was assigned to the

(RRRR-/SSSS-) isomer. The intimate mechanism by which this process occurs has not been established.

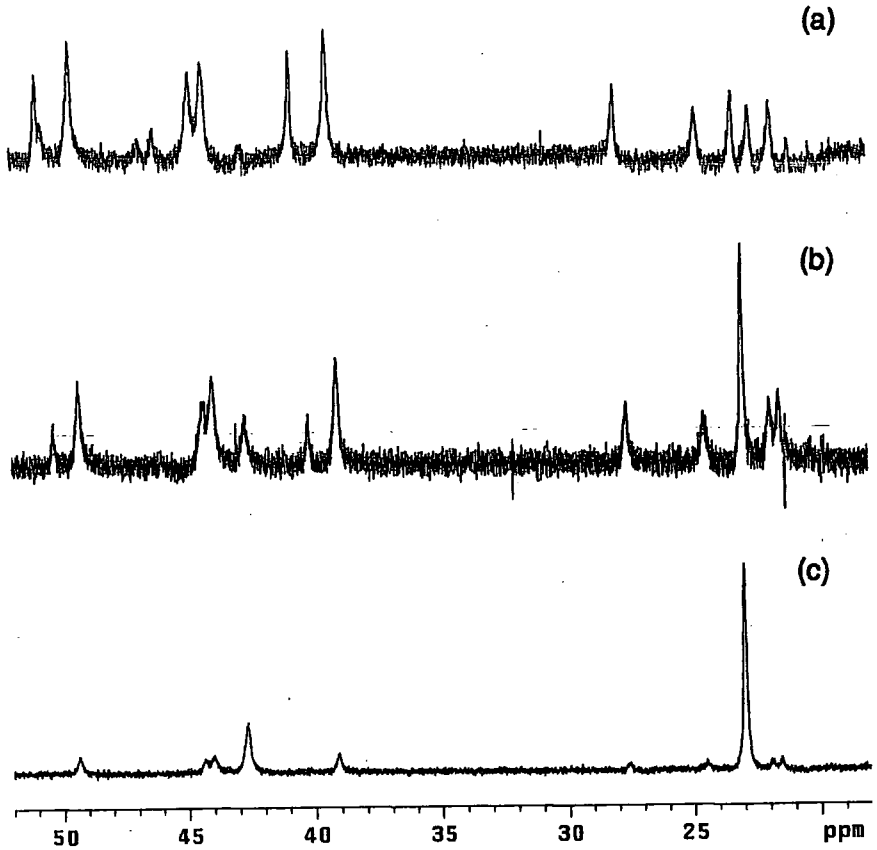

Figure 2.2 ^{1}H NMR spectra focusing on the axial proton region of europium(III) tetra(ethylcarboxy) DOTA when heated at 100°C, pH 12.5 (a) t = 0, (b) 1 week, (c) 1 month.

The diastereoisomers may interconvert as expected or alternatively, the complexes may undergo hydrolysis at high pH. Lanthanide hydroxides are insoluble at pH's higher than 6, so this process would be irreversible. If this were the case then the isomer remaining in solution is merely the one which is least susceptible to hydrolysis. The question was posed as to whether or not the corresponding gadolinium(III) complexes will behave in the same manner. To establish which mechanism was being observed, a hydrogen - deuterium exchange experiment was performed on the corresponding gadolinium(III) complexes.

Deuterium Exchange in Gadolinium(III) Complexes

Since the paramagnetic line broadening of gadolinium precludes the use of NMR in following this process, a different approach had to be employed. The incorporation of deuterium into a complex could easily be followed by electrospray mass spectrometry. A sample of [Gd.26] was heated in sodium

deuteroxide solution, pD 12.5. Aliquots were removed at regular intervals and electrospray mass spectrometry used to analyse the extent of deuterium incorporation. After 4 weeks no deuterium incorporation could be observed. Clearly, no enolisation had occured at pH 12.5 and the observed simplification of the europium ^{1}H NMR spectrum must have been due to hydrolytic decomplexation. The rate of this decomplexation must be faster for the isomers of lower symmetry.

Acid Catalysed Epimerisation

Enolisation may occur not only at high pH but also at very low pH. To establish whether or not this mechanism could be used to effect the epimerisation of the ligand **26**, a sample was heated at pD 1 in D_2O under argon. The extent of deuterium incorporation could be followed by ^{1}H NMR and electrospray mass spectrometry. If deuterium were incorporated into **26** under these conditions then enolisation must occur and the acid catalysed epimerisation of the corresponding complexes may be possible. The ^{1}H NMR spectrum revealed a significant decrease in the intensity of the methine proton resonances (3.8 - 4.3 ppm) within one week (Figure 2.3). This was ascribed to the incorporation of deuterium into the ligand.

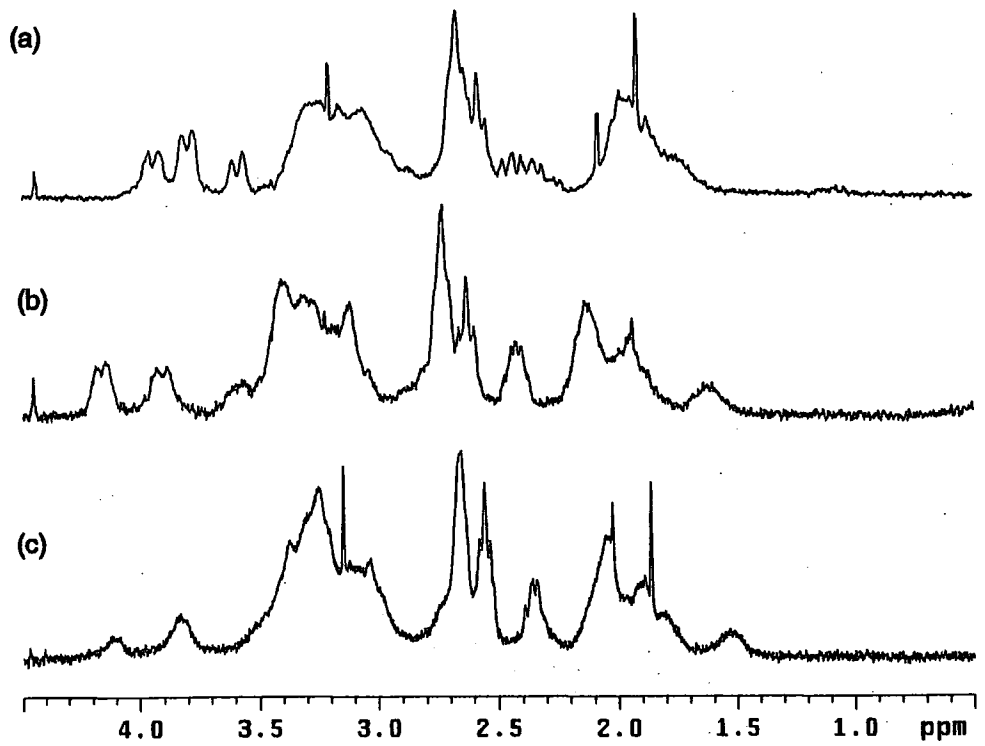

Figure 2.3 The ^{1}H NMR spectra of a sample of **26** when heated in D_2O at pD 1, (a) t = 0, (b) t = 18 hours and (c) t = 1 week, shows significant incorporation of deuterium at the methine carbon (3.8 - 4.3 ppm).

The incorporation of deuterium into **26** was then confirmed by electrospray mass spectrometry. The acid catalysed enolisation did not simplfy the form of the ^{1}H NMR spectrum of the ligand. A kinetically controlled statistical distribution of the four stereoisomers was expected and the complex NMR spectrum observed is consistent with prediction. Clearly the epimerisation of **26** to a single isomer will only occur in its complexes, where steric demands are expected to favour the (*RRRR*-)/(*SSSS*-) isomer. However, the lanthanide complexes of tetraacetate substituted cyclen derivatives are known to dissociate at pH as low as 1.[13]

The lanthanide(III) ions are strong Lewis acids and may in themselves represent a solution to the problem of competitive dissociation. The fortuitous discovery that during the synthesis of lanthanide(III) complexes of **26** the nature of the counter ion affected the stereoisomeric nature of the resulting complex suggested a solution to this problem. When the complexes were synthesised from mixtures of stereoisomeric ligands using the corresponding lanthanide(III) oxide, a preference for formation of the C_4 symmetric (*RRRR*-)/(*SSSS*-) isomer was observed. A control experiment was performed in which the oxide of europium(III) was heated with a sample of the (*RRRS*-)/(*SSSR*-) isomer of the ligand **26** (the pH (3) was not adjusted) Very rapidly the ^{1}H NMR spectrum revealed the presence of the [Eu.(*RRRR*-)], and after one week this was the only species observed in solution (Figure 2.4). In contrast to the base catalysed reaction no free ligand could be observed in the region 0 - 5 ppm.

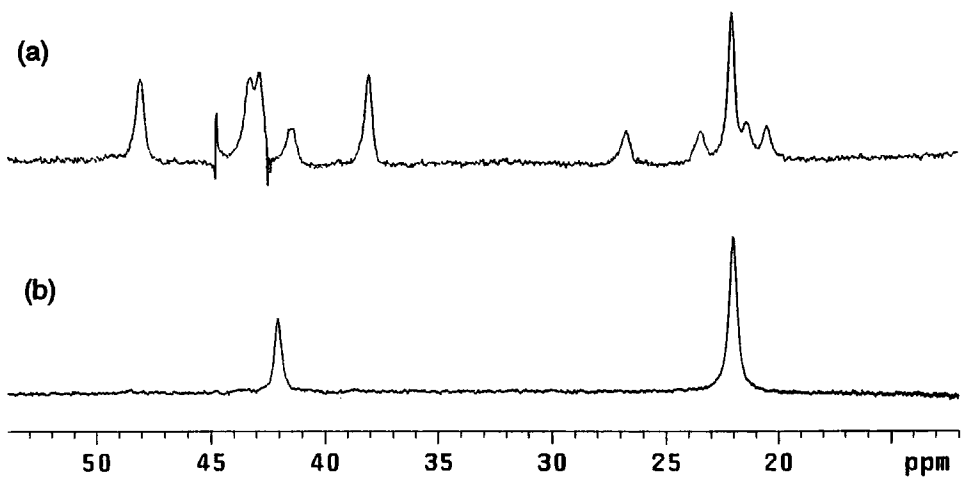

Figure 2.4 The epimerisation of **26** is mediated by europium(III) oxide. A sample of (*RRRS*-) **26** shows signs of epimerisation after just 18 hours (a) and the epimerisation is complete after 1 week (b).

The mixture of stereoisomeric lanthanide(III) complexes of **26** may be epimerised to the (*RRRR*-)/(*SSSS*-) isomer because the Lewis acidity of the

lanthanide(III) ion itself catalyses enolisation. The following mechanism is proposed to account for this observation.

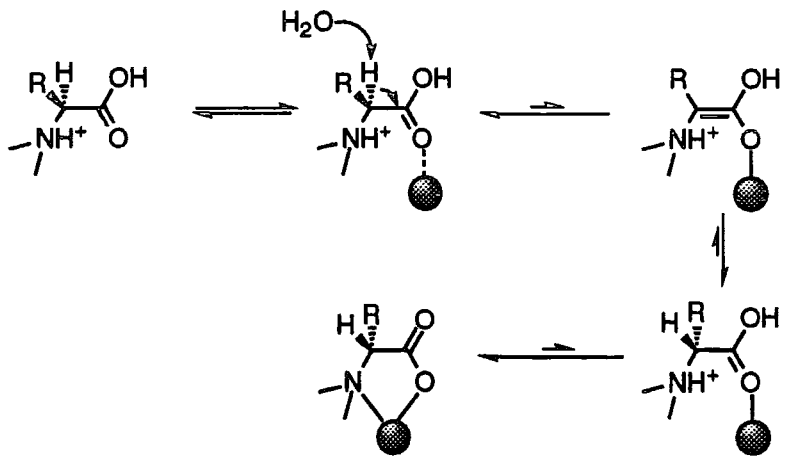

Figure 2.5 The epimerisation of **26** mediated by lanthanide(III) ions.

The Lewis acid catalysed enolisation occurs slowly with the uncomplexed ligand. However, the low pH of the reaction maintains a small population of the complexed ligand in solution, with the complex being slowly hydrolysed and then reforming. Since the (*RRRR*-)/(*SSSS*-) isomer of the complex is the most stable it dissociates more slowly than the others, and eventually predominates in solution. This enolisation and epimerisation mechanism has only been observed to a significant extent when the oxide of the lanthanide is employed. This may be simply because complexation with other lanthanide(III) salts results in the pH being raised to 5.5, preventing dissociation of the complex once formed. The epimerisation of a mixture of stereoisomers of **26** has been observed with neodymium(III), europium(III) and ytterbium(III) oxides.

Resolution of Diastereoisomers

The mixture of isomers obtained from the racemic synthesis of tetra(carboxyethyl) DOTA **26** was eventually resolved into the individual isomers by fractional crystallisation from water in work undertaken at Guerbet. In principle six stereoisomers may be expected from an unselective synthesis, *RRRR*-, (*SSSS*-), *RRRS*-, (*SSSR*-), *RRSS*- and *RSRS*-. Since two of these are enantiomeric pairs, four isomers were isolated (Figure 2.6).[14] The purity of each sample was established by reverse phase HPLC.

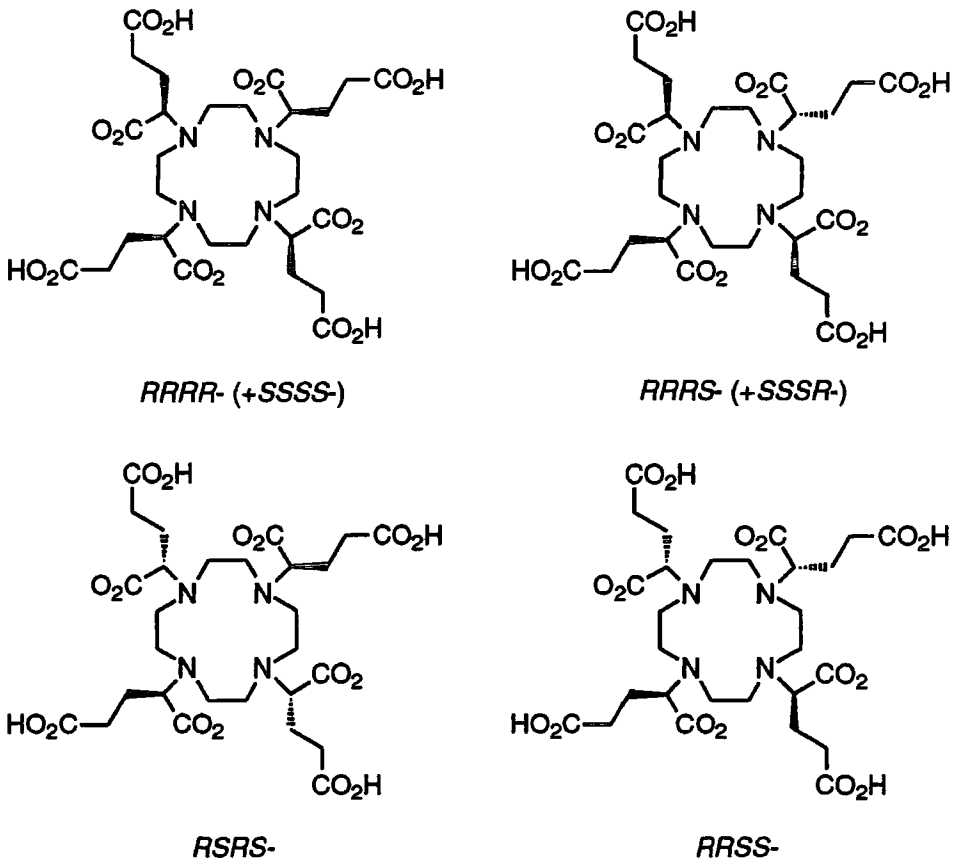

Figure 2.6 The four diastereoisomers of tetra(carboxyethyl) DOTA, **26**.

In an unselective synthesis of tetra(carboxyethyl) DOTA **26** a statistical distribution of the isomers would be expected. This distribution is summarised in Table 2.2 along with the symmetry of each isomer.

Isomer	Symmetry	Nature	Distribution
(*RRRR*-)	C_4	diastereoisomer	12.5%
(*RRRS*-)	none	diastereoisomer	50%
(*RRSS*-)	σ	*meso*-compound	25%
(*RSRS*-)	C_2	*meso*-compound	12.5%

Table 2.2 The distribution and symmetry functions of the four isomers of **26**.

It is worthy of note that although two of the free ligands consititute *meso*-compounds, once complexed each of the four isomeric structures becomes diastereomeric. However, the symmetry of each isomer remains the same.

The configuration of each isomer was determined by X-ray diffraction studies performed on crystals of three of the ligands, (*RRRS*-), (*RRSS*-) and

(*RSRS*-), grown from acidified aqueous solution. The structures are shown below (Figures 2.7-2.9).

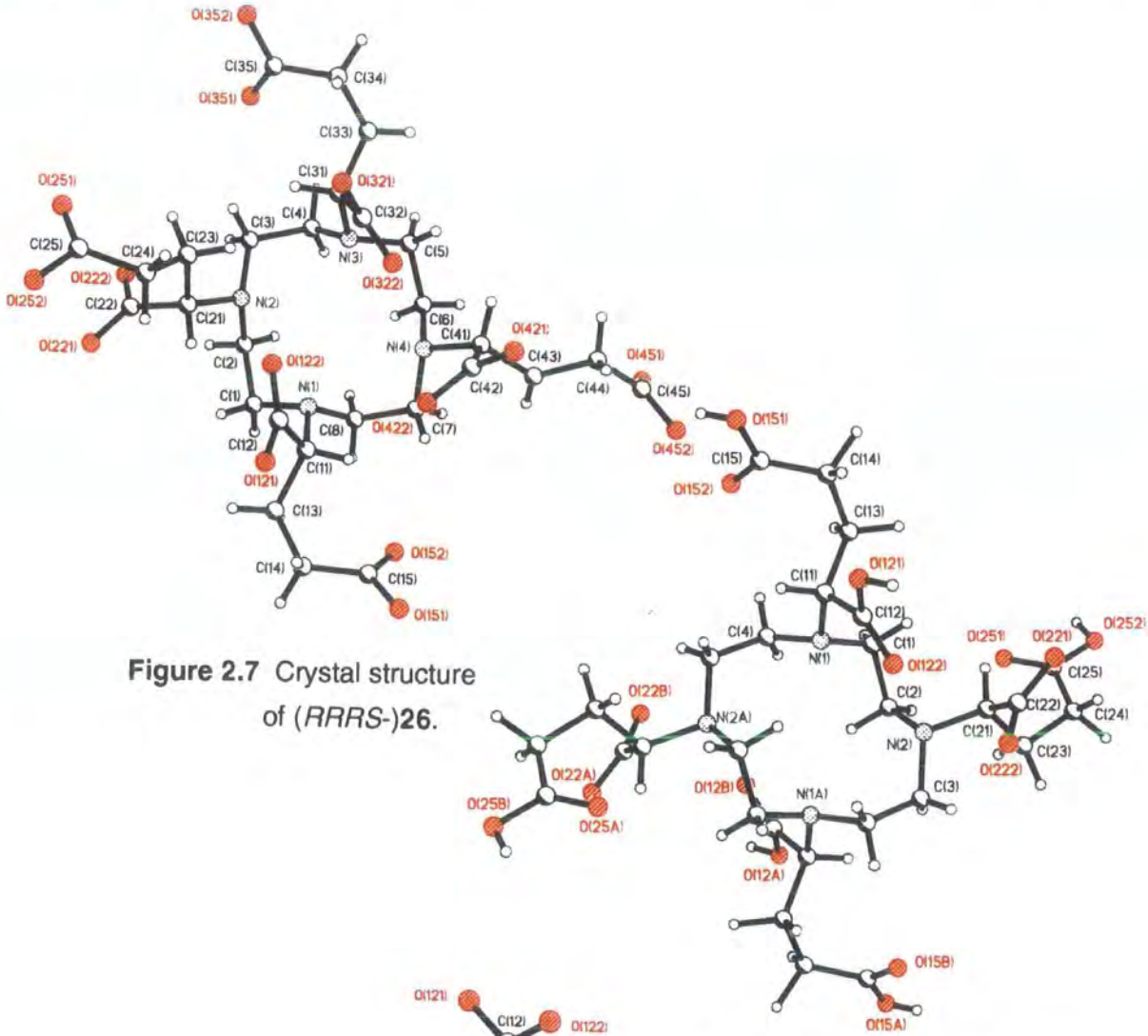

Figure 2.7 Crystal structure of (*RRRS*-)**26**.

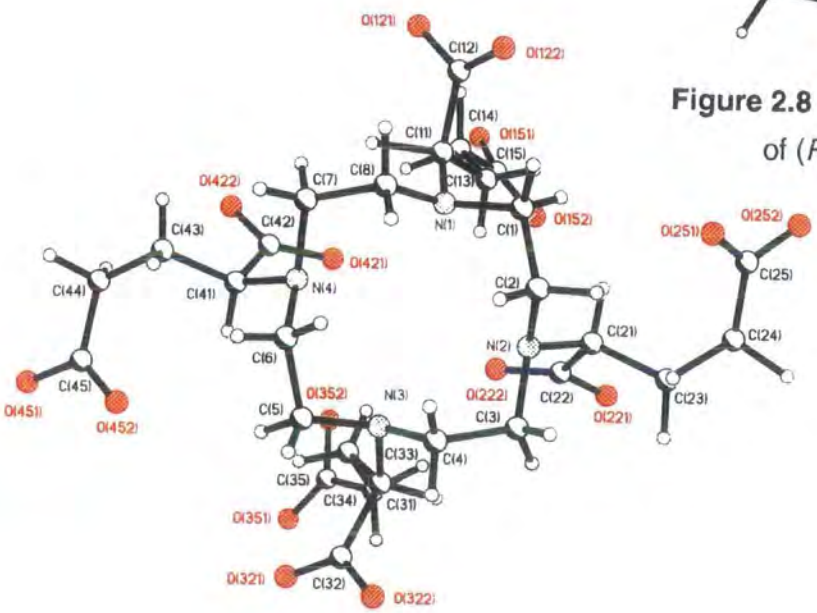

Figure 2.8 Crystal structure of (*RRSS*-)**26**.

Figure 2.9 Crystal structure of (*RSRS*-) **26**.

In both the (*RRRS*-) and (*RSRS*-) isomers the cyclen ring adopts the same [3333] conformation[15] as it does in all published structures of its complexes. The structure of the (*RRSS*-) isomer is very different. The ligand lies on an inversion centre, and this results in the distortion of the [3333] ring conformation. In this ligand the α-carboxylates are positioned two above and two below the plane of the macrocycle. Since the ligand lies on an inversion centre the arrangement is *trans*. All the arms are positioned such that they may be considered predisposed to binding. In contrast, the α-carboxylates of the (*RSRS*-) ligand are in a *cis*- arrangement above and below the ring. The positions of the α-carboxylates in each of the three ligands relative to nitrogen are consistent with a predisposed ligand.

Synthesis of the Lanthanide(III) Complexes

Having obtained samples of each diastereoisomer of **26**, a selection of the corresponding lanthanide(III) complexes was synthesised. Europium, gadolinium, terbium and erbium complexes were synthesised from the corresponding nitrate and holmium complexes from the chloride, in aqueous solution by heating for 18 hours at 90°C and pH 5.5. The neodymium and ytterbium complexes were synthesised from a suspension of stoichiometric quantities of the ligand and the metal oxide in water. Whilst this complexation requires heating for 3 days at 90°C, it avoids the production of salts as side products.

2.3. Structural and Dynamic Studies of Substituted Europium(III) Complexes

Europium(III) Complexes in Solution

The proton NMR spectra of the europium complex of each of the four isomers of **26** are pictured (Figure 2.10). The spectra highlight the symmetry of each complex. With the exception of the (*RRSS*-) isomer, two distinct species are observed in the NMR spectrum of each complex. This is best observed by examination of the shifted axial proton resonances between 20 and 50 ppm. Such features have also been observed with [Ln.DOTA]$^-$, (Chapter 1.3), and the two species assigned to two different co-ordination geometries of the complex - the square antiprism and the twisted square antiprism.[16] In contrast, only one species is apparent in the spectrum of the (*RRSS*-) isomer.

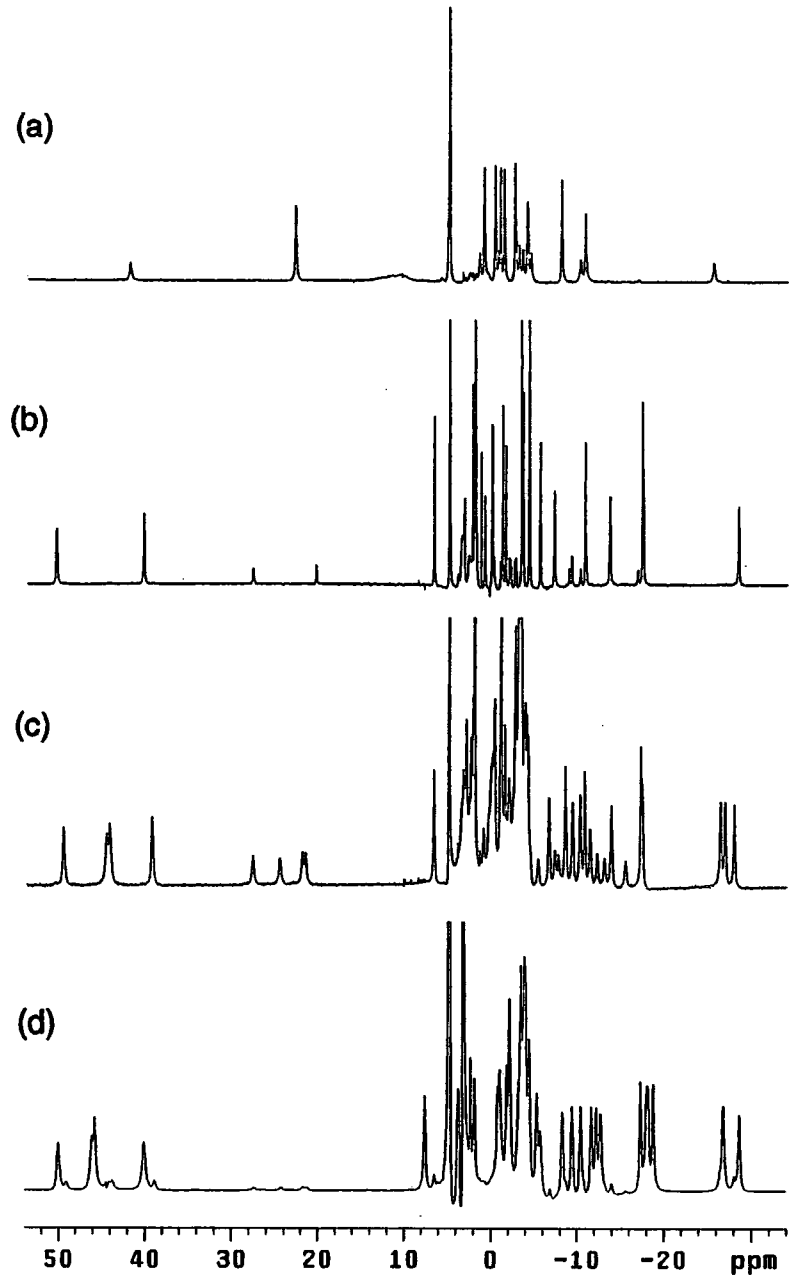

Figure 2.10 The ^{1}H NMR spectra of each diastereoisomer of (a) [Eu.(*RRRR*-)] (b) [Eu.(*RSRS*-)] (c) [Eu.(*RRRS*-)] (d) [Eu.(*RRSS*-)] (contaminated with a small amount of the [Eu.(*RRRS*-)] complex).

In [LnDOTA]$^-$ complexes the two co-ordination geometries are related as two enantiomeric pairs. The introduction of a stereogenic centre in the *N*-substituent alters this relationship. The result is determined by the configuration sequence of the chiral centres on the *N*-substituents. When the configuration of each chiral centre is the same, then the four isomeric structures of DOTA, Λ(δδδδ), Δ(λλλλ), Δ(δδδδ) and Λ(λλλλ), are rendered diastereomeric. Consequently, the ^{1}H NMR spectrum of the complex with (*RRRR*-)

configuration would be expected to reveal four chemically distinct species. 2-Dimensional ^1H-^1H correlation spectroscopy (COSY) experiments were performed on the [Eu.(*RRRR*-)] and [Eu.(*RSRS*-)] europium(III) complexes. The spectra obtained were assigned on the basis of comparison with the related spectra obtained for the complexes of DOTA.[7] The COSY spectrum of the [Eu.(*RRRR*-)] isomer confirms that there are only two diasteriomeric species present in solution. Clearly two of the four possible diastereoisomers are not present in solution at room temperature, to a significant extent (<5%).

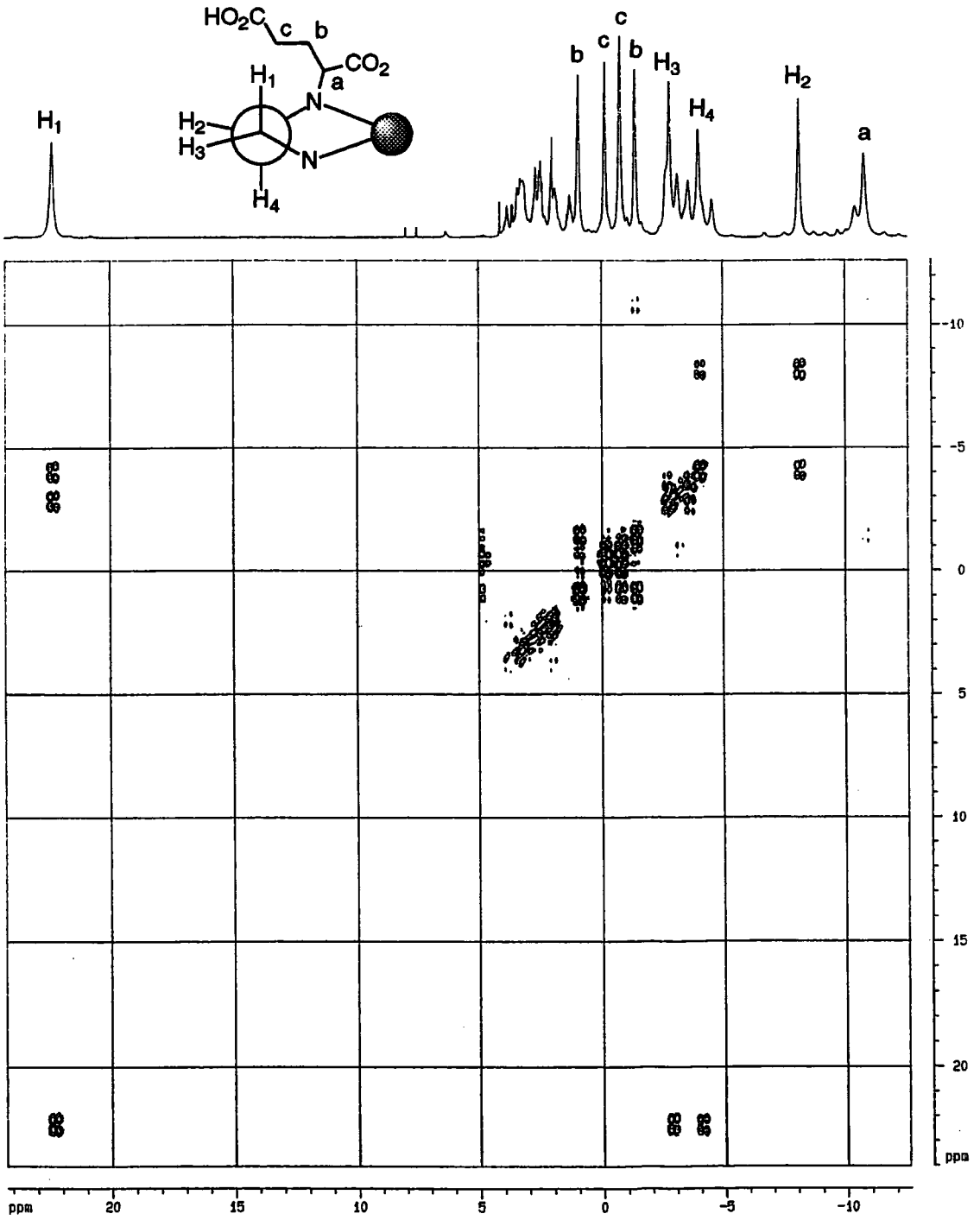

Figure 2.11 ^1H COSY spectrum of [Eu.(*RRRR*-)].

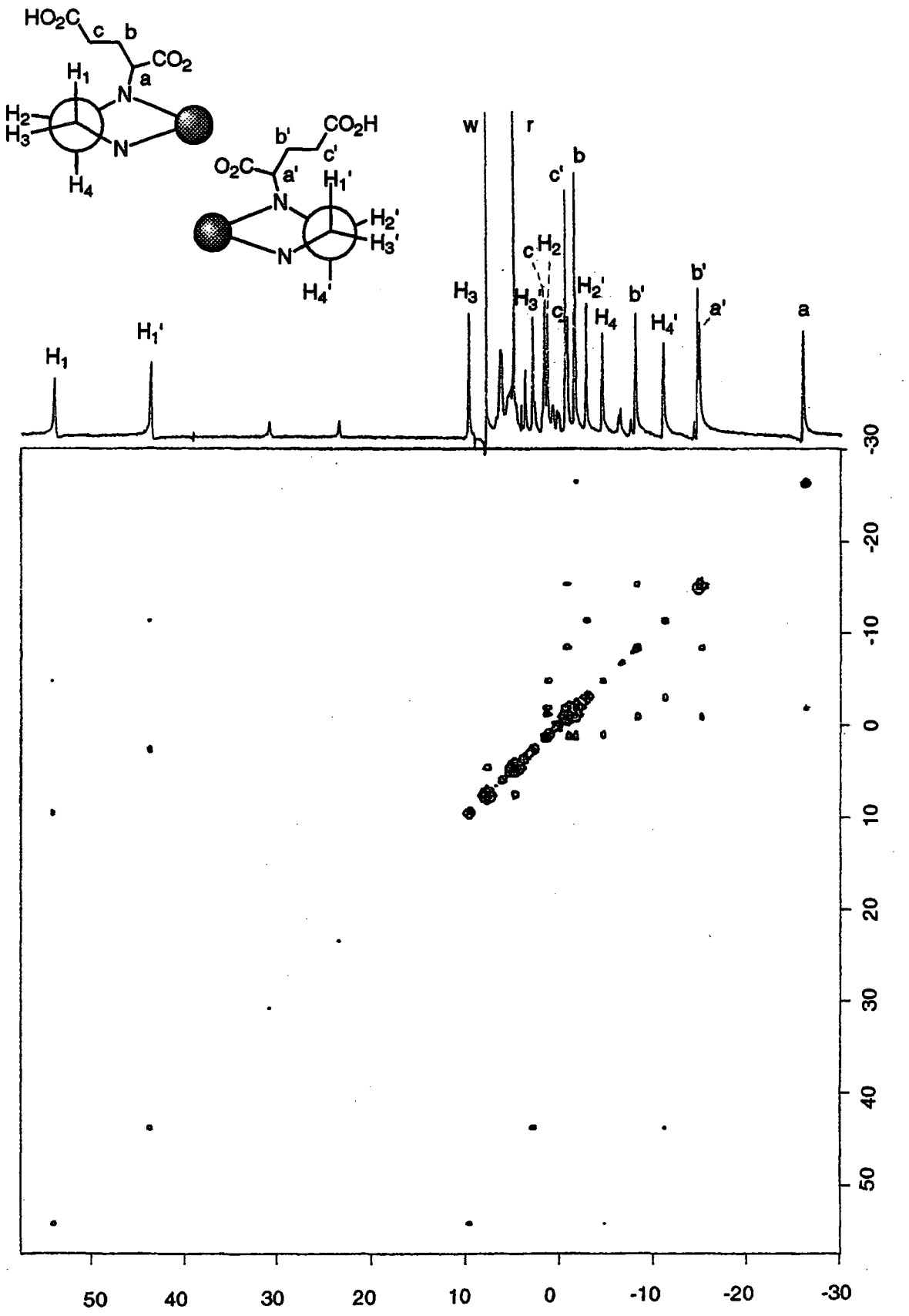

Figure 2.12 ^{1}H COSY spectrum of europium(III) (*RSRS*-) tetra(ethylcarboxy) DOTA

In the case of the [Eu.(*RSRS*-)] isomer, introduction of the chiral centres does not affect the enantiomeric relationship observed in DOTA. The mirror image of one co-ordination isomer may still be superimposed upon the same co-ordination isomer with opposing helicity. Thus two species should be observed in the NMR spectrum. The assignment of the NMR of the major species was undertaken from the ^{1}H-^{1}H COSY spectrum (Figure 2.12).

Satisfactory ^{1}H COSY spectra of the [Eu.(*RRRS*-)] and [Eu.(*RRSS*-)] isomers were not obtained. Inspection of the ^{1}H NMR spectra of the [Eu.(*RRRS*-)] complex suggests that only two species are present in solution. Four diastereoisomeric species would also be expected in a solution of this isomer. The [Eu.(*RRSS*-)] isomer is unique in that inspection of the ^{1}H NMR spectrum shows that only one species may be observed in solution. The two co-ordination isomers for this compound would be related as enaniomeric pairs as for [Eu.(*RSRS*-)], however, it appears that only one of the two possible co-ordination geometries is adopted by this complex.

Emission Spectra of Europium Complexes

Emission spectra of each isomer were recorded by direct metal excitation at 397 nm (Figure 2.13). In the range 500 - 800 nm the ΔJ = 0,1,2,3 and 4 transitions for $^5D_0$ -> ^7F_J are expected to be observed. These bands contain a substantial amount of information on the local co-ordination environment of the europium(III) ion.

The ΔJ = 0 transition (occurring at 580 nm) can reveal information regarding the number of species present in solution.[17] Since the $^5D_0$ level cannot experience crystal field splitting, any degeneracy in this band reflects the number of europium species present in solution. However, a high resolution emission spectrum is required to observe this degeneracy. The resolution of the LS-50B on which these spectra were recorded, is at best 1 nm, hence the ΔJ = 0 transition appears unresolved.

The general form of the spectra obtained for each complex is the same, although small variations in the intensity and splitting of transitions may be observed. From the close resemblance of these spectra it is clear that the local environment around the europium(III) ion is very similar.

Comparison of these spectra with that obtained for [Eu.DOTA]$^-$, (Figure 1.5)[18], show that the local co-ordination environment of europium(III) in each isomer of **26** is also similar to that observed for DOTA. It can therefore be concluded that europium(III) forms the same sort of complexes with these substituted ligands as it does with DOTA.

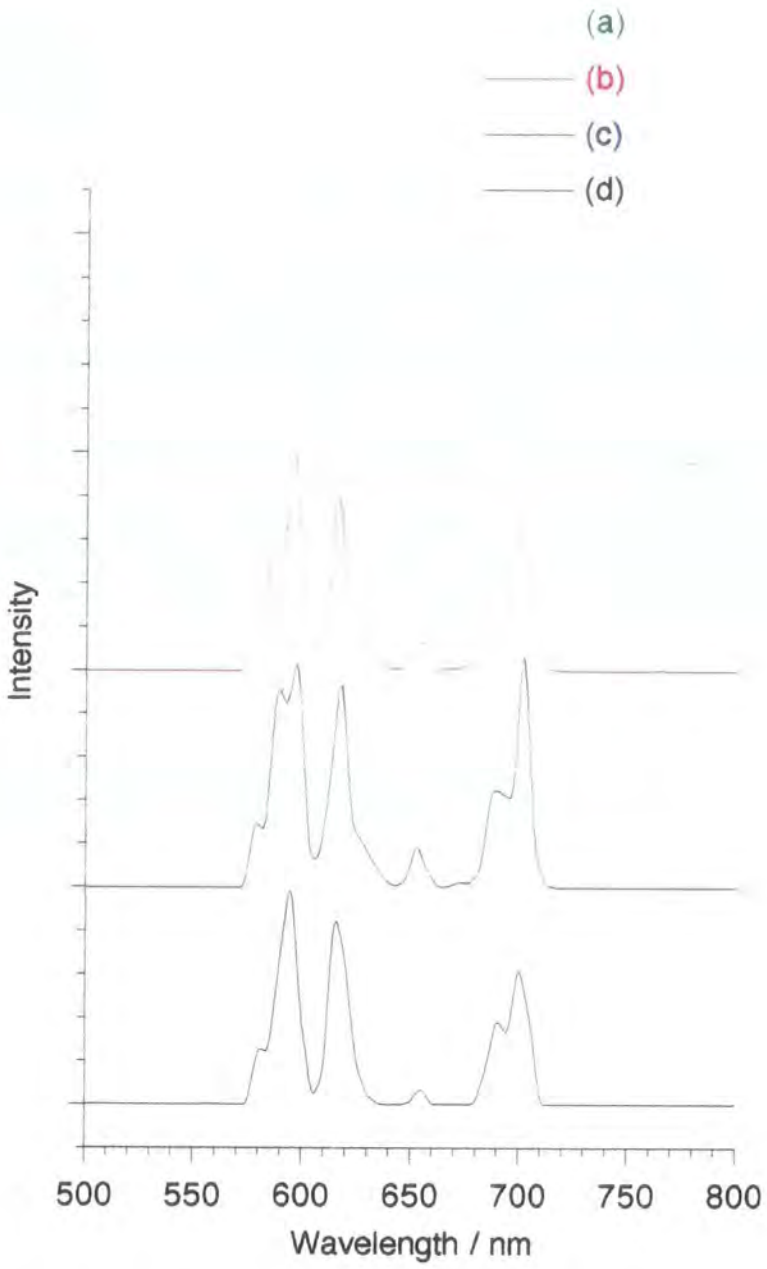

Figure 2.13 The emission spectra of a) [Eu.(*RRRR*-)] (green), b) [Eu.(*RRRS*-)] (red), c) [Eu.(*RRSS*-)] (blue), d) [Eu.(*RSRS*-)] (black).

Dynamics of the Europium(III) Complexes

The complex [Eu.DOTA]$^-$ exists as two enantiomeric pairs which are in dynamic exchange in solution and hence two species are observed by ^{1}H NMR, (Chapter 1.3). The two structures, the square antiprismatic and the twisted square antiprismatic geometries (Figure 1.10), are interchanged by a rotation of the arms or a flip in the ring conformation of the macrocycle. These motions exchange the positions of protons within the complex. Thus the axial proton of

the major isomer is exchanged with both the equatorial and axial proton of the minor isomer by ring flip or arm rotation respectively (Figure 2.14). Sequential arm rotation and ring flip allow exchange of the enantiomers of [Ln.DOTA]$^-$ complexes in solution.[19,20]

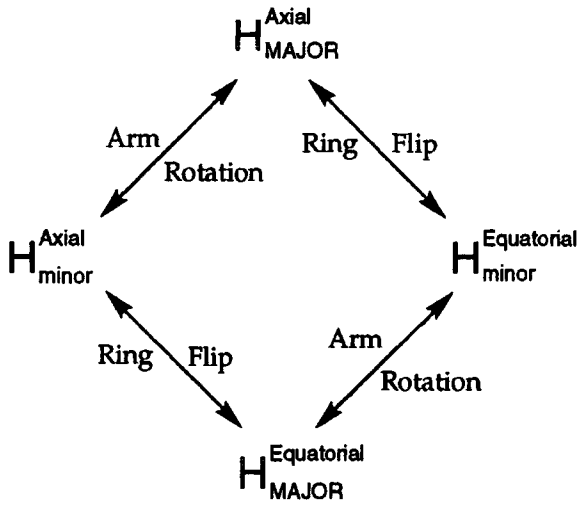

Figure 2.14 The positional exchange of a proton in the major and minor isomers of [Ln.DOTA]$^-$ complexes.

2-Dimensional exchange spectroscopy (EXSY) has been used to probe these processes in lanthanide(III) complexes of DOTA. A mixing time of 40 ms was used to record EXSY spectra of the three isomers exhibiting two species in solution [Eu.(*RRRR*-)], [Eu.(*RRRS*-)] and [Eu.(*RSRS*-)]. The first spectrum to be recorded was that of [Eu.*RSRS*-] (Figure 2.15).

The spectrum obtained is very reminiscent of that of [Eu.DOTA]$^-$.[21] Each of the resonances corresponding to a ring proton in the major isomer is correlated to two protons in the minor isomer. In particular, the axial protons at 40 and 50 ppm are seen to exchange with both axial and equatorial protons of the minor isomer. This corresponds exactly to the behaviour observed in Eu[DOTA]$^-$ and demonstrates that both ring inversion and arm rotation are occuring fairly quickly on the NMR time-scale at room temparature.

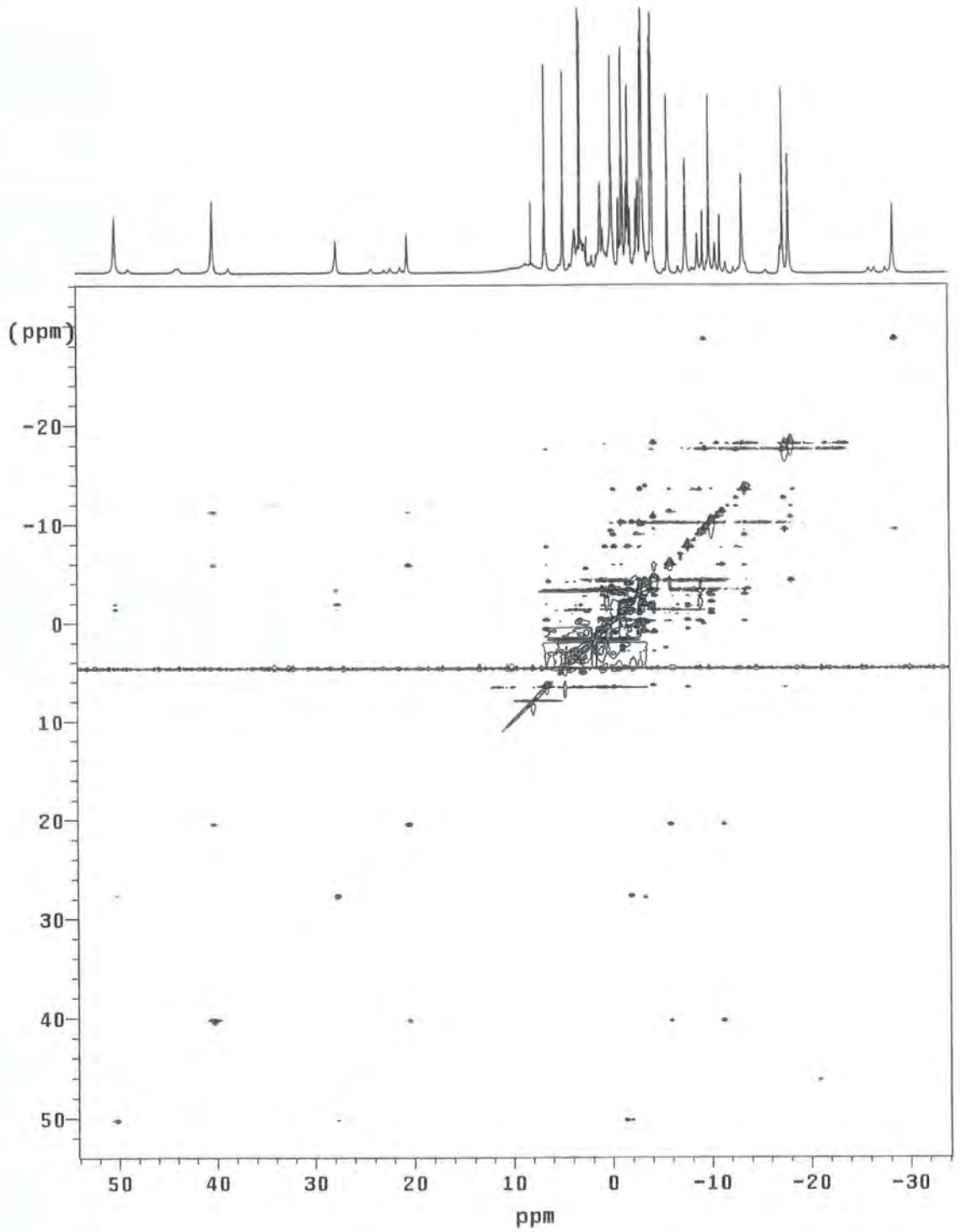

Figure 2.15 ^{1}H EXSY spectrum of [Eu.(*RSRS*-)] showing correlations relating to both arm rotation and ring inversion

The spectrum obtained for [Eu.(*RRRR*-)] was much less complex (Figure 2.16). Although the spectrum is simplified by an increase in symmetry in the complex, this is not the only cause of the increased simplicity. Each resonance of the major isomer gives rise to only one cross peak in the spectrum. In the case of the axial proton (δ 22 ppm) in the major isomer, the cross peak shows

that it exchanges with an equatorial proton in the minor isomer. Such an exchange is expected as a result of ring inversion. Exchange between the axial protons of the major and the minor isomers is not observed. It is thus evident that arm rotation does not occur at a measurable rate on the NMR time-scale at room temperature.

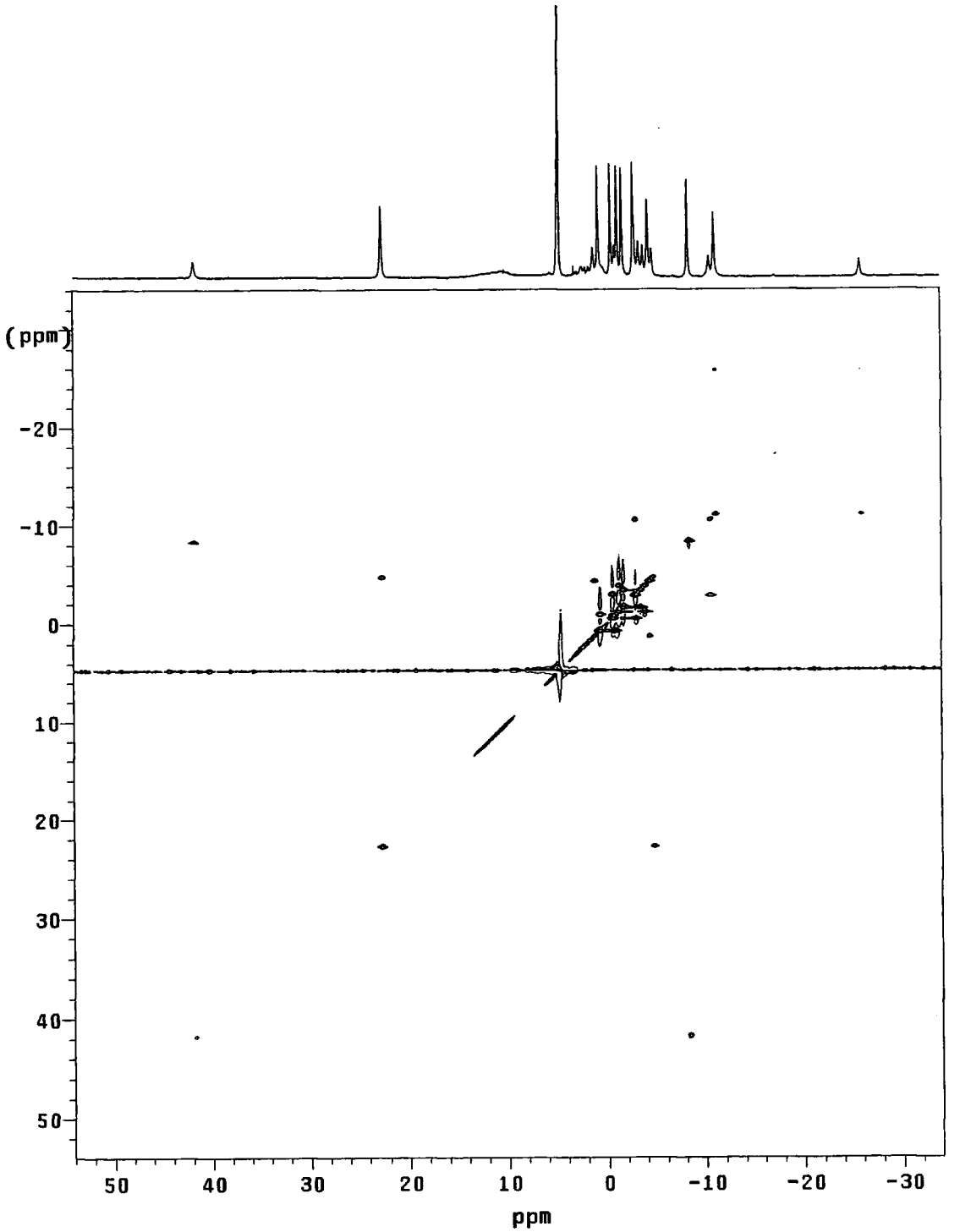

Figure 2.16 ^{1}H EXSY spectrum of [Eu.(*RRRR*-)] showing correlation relating to ring inversion but none relating to arm rotation.

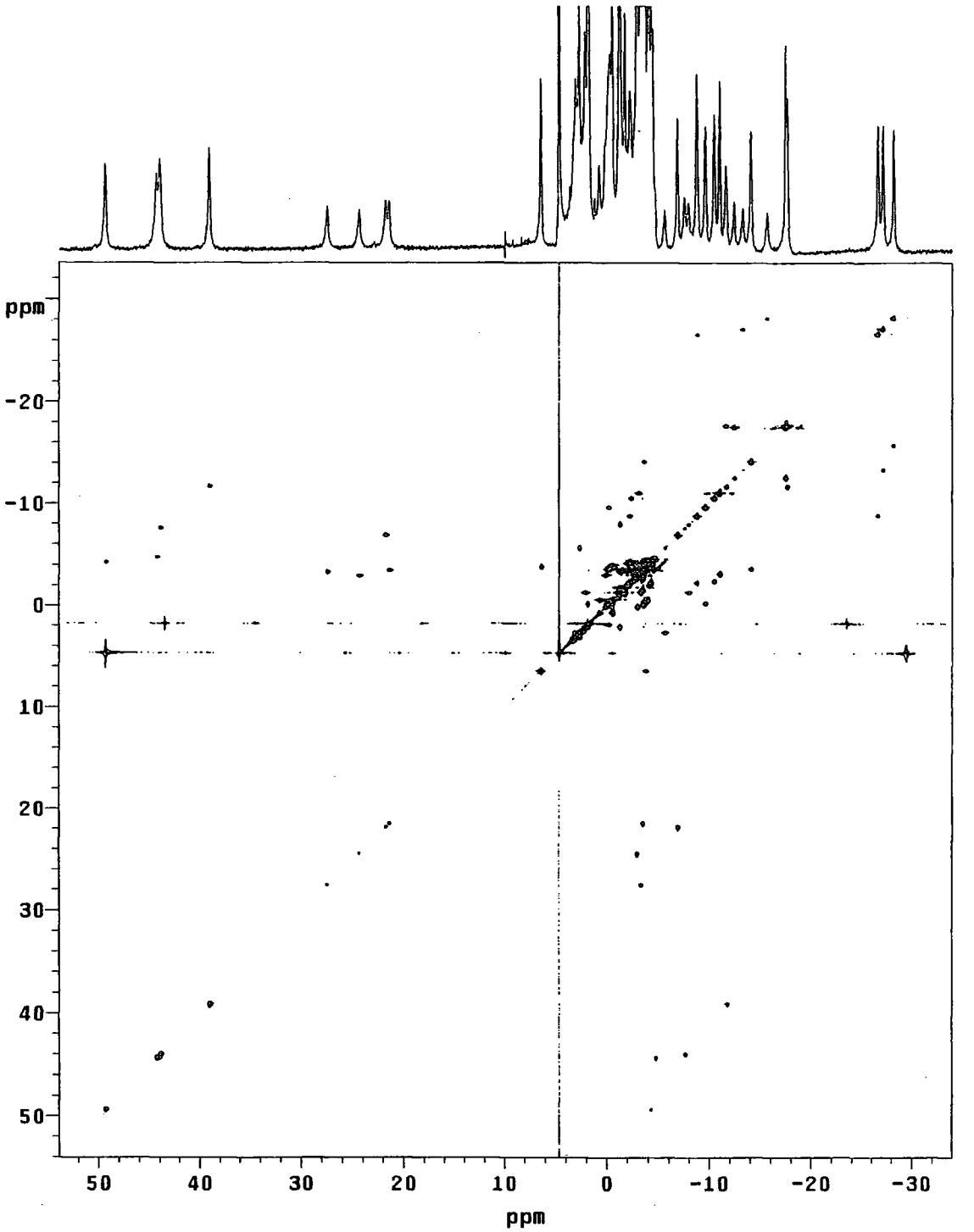

Figure 2.17 ^{1}H EXSY spectrum of [Eu.(*RRRS*-)].

The rate of ring inversion in the complex was probed using saturation transfer techniques.[22] If a resonance which is in exchange with another in the NMR spectrum of the complex is continually saturated by irradiation then the second resonance will also experience saturation. Both resonances will undergo spin-lattice relaxation. If the exchange rate is comparable to the relaxation rate, then the intensity of the second resonance will be the result of

competition between saturation from exchange and relaxation. Assuming that the longitudinal relaxation rates of each resonance are the same, then their rate of interconversion can be determined from (Eqn 2.1).

$$I_S = \frac{I_0 R_1}{(R_1 + k_{ex})} \qquad (2.1)$$

Where I_S and I_0 are the intensities with and without saturation, R_1 is the longitudinal relaxation rate and k_{ex}, the rate of saturation transfer. This latter term, k_{ex}, is the rate of chemical exchange. By monitoring the exchange of the axial proton at δ 44 ppm with the equatorial proton resonance at δ -8 ppm, the rate for the interconversion of the minor isomer with the major could be measured. A rate of 45 ± 15 s^{-1} was measured at 20°C. The reverse rate may then be estimated, within the accuracy of the experiment, by comparing the population densities. The ratio of the two isomers is 1:4, the rate for the interconversion of the major isomer to the minor isomer may then be estimated to be 11 s^{-1}.

The same observation can be made from the EXSY spectrum of [Eu.(*RRRS*-)] (Figure 2.17). The spectrum is complicated and, since a complete assignment of the 1-dimensional NMR spectrum of [Eu.(*RRRS*-)] is unavailable, a complete analysis of the intramolecular motion of this complex is has not been undertaken. However, examination of the four resonances relating to the axial proton (δ 40 - 50 ppm), reveals that the two axial positions are not in exchange. Exchange does occur between each of these resonances and equatorial ring protons in the minor isomer. Again, whilst ring inversion occurs on the NMR time-scale at room temperature, arm rotation is frozen out.

Variable temperature ^{1}H NMR experiments were performed on both the [Eu.(*RRRR*-)]and [Eu.(*RRRS*-)] isomers. Whilst the major and minor isomer resonances in both complexes move together as the temperature is increased (the large shifts are due to the temperature dependence of the paramagnetic shift), they do not coalesce below 60°C. This behaviour suggests that arm rotation can be observed at high temperatures, but this rate is likely to be more than two orders of magnitude less than that measured for the ring inversion, extrapolating back to room temperature.

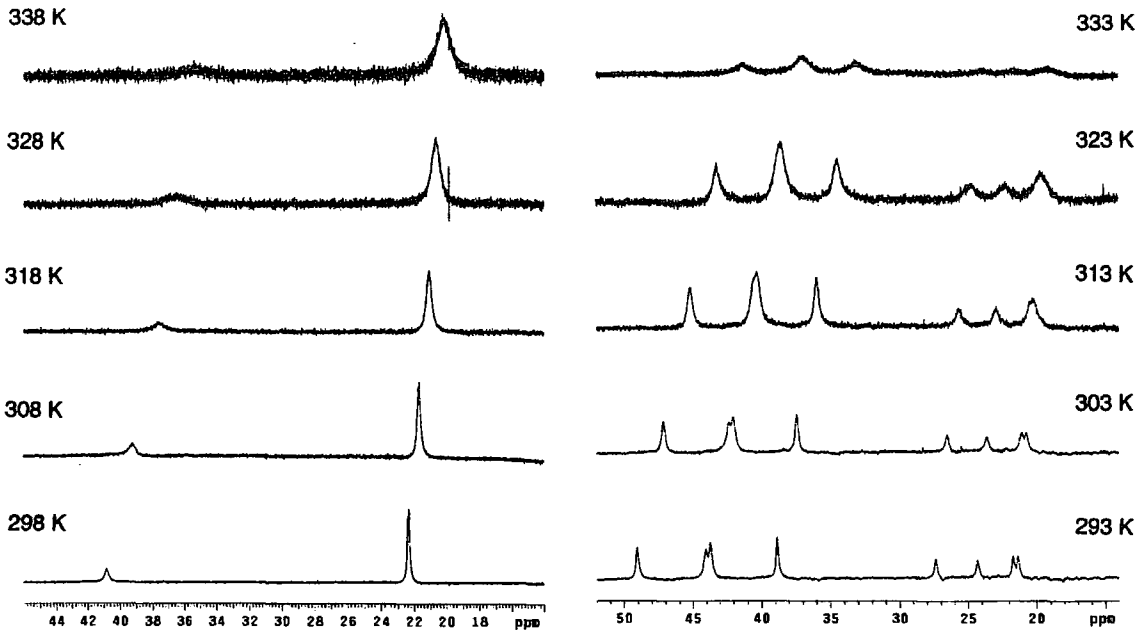

Figure 2.18 Variable temperature ^{1}H NMR spectra of the axial proton resonances in [Eu.(*RRRR*-)] (left) and [Eu.(*RRRS*-)] (right). In both cases the resonances move together.

The [Eu.(*RRSS*-)] isomer appears to exists in only one of the two possible co-ordination geometries. It is possible that either ring inversion or arm reorientation occur at room temperature, but since we cannot observe any second species in the NMR these motions may not be probed by the techniques employed previously. The reason why this complex should adopt only one co-ordination isomer is ambiguous. However, it may be assumed that the steric demands of juxtaposing chiral centres in this complex are greater than those of the other isomers. This forces the complex into adopting the co-ordination geometry which minimises the steric interactions of the substituents.

The Conformation of Europium(III) Complexes

In addition to the configuration of the chiral centres on each *N*-substituent, these complexes possess two further elements of chirality: the orientation of the pendant arms (Δ or Λ) and the conformation of the macrocyclic ring (δδδδ or λλλλ), (Chapter 1.3). Arm rotation and ring inversion occur rapidly on the NMR timescale in the lanthanide complexes of DOTA. These motions exchange these two elements of chirality (Δ <-> Λ and (δδδδ) <-> (λλλλ)). The results of the EXSY experiments show that this is also the case for [Eu.(*RSRS*-)]. However, for the [Eu.(*RRRR*-)] and Eu.(*RRRS*-)] complexes, arm rotation is frozen-out at room temperature. As a result only two of the four

possible co-ordination isomers (Δ(λλλλ), Λ(δδδδ), Δ(δδδδ), and Λ(λλλλ)) are significantly populated, (Figure 2.19).

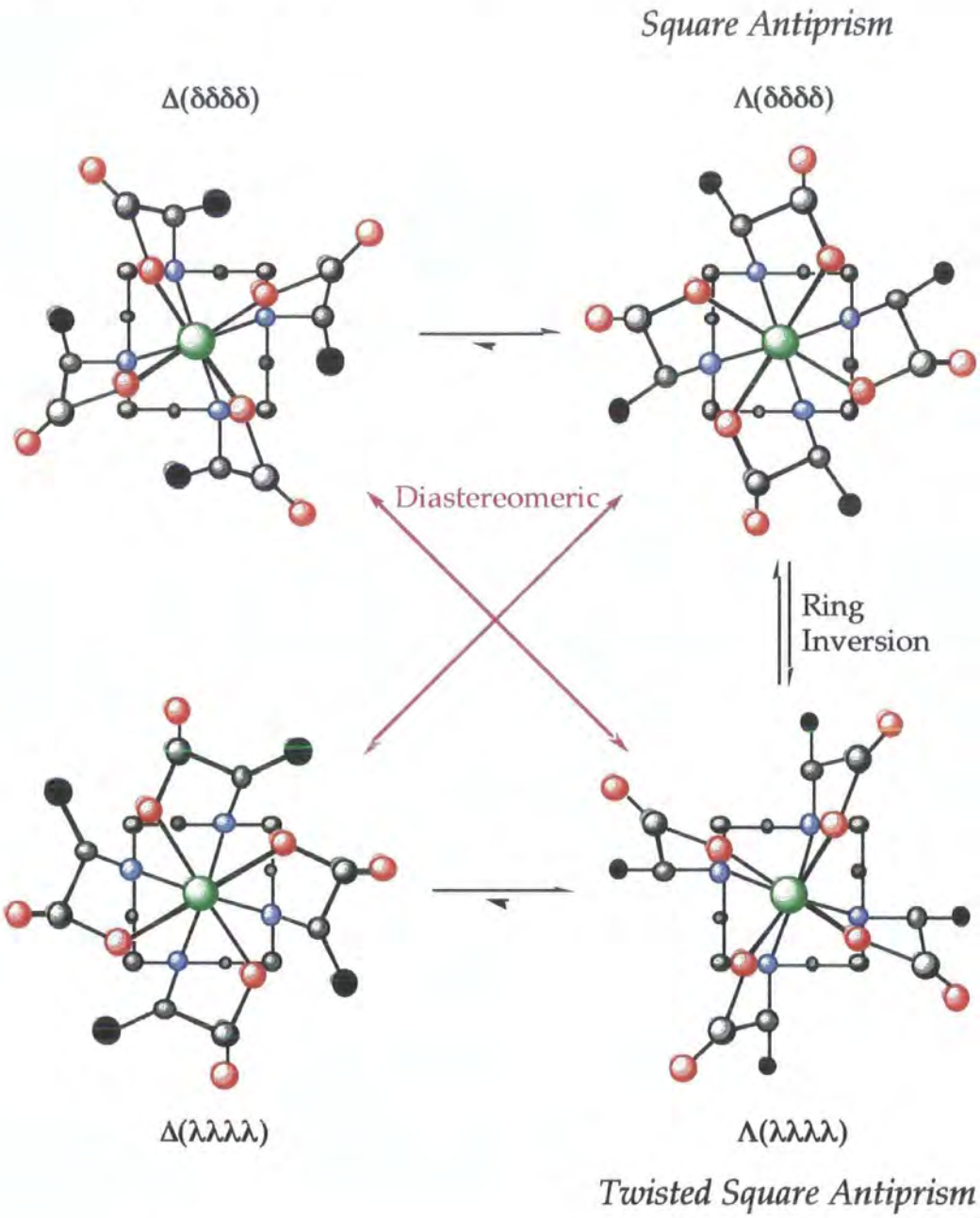

Figure 2.19 A schemtic representation of the intramolecular motion of [Ln.(*RRRR*-)] complexes. Arm rotation is effectively frozen-out and only two of the four possible structures are accessible. The bold spheres represent the carboxyethyl substituents.

The two structures observed in solution interconvert through ring inversion alone thus the orientation of the arms must be fixed. Crystals of the [Eu.(*RRRR*-)] complex were grown from an acidified aqueous solution. The crystal structure obtained (Figure 2.20) reveals a square antiprismatic complex. The orientation of the pendant arms is in the Λ conformation whilst that of the

macrocyclic ring is (δδδδ). In fact both [Eu.(*RRRR*-)] and [Eu.(*SSSS*-)] isomers co-crystallised in the unit cell from the racemic solution. The [Eu.(*SSSS*-)] isomer is the mirror image of the RRRR isomer (and hence is not shown) but must therefore have a Δ orientation of the arms with a (λλλλ) ring conformation.

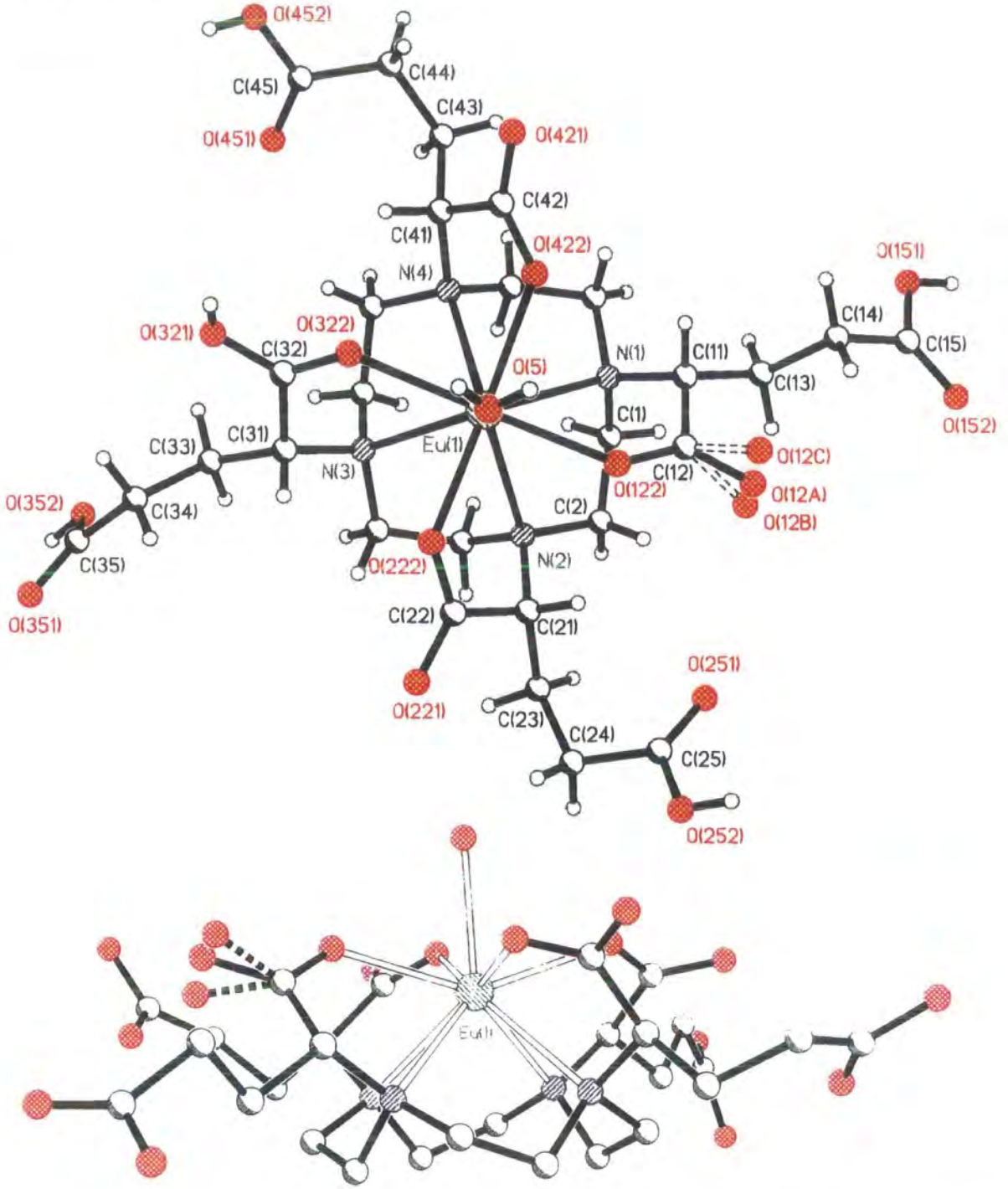

Figure 2.20 Crystal structure of [Eu.(*RRRR*-)] showing a square antiprismatic co-ordination geometry. The helicity of the pendant arms (Λ) is determined by the configuration of the stereogenic centre at carbon.

The crystal structures of the gadolinium, terbium and ytterbium complexes also show a anticlockwise arrangement of the arms (Λ) where the configuration is (*R*) and a clockwise orientation (Δ) when the configuration is (*S*).

Crystals of the corresponding gadolinium(III), terbium(III) and ytterbium(III) complexes were also grown from an acidified aqueous solution. The structure of [Gd.(*SSSS*-)] is shown (Figure 2.21). The complex is isostructural with that of the europium(III) complex. It adopts a square antiprismatic geometry and the orientation of the pendant arms appears to be controlled by the configuration at carbon. In this case the configuration is (*S*) and the arms are orientated in a Δ arrangement. The complex is an exact mirror image of the europium complex.

There is no significant change in the lanthanide(III)-water bond distance on passing from europium to gadolinium, (Table 2.2).

Complex	Ln(III)-H_2O distance (Å)
[Eu.(*RRRR*-)]	2.447(3)
[Gd.(*SSSS*-)]	2.432(2)
[Tb.(*RRRR*-)]	2.427(3)

Table 2.2 The lanthanide-water bond distances taken from the crystal structures.

In fact the [Tb.(*RRRR*-)] complex exhibits much the same metal-water bond distance (Figure 2.22). In common with the other two complexes a square antiprismatic geometry is observed. A small contraction is observed in that the terbium(III) ion lies closer to the macrocylic ring, rendering the complex more compact. Here again, the helicity of the pendant arms is determined by the configuration at carbon. It may be assumed that the orientation of the arms is defined by the configuration at the chiral centres for both the (*RRRR*-) and (*RRRS*-) isomers. The conformation of the macrocyclic ring then defines the co-ordination geometry as either a square or twisted square antiprism.

The structure of the [Yb.(*RRRR*-)] complex had not been completely solved at the time of writing. However, a preliminary solution suggests that the structure is radically different from those shown here. The C4 symmetry of the unit cell in which ytterbium lies precludes the possibility of a water molecule being co-ordinated to the ytterbium(III) ion.

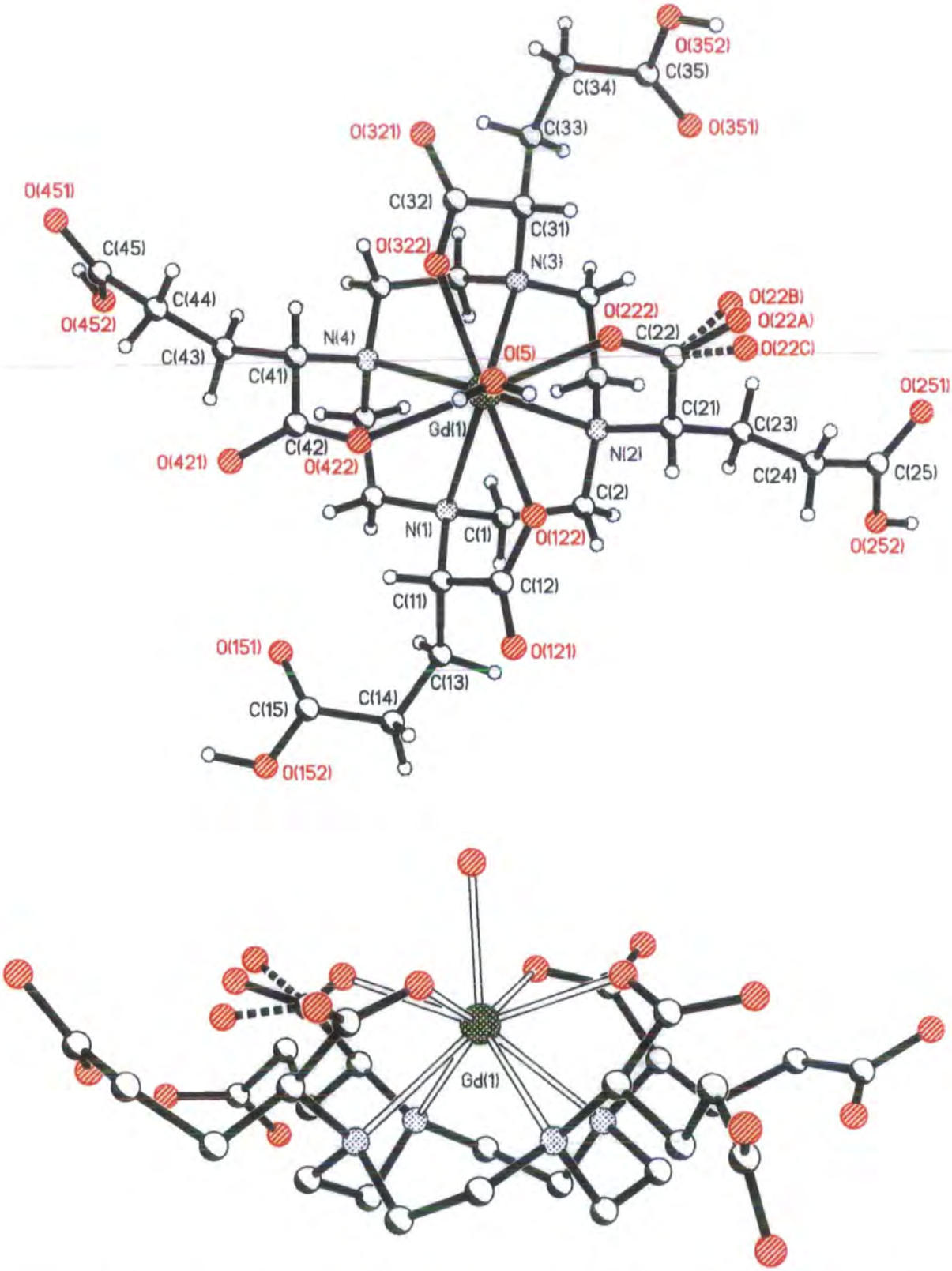

Figure 2.21 The crystal structure of [Gd.(*SSSS*-)] is isostructural with that of the europium(III) complex. It is a square antiprism with a (λλλλ) ring conformation and a Δ orientation of the pendant arms.

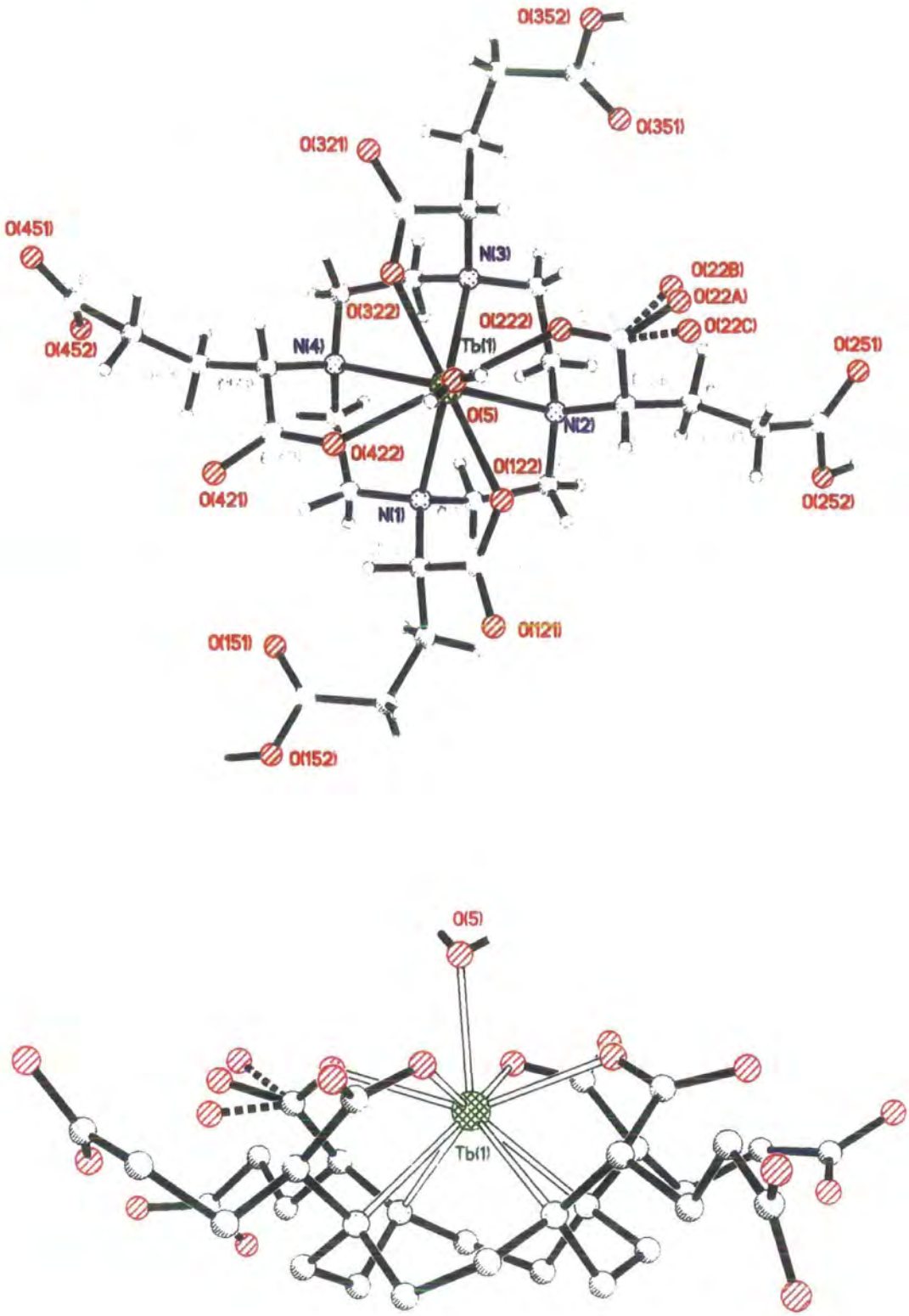

Figure 2.22 The crystal structure of [Tb.(*SSSS*-)], exhibiting a square antiprismatic geometry with a (λλλλ) ring conformation and a Δ orientation of the pendant arms.

The Hydration States of the Isomeric Europium(III) Complexes

The time resolved decay of the luminescence from europium was measured in H_2O and D_2O for each of the four complexes. This was performed by direct excitation of the metal centre at 397 nm, monitoring the emission at 617 nm. Treatment by the Horrocks' method[23] enabled a value for q, the number of directly co-ordinated water molecules, to be obtained (Table 2.3).

	τ_{H_2O} / ms	τ_{D_2O} / ms	q
[Eu.(*RRRR*-)]	0.62	2.08	1.1 ± 0.1
[Eu.(*RRRS*-)]	0.67	2.50	1.1 ± 0.1
[Eu.(*RRSS*-)]	0.67	2.00	1.0 ± 0.1
[Eu.(*RSRS*-)]	0.67	2.50	1.1 ± 0.1

Table 2.3 The luminescent lifetimes (τ) and hydration states (q) of the europium(III) complexes of the isomers of tetra(carboxyethyl) DOTA.

Deviations from integral values of q are very common.[12] Indeed Horrocks himself quotes an error of 0.5 in the values obtained. Realistically, the values can be expected to be much more accurate than this and experimental errors of 10% are usually quoted. A hydration state of one is observed for each isomer in solution, consistent with the observation of one bound water molecule in the crystal structure of [Eu.(*RRRR*-)] A further contribution to the measured q value arising from the quenching effects of outer sphere oscillators, (Chapter 1.3), is observed.

2.4. Lanthanide(III) Complexes of (*RRRR*-) Tetra(carboxyethyl) DOTA

The catalysis of water proton relaxation by a paramagnetic complex is a dynamic process. As a result, both the structure and the dynamics of a complex may strongly influence the effectiveness of the catalysis. It is, therefore, imperative to understand not only how a complex behaves in solution but also exactly what the structure of the solute is.

The Structure of the Europium(III) Complexes

As discussed previously, (Chapter 1.3), lanthanide(III) complexes based around the DOTA ligand may exist as one of two co-ordination isomers, the square antiprism, or the twisted square antiprism. Throughout most of the

lanthanide series, for the complexes of DOTA, the square antiprismatic geometry is favoured in the solid state.

However, in solution the complex is in dynamic equilibrium and both geometries may be observed. This is most clearly highlighted by considering the most shifted axial proton resonance in the ^{1}H NMR spectrum. The resonances of these protons in the four diastereomeric europium complexes are shown (Figure 2.23). The two co-ordination isomers may be clearly differentiated since one (resonating 40-50 ppm) experiences a greater shift than the other (resonating 20-30 ppm).

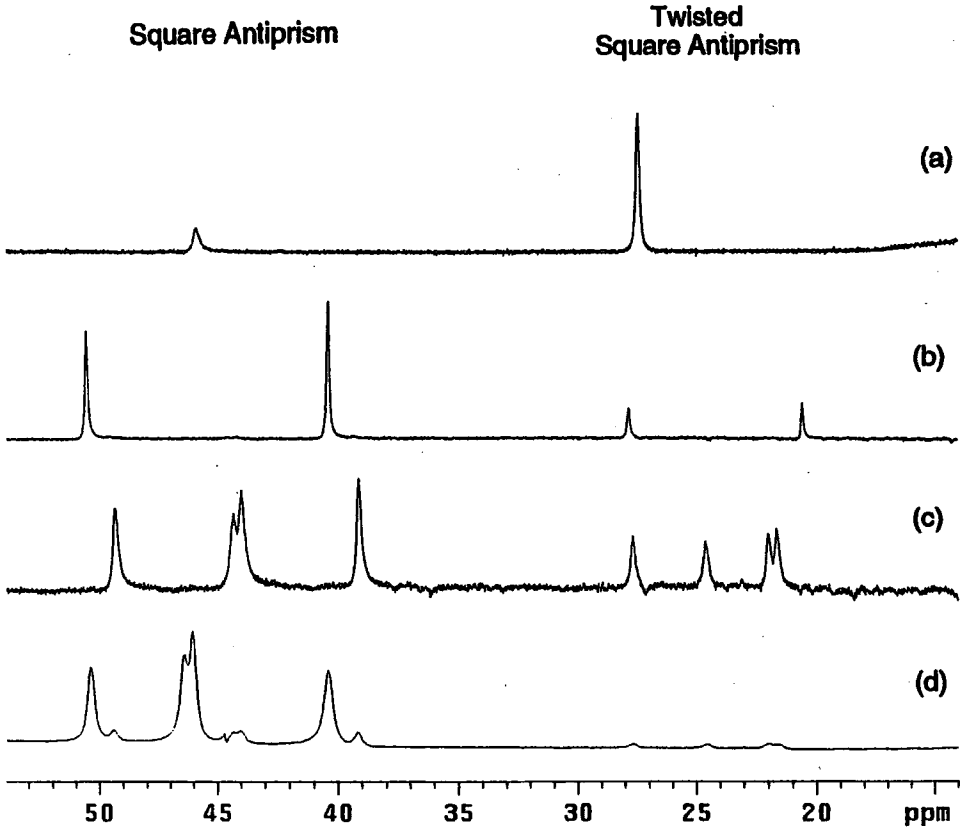

Figure 2.23 The shifted axial proton resonances in the ^{1}H NMR spectra of (a) [Eu.(*RRRR*-)], (b) [Eu.(*RSRS*-)], (c) [Eu.(*RRRS*-)], (d) [Eu.(*RRSS*-)], highlights the changes in preferred co-ordination geometry for the four isomers.

Whilst it is not possible to predict the NMR shift of a proton in a europium complex because of the contact contribution to the paramagnetic shift of europium, an assignment of the co-ordination isomers may still be made. It may be expected that the co-ordination isomer which experiences less paramagnetic shifting will have the greater distance between proton and the metal. The twisted square antiprismatic geometry has both longer metal-nitrogen and metal-oxygen bonds than the square antiprism.[21] The ring protons may be expected to reside further from the metal centre and hence experience a smaller paramagnetic shift. This is consistent with the

observations made for DOTA, in which the least shifted isomer is always the twisted square antiprism, across the lanthanide series.[24]

The ratio of the two co-ordination isomers of DOTA has been shown to be dependent upon ionic strength.[25] In particular the addition of lithium salts to a solution of [Eu.DOTA]$^-$ has been shown to enhance the tendancy of the complex to adopt a twisted square antiprismatic geometry. This can be understood by considering the high affinity of lithium towards the oxygen of a carbonyl. The interaction of lithium with the carboxylates of [Ln.DOTA]$^-$ will perturb the electron density through the carboxylate. The electron density is drawn away from the lanthanide(III) ion slightly weakening the bonding interaction with oxygen. The result is marginally longer metal-oxygen bonds, favouring the twisted square antiprismatic geometry. In contrast to the results obtained for [Eu.DOTA]$^-$, addition of lithium chloride to a sample of [Eu.(*RRRR*-)] resulted in very small changes in the isomer ratio (Figure 2.24).

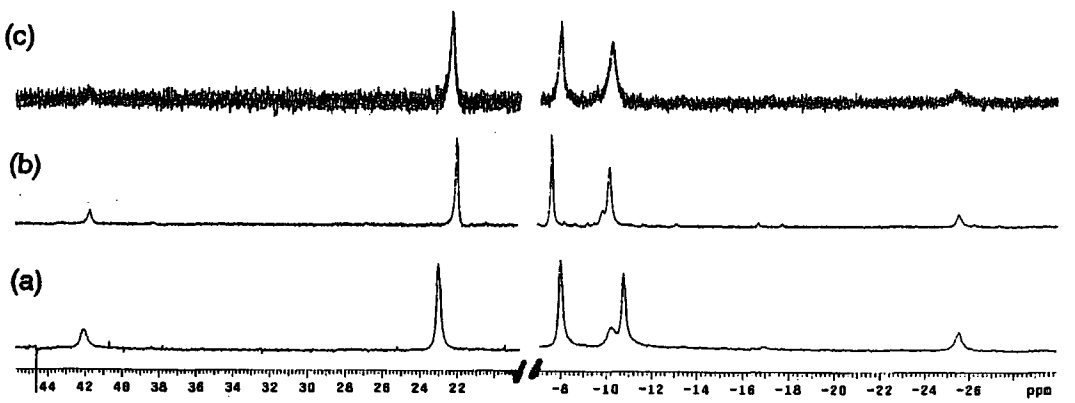

Figure 2.24 The addition of lithium chloride to 0.07 mmol dm^{-3} solution of [Eu.(*RRRR*-)] (a) [LiCl] = 0 mmol dm^{-3} (b) [LiCl] = 3.5 mmol dm^{-3} (c) [LiCl] = saturated.

The ratio of the isomers is reversed between these two complexes. [Eu.DOTA]$^-$ shows a ratio of 4:1 in favour of the most shifted isomer whereas [Eu.(*RRRR*-)] shows a ratio of 1:4. The observation that, even at saturation, addition of lithium chloride shows little change in the isomer ratio suggests that the complex already favours the twisted square antiprism, i.e. the least shifted co-ordination isomer.

The major isomer of [Eu.(*RRRS*-)], [Eu.(*RRSS*-)], and [Eu.(*RSRS*-)] may be assigned to the square antiprismatic geometry. The major isomer for [Eu.(*RRRR*-)] on the other hand is expected to be a twisted square antiprism, the opposite geometry to that exhibited in the solid state (Figure 2.20). This reversal in conformational preference may be the result of the strong hydrogen bonding interactions observed between the substituent carboxylates. This

structure must be the lowest in energy conformation in the solid state. In the solution state, a favourable entropy contribution or preferential solvation of the substituent carboxylates may cause the twisted square antiprismatic co-ordination geometry to become more favourable.

The Structure Across the Lanthanide Series

So far the discussion has been confined to the complexes of europium(III). Whilst analogies regarding the behaviour of the corresponding gadolinium(III) complexes may be drawn from these results, it is important to remember that due to contraction of the lanthanide series the behaviour of the gadolinium complexes will differ slightly. In order to develop a full picture of the structure of these gadolinium(III) complexes in solution, the analogous terbium(III) complexes must be studied. The structure of the gadolinium(III) complex may be expected to lie somewhere between the two. Two factors are of particular interest, the hydration state and the ratio of the co-ordination isomers in solution.

To develop a complete picture of the relationship between the ratio of the two co-ordination isomers with lanthanide contraction, a selection of [Ln.(*RRRR*-)] complexes was synthesised. The relative ratio of square to twisted square antiprism was measured by examination of the axial proton resonances in their ^{1}H NMR spectrum (Figure 2.25). The ratios of the two isomers are summarised in Table 2.4.

(±)-*RRRR*- Complex	Square Antiprism	Twisted Square Antiprism
Praseodymium	1	28
Neodymium	1	8
Europium	1	4
Terbium	1	1.5
Holmium	1	4
Ytterbium	1	15

Table 2.4 The relative ratios of square to twisted square antiprismatic geometries for a selection of lanthanides across the series.

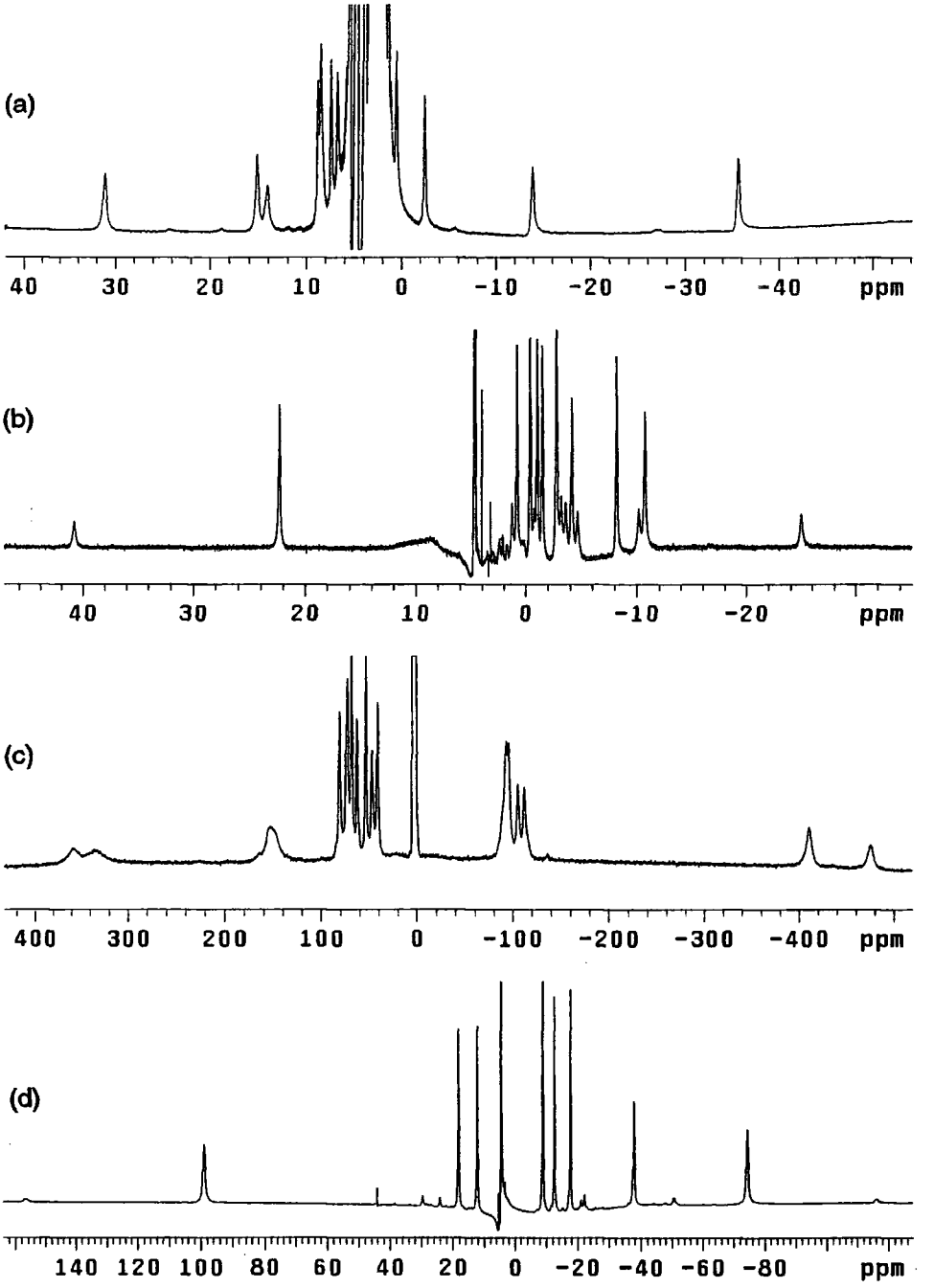

Figure 2.25 ^{1}H NMR spectra of (a) [Pr.(*RRRR*-)], (b) [Eu.(*RRRR*-)], (c) [Tb.(*RRRR*-)] and (d) [Yb.(*RRRR*-)].

The ratio of the two isomers changes dramatically across the lanthanide series. This is not surprising since a similar observation is made for the lanthanide(III) complexes of DOTA. As found in the complexes of DOTA, the change in isomer ratio is not linear across the series. This is most clearly illustrated by plotting the mole fraction of each isomer across the lanthanide series (Figure 2.26)

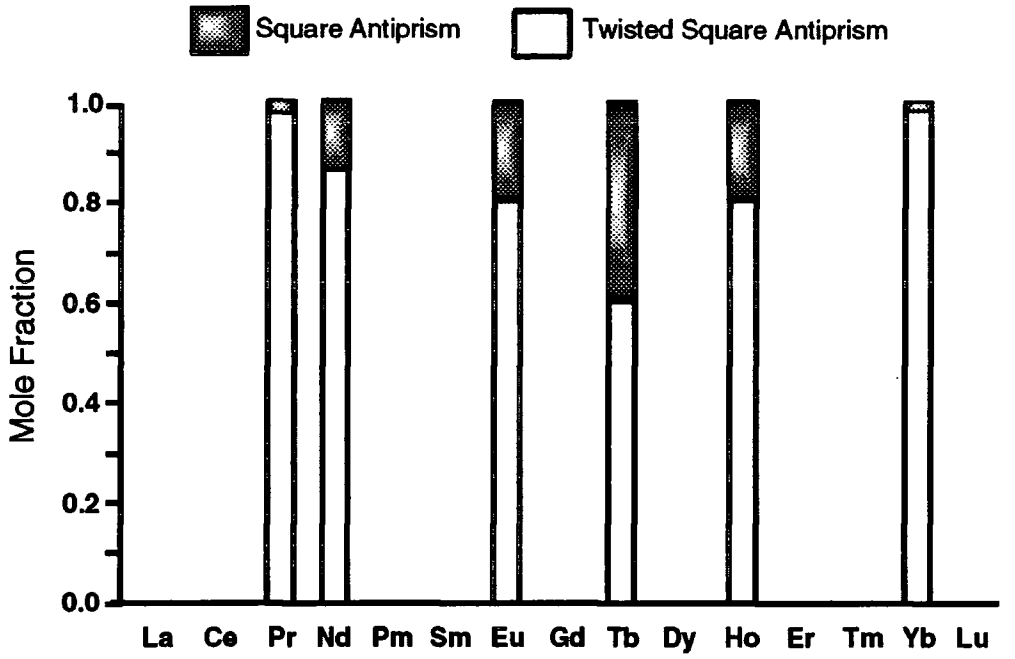

Figure 2.26 A plot of the relative mole fractions of square versus twisted square antiprismatic geometries in the solution state for a selection of lanthanides across the series.

Although these complexes exhibit a clear preference for a twisted antiprismatic geometry across the whole series, the overall trend is similar to that observed for [Ln.DOTA]$^-$ (Figure 1.8). The mole fraction of the square antiprism increases steadily across the early part of the series, reaching a maximum at or after terbium. It then decreases across the rest of the series until at ytterbium the complex exists almost solely as a twisted square antiprism.

This reversal in the trend for complexes across the series was explained by Aime *et al.*[26]. Early in the series as the ionic radius decreases, the metal-donor distances shorten and the more compact square antiprism becomes increasingly more favoured. Eventually the ionic radius is decreased to such an extent that, in the minor isomer, the bound water molecule is pushed away from the lanthanide ion by the steric demands of the ligand. This dissociation increases the disorder of the system, and hence a favourable entropy term is associated with the twisted square antiprismatic geometry becoming increasingly favoured towards the end of the series. This rationale may be used to explain the trend observed in [Ln.**26**] complexes, provided the hydration states measured in solution tally with those predicted by theory.

The Hydration State Across the Lanthanide Series

Recent advances in the study of luminescent lanthanide ions has allowed the method of Horrocks for measuring the hydration states of lanthanides to be extended to ytterbium.[27] Such methods have been employed to determine the hydration states of the [Eu.(*RRRR*-)], [Tb.(*RRRR*-)] and [Yb.(*RRRR*-)] complexes. The results are shown in Table 2.5.

Complex	τ_{H_2O}/ns	τ_{D_2O}/ns	q
[Eu.(*RRRR*-)]	621.1	2083	1.1 ± 0.1
[Gd.(*RRRR*-)]	/	/	(1)[a]
[Tb.(*RRRR*-)]	2083	3333	0.76 ± 0.08
[Yb.(*RRRR*-)]	0.974	3.588	0.54 ± 0.07[b]

Table 2.5 The luminescent lifetimes, τ, and hydration states, q, of a series of [Ln.(*RRRR*-)] complexes. a) Deduced from the NMRD profile (Chapter 2.6). b) in accordance with the published procedure for ytterbium complex, adjustment has been made in this figure for the outer sphere contribution.[27]

The hydration state of the europium(III) complex was determined to be one. This is consistent with the observation of one bound water molecule in the crystal structure (Figure 2.19). On passing to terbium(III), however, a clear cut change is observed. The lanthanide hydration state is reduced by approximately a quarter of one water molecule. This may be a consequence of the so-called "gadolinium break". On passing from the lighter to the heavier lanthanides a change in co-ordination number of the lanthanide(III) aquo ion from nine to eight is observed. This "break" is generally considered to occur at gadolinium.

However, and in common with the aquo ions, this "break" is not a clean break. The observed value of q = 0.76, is neither one nor zero. Non-integral values of q are not uncommon in these types of complex.[28] The value of q obtained for the corresponding ytterbium complex is also equivalent to approximately half a bound water molecule. Clearly then the major isomer of [Yb.(*RRRR*-)] (corresponding to the minor isomer of [Yb.DOTA]-) is not a simple q = 0 complex. Another explanation must be found for these observations.

There are two possible limiting cases which should be considered. Firstly, there may be a mixture of q = 1 and q = 0 states for the major isomer of

the [Yb.(*RRRR*-)] complex. These two structures are time averaged on the NMR timescale. The second scenario involves only a $q = 1$ species in which the water is forced away from the metal ion by the increasing steric demands of the ligand. When considering these two cases it is important to keep in mind the observed ratio of the two isomers, for each complex. After all, the two co-ordination isomers need not behave in a similar manner and the hydration state may be pivotal in establishing which isomer is favoured.

In the situation where a significant proportion of the major isomer of a complex in solution possesses a vacant co-ordination site, then the observed water exchange rate of the bulk material would be very fast. Since water exchange occurs *via* a dissociative mechanism, the rate is controlled by the rate of metal-water bond cleavage. If a large population exists in this state then the apparent exchange will be very fast. It is reasonable to suppose that this will be of the order of 10^8 s^{-1}. The timescale of the non-radiative quenching of luminescence is much slower, of the order of 10^6 s^{-1} for ytterbium and 10^3 s^{-1} for terbium. The observed hydration state is therefore a time averaged value. The hydration state in a preliminary solution of the solid state structure of [Yb.(*RRRR*-)] is zero. This supports the hypothesis that a proportion of the complex possesses no bound water molecule.

The second limiting case is that a water molecule remains bound to the lanthanide(III) ion but is pushed away by the steric demands of the ligand. This idea is supported by the solid state structure of [Tb.(*RRRR*-)] which has one bound water molecule. In the heavier lanthanides, after the "gadolinium break", steric crowding of the vacant binding site may be expected. This is likely to be more pronounced in the twisted square antiprismatic geometry where, although the metal-oxygen bond lengths are longer, the oxygens are pushed up, closer to the apical position occupied by the water. Such crowding may result in a lengthening and weakening of the metal-water bond. Since vibrational transfer from the excited lanthanide(III) ion to the water molecule, which results in luminescence quenching, follows an r^{-6} dependence, relatively small increases in the terbium-water bond distance may have a significant effect upon the observed value of q.

The metal-water bond length can only increase so far before the bonding interaction is broken. Let's suppose that the water lies at the farthest limit of the bonding interaction in the twisted square antiprismatic geometry of [Tb.(*RRRR*-)]. The bonding interaction will be weak and this may be expected to give rise to a more readily dissociated complex. As the steric demands of the ligand increase with decreasing ionic radius across the series, the dissociation of the water molecule will be increasingly more favoured. An increasingly

significant population density of the twisted square antiprismatic geometry will then be $q = 0$. The weak metal-water bonding interactions which lead to this increased dissociation must also lead to faster water exchange rates (since the mechanism of water exchange must be dissociative). Since water exchange is fast on the time-scale of a luminescence experiment (k_{ex} ~100 ns) then a time averaged position of the inner co-ordination sphere of water will be observed. Thus in terms of the luminescence measurements, the apparent metal-water bond length increases in the twisted square antiprismatic geometry of [Gd.(*RRRR*-)] complexes on passing from gadolinium to ytterbium.

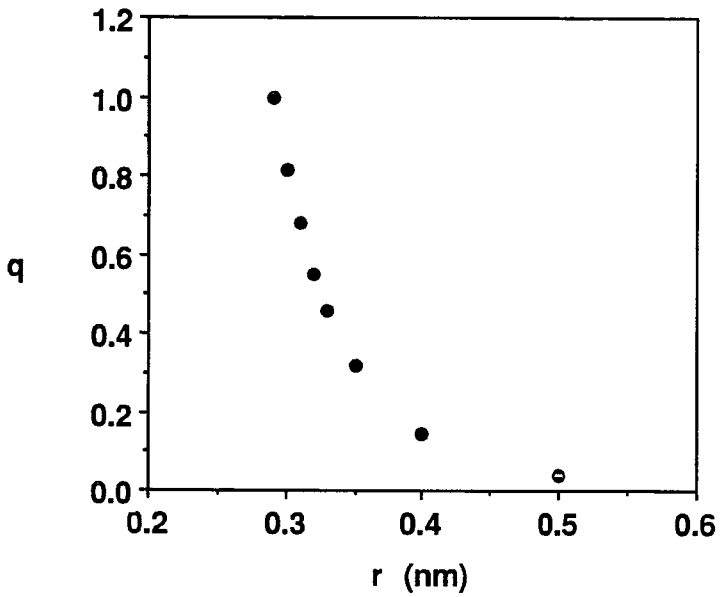

Figure 2.27 The value of q is dependent upon the distance, r, of the water molecule from the lanthanide(III) ion.

In reality the twisted square antiprism is expected to favour the dissociation of the water molecule to give an increasing proportion of $q = 0$ complex along the series. In the square antiprismatic geometry the metal-water bond distances, taken from the crystal structures of [Eu.(*RRRR*-)], [Gd.(*RRRR*-)] and [Tb.(*RRRR*-)], do not vary significantly, it is therefore assumed that these complexes remain fully hydrated.

2.5. Relaxation Measurements of Gadolinium(III) Complexes

The isomeric complexes of gadolinium(III) tetra(carboxyethyl) DOTA **26** may be expected to exhibit broadly similar nuclear magnetic relaxation characteristics. They are, after all, the same size and each has one bound water molecule. However, substantial differences in the structural and dynamic properties of the four isomers have been illustrated. The symmetry and shape of the complexes differ. So, whilst characteristics which are dependent upon

size, such as τ_R, may be expected to be broadly similar for each isomer, τ_S which is thought to be related to the symmetry and rigidity of the complex[29] may differ dramatically, and different rates of water exchange may also occur. The three complexes [Gd.(*RRRR*-)], [Gd.(*RRRS*-)] and [Gd.(*RSRS*-)] were investigated.

^{17}O NMR Studies

The role of the bound water molecule is crucial to the effectiveness of a contrast agent. In [Gd.DOTA]$^-$ half of the overall relaxivity of the complex arises through an inner sphere mechanism, i.e. through exchange of the bound water molecule. This contribution was quantified, by the work of Solomon, Bloembergen and Morgan (Chapter 1.2), by the following equations (2.2 - 2.4) where τ_M is the residence lifetime of a water molecule.

$$R_1 = \frac{[C]q}{55.6}\left(\frac{1}{T_{1M} + \tau_M}\right) \tag{2.2}$$

$$T_{1M} = \frac{2/15 S(S+1)g^2\beta^2\gamma_I^2}{r^6}\left\{\frac{7\tau_C}{(1+\omega_S^2\tau_C^2)} + \frac{3\tau_C}{(1+\omega_I^2\tau_C^2)}\right\} + \frac{2}{3}\frac{A^2}{\hbar^2}S(S+1)\left\{\frac{\tau_S}{(1+\omega_S^2\tau_S^2)}\right\} \tag{2.3}$$

$$\frac{1}{\tau_C} = \frac{1}{\tau_S} + \frac{1}{\tau_R} + \frac{1}{\tau_M} \tag{2.4}$$

From these equations it is clear that fast exchange conditions must prevail if a complex is to exhibit significant inner sphere relaxivity. For a slowly tumbling system, where τ_R is long, the characteristic correlation time τ_C, and hence at imaging fields the relaxivity will be limted by τ_M. For this reason it is important to be able to measure water exchange rate. Since the protons of a water molecule may themselves undergo exchange in a separate process from water exchange, the proton does not offer an effective probe for this process.[30] Fortunately ^{17}O is also NMR active and, since it is the metal-oxygen lability which is under scrutiny, offers an ideal probe for water exchange. As a result of co-ordination to a paramagnetic ion the relaxation of the quadrupolar ^{17}O nucleus is catalysed in an NMR experiment. Since T_2 is shortened, the linewidth of the signal arising from the bound oxygen is broadened. If the exchange of the bound water is sufficiently fast then this effect will be transferred to the bulk water, in the same way that proton relaxation is.

By measuring the effect of temperature on the linewidth of an ^{17}O enriched solution of a paramagnetic complex and correcting for natural

linewidth, a profile of the paramagnetic transverse relaxation rate may be built up. Since this relaxation rate is almost entirely dependent upon the contribution from coordinated water molecules, it is also dependent upon τ_M. A fitting procedure may be undertaken, usually in conjunction with the fitting of an NMRD profile, which will enable a value of τ_M to be calculated. An approximate value for τ_V, the correlation time characterising the proton relaxation time, may also be estimated from this profile.

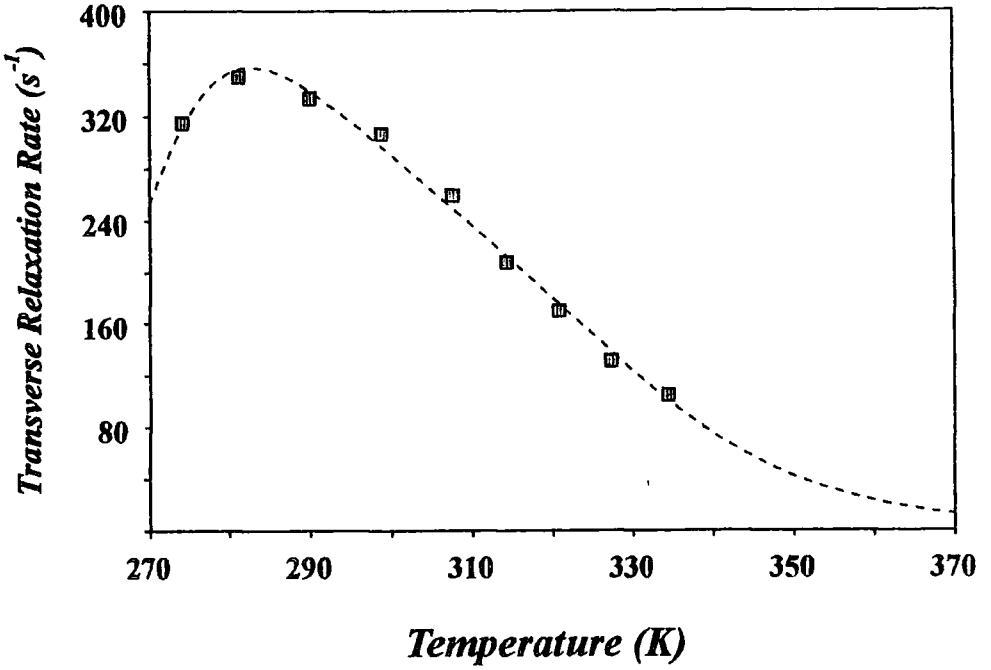

Figure 2.28 The VT ^{17}O profiles of [Gd.(*RRRR*-)] (44mM).

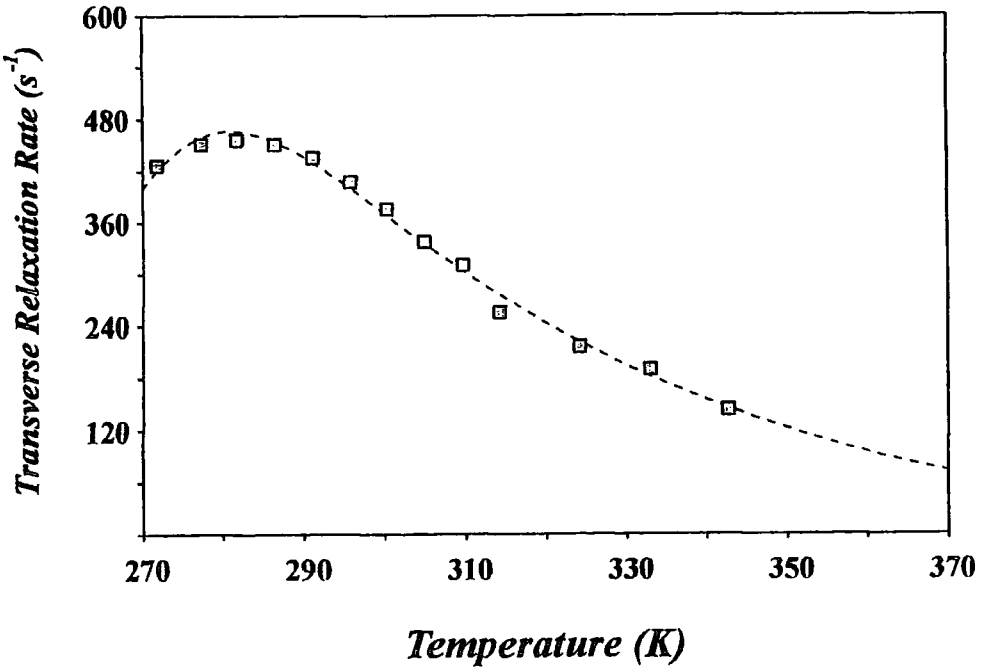

Figure 2.29 The VT ^{17}O profiles of [Gd.(*RRRS*-)] (41 mM).

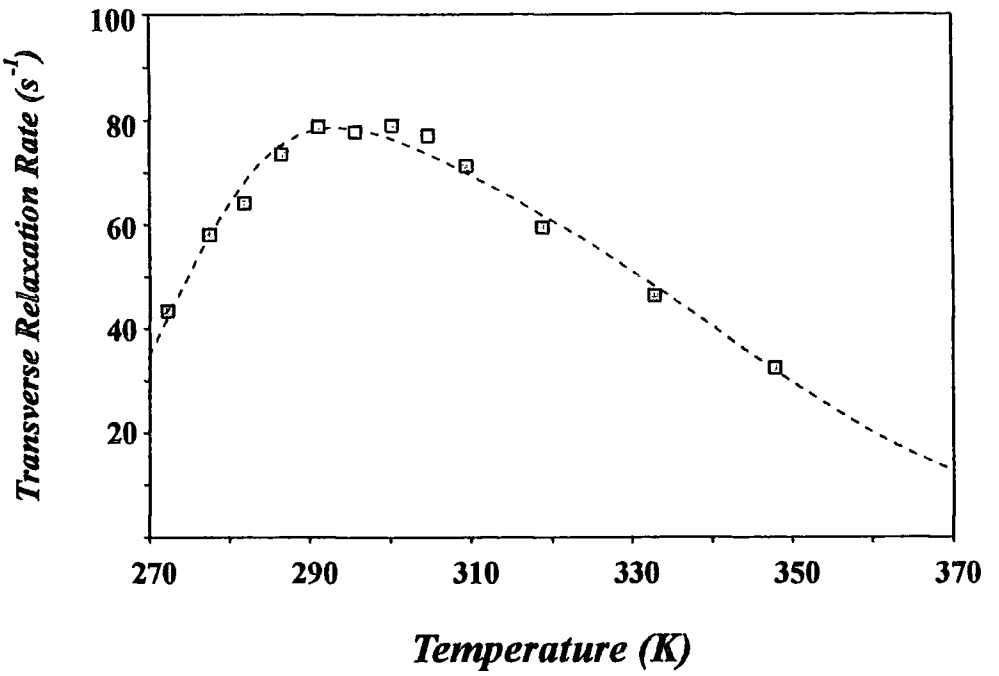

Figure 2.30 The VT ^{17}O profiles of [Gd.(*RSRS*-)] (16mM).

^{17}O Profiles for the three isomers are shown in Figures 2.28-2.30. In general the flatter the profile the slower the water exchange rate. Faster exchange rates give rise to profiles with more exponential character. Inspection of the three profiles shows that the flattest is that of the (*RSRS*-) isomer, and hence this is the isomer with the slowest rate of water exchange. In contrast the profile for [Gd.(*RRRR*-)] is very steep, indicating that the complex possesses a short value of τ_M. Values of τ_M and τ_V at 25°C were calculated from the fitting of these profiles, and the results are summarised in Table 2.6 A full list of fitting parameters is included in Appendix I.

Complex	τ_M / ns	τ_V / ps
[Gd.(*RRRR*-)]	71	13
[Gd.(*RRRS*-)]	140	12.1
[Gd.(*RSRS*-)]	270	13.3

Table 2.6 The values of τ_M and τ_V at 25°C obtained from the ^{17}O profile of each complex.

The values of ~13 ps obtained for τ_V in each of the three complexes are the same, within experimental error. This is not particularly surprising in view of the strong relationship between τ_V and the nature of the chelating agent. All three ligands chelate the gadolinium in much the same way The value of

τ_V obtained for DOTA is 7.2 ps, the values obtained here are not so dissimilar. The values of τ_M on the other hand differ markedly between the three isomers. The [Gd.(*RSRS*-)] complex exhibits a water exchange rate comparable to that of DOTA (244 ns).[31] This is entirely expected since the solution state structure and dynamics of this complex are identical to those of DOTA. It may be noted that as the number of juxtaposing chiral centres within the complex is reduced, so is τ_M. The value of τ_M obtained for the [Gd.(*RRRS*-)] complex is intermediate, whereas that observed in the [Gd.(*RRRR*-)] isomer is far shorter.

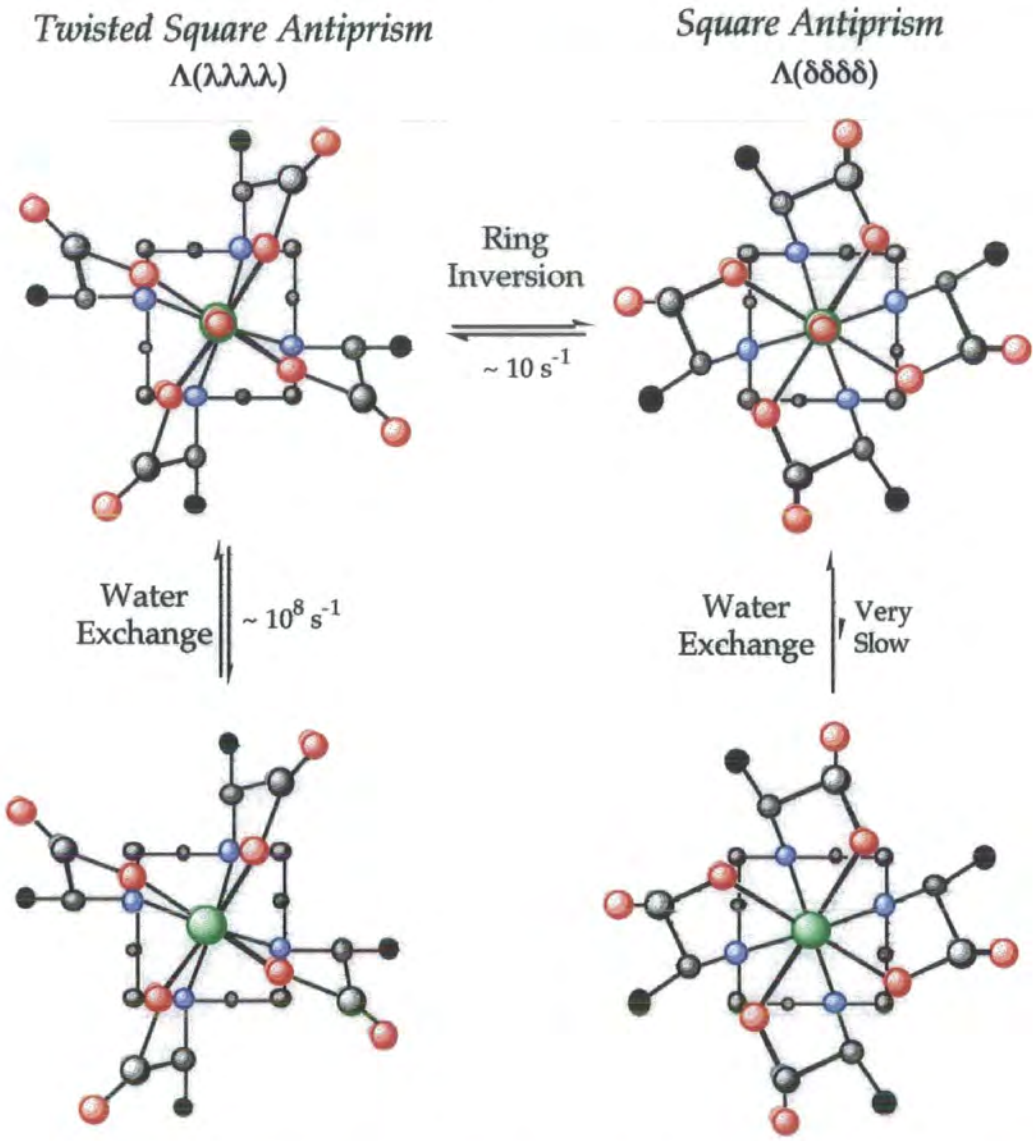

Figure 2.31 Water exchange is almost exclusive to the twisted square antiprisatic geometry. The observed rate of water exchange is therefore dependent upon the proportion of the complex adopting this conformation; shown here for [Ln.(*RRRR*-)].

Indeed the observed value of 40 ns at 39°C is approaching the optimum value of 30 ns calculated by Aime *et al.* for a slowly tumbling system.[32] The

water exchange rate increases with both an increase in the rigidity of the complex and also the proportion of the complex which exists in the twisted square antiprismatic geometry in solution. This latter factor would appear to be most important in determining the extremely fast water exchange rate observed for the (*RRRR*-) isomer.

Merbach and Pubanz have used variable pressure NMR experiments to probe the water exchange processes in [Gd.DOTA]$^-$ and [Gd.DTPA]$^{2-}$.[33,26] The activation volume for this process may be measured in this way. Since water exchange in [Gd.DOTA]$^-$ must proceed *via* a dissociative mechanism, this *activation volume* would be expected to be positive. The authors found that although the activation volume was indeed positive it was much smaller than expected. The value obtained matched that expected for a situation in which the minor co-ordination isomer of [Gd.DOTA]$^-$ was the *only* species undergoing water exchange (Figure 2.31). Thus it was concluded that the dissociation of the major isomer had to overcome a large energy barrier and thus in the region 20-40°C only the minor, twisted square antiprismatic, isomer exchanged with the bulk solvent.

In view of these results the water exchange rate $(1/\tau_M)_{[Gd.26]}$ and the mole fraction(twisted square antiprism)$_{[Eu26]}$ were compared for each of the three isomers, (Figure 2.32).

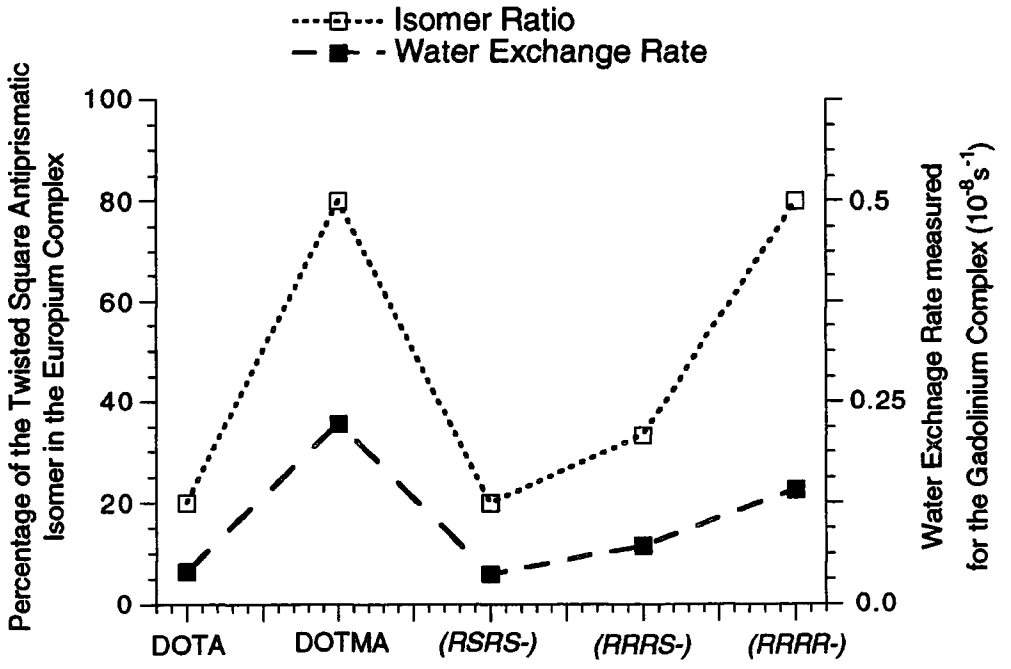

Figure 2.32 Plots of the water exhange rate measured for the Gd(III) chelates and the proportion of each chelate adopting a twisted square antiprismatic geometry in the Eu(III) complexes of DOTA, DOTMA, **26**(*RSRS*-), **26**(*RRRS*-) and **26**(*RRRR*-).

A close relationship between these two parameters is clear. This suggests that τ_M is indeed dependent upon the proportion of the complex which adopts a twisted square antiprismatic geomety and that in the complex with a square antiprismatic geometry, the water does not exchange to a significant extent with the bulk.

Nuclear Magnetic Relaxation Dispersion Studies

The NMRD profiles for the three gadolinium(III) complexes were recorded at 15, 25 and 39°C (Figures 2.33-2.35). The simultaneous fitting of the three profiles of each complex with the ^{17}O profile allows values of τ_S and τ_R to be obtained.

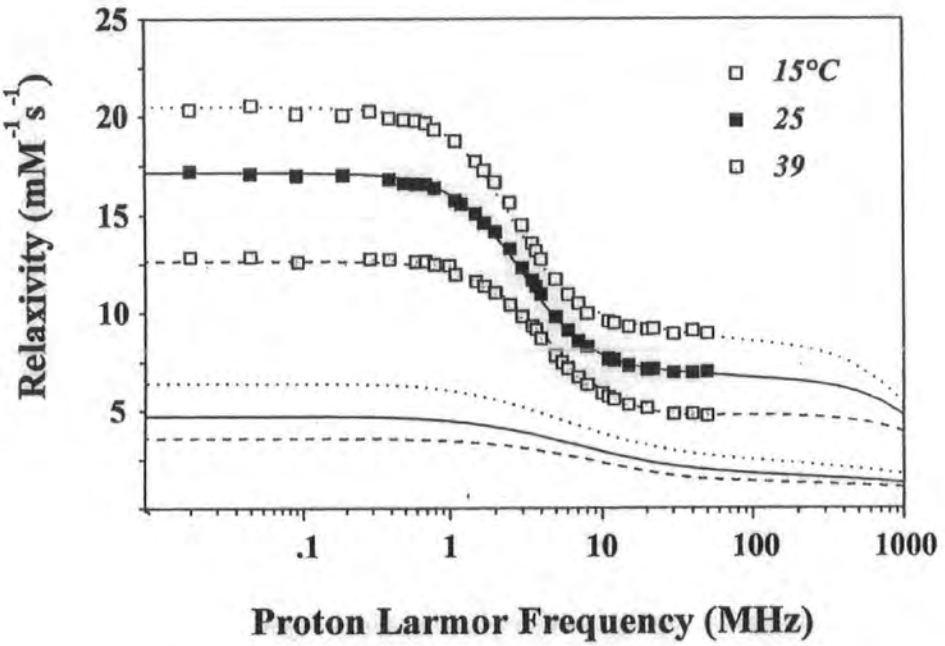

Figure 2.33 The NMRD profile of [Gd.(*RRRR*-)].

The first feature to note is the strong temperature dependence of the relaxivity across the frequency spectrum. In common with most known gadolinium complexes, each of the three complexes shows a reduced relaxivity with increasing temperature. For this reason it is important to compare only profiles recorded at the same temperature. For the purposes of this discussion the profiles at 25°C will be considered, however, a full list of best fitting parameters is appended (Appendix I). One other feature of the profile worthy of note is the characteristic inflection about 5-10 MHz, indicating the presence of a bound water molecule, cf. [Gd.DOTA]$^-$ (Figure 1.3). This aids the fitting process, since q may be fixed to one.

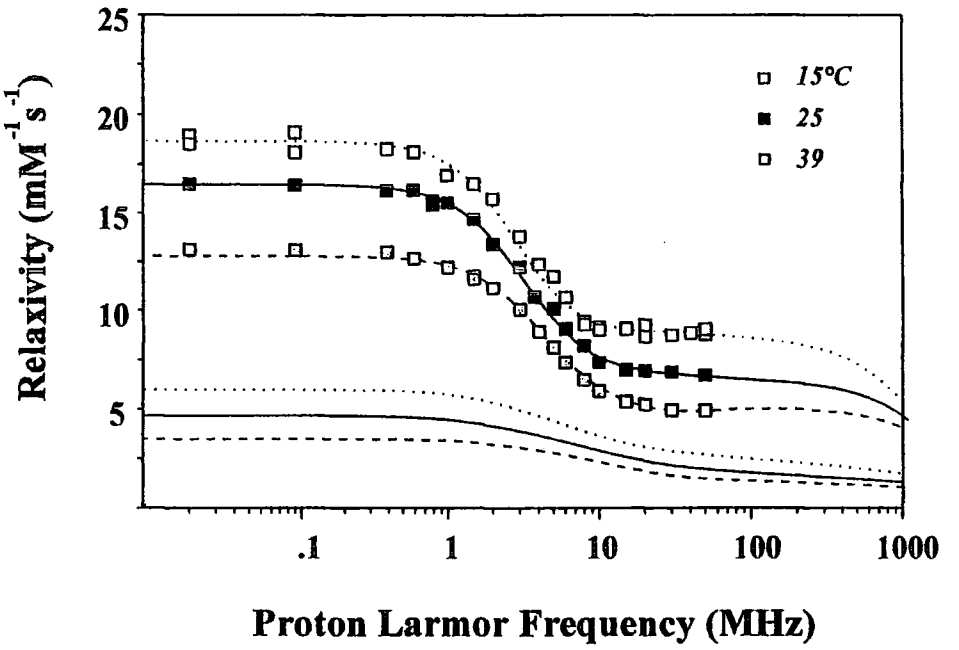

Figure 2.34 The NMRD profile of [Gd.(*RRRS*-)].

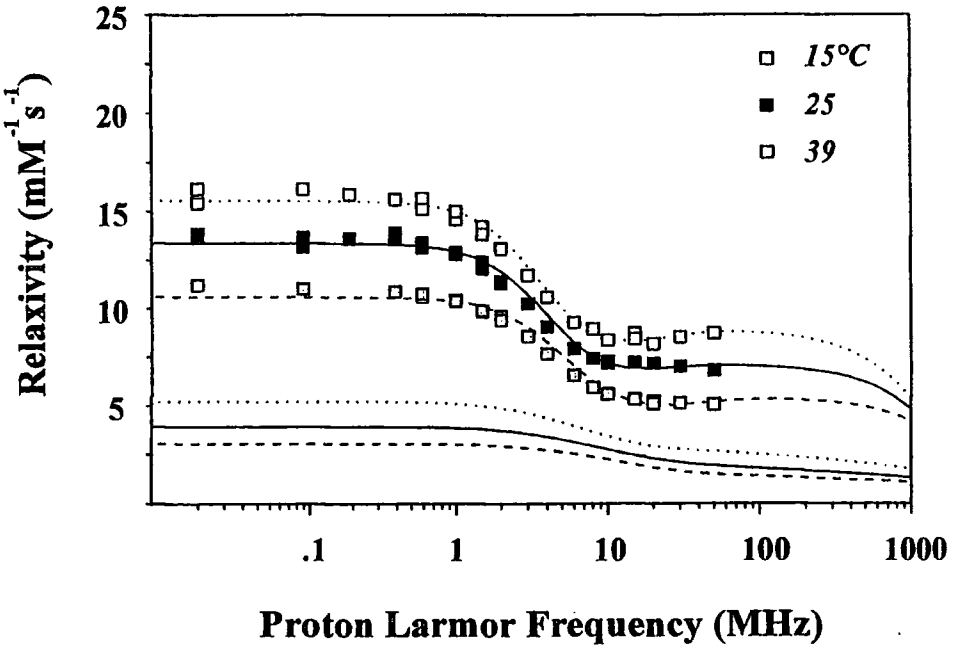

Figure 2.35 The NMRD profile of [Gd.(*RSRS*-)].

The high field region for the three NMRD profiles bear a marked resemblance to each other. For small gadolinium chelates such as these, this region of the profile is controlled by τ_R. Because the three complexes under investigation have the same molecular weight and approximately the same molecular dimensions, they would be expected to tumble at much the same rate. This is reflected in the values of τ_R obtained from the fitting of the profiles (Table 2.7).

Complex	τ_R/ps	τ_{S0}/ps
[Gd.(*RRRR*-)]	108	368
[Gd.(*RRRS*-)]	103	349
[Gd.(*RSRS*-)]	115	137

Table 2.7 Values of τ_R and τ_S obtained from the NMRD profiles at 25°C

It is the low field region of the profiles which reveal the major differences between the complexes. This region is primarily influenced by the value of τ_{S0}, the electron spin relaxation time at zero field. The factors which govern τ_{S0} are not understood. This study of chemically identical gadolinium(III) chelates may provide a useful insight into the factors which determine this parameter. Values of τ_{S0} in excess of 300 ps are observed for the [Gd.(*RRRR*-)] and [Gd.(*RRRS*-)] complexes, whereas that for [Gd.(*RSRS*-)] is a factor of three smaller. This suggests that structural or dynamic features of these first two complexes, which are not exhibited by [Gd.(*RSRS*-)], are responsible for longer electron spin relaxation times. The only structural feature shared by [Gd.(*RRRR*-)] and [Gd.(*RRRS*-)] which is not shared by [Gd.(*RSRS*-)] is the freezing of arm rotation. This reduced motion renders these complexes more rigid (and hence more inert) than the other isomer. Since the donor atoms exhibit less motion relative to the gadolinium(III) ion in the [Gd.(*RRRR*-)] and [Gd.(*RRRS*-)] isomer, the unpaired electrons of the gadolinium may experience less perturbation from those in the donor atoms. If this perturbation were the cause of the electron relaxation then clearly a longer electronic relaxation time would be expected for those isomers with least internal motion, ie. [Gd.(*RRRR*-)] and [Gd.(*RRRS*-)]. The value of τ_{S0} may then be related to the rigidity of the chelate. Attempts to relate it to the symmetry of the complex clearly have no foundation.

Macromolecular Gadolinium(III) Complexes

The reason for introducing the substituents in these gadolinium complexes was to enable the paramagnetic centre to be secured at the centre of a slowly tumbling macromolecular structure. In order to obtain a clear picture of the effect of increasing the mass of the complex, it was thought appropriate to synthesise a monodisperse macromolecular gadolinium complex. In order to increase the mass sufficiently to realise significant gains in relaxivity,

substituents of molecular mass greater than 1000 Daltons were required. A derivatised β-cyclodextrin was chosen. Permethyl monoamino β-cyclodextrin **34** was synthesised by Phillip Skinner utilising the methods of Chen *et al.*[34] An EDC mediated coupling reaction was then performed with a racemic sample of the gadolinium complex, [Gd.**26**] in water (Scheme 2.6). The lower-molecular weight reaction by-products were then removed by dialysis through a semi-permeable membrane with a molecular weight cut-off of 2000.

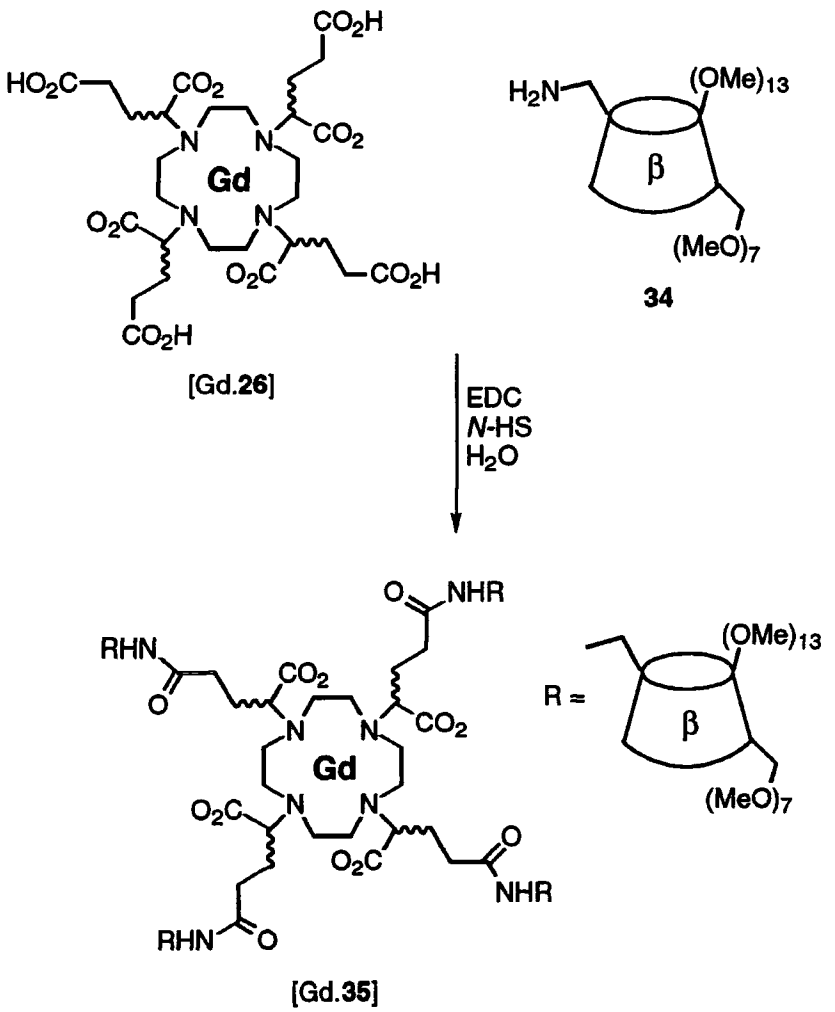

Scheme 2.6 The synthesis of the macromolecular gadolinium(III) β-cyclodextrin conjugate **35** with a molecular weight ~ 6500.

The NMRD profiles at 15 and 39°C and ^{17}O VT profile of this macromolecular complex were then recorded, (Figures 2.36 and 2.37).

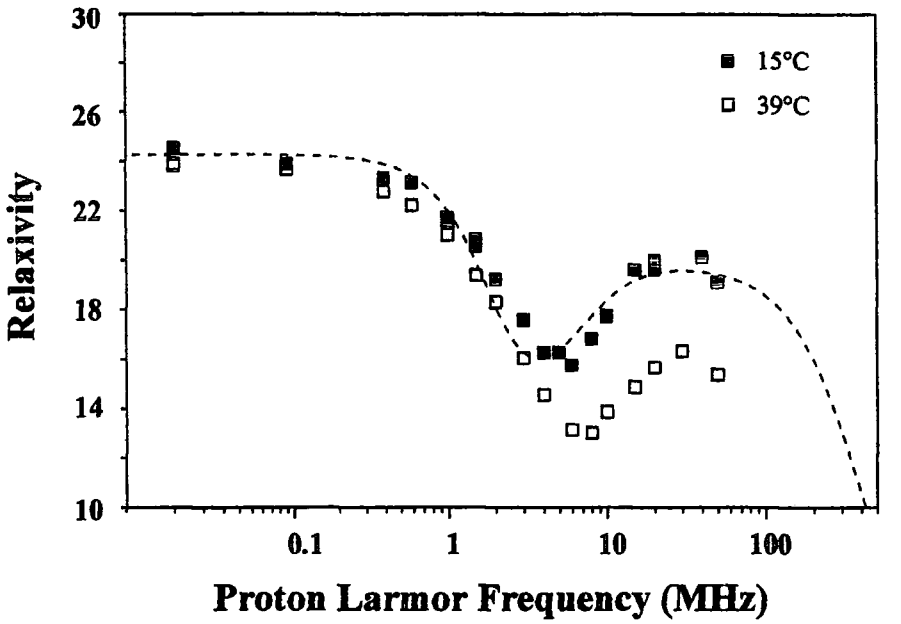

Figure 2.36 NMRD profile for [Gd.35]

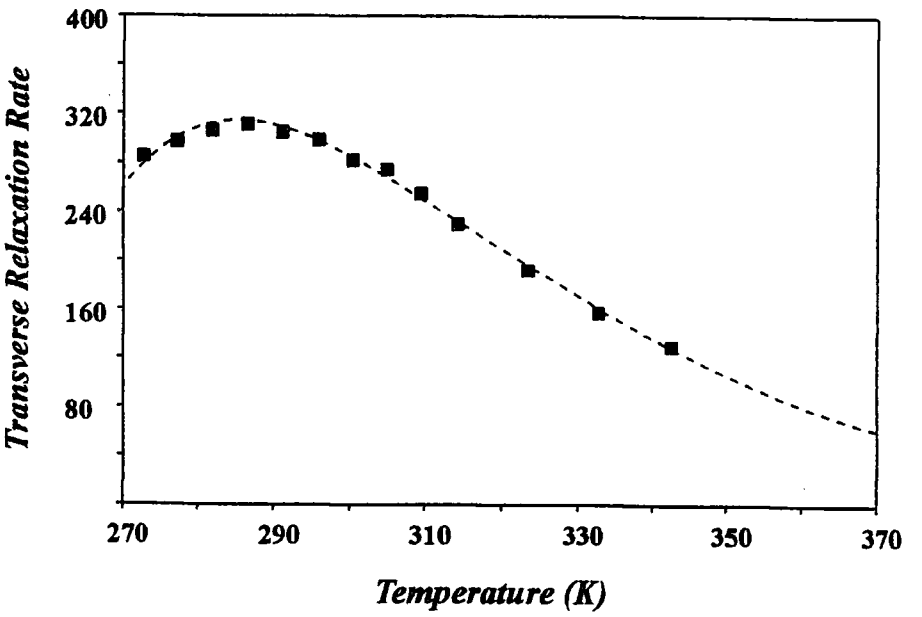

Figure 2.37 ^{17}O Profile for [Gd.35]

The most important aspect of these results is the high field (5 - 50 MHz) region of the NMRD profiles. This is similar to the fields used in clinical imaging, which are typically (20 - 50 MHz). For small chelates this region of the profile is also controlled by the value of τ_R. By increasing the value of τ_R the effect of the reorientational correlation time is diminished according to Eqn 2.2 - 2.4.

$$R_1 = \frac{[C]q}{55.6}\left(\frac{1}{T_{1M} + \tau_M}\right) \tag{2.2}$$

$$T_{1M} = \frac{2/15 S(S+1)g^2\beta^2\gamma_I^2}{r^6}\left\{\frac{7\tau_C}{\left(1+\omega_S^2\tau_C^2\right)} + \frac{3\tau_C}{\left(1+\omega_I^2\tau_C^2\right)}\right\} + \frac{2}{3}\frac{A^2}{\hbar^2}S(S+1)\left\{\frac{\tau_S}{\left(1+\omega_S^2\tau_S^2\right)}\right\} \tag{2.3}$$

$$\frac{1}{\tau_C} = \frac{1}{\tau_S} + \frac{1}{\tau_R} + \frac{1}{\tau_M} \tag{2.4}$$

An increase in relaxivity is expected in this region for larger chelates. Indeed a characteristic hump in the region 5 - 100 MHz is observed indicating a longer τ_R. From the fitting of the profile at 15°C, a value of 414 ps is obtained for τ_R. The parameters obtained from the fitting procedure at 15°C are shown in Table 2.8.

Parameter	Value at 15°C
τ_{S0}	200 ps
τ_V	47 ps
τ_R	414 ps
τ_M	98 ns

Table 2.8 The best fitting parameters for [Gd.**35**] at 15°C

Since the chelate is a mixture of stereoisomers the values obtained are averaged over the four isomers present. The values of τ_M and τ_{S0} are not significantly affected by the increase in mass. In contrast τ_R and τ_V are significantly increased by the increase. The increase in τ_R was the intentional result of appending the β-cyclodextrin derivatives. The value of τ_V, however is also likely to increase with increasing size, since it is dependent upon the rate of collision of the chelate. The addition of the β-cyclodextrin derivatives to the chelate will reduce the sensitivity of the gadolinium centre to collision, resulting in an increase in τ_V.

Although there is a substantial increase in the relaxivity at imaging fields (R_1 = 15 $mM^{-1}s^{-1}$ at 39°C and 20MHz) this increase is not as high as might have been expected. An extrapolation of a comparison of relaxivity against molecular weight for a number of smaller gadolinium chelates reveals that further increases in relaxivity may yet be possible (Figure 2.38). The

gadolinium(III) β-cyclodextrin conjugate **35** has a molecular mass of over 6000 and thus relaxivities in the region of 35 - 45 mM^{-1} s^{-1} may be predicted.

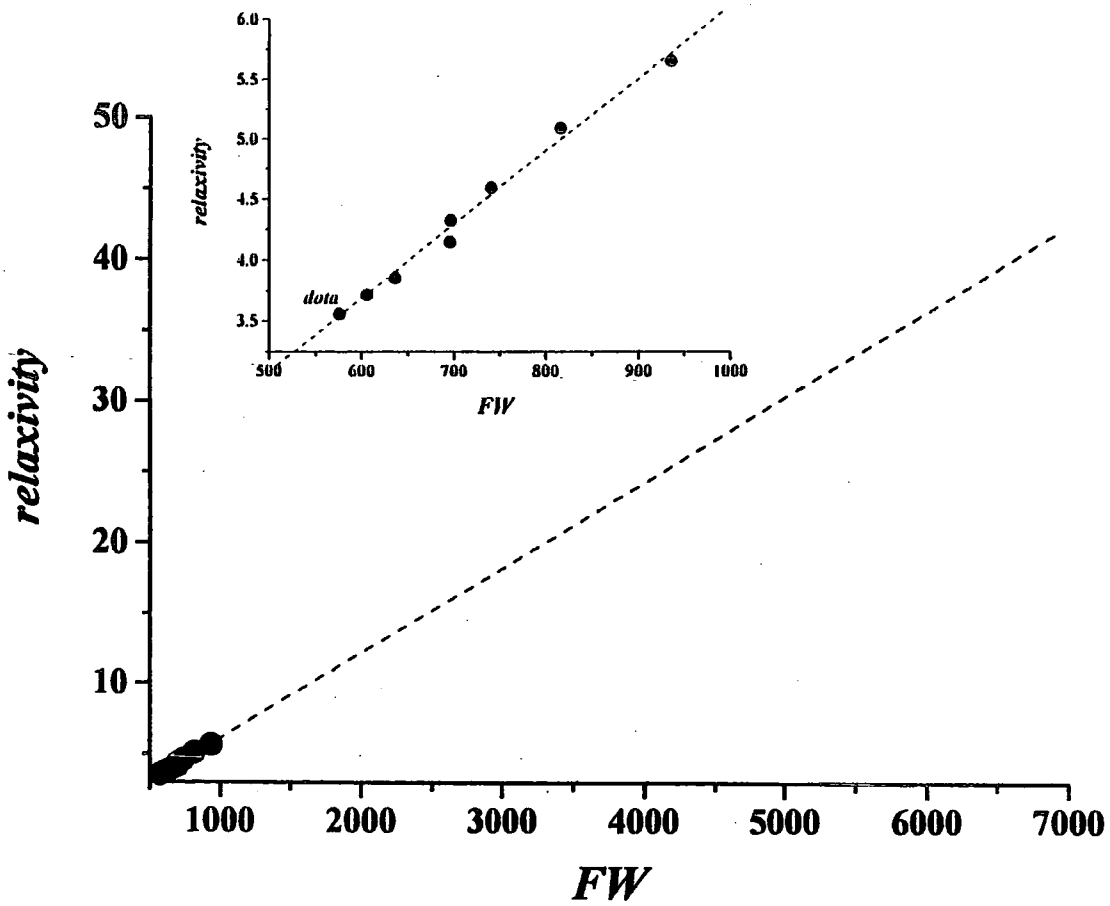

Figure 2.38 A plot of relaxivity versus molecular weight for a series of small gadolinium(III) chelates, extrapolated to higher masses predicts large gains in relaxivity.

It is important to consider why [Gd.**35**] does not exhibit the relaxivity of around 40 $mM^{-1}s^{-1}$ predicted. It has been shown that when τ_R ceases to limit the relaxivity at high field then the water exchange rate becomes limiting.[32] Since the macromolecular chelate [Gd.**35**] is a mixture of stereoisomers and each isomer exhibits a different water exchange rate, each isomeric form of the chelate will contribute to the observed relaxivity with the more abundant (*RRRS*-) isomer predominating. It is important therefore to use only a chelate with a fast water exchange rate, ie. the (*RRRR*-) isomer, at the centre of the macromolecular array.

Comparison of the proton relaxation rate of the macromolecular gadolinium(III) chelate [Gd.**35**] and a complex exhibiting a fast water exchange rate, such as [Gd.(*RRRR*-)]shows the limiting behaviour of the two parameters τ_M and τ_R. The proton relaxation rates, as a function of temperature, are shown for these two complexes at 20 MHz (Figure 2.39)

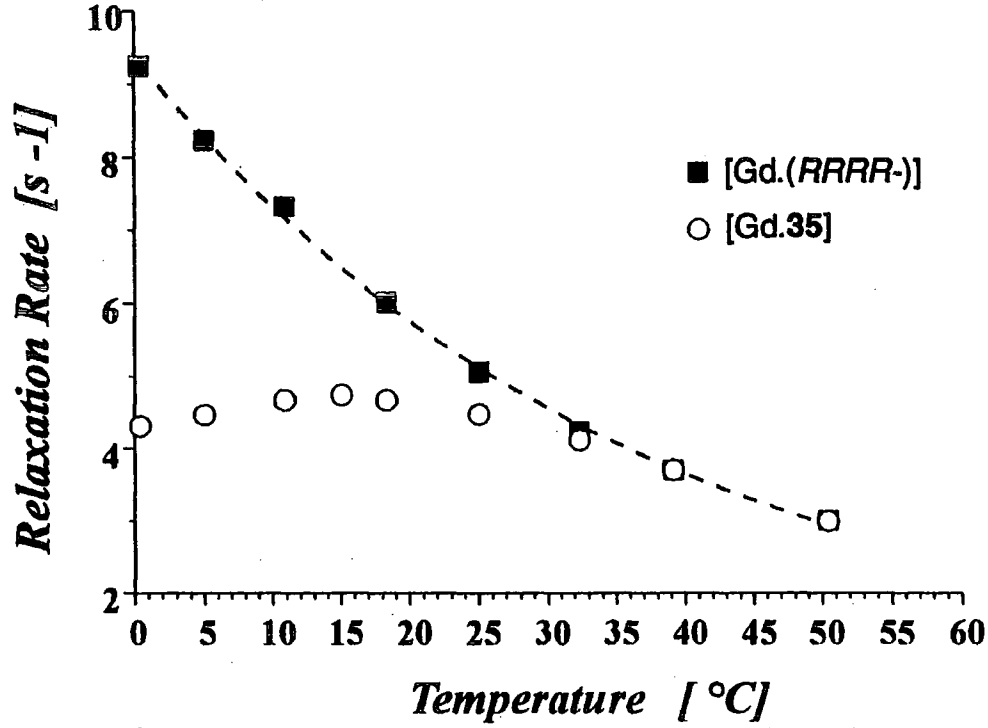

Figure 2.39 The longitudinal relaxation rate of the 'fast exchange' complex [Gd.(*RRRR*-)] and the macromolecular chelate [Gd.**35**] as a function of temperature at 20 MHz.

The reorientational correlation time becomes longer at lower temperatures. As a result the limiting effect of τ_R upon relaxivity is reduced as the temperature is dropped. In the case of a small gadolinium(III) chelate, with a fast water exchange rate, a continuous increase in relaxivity is observed because τ_M does not become limiting. In the case of the macromolecular chelate [Gd.**35**], the limiting effect of τ_R ceases as the temperature drops and the proton relaxation rate becomes limited by τ_M. Because τ_M is not sufficiently fast, the relaxivity does not increase as the temperature continues to drop and the profile remains much flatter.

One other feature, which may limit the relaxivity is the value of τ_R. If the motion of the gadolinium(III) ion, and the associated water molecule, is not efficiently coupled to the motion of the whole tetra-β-cyclodextrin conjugate then τ_R will not be maximised. Independent rotary motion about a C_2 axis of the conjugate may also occur, this motion may be faster than the overall tumbling motion of the conjugate (Figure 2.40).

In order to optimise the relaxivity gained by increasing the molecular mass of a chelate it is necessary to consider carefully the choice of macromolecule. Clearly compact structures are *not* ideal as this allows certain motions to persist , if at a somewhat reduced rate. Rather a structure which branches outward rapidly, forming a globular complex is likely to be preferred.

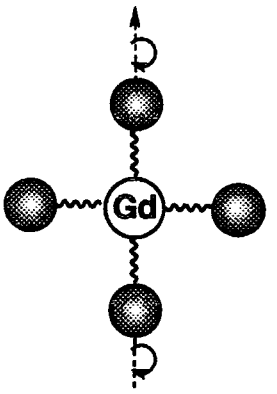

Figure 2.40 A gadolinium(III) chelate secured by point masses does not ensure effective coupling to the slow molecular motion of the macromolecule.

2.6. Conclusions

Very different proton relaxation behaviour is observed for diastereoisomeric gadolinium(III) complexes of tetrasubsubstituted DOTA derivatives such as **26**. The relaxation catalysis occurs *via* both an inner and an outer sphere mechanism. Since the catalysis of this relaxation is a dynamic process, the structural and dynamic properties of each isomer affect the efficiency of the catalysis.

To probe the structure and dynamics of each isomer the europium(III) complexes of each isomer were studied. The emission spectra of the four diastereoisomeric complexes reveal that the co-ordination environment of the europium(III) ion is similar in each of the four complexes. The hydration state, q of each isomer in solution was determined to be one by Horrocks' method. However, the preferred co-ordination geometry of the four isomers varies considerably. [Eu.(*RRRR*-)] exhibits a clear preference for a twisted square antiprismatic geometry over a square antiprism (a ratio of 4:1 was measured by ^{1}H NMR). As the number of juxtaposing chiral centres in the complex increases this preference changes. [Eu.(*RRRS*-)] favours the square antiprism 2:1, and [Eu.(*RSRS*-)] the square antiprism by 4:1. The [Eu.(*RRSS*-)] complex is notable in that only the square antiprismatic geometry could be observed in the ^{1}H NMR spectrum.

The rates of ring inversion and arm rotation, which may interconvert the two co-ordination isomers must be slow in this complex. In the case of [Eu.(*RSRS*-)] both ring inversion and arm rotation may be observed on the NMR timescale at room temperature. The ratio of the two co-ordination isomers (which are also related as enantiomeric pairs) and the rates of

interconversion resemble those observed with [Eu.DOTA]$^-$. It is not surprising therefore to observe that the proton relaxation behaviour of the [Gd.(*RSRS*-)] complex mirrors that observed for [Gd.DOTA]$^-$. The [Eu.(*RRRR*-)] and [Eu.(*RRRS*-)] complexes undergo ring inversion at a rate of ~45 ± 15 s^{-1} at room temperature. In contrast, the rate of arm rotation is very much slower, by at least two orders of magnitude. This effective locking of the pendant arm orientation is the result of the acetate substituents. The configuration of the chiral centre determines the sense in which the arms orientate in these two complexes, Δ for an (*S*) configuration and Λ for an (*R*) configuration. This can be seen most clearly in the crystal structure of [Eu.(*RRRR*-)] which surprisingly adopts a square antiprismatic co-ordination geometry in which the arms lie in a Λ orientation. The [Gd.(*RRRR*-)] and [Gd.(*RRRS*-)] complexes exhibit quite different proton relaxation behaviour to that observed for [Gd.(*RSRS*-)] and [Gd.DOTA]$^-$. The values of τ_{S0} for each complex are very different. Longer values are obtained for the [Gd.(*RRRR*-)] and [Gd.(*RRRS*-)] complexes, which also exhibit less intramolecular motion, suggesting that this hitherto unexplained parameter is strongly related to the rigidity and dynamics of a complex. More importantly, in terms of imaging applications, the values of τ_M obtained vary substantially from complex to complex. The values of τ_M show a strong dependence upon the proportion of the complex adopting a twisted square antiprismatic geometry.

Studies of a number of [Ln.(*RRRR*-)] complexes show that the hydration state of the complex, as determined by luminescence, changes dramatically on passing to the heavier lanthanide(III) ions. This appears to be a consequence of changes in the twisted square antiprismatic geometry. The square antiprismatic geometry observed in the crystal structures of [Eu.(*RRRR*-)], [Gd.(*RRRR*-)] and [Tb.(*RRRR*-)] shows little variation in the lanthanide-water bond distances, all three complexes possessing one co-ordinated water molecule. It is proposed therefore that the twisted square antiprismatic geometry begins to crowd the water binding site of the [Ln.(*RRRR*-)] complex after the 'gadolinium break'. Thus the water molecule is pushed away from the lanthanide ion, and the effective quenching of the lanthanide(III) ion by OH oscillators is reduced, reducing the observed value of *q*. Eventually the water molecule is pushed so far off the lanthanide(III) ion that the complex dissociates, hence the observation in the preliminary solution to the crystal structure of [Yb.(*RRRR*-)] that there is no directly bound water molecule. This steric crowding of the co-ordinated water molecule in the twisted square antiprism increases the rate of dissociation and since water exchange must

occur through a dissociative mechanism, so the rate of water exchange is increased.

The rate of water exchange becomes important as the rotational correlation time becomes longer. In the gadolinium(III) β-cyclodextrin conjugate **35**, an increase in relaxivity at imaging fields is observed. This increase is the result of reducing the rate at which the gadolinium(III) ion and the associated water tumble in solution. However, the magnitude of this increase may be limited by the water exchange rate. It is important therefore to have the (*RRRR*-) isomer at the centre of the macromolecular array in order to harness the faster water exchange rate of this isomer. The [Gd.(*RRRR*-)] complex may be synthesised from a mixture of isomers of **26** by performing the reaction at low pH from the corresponding oxide as a suspension in water.

2.7. References

1 Brittain, H.G.; Desreux, J.F.; *Inorg. Chem.*, (1984), **23**, 4459.

2 Horrocks W. DeW. Jr.; Sudnick, D.R.; *J. Am. Chem. Soc.*, (1979), **101**, 334.

3 Seri, S.; Hashiguchi, Y.; Kubomura, K.; Abe, Y.; Iguchi, T.; Iwai, K.; Watanabe. T.; *Nippon Kagaku Kaishi,*. (1993), **5**, 528.

4 Chen, D.F.; Jin, T.Z.; *Chem. J. Chinese Univ.*, (1996), **17**, 1179.

5 Kang, S.I.; Ranganathan, R.S.; Emswiler, J.E.; Kumar, K.; Gougoutas, J.Z.; Malley, M.F.; Tweedle, M.F.; *Inorg Chem.*, (1993), **32**, 2912.

6 Tweedle, M.F.; Shukla, R.; Weber, R.; Zhang, X.; *Abstracts from the COST D1 Meeting*, The Hague, 17-20 October 1996.

7 Aime, S.; Botta, M.; Ermondi, G.; Fedeli, F.; Uggeri, F.; *Inorg. Chem.*, (1992), **31**, 1100

8 Kumar, K.; Tweedle, M.F.; *Inorg. Chem.*, (1993), **32**, 4193.

9 Effenberger, F.; Burkard, U.; Willfarht, J.; *Angew. Chem. Int. Ed. (Engl.)*, (1983), **22**, 65

10 Effenberger, F.; Burkard, U.; Willfarht, J.; *Liebigs. Ann. Chem*, (1986), 314

11 Kumar, K.; Tianzhu, J.; Xiangyun, W.; Desreux, J.F.; Tweedle, M.F.; *Inorg. Chem.*, (1994), **33**, 3823.

12 Dickins, R.S.; Parker, D.; de Sousa, A.S.; Williams, J.A.G.; *J. Chem. Soc. Chem. Commun.*, (1996), **36**, 697.

13 Norman, T.J.; *PhD Thesis*, University of Durham, 1994.

14 Henceforth the isomers are referred to as (*RRRR*-), (*RRRS*-), (*RRSS*-) and (*RSRS*-)

15 Dale, J.; *Acta Chem. Scand.*, (1973), **27**, 1115.
Dale, J.; *Top. Stereochem.*, (1976), **9**, 199.

Dale, J.; *Isr. J. Chem.*, (1980), **87**, 1070.

16 Aime, S.; Botta, M.; Ermondi, G.; *Inorg. Chem.*, (1992), **31**, 4291.

17 Bunzli, J-C.G.; In *"Lanthanide Probes in Life, Chemical and Earth Sciences"*, Eds. Bunzli, J-C.G.; Choppin, G.R., Elsevier, Amsterdam, (1989), Chapter 7.

18 A sample of Eu.DOTA was prepared by the author using methods published by Kumar, K.; Chang, C.A.; Francesoni, L.C.; Dischino, D.D.; Malley, M.F.; Gougoutas, J.Z.; Tweedle, M.F.; *Inorg. Chem.*, (1994), **33**, 3567. X-ray quality crystals were grown from acidfied aqueous solution. The corresponding europium(III) complex was synthesised from the nitrate in aquaoues solution at pH 5.5.

19 Aime, S.; Botta, M,; Ermondi, G.; *Inorg. Chem.*, (1992), **31**, 4291.

20 Jacques, V.; Desreux, J.F.; *Inorg. Chem.*, (1994), **33**, 4048.

21 Hoeft, S.; Roth, K.; *Chem. Ber*, (1993), **126**, 869.

22 Sanders, J.K.M.; Hunter, B.K.; In *"Modern NMR Spectroscopy"*, Oxford University Press, Oxford, (1988), 224.

23 Horrocks W.de W.Jr.; Sudnick, D.R.; *Acc. Chem. Res.*, (1981), **14**, 384.

24 Jacques, V.; Desreux, J.F.; *Inorg. Chem.*, (1994), **33**, 4048.

25 Geraldes, C.F.G.C.; Merbach, A.E.; Pubanz, D.; Aime, S.; Botta, M.; *J. Alloys Comp.*, (1995), **225**, 303.

26 Aime, S.; Botta, M.; Fasono, M.; Marques, M.P.M.; Geraldes, C.F.G.C.; Pubanz, D.; Merbach, A.E.; *Inorg. Chem.*, (1997), **36**, 2059.

27 Beeby, A.; Dickins. R.S.; Faulkner, S.; Parker, D.; Williams, J.A.G.; *J. Chem. Soc. Chem. Commun.*, (1997), **37**, 1401.

28 Aime, S.; Botta, M.; Parker, D.; Williams, J.A.G.; *J. Chem. Soc., Dalton Trans.*, (1996), 17.

29 Sherry, A.D.; Brown, R.D.; Geraldes, C.F.C.G.; Koenig, S.H.; Kuan, K-T.; Spiller, M.; *Inorg. Chem.*, (1989), **28**, 620.

30 Aime, S.; Barge, A.; Botta, M.; Parker, D.; de Sousa, A.S.; *J. Am. Chem. Soc.*, (1996), **119**, 4767.

31 Aime, S.; Botta, M.; Personal communication.

32 Aime, S.; Botta, M.; Fasano, M.; Terreno, E.; *Chem. Soc. Rev.*, (1998), **27**, 19.

33 Pubanz, D.; *PhD Thesis*, University of Lausanne, (1997).

34 Chen, Z.; Bradshaw, J.S.; Lee, M.L.; *Tetrahedron. Lett.*, (1996), **37**, 6831.

Chapter Three

Substituted DO3A Derivatives

3.1. Introduction

The gadolinium complex of the triacetate substituted cyclen derivative DO3A **7** has received a certain amount of attention as a consequence of its possible application as a contrast agent. It is a heptadentate ligand, therefore in its neutral gadolinium(III) complex, there are expected to be two bound water molecules leading to a larger relaxivity than the corresponding $q = 1$ complexes such as [Gd.DOTA]$^-$. The [Ln.DO3A] complexes, although relatively stable, do not exhibit sufficient kinetic inertness for their safe use *in vivo*. The more rigid chelate, DO3MA **8**, forms a complex with gadolinium which is much less prone to dissociation.[1] The potential increases in relaxivity that may be expected to arise from an increase in hydration state render this class of compound an interesting group for study.

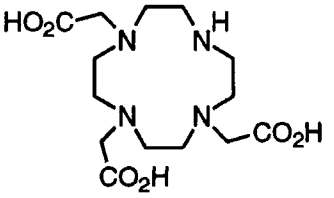

7
DO3A

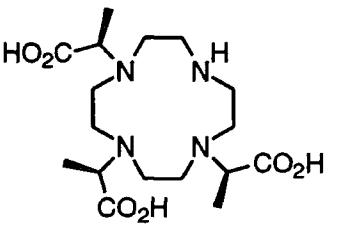

8
DO3MA

Since one of the four nitrogens in the cyclen ring must remain unsubstituted, the synthesis of these triacetate based ligands is less straightforward than that of DOTA or its derivatives.

Strategies for the Synthesis of DO3A Derivatives

Ostensibly, two methods for the mono-protection of cyclen have been developed. The first is a variation on the 1,7-*trans*-ditosylation procedure developed by Desreux,[2] which relied upon the steric demands of the tosyl group and the difference in pK_a of the ring amines to allow selective protection of two of the nitrogens. When equimolar quantities of *p*-methoxytoluenesulfonyl chloride and cyclen are reacted in dichloromethane with triethylamine as a base then the mono-protection of cyclen may be achieved.[3] Although further purification is required, the yields of this reaction are generally good, and typically greater than 70%.

The remaining three nitrogens may then be alkylated under standard conditions before the protecting group is removed. This can be achieved under a variety of conditions, such as HBr in acetic acid,[4] although the use of sodium in liquid ammonia is often favoured.

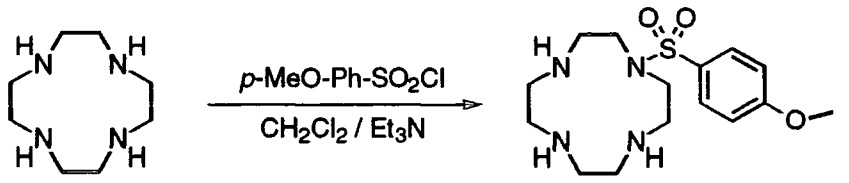

5 36

Scheme 3.1 The mono-arylsulfonylation of cyclen.

Atkins developed a method for the mono functionalisation of cyclen by formation of 1,4,7,10-tetraazatricyclo[5.5.1.0]tridecane **37**.[5] The more robust nature of this reaction makes it more applicable to industrial application. Tweedle subsequently showed that partial hydrolysis of the tricycle **37** yielded 1-formyl cyclen **38**, hence facilitating mono-protection of cyclen.[6] This highly efficient method of protecting cyclen was chosen by Tweedle for the synthesis of DO3MA **8**.[7]

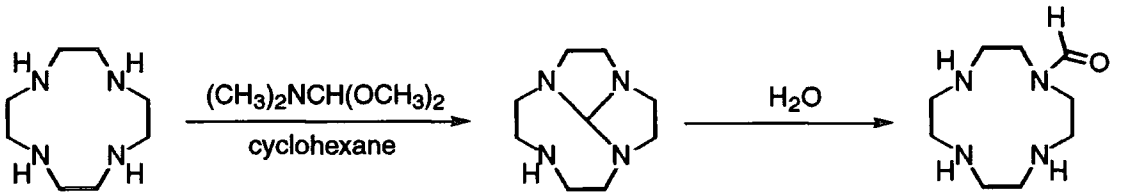

5 37 38

Scheme 3.2 The mono-*N*-formylation of cyclen proceeds in almost quantitative yield.

Once again standard conditions may be used to add the carboxymethyl groups to the mono-formyl cyclen **38**. The formyl protecting group can be removed under mild acidic conditions, thereby enabling concomitant removal of the formyl and acetate protecting groups, such as *tert*-butyl esters, to be achieved.

3.2. Synthesis of Tri(carboxyethyl) DO3A

The serendipitous discovery that cyclen could be selectively alkylated three or four times depending upon the nature of the base employed (Chapter 2.2), suggested a facile synthetic route to DO3A **7**, and its substituted derivatives. Since C-substitution of the carboxymethyl groups has been shown to render such compounds more stable than their unsubstituted counterparts, their viability as potential contrast agents is enhanced.[1]

The use of highly moisture sensitive reactions, as are required for the synthesis and use of triflates, is generally avoided in industrial processes. Thus a substitute for the reaction of the triflate of diethyl malate **21** with cyclen **5**

(Scheme 2.3) had to be found. As this substitution reaction did not proceed with complete inversion of configuration, leading to a mixture of diastereoisomers, racemic dimethyl α-bromoglutarate **27** was employed. The reaction of dimethyl α-bromoglutarate **27** with cyclen **5** in acetonitrile is much more rapid than that of the triflate **21**. When triethylamine was used as a base in this reaction, a significant quantity of the tetraalkylated cyclen **24** was obtained. The use of a substantially weaker base might be expected to increase the selectivity of the reaction. This hypothesis was supported by Pillia's use of sodium hydrogen carbonate to selectively trialkylate cyclen in the preparation of DO3A derivatives.[8] When sodium hydrogen carbonate was employed as a base, in the presence of 4Å molecular sieves, the rate of reaction dropped dramatically. After one week, the reaction was still not complete, but gentle warming to 50°C for 2 days increased the rate sufficiently to allow formation of reasonable quantities (33%) of the desired trialkylated cyclen **39** (Scheme 3.3). The tetraalkylated product was still formed, but was easily separated by column chromatography.

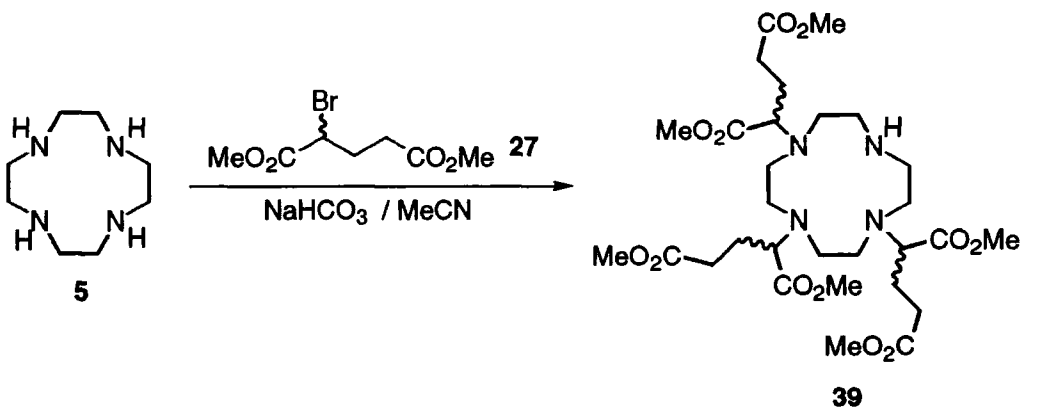

5 39

Scheme 3.3 Synthesis of **39** from cyclen **5** and dimethyl α-bromoglutarate **27**.

Purification of the trialkylated cyclen **39** was performed over silica gel eluting with an ammonia solution in tetrahydrofuran, with methanol and dichloromethane. This method of separation was used in preference to chromatography over alumina, and gave an improved separation.

The Complexation of Lanthanide(III) Ions with DO3A Derivatives.

The hydrolysis of the methyl esters of **39** initially proved problematic. Acid catalysed hydrolysis proved remarkably ineffectual. Heating under reflux in 6M hydrochloric acid led to the formation of an insoluble precipitate. On the other hand, the purification of the organic insoluble ligand proved troublesome after base catalysed hydrolysis. In the light of these difficulties, alternative

In each spectrum the hypersensitive $\Delta J = 2$ band is significantly more intense than the magnetic dipole allowed $\Delta J = 1$ transition. This is a clear indication that each complex adopts a similar coordination geometry and experiences a ligand field of approximately the same symmetry. Although there may be much more information to be gained from a more detailed analysis of these spectra, the limitations of our current understanding do not allow any further conclusions to be drawn.[11]

NMR Studies

Proton NMR spectroscopy has proved a useful probe into the structural and dynamic properties of lanthanide(III) complexes.[12] In particular, its application to the well defined complexes of polyamino-carboxylate ligands has been particularly enlightening.[13] The complexes of ligands derived from DO3A have received much less attention than their counterpart with four pendant arms. This is primarily because their use *in vivo* is restricted by their lability to acid catalysed dissociation.

In contrast to the rigid, well-defined coordination geometries adopted by the lanthanide(III) complexes of cyclen derivatives appended with four ligating arms, the coordination geometries adopted by heptaco-ordinate complexes are less well defined. Three coordination geometries may exist in the complexes of such 7-coordinate ligands.

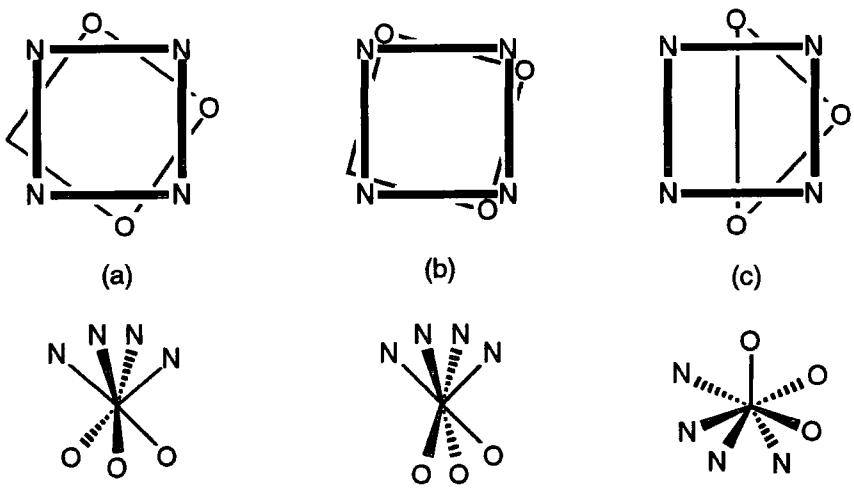

Figure 3.2 The three possible coordination geometries of Ln.DO3A based complexes (a) the pseudo-square antiprism, (b) the psuedo-twisted square antiprism and (c) the mono-capped octahedron.

These may be considered to approximate to a psuedo-square antiprism (Figure 3.2a), a psuedo twisted square antiprism (Figure 3.2b), and what may be considered either as a bi-capped trigonal bipyramid or a mono-capped octahedron. (Figure 3.2c). However, all three structures may also be considered to be distorted bi-capped trigonal bipyramids and so distinguishing one from another is likely to be difficult. It is reasonable to expect that a complex will interconvert freely between these geometries by means of ring inversion and arm rotation. The ^{1}H NMR spectra recorded at room temperature, (Figure 3.3) confirms this.

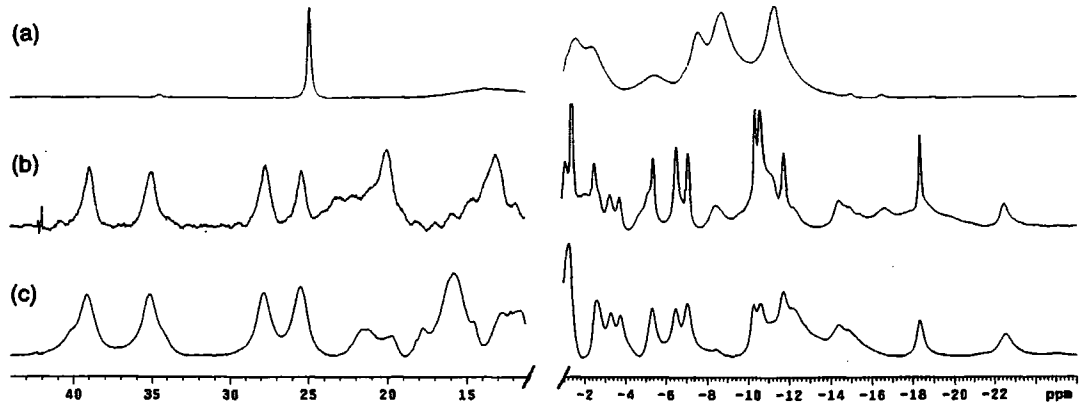

Figure 3.3 Extended sweep width ^{1}H NMR spectra of (a) [Eu.DO3A] (b) [Eu.**41**] and (c) [Eu.**40**], recorded at 200 MHz, 294K.

The spectrum of each complex revealed broad peaks which characterise a system that is in intermediate exchange on the NMR timescale. In an attempt to elicit more information about the structure of the complexes in solution, the NMR spectra were also recorded at 273K (Figure 3.4).

In the case of [Eu.**40**] the spectrum is further complicated by the presence of three diastereoisomers of the complex. However, at 273K (Figure 3.4c) the lines are much sharper and it is clear that the signals cannot be assigned to a given coordination geometry. It is worth noting the similarity between this spectrum and that of [Eu.**41**], (Figure 3.4b). This latter spectrum is marginally less complex because of the lack of stereoisomers in the ligand. Again the signals may not be assigned with confidence to a particular proton in a particular coordination geometry. The spectrum of [Eu.DO3A] (Figure 3.4a) is notable in two respects. Firstly, the spectral width is much narrower than those of the other two complexes. Secondly, at 273K it is similar in form to those of the other two complexes at room temperature. This complex is evidently undergoing more rapid exchange and the distinction of coordination isomers is therefore impossible.

Although a tentative assignment of some of the peaks in the spectra can be made, in particular those between 35 and 45 ppm in the spectra of Eu.MeDO3A and Eu.g-DO3A (axial protons in a pseudo-square antiprismatic arrangement), in general the spectra are too complex for a complete assignment to be performed.

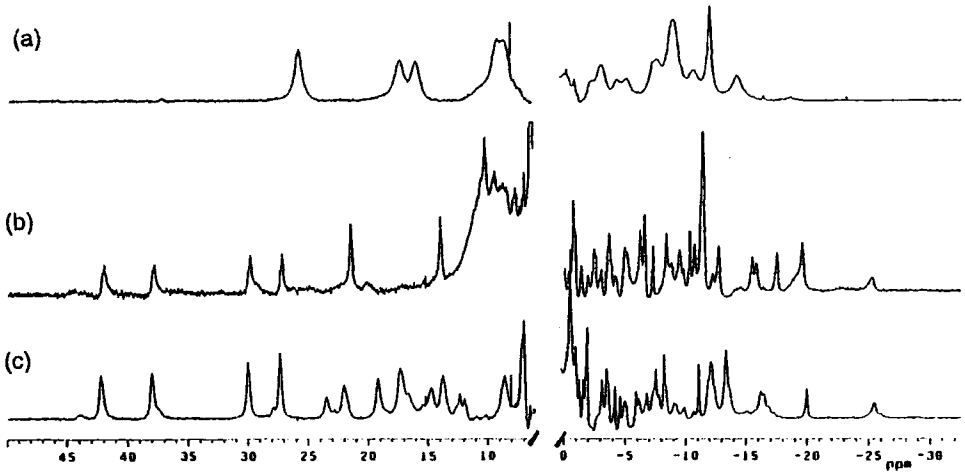

Figure 3.4 Low temperature (273K), extended sweep width ^{1}H NMR spectra of (a) [Eu.DO3A] (b) [Eu.**41**] and (c) [Eu.**40**].

It is clear from comparison of the spectra at 21 and 0°C that all three complexes undergo rapid exchange between different co-ordination isomers at room temperature. However, the complex of DO3A is far more fluxional that those of **40** and **41**, exhibiting relatively broad resonances even at 0°C. It would appear that the inclusion of substituents on the acetates or on the free nitrogen imparts a degree of rigidity upon the complex, reducing the rate of arm rotation in the complex.

The Hydration State, q.

The hydration state of each of the three europium(III) complexes was measured by Horrocks' method.[14] The results are summarised (Table 3.1).

The measured value of q for each of the three europium(III) complexes is slightly lower than the expected value of two. However, the values are much higher than would be expected for a complex in which the lanthanide luminescence is quenched by only one coordinated water molecule. The values obtained may be understood in terms of a situation in which there are two water molecules close to the metal centre, each of which contributes differently to the quenching of luminescence. Two models may be proposed which may account for such a situation.

	τ_{H_2O}/ms	τ_{D_2O}/ms	q
[Eu.DO3A]	0.44	1.9	1.8 ± 0.2
[Eu.**40**]	0.44	1.9	1.8 ± 0.2
[Eu.**41**]	0.42	1.3	1.7 ± 0.2

Table 3.1 The hydration states for the europium complexes of the three heptadentate ligands.

As the lanthanide(III) ions decrease in ionic radius across the series, the coordination number of the aqua ion decreases from 9 to 8 at gadolinium.[15] It is generally accepted that the europium(III) aqua ion exists in solution as a mixture of both eight and nine co-ordinate species, albeit in rapid exchange.[16] It is possible then that the use of a heptadentate ligand does not, in fact, vacate two co-ordination sites on the lanthanide(III) ion and only one site is then occupied by a water molecule, i.e. the europium exists as an eight co-ordinate ion with only one bound molecule. A second water molecule binds close to the metal centre in a second coordination sphere. The situation depicted in Figure 3.5 may thereby be envisaged.

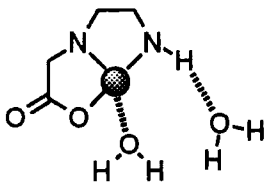

Figure 3.5 A schemetic representation of a lanthanide(III) DO3A complex with one inner sphere and one second sphere water molecules.

Since the water molecule in the second coordination sphere is much further from the lanthanide(III) ion than the bound water molecule, its effectiveness at quenching europium(III) luminescence is reduced. Hence the fractional value of q. If this model was correct then an integral value of q would be expected for a compound in which the hydrogen bond donor giving rise to this second coordination sphere was removed. The methylation of the remaining secondary amine in the cyclen ring allows the removal of this hydrogen bond donor. The hydration state of the complex [Eu.**41**] does not vary within experimental error from that observed in the other two complexes.

It seems unlikely therefore that this model provides an accurate picture of the local hydration state of the lanthanide(III) ion in these complexes.

The second model involves the co-ordination of two water molecules in the first co-ordination sphere. However, these two water molecules are not equivalent. One is in fast exchange with the bulk solvent. This exchange is a dissociative process and must involve an unsaturated eight co-ordinate complex. In this complex the remaining co-ordinated water molecule will be more strongly bound to the lanthanide and so will not dissociate as readily. This hypothesis is supported by crystallographic data obtained by Desreux *et al.* for the gadolinium complex of ODO3A **47**. The complex [Gd.ODO3A] exhibits an extremely long bond to the water molecule in the apical position, 2.559(7)Å, compared to a distance of 2.447Å for that of the corresponding DOTA complex.[17] The ninth donor atom is provided by the carboxylate of a neighbouring complex molecule which is replaced by a water molecule in solution.

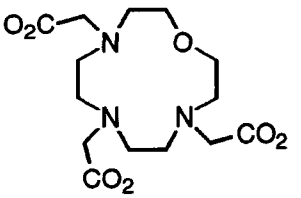

47

ODO3A

The long metal-water bond may reasonably be expected to be weaker and therefore more labile than that of [Gd.DOTA]-. This water molecule may therefore be expected to be in fast exchange. Dissociation of the water-lanthanide complex is only likely to occur from the nine co-ordinate complex. Given that the lifetime of the nine co-ordinate complex is short, because the first water molecule is in fast exchange, the probability of the second water molecule dissociating simultaneously, is very low.

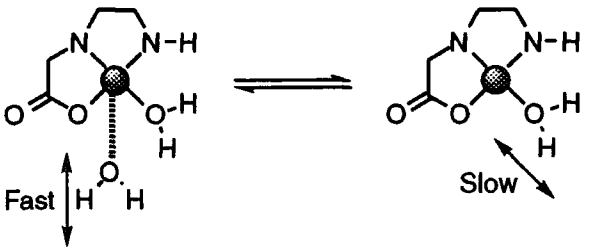

Figure 3.6 A schematic representation of a lanthanide(III) DO3A complex one co-ordinated water molecule is in fast exchange whereas the other remains bound.

Such a situation implies, that when two water molecules are coordinated at a lanthanide centre bound to a heptadentate ligand, one will exhibit fast exchange whilst the other will undergo a much slower rate of water exchange, (Figure 3.6).

The rate of water exchange is an important factor in determining the inner sphere relaxivity of a complex. If one of the two bound water molecules is in slow exchange, then its contribution to the overall relaxivity will be reduced. A study of the relaxivity of [Gd.DO3A] and [Gd.ODO3A] revealed that these complexes do *not* exhibit the relaxivity expected for a $q = 2$ complex under fast exchange conditions.[17] The NMRD profiles of these complexes at 25 and 37°C were compared with the calculated profiles for a hypothesised $q = 2$ DOTA complex (Figure 3.7).

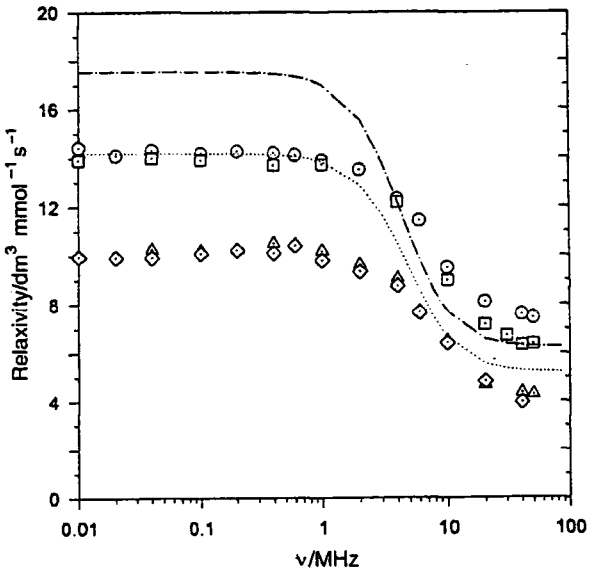

Figure 3.7 NMRD profiles of [Gd.DO3A] (squares, 25°C and triangles, 37°C) and [Gd.ODO3A] (circles, 25°C and diamonds, 37°C). The calculated profiles for [Gd.DOTA]- with a hydration state of two, at 25°C (dashed line) and 37°C (dotted line) are also shown. Reproduced from reference (17).

Neither of these complexes exhibit the relaxivity calculated for a $q = 2$ complex although they do exhibit higher relaxivities than than those of $q = 1$ complexes (Table 3.2)

These observations are entirely consistent with idea that these heptadentate lanthanide(III) chelates are $q = 2$ complexes, but the two water molecules are different. One is tightly bound and does not undergo fast exchange, while the other is less tightly bound and is in rapid exchange with the bulk solvent. The result is that the complexes behave as if they were less than $q = 2$.

Complex	Relaxivity at 20 MHz, 40°C
[Gd.DOTA]$^-$	3.5 $mM^{-1}s^{-1}$
[Gd.DO3A]	4.8 $mM^{-1}s^{-1}$

Table 3.? The relaxivity values of [Gd.DOTA]$^-$and Gd[DO3A].[6]

For these conformationally rigid chelates of gadolinium(III) the application of Solomon - Bloembergen - Morgan theory to the complex as a whole may represent an unjustifiable simplification. In the light of these results it is clear that each water molecule should be considered individually. Since the two water molecules cannot both be in fast exchange in the application of Solomon - Bloembergen - Morgan theory they should be treated such that one is considered to be in slow exchange and the other is in fast exchange. Their respective contributions to the relaxivity may then be summed.

3.4. A Tri-acetate substituted DOTA Derivative

The use of heptadentate chelating agents to produce charge neutral gadolinium(III) complexes does not result in the relaxivity enhancement expected for two water molecules. The accompanying loss of complex stability, particularly with respect to kinetic dissociation, is therefore not offset by the desired increase in relaxivity. Clearly then, a complex in which the secondary amine of **39** was substituted with a further chelating group, would be expected to exhibit greater stability without substantial detriment to the relaxivity. In this manner a number of different gadolinium(III) complexes, related to [Gd.DOTA]$^-$ and [Gd.HP-DO3A], could be secured at the centre of a macromolecular structure by just three linkage points. For the purposes of the present work, addition of an acetate arm to yield a tri-substituted DOTA derivative was considered.

Synthesis

Having already synthesised the substituted DO3A derivative **39** the addition of the remaining acetate was trivial. The nucleophilic substitution of methyl bromoacetate with **48**, in acetonitrile in the presence of caesium carbonate, proceeds to completion, overnight, at room temperature, (Scheme 3.7). The heptamethyl ester **49** was purified over silica gel, eluting with 5%

methanol in dichloromethane. The base hydrolysis of the esters was performed in a 1M solution of lithium hydroxide.

The ligand **50** was obtained from the reaction by elution of the reaction mixture over Dowex 50W cation exchange resin. Eluting with a 12% solution of ammonia afforded the ligand **50** as the corresponding ammonium salt. No further purification was undertaken and the ligand was used directly in complex formation.

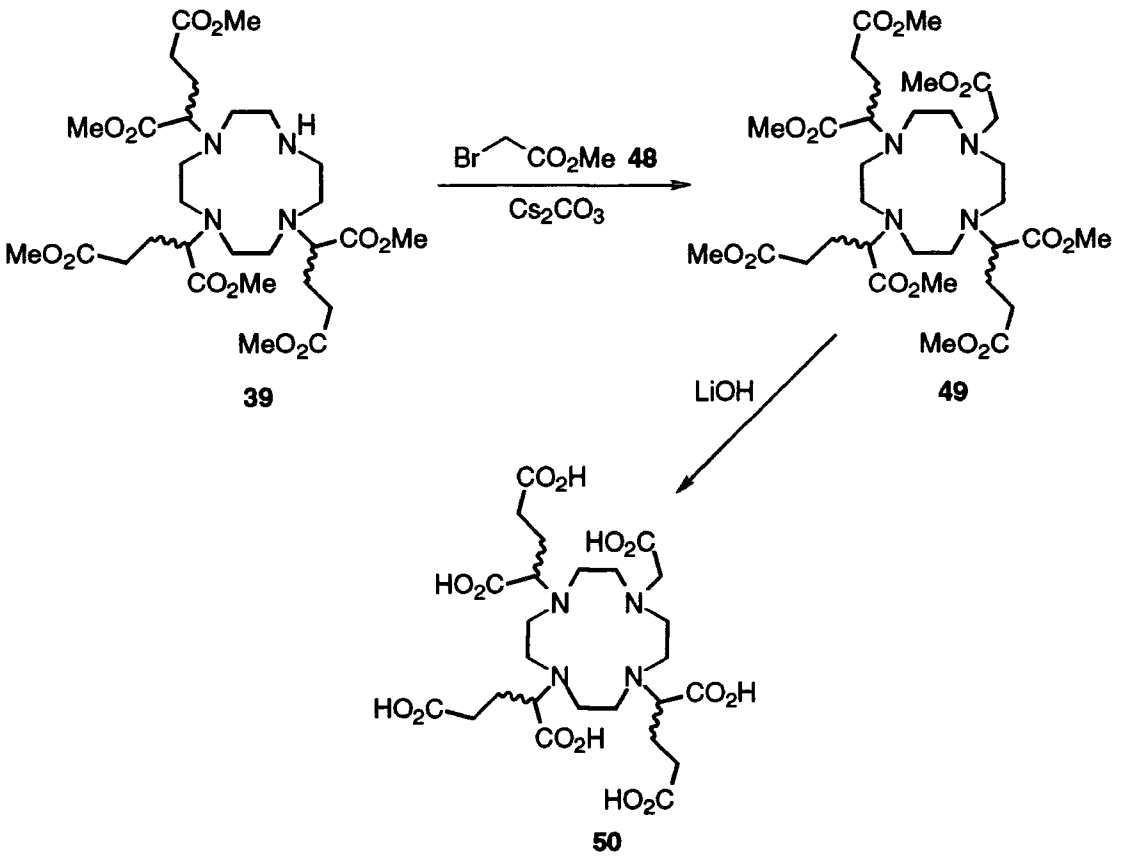

Scheme 3.7 Synthesis of the octadentate ligand **50**.

The Europium(III) Complex of Tri(carboxyethyl) DOTA

The europium(III) complex of **50** was synthesised from the corresponding oxide in aqueous solution, by heating at 90°C for 2 days. The structure of this complex was probed using ^{1}H NMR and luminescence spectroscopy. The emission spectrum of [Eu.**50**] was recorded by direct metal excitation at 397 nm (Figure 3.8).

In contrast to the spectra obtained for [Eu.**39**], the hypersensitive $\Delta J = 2$ band is less intense than the $\Delta J = 1$ band. As a result, the spectrum looks much more like that obtained for [Eu.DOTA]$^-$ and the isomeric complexes of [Eu.**26**]. The proton NMR spectrum (Figure 3.9) is much better resolved than that of

[Eu.39]. The resonances pertaining to the square antiprismatic co-ordination geometry may now be observed.

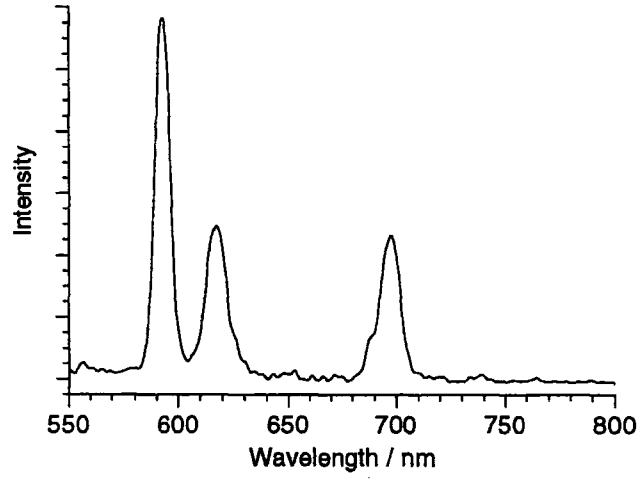

Figure 3.8 The emission spectrum of [Eu.**50**] recorded by direct metal excitation at 397 nm.

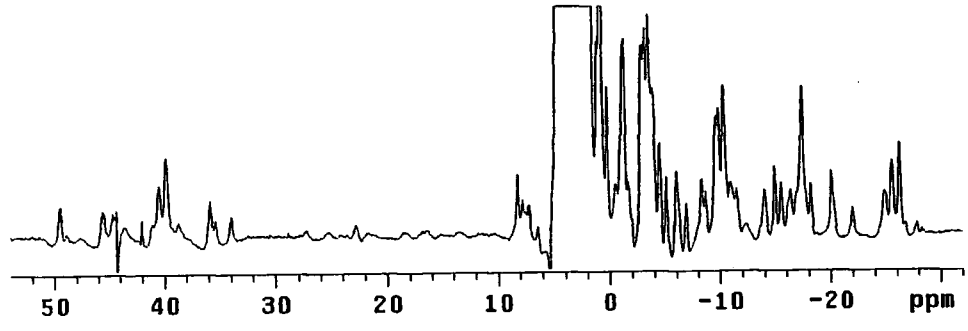

Figure 3.9 1H NMR spectrum of [Eu.**50**] (200MHz, 21°C).

The complex is a mixture of three diastereoisomers, and the spectrum is accordingly difficult to assign. However, it clear that the structure of the complex is similar to that of the corresponding DOTA complex and it is reasonable to assume that the complex is in dynamic exchange between the two limiting co-ordination geometries.

3.5. Conclusions

An increase in the hydration state of the lanthanide(III) ion from one to two may not necessarily lead to a doubling in the inner sphere contribution to the relaxivity of a complex. This study of the three heptadentate ligands DO3A 7 Me-DO3A **41** and **39** has shown that it is likely that two water molecules are bound to the lanthanide(III) ion. However, in these complexes, in terms of both the proton relaxation and luminescence quenching effects the effective hydration state is less than two. This may be explained by considering the

position of the two water molecules. One is tightly bound (~2.44Å) and effectively quenches luminescence. The other is situated further way from the lanthanide(III) ion (~2.55Å) and, as a result of the r^{-6} dependence, quenches the luminescence much less effectively. The rate of exchange of the two water molecules may then also be expected to differ. If the water exchange rate of one water molecule is fast, and dissociation is required to exchange water molecules, then the probability of dissociation of the other water molecule is reduced. This results in a lower than expected relaxivity for these complexes.

Solomon - Bloembergen - Morgan theory tells us that τ_M, the residence lifetime of a water molecule on the complex becomes limiting as τ_R becomes longer. Hence positioning a gadolinium(III) chelate with a slow water exchange rate at the centre of a slowly tumbling system would not be expected to give rise to large increases in relaxivity at higher fields. As a result these heptadentate chelates, when linked to three macromolecular arrays, are not expected to be significantly more effective as contrast agents than their octadentate counterparts.

The addition of a fourth ligating substituent to the complex, is unlikely to have any adverse effect upon the observed relaxivity in a slowly tumbling system. In this work an acetate substituent was added, and the resulting complex was found to adopt a similar solution structure to those observed in [Ln.DOTA]$^-$ complexes. However, the synthesis of this type of complex is much lower yielding than that of [Ln.**26**] and hence is only likely to be employed if a neutral complex were desired, in which case a hydroxypropyl arm could be added. This would, in effect, create a neutral structure at the centre of the macromolecule.

3.6. References

1 Kumar, K.; Chang, C.A.; Tweedle, M.F.; *Inorg. Chem.*, (1993), **32**, 587.
Kumar, K.; Tweedle, M.F.; *Inorg. Chem.*, (1993), **32**, 4193.
Kumar, K.; Jin, T.; Wang, X.; Desreux, J.F.; Tweedle, M.F.; *Inorg. Chem.*, (1994), **33**, 3823.

2 Dumont, A.; Jacques, V.; Quixin, P.; Desreux, J.F.; *Tetrahedron Lett.*, (1994), **35**, 3707.

3 Parker, D.; de Sousa, A.S.; Personal communication.

4 Greene, T.; Wuts, P.G.M.; In *"Protecting Groups in Organic Synthesis"*, 2nd Ed, Wiley and Sons, New York, (1991).

5 Atkins, T.J.; U.S. Patent No. 4 085 106, April 18, (1978).

6 Dischino, D.D.; Delaney. E.J.; Emswiler, J.E.; Gaughan, G.T.; Prasad, J.S.; Srivastava, S.K.; Tweedle, M.F.; *Inorg. Chem.*, (1991), **30**, 1265.

7 Kang, S.I,; Ranganathan, R.S.; Emswiler, J.E.; Kumar, K.; Gougoutas, J.Z.; Malley, M.F.; Tweedle, M.F.; *Inorg. Chem.*, (1993), **32**, 2912.

8 Pillai, R.; Fan, H.; Ranganathan, R.S.; *Abstracts of Papers of the Am. Chem. Soc.*, (1996), 359.

9 Kalesse, M.; Loos, A.; *Bioorg. Med. Chem. Lett.*, (1996), **6**, 2063.

10 Yanouanc, J.; Le Bris, N.; Le Gall, G.; Clément, J-C.; Handel, H.; des Abbayes, H.; *J. Chem. Soc. Chem. Commun.*, (1991), **31**, 206.

11 Bunzli, J-C.G.; In *"Lanthanide Probes in Life, Chemical and Earth Sciences"*, Eds. Bunzli, J-C.G.; Choppin, G.R., Elsevier, Amsterdam, (1989), Chapter 7.

12 Sherry, A.D.; In *"Lanthanide Probes in Life, Chemical and Earth Sciences"*, Eds. Bunzli, J-C.G.; Choppin, G.R., Elsevier, Amsterdam, (1989), Chapter 4.

Eads, C.D.; Mulqueen, P.; Horrocks, W.de W.Jr.; Villafranca, J.J.; *Biochemistry*, (1985), **24**, 1221.

Holz, R.C.; Horrocks, W.de W.Jr.; *J. Magn. Reson.*, (1990), **89**, 627.

13 Jenkins, B.G.; Lauffer, R.B.; *J. Magn. Reson.*, (1988), **80**, 337.

Jenkins, B.G.; Lauffer, R.B.; *Inorg. Chem.*, (1988), **27**, 4730.

Spirlet, M-R.; Rebizant, J.; Dereux, J.F.; Loncin, M-F.; *Inorg Chem.*, (1984), **23**, 359.

Aime, S.; Botta, Ermondi, G.; *Inorg. Chem.*, (1992), **31**, 4291.

14 Horrocks, W.de W.Jr.; Sudnick, D.R.; *J. Am. Chem. Soc.*, (1979), **101**, 334.

Horrocks, W.de W.Jr.; Sudnick, D.R.; *Acc. Chem. Res.*, (1980), **14**, 384.

15 Kowall, T.; Foglia, F.; Helm, L.; Merbach, A.E.; *J. Am. Chem. Soc.*, (1995), **117**, 3790.

Cossy, C.; Helm, L.; Powell, D.H.; Merbach, A.E.; *New. J. Chem.*, (1995), **19**, 27

16 Grygiel, W.; Starzak, M.; *J. Luminescence*, (1997), **71**, 21.

17 Spirlet, M-R.; Rebizant, J.; Wang, X.; Jin, T.; Gilsoul, D.; Comblin, V.; Maton, F.; Muller, R.N.; Desreux, J.F.; *J. Chem. Soc., Dalton Trans.*, (1997), 497.

Chapter Four

Iron(III) Templated Aza-crown Syntheses

4.1. A Brief History of the Synthesis of Cyclens

The first synthesis of cyclen **5** was published in 1961 by Stetter and Mayer.[1] In keeping with many of the syntheses currently employed, it is a long and non-trivial procedure. Ethylenediamine is first protected using tosyl chloride and the resultant ditosylamide **51** is alkylated with methyl bromoacetate **48**, (Scheme 4.1). The diester **52** is hydrolysed in base and then subsequently converted to the diacid chloride **53** with thionyl chloride.

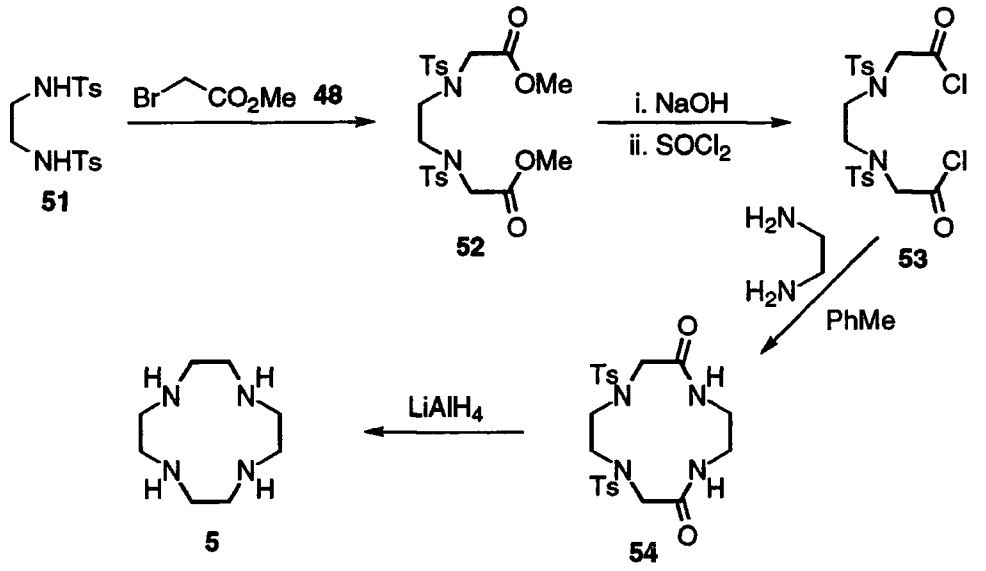

Scheme 4.1 The original route to cyclen devised by Stetter and Mayer.[1]

Condensation of the diacid chloride **53** with ethylenediamine yields the cyclic diamide **54** in 68% yield. Reduction of the amides and removal of the tosyl groups is achieved in one step using lithium aluminium hydride to yield cyclen **5** in six steps and a 15% overall yield. It has since been shown that cyclisation can be effected by condensation of ethylenediamine with the methyl,[2] ethyl[3] or *N*-hydroxysuccinimide[4] diester.

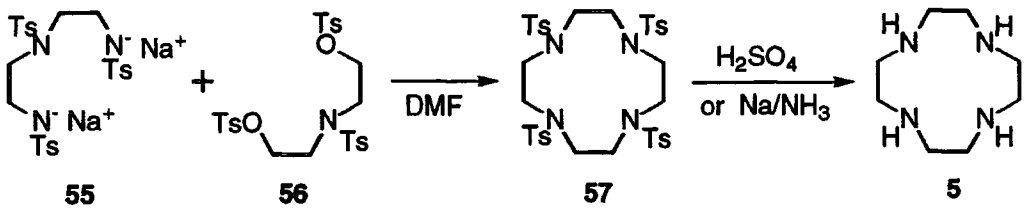

Scheme 4.2 The Richman-Atkins synthesis of cyclen **5**.

Until very recently cyclen has been synthesised commercially using the methods developed by Richman and Atkins in 1974.[5] Originally, the sodium

salt of a ditosyl amide **55** was condensed with an appropriate ditosyl ester **56** in DMF, (Scheme 4.2), thereby avoiding the use of acid chlorides.

In 1985 Iwata and Kuzuhara showed that deprotonation of the ditosyl amide **55** with potassium or caesium carbonate in DMF was equally effective.[6] The tosyl groups can be removed from the cyclic tetrasulfonamide **57** in a number of ways, the most popular of which involve sulfuric acid[7] or sodium in liquid ammonia.[8,9] Pure cyclen may then be obtained by sublimation.

Recently a much shorter synthesis of cyclen has been developed by Gary Weisman.[10] Cyclen can be synthesised in 68% yield in just two steps by the condensation and reduction of triethylenetetraamine **58** and dithiooxamide **59** (Scheme 4.3).

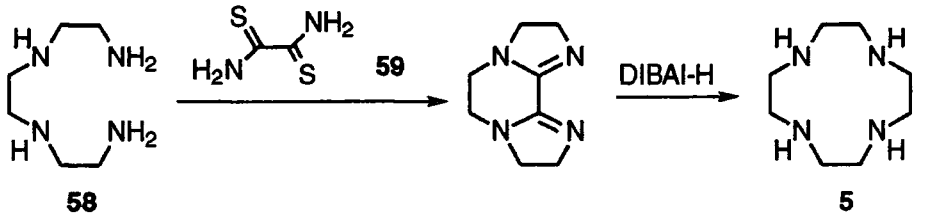

Scheme 4.3 The Weisman synthesis of cyclen.[10]

A number of derivatives of cyclen substituted on carbon have also been synthesised, (Figure 4.1). Functionalisation of the macrocyclic skeleton has facilitated the covalent linkage of the ligand to targeting vectors such as F_{ab} antibody fragments.[11] In general such compounds (**60-62**) are synthesised by variations on the Atkins approach.[8,9,12] Takenouchi *et al.*[2] provided the exception when, in 1993 they employed the orginal method of Stetter and Mayer[1] to prepare cyclen derivatives with appended nitrobenzyl groups, **62** and **64**, .

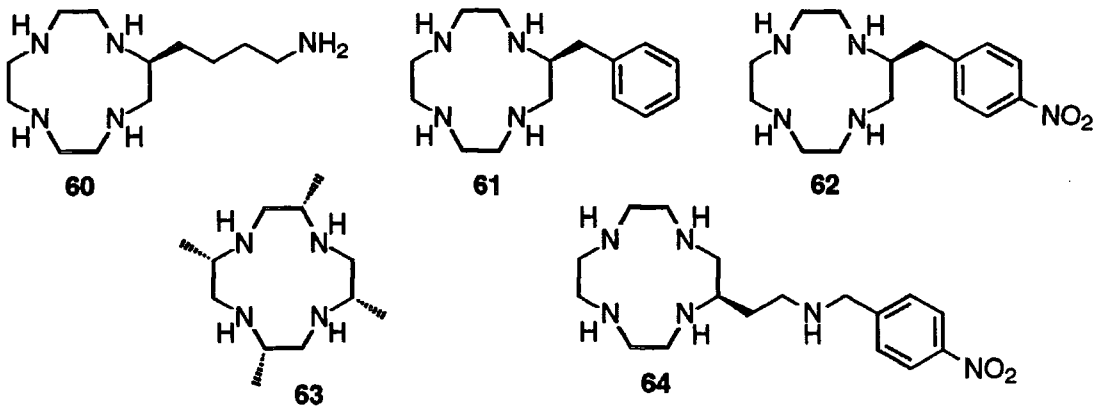

Figure 4.1 Substituted cyclen derivatives

In addition to mono-substituted cyclen derivatives, (*S,S,S,S*)-tetramethyl cyclen, **63** has been synthesised by Pillia *et al.*[13] The cyclotetramerisation of (*S*)-methyl *N*-benzylaziridine is catalysed by *p*-toluenesulfonic acid. The *N*-benzyl groups can be removed under catalytic hydrogenation to afford enantiopure tetramethylcyclen in two steps. However, this reaction suffers from the obvious disadvantages arising from the high toxicity of aziridines.

In recent years patents have been filed on two new syntheses of cyclen,[14,15] which, similarly to a recently published synthesis, by Handel *et al.* involve templating with a two carbon fragment prior to cyclisation.[16] The approach taken by Handel *et al.* used butanedione to template triethylenetetraamine **58**, the ring closure was then effected by condensation of the tricycle **65** with dibromoethane (Scheme, 4.4). Free cyclen was subsequently liberated by mild acid hydrolysis.

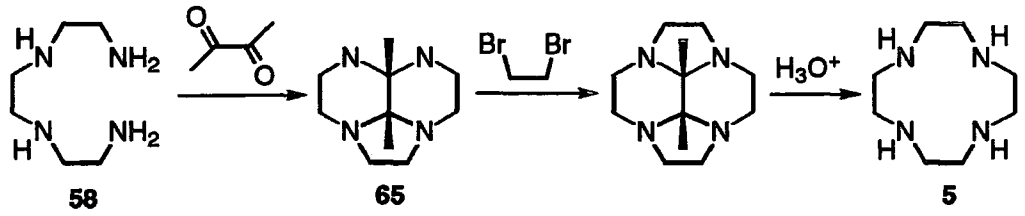

58 **65** **5**

Scheme 4.4 The three step synthesis of cyclen devised by Handel *et al.*

4.2. Iron(III) Templated Synthesis of Aryl Substituted Cyclen Derivatives

Many macrocyclic syntheses employ transition metals to template the ring closure thereby avoiding polymerisation.[17] Transition metal templates had not previously been applied to the synthesis of cyclen or its substituted derivatives. Work previously carried out in Durham in 1995 has shown that iron(III) chloride could be used to template the synthesis of a cyclen derivative with a phenyl substituent in the 2- position **66**.[18] The reaction can be carried out in a single step and in good yield.

The iron(III) chloride templated condensation of triethylenetetraamine and phenyl glyoxal **67** was found to be effective in methanol, (Scheme 4.5). The resulting *cis*-diimine **68** was reduced *in situ* with sodium borohydride and the cyclen derivative liberated in an acid/base work-up.

Not only is this a simple and convenient synthesis of cyclen derivatives but it may be readily modified to allow subsequent functionalisation. If the phenyl ring can be substituted with a suitable functional group, such as a primary amine, this may allow the covalent linkage of the ligand to a targeting vector, macromolecule or protein. The scope of this reaction would then be considerably enlarged. With this in mind, the preparation of two aryl cyclen

derivatives bearing functional groups (nitro and nitrile groups) was undertaken.

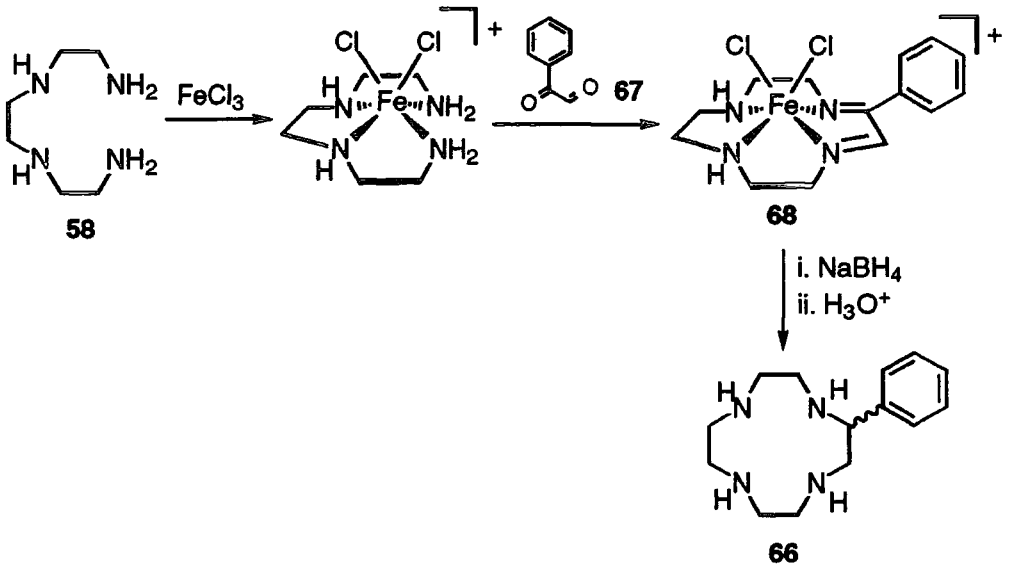

58 68 66

Scheme 4.5 The one-pot synthesis of phenyl cyclen

Glyoxal Synthesis

Although phenyl glyoxal is commercially available, its functionalised analogues are not. An effective synthetic route to such functionalised aryl glyoxals had already been established[19,20] (Scheme 4.6). Oxidation of the appropriate acetophenone with selenium(IV) oxide in a mixture of water and dioxane as solvent, afforded the corresponding glyoxal. However, purification of these functionalised glyoxals proved to be difficult. Whilst residual inorganics and starting materials could be removed by column chromatography over silica, this procedure did not yield the pure glyoxal.

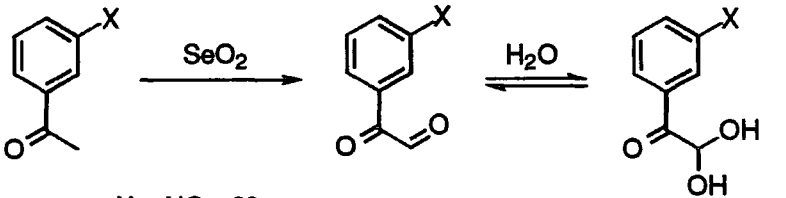

Scheme 4.6 The synthesis of substituted phenyl glyoxals **69** and **70**.

Purification was complicated by the fact that glyoxals exist as a mixture of the di-carbonyl compound and its corresponding hydrate. The water may be removed by distillation and the glyoxal purified by Kugelröhr distillation. Both

the *meta*-nitro and cyano phenyl glyoxals **69** and **70** were synthesised in this manner and obtained as bright yellow glassy solids in over 60% yield.

Synthesis of Aryl Substituted DOTA Derivatives

The synthesis of *meta*-cyano phenyl DOTA was undertaken (Scheme 4.7). Work carried out by Dr Matt Wilkinson in Durham had shown that aryl cyclen derivatives with electron withdrawing groups in the *para*-position were not stable with respect to oxidative decomposition in air or in aqueous solution. Having synthesised and purified *meta*-cyanophenyl glyoxal **70**, the iron(III) templated cyclisation with triethylenetetraamine **58** was carried out as previously described. After purification over silica gel, the desired macrocycle was obtained in 54% yield.

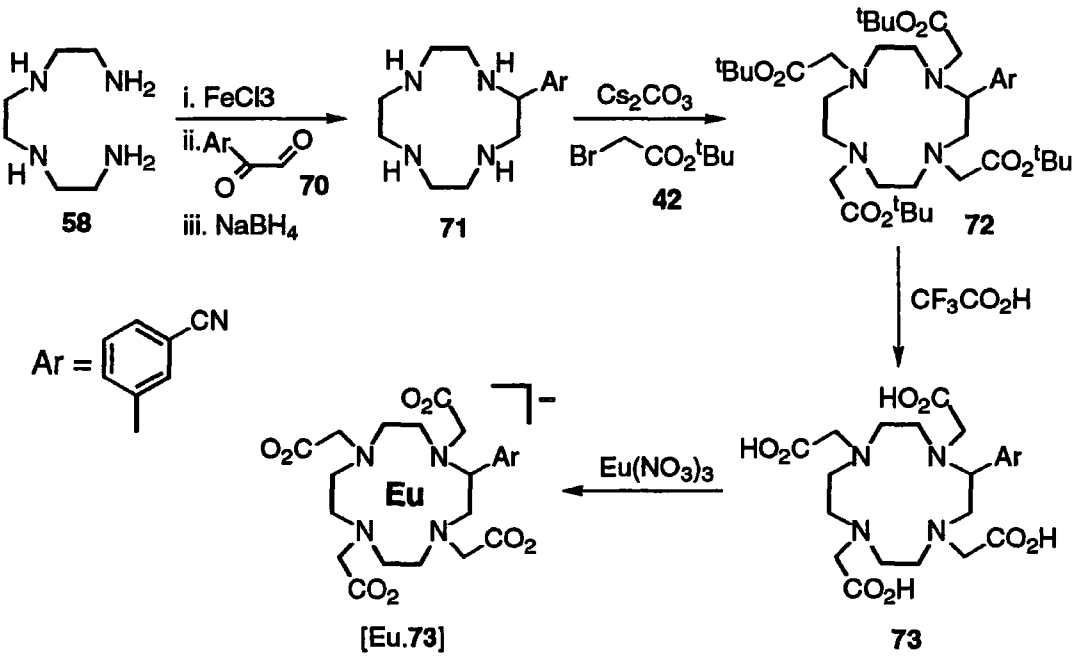

Scheme 4.7 The synthesis of [Eu.2-(*m*-CN-Ph) DOTA]$^-$.

In contrast to the synthesis of DOTA **2**, the alkylation of 2-aryl cyclen derivatives must be undertaken with caution. When four equivalents of *tert*-butyl bromoacetate **42** were used, quaternisation of one of the ring nitrogens was observed (ESMS). This compound could not be separated from the desired DOTA derivative. By careful monitoring of the reaction by ESMS and using just 3.5 equivalents of the bromoacetate **42** this problem could be circumvented. The tetra-*tert*-butyl ester, **72** was purified over silica gel and obtained as a colourless oil. The esters were then hydrolysed with trifluoroacetic acid. The corresponding europium(III) complex [Eu.**73**] was synthesised in the same manner as described for DOTA (Chapter 2). A solution of europium(III) nitrate

in water was added to the ligand **73** and heated at pH 5.5 and 60°C for 6 hours. Unlike the lanthanide complexes of DOTA the complex [Eu.**73**] could not be crystallised from aqueous solution.

4.3. The Properties of Lanthanide 2-Aryl DOTA Derivatives

Hydration States

In addition to the 2-(*m*-cyanophenyl)-DOTA **73** described above the europium and terbium complexes of 2-(phenyl)-DOTA **68** had also been synthesised at Durham by Dr Stephen Faulkner. In contrast to the complexes discussed in Chapters 2 and 3, 2-aryl-DOTA derivatives have a chromophore which allows indirect excitation of the lanthanide ion. The lanthanide ions have very small extinction coefficients (typically 1 dm^3 mol^{-1} cm^{-1}) so direct excitation of the metal ion, as used for the DOTA complexes (λ_{Tb} = 366 nm and λ_{Eu} = 397 nm), is a particularly inefficient process. In cases where a suitable chromophore is present in the complex that can be used as an antenna to sensitise formation of the excited lanthanide(III) ion, thus enabling higher quantum yields to be obtained.[23]

The aryl DOTA derivatives were irradiated at shorter wavelength (λ_{Ex} = 250nm), exciting the aromatic substituent to the (S_1) singlet state. After intersystem crossing to the triplet state, the excited lanthanide is obtained following intramolecular energy transfer (Figure 4.2).

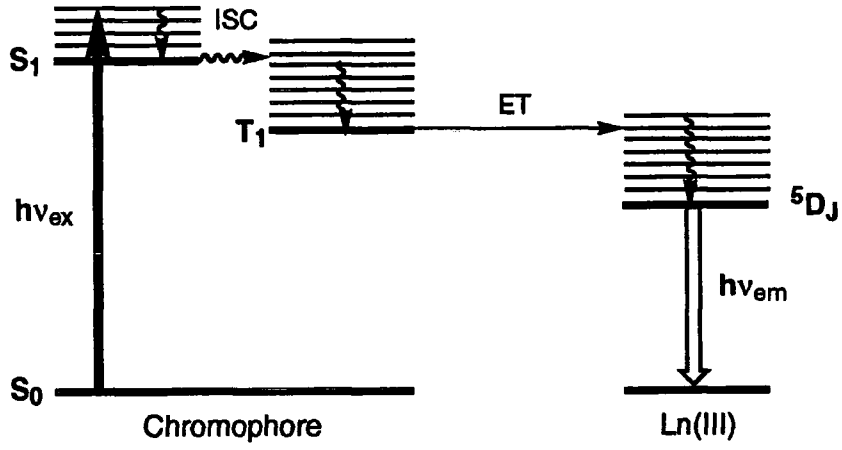

Figure 4.2 A Jablonski energy level diagram showing the sensitisation of a lanthanide(III) ion by the aromatic 'antenna' of the ligand

The lifetimes of these complexes were measured in both water and deuterium oxide, allowing the calculation of their hydration state *via* Horrocks' method.[21] The results are summarised in Table 4.1.

The values of Δk and q obtained for each complex are almost identical to those observed for DOTA. Deviations from integral values of q have been discussed in Chapter 1.3. Although non-integral values for the hydration states of each complex are obtained, these values are consistent with the presence of one coordinated water molecule. The only deviation from the behaviour of DOTA was in the observed lifetime for [Tb.Ph-DOTA]$^-$. The reason why the lifetime of terbium DOTA is a factor of three longer than that of [Tb.Ph-DOTA]$^-$ is not fully understood. Since the lifetime is so much shorter in both H_2O and D_2O then this observation would seem to be a facet of the ligand's properties rather than an increase in hydration.

Complex	$\tau_{(H_2O)}$ / ms	$\tau_{(D_2O)}$ / ms	q
[Eu.Ph-DOTA]$^-$	0.57	1.59	1.18
[Tb.Ph-DOTA]$^-$	0.53	0.62	1.15
[Eu.DOTA]$^-$	0.60	2.13	1.20[22]
[Tb.DOTA]$^-$	1.51	2.54	1.13[23]

Table 4.1 Hydration states, q, of Eu and Tb Ar-DOTA and DOTA complexes. $\tau_{(H_2O)}$ and $\tau_{(D_2O)}$ are the luminescent lifetimes in H_2O and D_2O respectively.

Complex Stabilities

The gadolinium complex of *p-N,N*-dibenzyl aminophenyl DOTA **74**, was synthesised by colleagues working at Guerbet, using the same procedure described above. In order for this compound, or its derivatives to be viable as a contrast agent the complex must satisfy certain criteria. In addition to the issue of relaxivity the complex must also be sufficiently stable to allow its use *in vivo*. In practical terms a stability constant of 10^{18} represents the absolute minimum, and adequate kinetic stability must also be demonstrated.

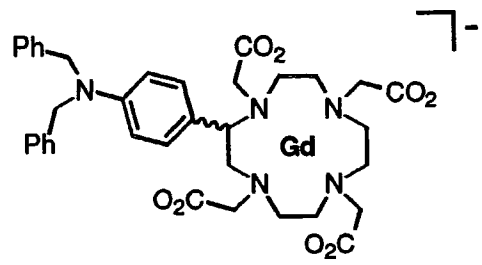

Gd.**74**

The stability of a complex may be evaluated by challenging the complex with a series of other ligands. As part of the stability evaluation, [Gd.**74**]$^-$ was challenged with a ten fold excess of EDTA at pH 5.5. Electrospray mass spectrometry was employed to analyse the results. After just 30 minutes only [Gd.EDTA]$^-$ was detected in negative ion mode. When the positive ion mode was scanned, free [H_5**74**]$^+$ was also clearly visible. The complex with EDTA is clearly stronger than that with the ligand **74**. EDTA is a hexadentate ligand and does not form strongly associative complexes with the lanthanide(III) ions (log K_a is typically 17.3).[24] The rapid dissociation of the [Gd.**74**]$^-$ upon introduction of EDTA implies that the stability of the complex is $< 10^{10}$.

These observations were confirmed by a similar experiment performed on [Eu.**68**]$^-$. When this complex was challenged with a ten fold excess of EDTA at pH 5.5 a similar analysis was performed using luminescence. An eight or nine coordinate lanthanide(III) EDTA complex has a hydration state of three. The hydration state of [Ln.**68**]$^-$, was previously established to be one. The luminescent lifetime of the lanthanide ion would therefore be expected to drop substantially on passing from the **68** complex to the EDTA complex. Indeed this was what was observed; the measured europium lifetime dropped from τ = 0.57ms to τ < 0.1ms in H_2O and from τ = 1.59ms to τ = 0.5ms in D_2O. Such behaviour is consistent with dissociation of the lanthanide(III) ion followed by sequestration by EDTA.

Lanthanide(III) complexes of DOTA derivatives with alkyl substituents appended to the macrocyclic framework are known to be stable.[9] When the alkyl substituent is replaced by an aryl ring it appears that this stability is lost. The electronic effects of the aromatic substituent can affect the macrocycle, as in the case of *p*-nitrophenyl cyclen. Such effects are, however, unlikely to affect donor atoms, separated from the substituent by saturated carbon atoms. Hence electronic effects may be ruled out as a source of the low effective stability of these complexes.

Consideration of the steric demand imparted by the substituent is more revealing. Crystal structures of lanthanide DOTA complexes[25] and substituted derivatives such as those in Chapter 2, show that the lanthanide is sandwiched between the four ring nitrogens and the coplanar oxygen atoms of the pendant arms below. The co-operative nature of this binding mode leads to the extremely high stability constants observed for these complexes. In all of these structures, the macrocycle adopts a square [3333] conformation. Force-field calculations for cyclododecane and related tetraoxa and tetraaza macrocycles have shown this to be the least strained conformation.[26] In this conformation

the five ring chelates are skewed into the same configuration with all the hydrogen atoms staggered, thus minimising steric interaction.

To gain some appreciation of the steric effects operative in of these systems, space filling molecular models were constructed of both DOTA and **68**. In the [3333] ring conformation the model of DOTA could be readily manipulated to invert the conformation of the ring. The ligand **68**, on the other hand, could not accommodate the phenyl ring and undergo ring inversion whilst maintaing a [3333] ring conformation. The ^{1}H NMR spectrum of both 2-(*m*-cyanophenyl)cyclen **71** and the derived tetraacetate **73** showed broad resonances for the macrocyclic ring. Such behaviour suggests that ring inversion may take place on the NMR timescale at room temparature. If this is the case, then the macrocycle is not expected to adopt a [3333] ring conformer. The steric constraints imposed by the phenyl ring must therefore prevent the macrocycle from adopting this conformation. Of the remaining conformers, the [2334] is the next lowest energy conformation in terms of total strain (Figure 4.3).

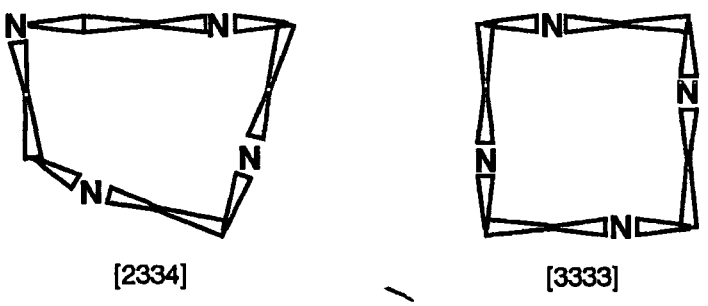

Figure 4.3 Representations of the [2334] and [3333] ring conformations of cyclen following the nomenclature of Dale.[27]

This hypothesis is substantiated by the observation that one of the ring nitrogens of **68** and **73** can be quaternised during alkylation. Quaternisation is not usually observed during the synthesis of DOTA itself. The [3333] ring conformation observed in both cyclen and DOTA will position the lone pair of each nitrogen such that they point inward. As can be seen from the representation of the two conformations using the Dale nomenclature (Figure 4.3), in the [2334] conformer one ring nitrogen is situated on a corner of the macrocycle. The lone pair of this nitrogen would be exposed, pointing away from the macrocycle. Quaternisation of nitrogen is only likely to occur if the lone pair of nitrogen is accessible, as in the [2334] conformer.

When a space filling model of [Ph-DOTA] was constructed with this conformation, the macrocycle was able to accommodate the phenyl ring and

also to ring invert. It is quite possible therefore that **68** has a [2334] macrocyclic ring conformation (Figure 4.4)

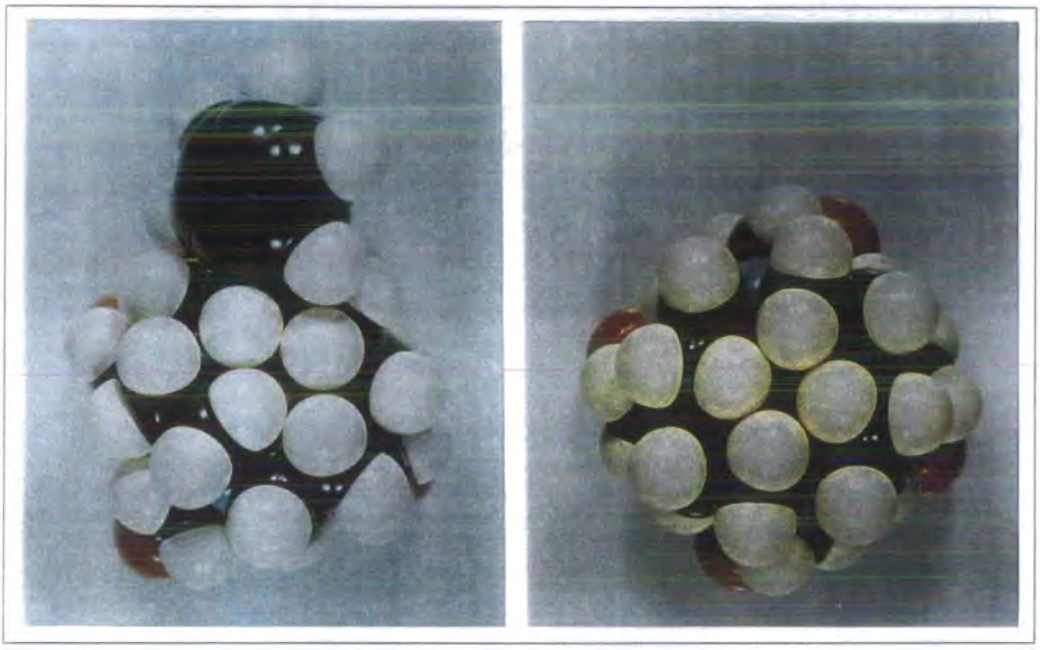

Figure 4.4 Space filling models of 2-Phenyl DOTA **68** (left) in a [2334] ring conformation and DOTA **2** (right) in a [3333] ring conformation

With the macrocycle in the [2334] ring conformation, the nitrogen donor atoms are not co-planar. Also, the nitrogen lone pairs are not directed toward the same point. Thus it is clear that **68** and its derivatives are unable to effect the same degree of co-operative binding mode for lanthanide(III) ions exhibited by DOTA.

To probe the local coordination environment of the lanthanide(III) ion in a 2-aryl DOTA ligand an emission spectrum of [Eu.**73**] was recorded (Figure 4.5). When compared to the spectrum obtained for the [Eu.DOTA]$^-$ the differences are immediately apparent. The most significant difference is in the intensity of the hypersensitivity of the $\Delta J = 2$ band centred around 620 nm. This band is extremely sensitive to the europium(III) coordination environment.[28] The sensitivity of this band to coordination environments is particularly informative when compared to the intensity of the relatively insensitive $\Delta J = 1$ band. In contrast to [Eu.DOTA]$^-$ where the $\Delta J = 2$ band is relatively weak, it is extremely intense in the spectrum of [Eu.**73**]. Indeed the general form of the two spectra are very different. This suggests that the europium(III) ion does not experience similar coordination environments in the two complexes [Eu.**73**] and [Eu.DOTA]$^-$.

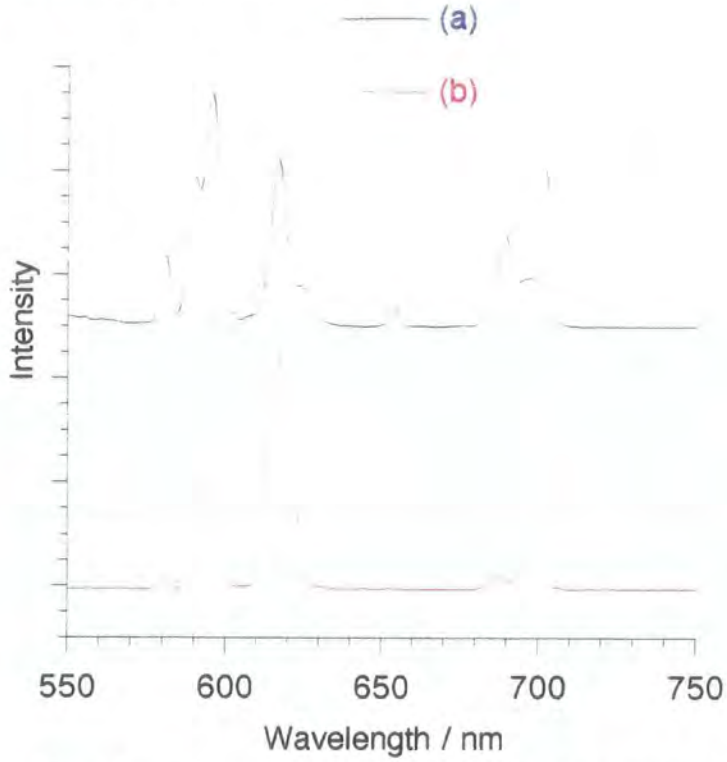

Figure 4.5 The emission spectrum of (a) [Eu.DOTA]$^-$ (blue) and (b) [Eu.**73**] (red).

The ^{1}H NMR spectrum of [Eu.**73**]$^-$ (Figure 4.6) is uncharacteristically broad and is not shifted to the same extent as those shown in Chapters 2 and 3.

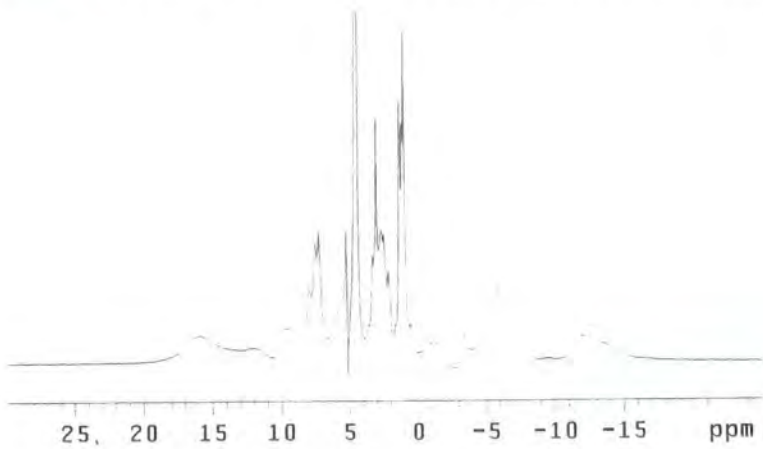

Figure 4.4 The ^{1}H NMR Spectrum of [Eu.**73**].

Three configurations of the [2334] conformer exist, and in the complex, the macrocycle is likely to interconvert between them. Whilst complexes of DOTA deviating from a [3333] ring conformation are previously unknown, such a deviation would seem to explain the broad and unassignable nature of the NMR spectrum of the complex. The weak binding of the ligand (and possibly longer metal-oxygen and metal-nitrogen bond lengths) and distortions to the macrocycle imply that the metal proton distances are greater than those

observed in [Ln.DOTA]$^-$ complexes. The lanthanide induced shift of the ligand protons is consequently smaller. Thus, for example, the most shifted axial ring proton resonates at 38 ppm in [Eu.DOTA]$^-$, but in [Eu.**73**], an exchange broadened resonance at 16 ppm was observed under similar conditions.

The loss of complex stability may tentatively be attributed to the steric demand imposed by the aryl substituent, preventing the ligand from adopting the most favoured conformation for lanthanide binding. The contribution of electronic effects may not be completely discounted but is unlikely to be the major cause of stability loss.

4.4 Extending the Use of Iron(III) Templated Cyclen Syntheses

As previously mentioned, 2-benzyl cyclen, **61** had been synthesised following Atkins procedure in 1993 by Moi *et al.*[8] The corresponding DOTA derivative has been used to complex lanthanide(III) ions, and these complexes are known to be as stable as those of DOTA itself. Hence the introduction of a methylene group between the aromatic group and the macrocycle serves to alleviate the steric problems encountered with the 2-aryl DOTA derivatives. It was unclear however, how the introduction of this methylene carbon would affect the iron(III) templated cyclisation discussed above.

Synthesis of Benzyl Glyoxal

The oxidation of 3-phenylpropionaldehyde **75** with selenium dioxide has been reported to give benzyl glyoxal **76** in one step.[29] Using the conditions reported, repeated attempts failed to give the desired glyoxal as the reaction product. Nor could benzyl glyoxal **76** be obtained under the conditions previously employed for the synthesis of aryl glyoxals **69** and **70**. Partial oxidation to the α-hydroxyaldehyde, appears to have been followed by rapid acid catalysed elimination, to give cinnamaldehyde **77** (Figure 4.8). This was the only product isolated from this reaction.

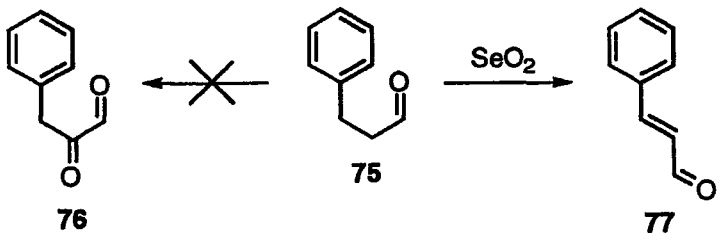

76 **75** **77**

Scheme 4.8 The oxidation of 3-phenylpropanionaldehyde **77**.

A similar approach to that employed by Dakin and Dudley was then considered, (Scheme 4.9).[30] Thiolane protection of the aldehyde was used in preference to the reported acetal protection as ethyl 1,3-dithiolane-2-carboxylate **78** is commercially available. The ethyl ester was hydrolysed in aqueous lithium hydroxide solution in almost quantitative yield. The piperidine amide, **80** was synthesised *via* the acid chloride, in turn prepared *in situ* with thionyl chloride.

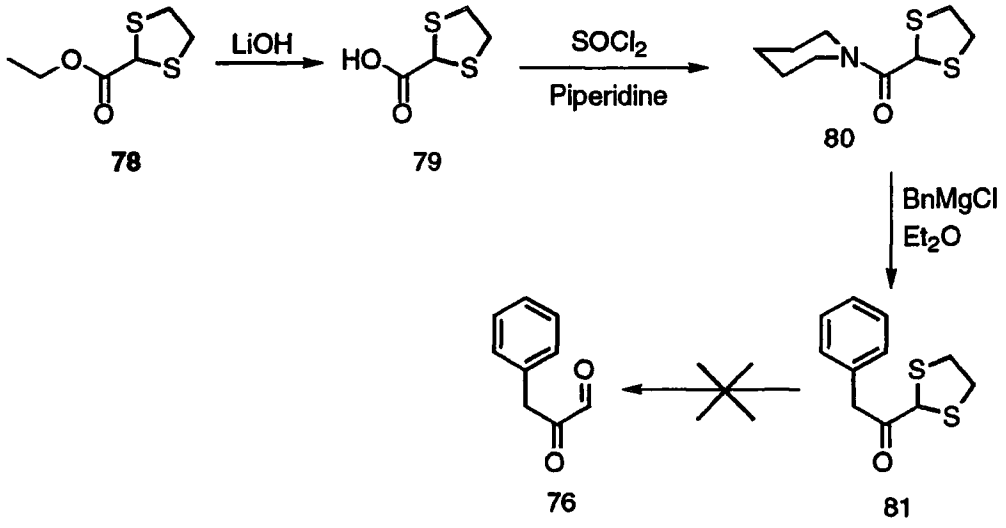

Scheme 4.9 The attempted synthetic route to benzyl glyoxal **76**.

The choice of solvent for the Grignard reaction is critical. The reaction of the amide, **80** with benzylmagnesium chloride proceeded smoothly in diethyl ether to afford the thiolane protected benzyl glyoxal **81** in 79% yield. When the solvent was changed from diethyl ether to tetrahydrofuran the desired product was not obtained.

Suitable conditions to liberate the glyoxal **76** from the α-keto thioacetal **81** proved elusive. Standard conditions employing mercury(II) salts were found to be ineffectual. Boiling a solution of the thioacetal, **81** in aqueous acetone with mercury(II) acetate did not afford any products with a characteristic aldehyde resonance in the ^{1}H NMR. Attempts to deprotect using silver nitrate[31] in a solution of water and dioxane proved unsuccessful. Whilst the thiolane was removed quickly at room temperature, ^{1}H NMR showed that the ensuing aldehyde was rapidly oxidised to the acid by the silver(I). A change in catalyst to copper(II) acetate in aqueous acetone did not react with the thioacetal **81**. After two days at reflux, t.l.c. analysis revealed the presence of only starting material. Olah *et al.* have reported that thiolanes may be deprotected effectively by trimethylsilyl halides in methylsulfoxide.[32] This method was undertaken, however, the horrendous stench arising from reaction

by-products prevented completion of the reaction work-up. It was never established whether or not this method afforded benzyl glyoxal **76** or not. *N*-Bromosuccinimide has been reported to remove thioacetals in aqueous acetone[33], but when this reagent was used the reported conditions were presumably insufficiently forcing to afford the desired glyoxal.

The problems experienced in attempting to remove the thioacetal appear to arise from the sensitive nature of the aldehyde in the desired glyoxal **76**. A compromise between the more forcing removal conditions exemplified silver(I) nitrate, and the mild conditions offered by *N*-bromosuccinimide is required. Such a compromise will inevitably result in a sensitive reaction, seriously limiting the application of this glyoxal in the synthesis of substituted cyclen derivatives.

4.5 Conclusions

The use of iron(III) to template the condensation reaction of a suitably activated glyoxal with triethylenetetraamine **58** to yield a derivatised cyclen derivative was shown to be efficient. The reaction may be extended to the synthesis of functionalised 2-aryl substituted cyclen systems **66** and **71**,[18] allowing incorporation of functionalised substitutuents into the product. The cyclisations were performed in "one-pot" and employed mild conditions throughout. The reaction does, however, appear to be limited in application to glyoxals with a substituent bearing activating π-electrons, such as an aromatic moiety. The reaction therefore seems not to be applicable to the synthesis of cyclen itself.

The tetraacetate ligands derived from these 2-aryl cyclen derivatives 2-Ph-DOTA and **73** were found to complex lanthanide(III) ions. Hydration states of one were measured for the europium(III) and terbium(III) complexes. The emission spectra of the europium(III) complex reveals that the local coordination geometry of the europium does not resemble that of the corresponding $[Eu.DOTA]^-$ complex, the hypersensitive $\Delta J = 2$ band being far more intense in the former spectrum. This difference in coordination environment is ascribed to be the reason for low stability of these lanthanide(III) 2-aryl DOTA complexes. In competition reactions with EDTA the lanthanide(III) ion is quickly removed from these ligands and a stability constant in the region of $<10^{10}$ has been estimated. The steric demands of an aromatic substituent on the macrocycle appears to distort the conformation of the ring from a [3333] into a [2334] ring conformation. This ring deformation distorts the N_4 plane of the cyclen, resulting in the loss of co-operative binding

by the ligand. This loss of stability precludes the use of this type of compound in practical applications where high kinetic stability is required.

4.6 References

1 Stetter, H.; Mayer, K.H.; *Chem. Ber.*, (1961), **94**, 1410

2 Takenouchi, K.; Tabe, M.; Watanabe, K.; Hazato, A.; Kato, Y.; Shionoya, M.; Koike, T.; Kimura, E.; *J. Org. Chem.*, (1993), 6895.

3 Wei, J.F.; Zhou, R.X.; Yan, G.P.; Du, P.; *Chem. J. Chin Uni.*, (1997), **18**, 658.

4 McMurray, T.J.; Brechbiel, M.W.; Kumar, K.; Gansow, O.A.; *Bioconjugate Chem.* (1992), **2**, 108.

5 Atkins, T.J.; Richman, J.E.; *J. Am. Chem. Soc.*, (1974), **96**, 2268.
Atkins, T.J.; Richman, J.E.; Oettle, W.F.; *Org. Synth.*, (1978), **58**, 86.

6 Iwata, M.; Kuzuhara, H.; *J. Chem. Soc., Chem. Commun.*, (1985), 918

7 Hettich, R.; Schnieider, H-J.; *J. Am. Chem. Soc.*, (1997), **119**, 5638.
Matsumoto, N.; Hirano, A.; Hara, T.; Ohyoshi, A.; *J. Chem. Soc. Dalton. Trans.*, (1983), 2405.
Luk'yanenko, N.G.; Basok, S.S.; Filonova, L.K.; Kulikov. N.V.; Pastushok, V.N.; *Chem. Hetrocycl. Compd. (Eng. Transl.)*, (1990), **26**, 346.

8 Garrity, M.L.; Brown, G.M.; Elbert, J.E.; Sachleben, R.A.; *Tetrahedron Lett.*, (1993), 5531.

9 Cox, J.P.L.; Craig, A.S.; Helps, I.M.; Jankowski, K.J.; Parker, D.; Eaton, M.A.W.; Millican, A.T.; Millar, K.; Beely, N.R.A.; Boyce, B.A.; *J. Chem. Soc. Perkin. Trans. 1*, (1990), 2567.

10 Weisman, G.R.; Reed, D.P.; *J. Org. Chem.*, (1996), **61**, 5186.
Weisman, G.R.; Reed, D.P.; *J. Org. Chem.*, (1997), **62**, 4548.

11 Norman, T.J.; Parker, D.; Harrison, A.; Royle, L.; Antoniw, P.; King, D.J.; *J. Chem. Soc. Chem. Commun.*, (1995), **35**, 1877.
Norman, T.J.; Parker, D.; Smith, F.C.; King, D.J.; *J. Chem. Soc. Chem. Commun.*, (1995), **35**, 1879.

12 Moi, M.K.; Meares, C.F.; DeNardo, S.J.; *J. Am. Chem. Soc.*, (1988), **110**, 6266.

13 Pillai, R.; Fan, H.; Ranganathan, R.S.; *Abstracts of Papers of the Am. Chem. Soc.*, (1996), 359.

14 Athey, P.S.; Kiefer, G.E.; Dow Chem. Co.: U.S. Pat 5 587 451, 24 Dec 1996; *Chem. Abstr.*, (1997), **126**, 144300r.

15 Sandes, R.W.; Vaasilevskis, J.; Undheim, K.; Gacek, M.; Nycomed Imaging A/s Norwary: PCT Int Appl. WO96 28 432, 19 Sept 1996; *Chem Abstr.*, (1996), **125**, 301031c.

16 Hervé, G.; Bernard, H.; le Bris, N.; Yaouane, J-J.; Handel, H.; Toupet, L.; *Tetrahedron Ltt.*, (1998), **39**, 6861.

17 Barefield, E.K.; *Inorg. Chem.*, (1972), **11**, 2273.

18 Edlin, C.D.; Faulkner, S.; Parker, D.; Wilkinson, M.P.; *J. Chem. Soc. Chem. Commun.*, (1996), **35**, 1249.

19 Evans, W.L.; Witzemann, E.J.; *J. Am. Chem. Soc.*, (1911), **33**, 1772.

20 Goldberg, M.W.; Rachlin, A.I.; Hoffmann-La Roche, US Patent 2641601, (1953).

21 Horrocks, W.D.; Sudnick, D.R.; *Acc. Chem. Res.*, (1981), **14**, 384

22 Bryden, C.C.; Reilley, C.N.; *Anal. Chem.*, (1982), **54**, 610.

23 Williams, J.A.G.; *PhD Thesis*, University of Durham (1995).

24 Smith, R.M.; Martell, A.E.; In *"Critical Stability Constants"*, Plenum Press, New York, Vol 1, (1974), 204.

25 Spirlet, M.; Rebizant, J.; Desreux, J.F.; *Inorg. Chem.*, (1984), **23**, 359.
Dubost, J-P.; Leger, M.; Larglois, M-H.; Meyer, D.; Schaefer, M.; *R. Acad. Sci. Paris Ser. 2*, (1991), **312**, 349.

26 Meyer, M.; Dahaoui-Gindrey, V.; Lecomte, C.; Guilard, R.; *Coord. Chem. Rev.*, (1998) in press, and references cited therein

27 Dale, J.; *Acta Chem. Scand.*, (1973), **27**, 1115.
Dale, J.; *Top. Stereochem.*, (1976), **9**, 199.
Dale, J.; *Isr. J. Chem.*, (1980), **87**, 1070.

28 Bunzli, J-C.; In *"Lanthanide Probes in Life, Chemical and Earth Sciences"*, Eds. Bunzli, J-C.G; Choppin, G.R., Elsevier, Amsterdam, (1989), Chapter 7.

29 Rioux-Lacoste, C.; Viel, C.; *Bull. Soc. Chim. Fr.*, (1974), **11**, 2463.

30 Dakin, H.D.; Dudley, H.W.; *J. Biol. Chem.*, (1914), **18**, 29.

31 Reece, C.A.; Rodin, J.O.; Brownlee, R.G.; Duncan, W.G.; Silverstein, R.M.; *Tetrahedron*, (1968), **24**, 4249.

32 Olah, G.A.; Narang, S.C.; Mehrotra, A.K.; *Synthesis*, (1982), 965.

33 Cain, E.N.; Welling, L.L.; *Tetrahedron Lett.*, (1971), **36**, 3553.

Chapter Five

Substituted Cyclen Synthesis

5.1. Introduction

As discussed in Chapter 1, a gadolinium ion secured at the centre of a macromolecule by three linkers may be expected to possess the same degree of rotational freedom as one secured by four linkers. The lanthanide complexes of polyamino carboxylate ligands with both three and four acetate substituents have been investigated in Chapters 2 and 3. In Chapter 4, a number of mono-functionalised cyclen derivatives were introduced. Derivatives of cyclen with three substituents can be envisaged which would also enable a lanthanide(III) ion to be secured at the centre of a macromolecular structure. The synthesis of suitable substituted cyclen derivatives was therefore pursued. This work proved to be more difficult than initially conceived. Two synthetic routes were employed, each of which is discussed separately.

The substitution of carbon in cyclen results in the introduction of a stereocentre. It is important to control the configuration of these centres as a mixture of diastereoisomers would otherwise arise in compounds with more than one substituent. In order to control the stereochemistry of the target molecules, it was necessary to use enantiopure starting materials. Amino acids provided an ideal starting point, as they are available as single enantiomers and their chemistry is well described in the literature.

5.2. An Iron(III) Templated Synthesis

At the outset of this work, it had not been established that lanthanide(III) complexes derived from cyclen derivatives bearing an aromatic substituent were surprisingly unstable. The synthesis of such a ligand was conducted first and is reported here.

A suitable triethylenetetraamine backbone had first to be synthesised. In order to effect this synthesis with control of stereoselectivity, (*S*-)-lysine was chosen as a starting material. The condensation of two equivalents of a Boc protected lysine active ester **82** with ethylenediamine **83** afforded the protected diamide **84** in 97% yield. In this manner, a suitable tetraamine backbone could be obtained following reduction of the amides. Attempts to directly reduce the Boc protected diamide **84** with borane-tetrahydrofuran complex proved fruitless: ESMS analysis of the reaction products revealed a mixture of reduction products. Hence the amines were deprotected using trifluoroacetic acid before the reduction was undertaken, (Scheme 5.1). The borane reduction of the resulting trifluoracetate salt of the amine **85** proved extremely effective. Almost quantitative conversion of the diamide **85** to the hexaamine **86** was

achieved after hydrolysis of the amino-borane complex with 2M hydrochloric acid.

The amine **86** was obtained as the corresponding hydrochloride salt, but the free amine would be required for the templated condensation in the presence of iron(III) in methanol. Anion exchange chromatography was employed to liberate the free amine using an Amberlite resin in the OH^- form.

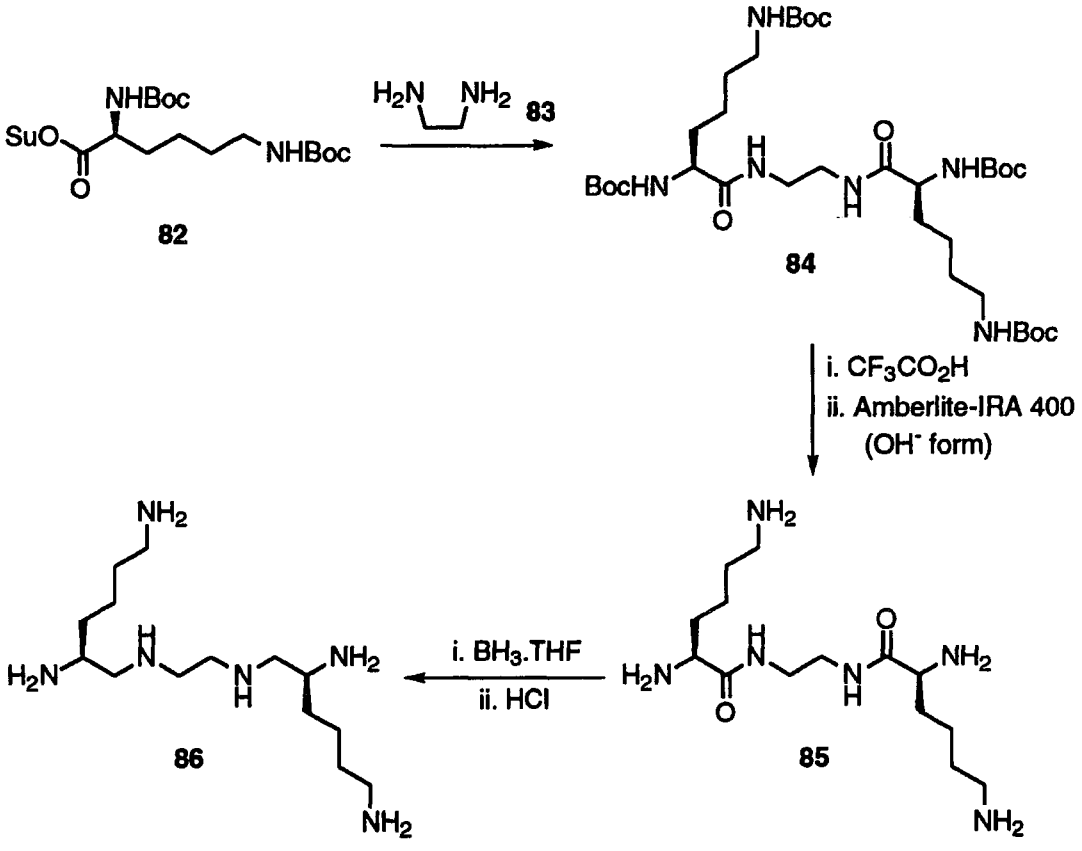

Scheme 5.1 The synthesis of enantiomerically pure substituted triethylenetetraamine derivatives

The iron(III) templated cyclisation of the hexaamine **86** required modification from the procedure set out in Chapter 4. The remote amines of the substituent arms may be expected to react much more quickly than those of the triethylenetetraamine in the iron(III) complex. For this reason it was necessary to protect them before addition of the aryl glyoxal. Since the Boc protection of amines is readily effected in methanolic solution this was the chosen method of protection.

The hexaamine **86** was added to a methanolic solution of iron(III) chloride and an orange precipitate was duly formed, as had previously been observed.[1] The nature of this iron(III) complex not only served to template the subsequent cyclisation reaction but also allowed the selective protection of the

remote amines. Di-*tert*-butyldicarbonate was then added to the suspension to protect the two remote amines of the substituents (Figure 5.2).

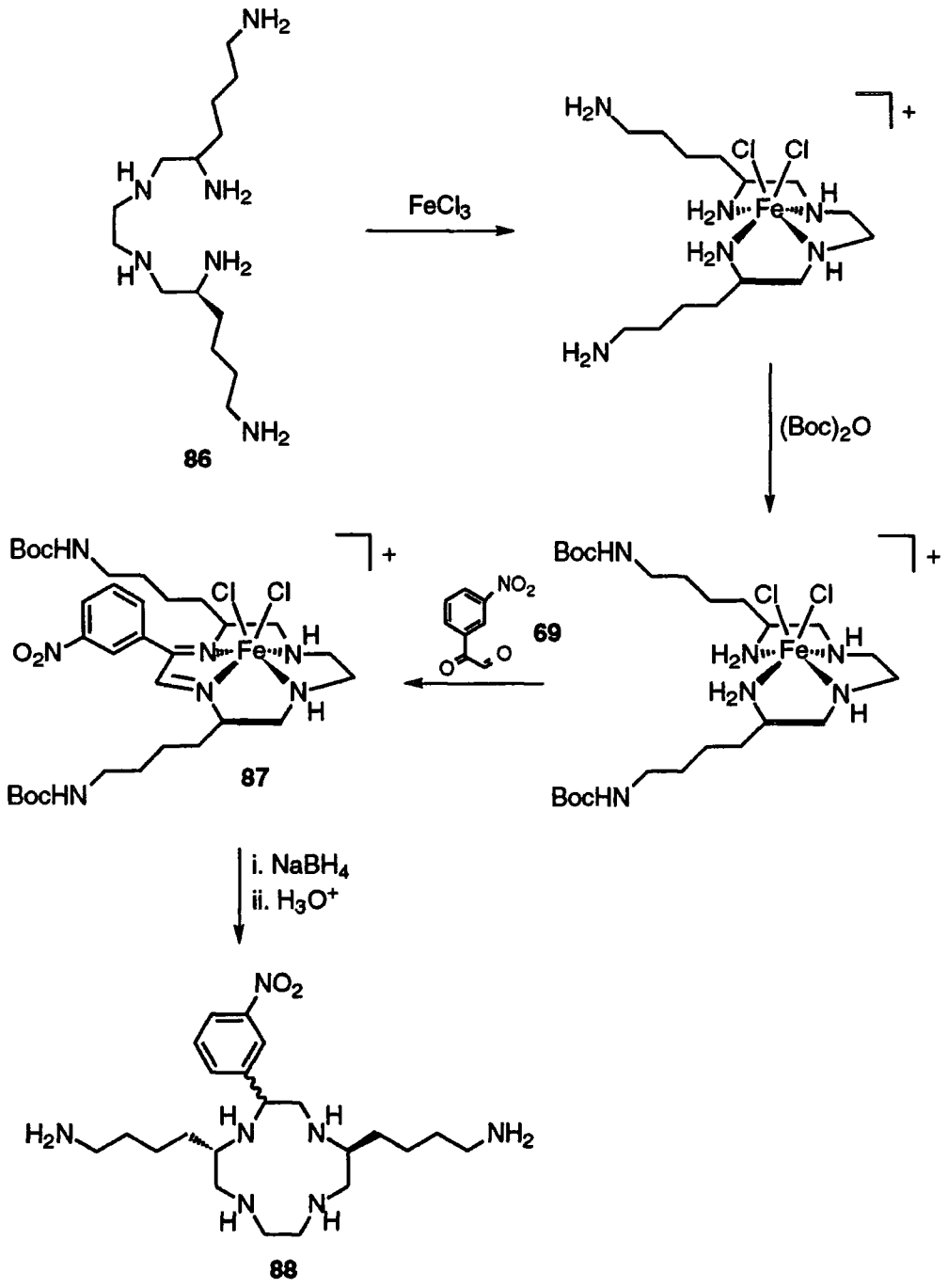

Scheme 5.2 The one-pot cyclisation of **88** performed in methanolic solution

The preparation of *m*-nitrophenyl glyoxal **69** was described previously (Chapter 4.2). The reported cyclisation procedure was followed again, and the glyoxal added to the reaction as a solid. The resulting *cis*-diimine **87** was then reduced *in situ* with sodium borohydride. In addition to reducing the diimine, the borohydride also partially reduced the nitro- group of the aromatic

substituent as revealed by ^{1}H NMR. After the reduction of the imine was complete, the excess borohydride was quenched by the addition of hydrochloric acid. Whilst the addition of acid ensures decomplexation of the iron(III) it also removes the Boc protecting groups. The reaction mixture was washed with dichloromethane before the pH was raised to 13 with sodium hydroxide and the reaction product isolated following exhaustive extraction with chloroform.

The presence of the desired product **88** was confirmed by ^{1}H NMR analysis of the crude reaction products. This mixture was also shown to contain the amino-phenyl substituted cyclen corresponding to reduction of the nitro group. However, the discovery that ligands derived from these 2-aryl substituted cyclen derivatives did not form sufficiently stable complexes with lanthanide(III) ions, the attempts to perform the complicated purification of this compound were abandoned at this point. A different target had to be found.

5.3. A Richman-Atkins Type Synthesis

Although the Richman-Atkins approach to cyclen is long and complex, it has been used to synthesise several mono-substituted derivatives of cyclen.[2,3] In 1988 a derivative of cyclen appended with a protected aminobutyl chain, **60**, was synthesised by this method.[2] A variation on this synthesis was envisaged enabling the synthesis of a cyclen derivative substituted with three amine bearing chains, **87**.

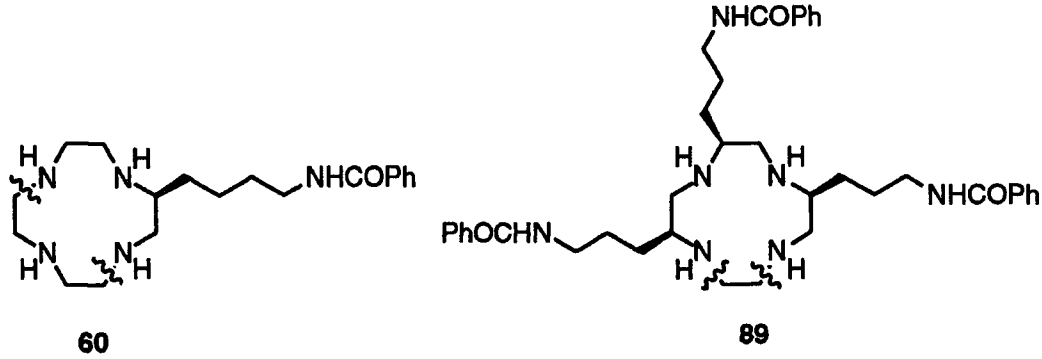

60 **89**

Figure 5.1 The substituted cyclen derivative **60** synthesised by Parker *et al.*[2] marked with the relevant disconnections and the proposed cyclen derivative **89** with the envisaged disconnections.

A different disconnection of the macrocyclic ring needed to be employed in the synthesis of **89** in order to prevent the formation of regioisomers during the cyclisation step. This is achieved by cyclisation with an unsubstituted

ethyleneglycol bis-tosylate. A suitable, enantiomerically pure triethylenetetraamine derivative was thus required, to complete the cyclisation.

The Synthesis of Chiral Triethylenetetraamine Derivatives

In the synthesis of **60**, lysine was used as the macrocyclic precursor in order to incorporate a functionalised substituent. The incorporation of lysine into the synthesis of **89** requires complex and unnecessary orthogonal protection of the two amines. By employing glutamine as a starting point of the synthesis this problem may be circumvented. The primary amide of the glutamine side chain acts as a natural functional group protection. Reduction of tri-glutamine amide would afford a polyamine with an enantiopure triethylene tetraamine backbone.

The synthesis of the desired peptide was achieved by using traditional peptide synthesis techniques (Scheme 5.3). As *p*-nitrophenol is ether soluble, the *p*-nitrophenol ester was chosen because the glutamine derivatives were anticipated to be water soluble. Ammonia was condensed onto the *p*-nitrophenol ester of *N*-Boc-glutamine **90** in dichloromethane. The resulting diamide **91**, whilst providing protection to the C terminus of the peptide, also facilitated the introduction of the fourth nitrogen to the end of the peptide chain.

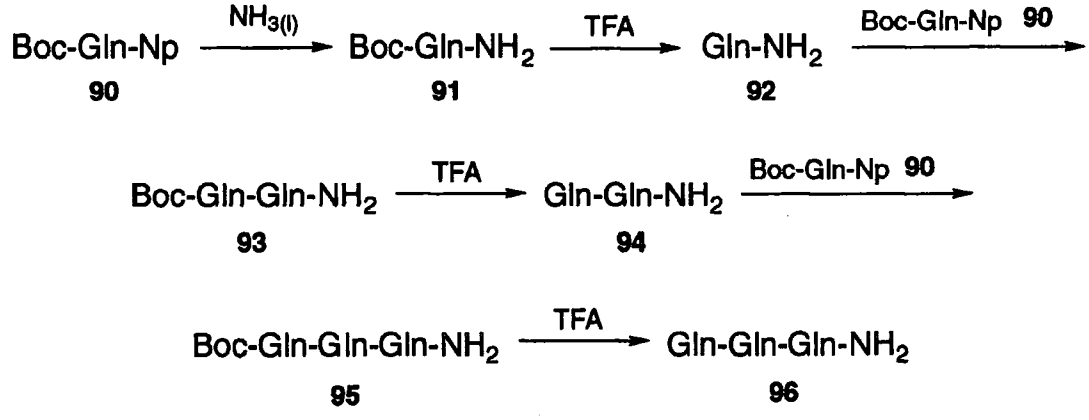

Scheme 5.3 The synthesis of triglutamine amide using established peptide synthesis techniques

Sequential deprotection with trifluoroacetic acid and condensation with the *N*-Boc glutamine *p*-nitrophenol ester **90** enable the desired triglutamine amide **96** to be synthesised effectively in good yield, 53% overall. The reduction of the amides was achieved using a 1M solution of borane tetrahydrofuran complex (Scheme 5.4).

The formation of the intermediate amino-borane complexes was followed by infra-red spectroscopy, observing the disappearance of the amide bands at 1642 and 1656 cm^{-1}. It should be noted that an NH bend is often revealed as the amide bands diminish. The characteristically low intensity of this band enables it to be distinguished from those of the amide. Hydrochloric acid was used to hydrolyse the resulting borane complex and the trisubstituted triethylenetetraamine **97** was obtained as its hydrochloride salt.

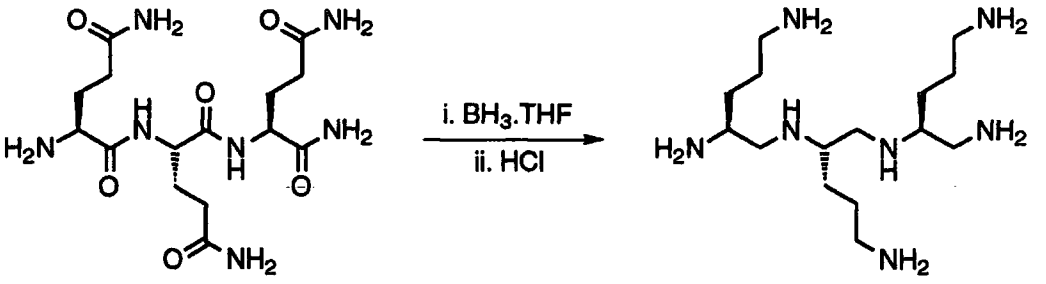

Gln-Gln-Gln-NH_2 **96** **97**

Scheme 5.4 The borane reduction of triglutamine amide.

Before cyclisation could be attempted, protection of the remote amines on the substituent alkyl chains was necessary. An analogous procedure to that used in the selective protection of lysine was employed (Figure 5.5). *N*δ-protection of lysine was achieved through the use of basic copper carbonate to chelate the α-amino and carboxylate groups. This left the remote amines free to be protected. This method has been used to protect remote amines in other polyamino systems.[2] A solution of the hexaamine hydrochloride **97** in water was neutralised with sodium hydroxide and basic copper carbonate was added. A deep blue colour rapidly ensued. To establish that the copper was chelating the four amines as desired, a solution of copper(II) triethylenetetraamine was prepared and the UV/visible spectra compared. Both spectra revealed the same broad absorption band centred around 590 nm. This indicates that both copper(II) complexes possess the same ligand field, presumably adopting the same coordination geometry around copper. It was inferred that the triethylenetetraamine backbone was therefore protected by the copper(II) ion and the three remote amines were free to be protected.

N-Hydroxysuccinimide benzoate ester **98**, prepared by an EDC mediated coupling of benzoic acid and *N*-hydroxysuccinimide, was used to protect the free amines as their *N*-benzoyl amide. Removal of the copper(II) was effected using hydrogen sulfide, and after an acid/base work-up the protected amine **99** was obtained in a 50% yield over the three steps.

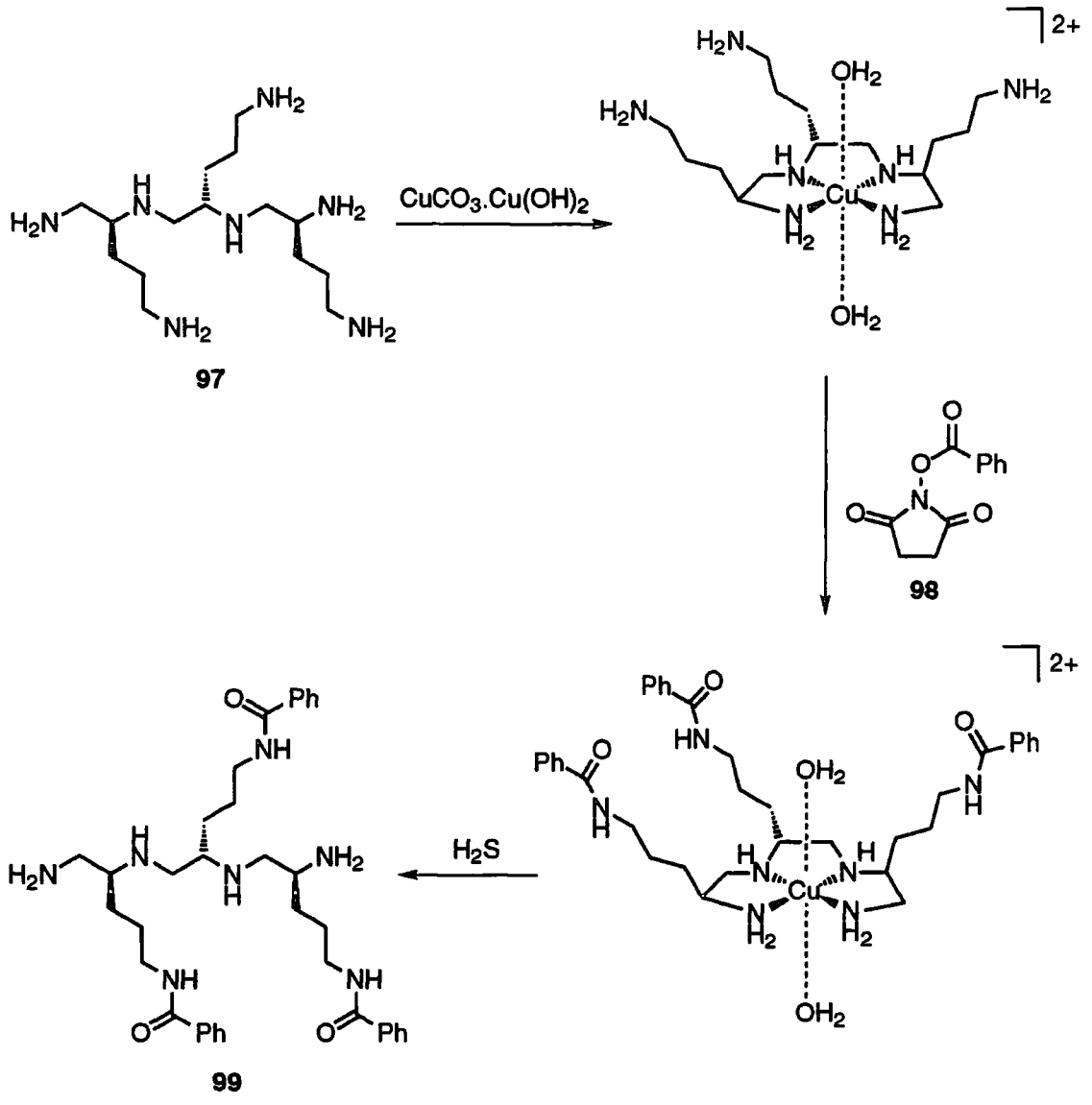

Scheme 5.5 Protection of the remote amines in **99** with the *N*-hydroxysuccinimide ester of benzoic acid achieved *via* copper(II) protection of the triethylenetetraamine moiety was undertaken in aqueous solution.

Ring Closure

Having synthesised a suitable polyamine **99** with which to effect a Richman-Atkins type cyclisation, the dual protection and activation of the triethylenetetraamine nitrogens as tosylamides was undertaken. The tosyl substituents increase the acidity of the amino protons allowing cyclisation. However they also serve to protect the secondary amines: mono-protection of the primary amines prevents a second reaction at this site.

The reaction of tosyl chloride with the tetraamine **99** was tried under a number of different conditions. Little or none of the required tetratosylamide

100 was observed in the ESMS spectrum when the reaction was performed in water with potassium carbonate or in dichloromethane with triethylamine. The desired product **100** was obtained when pyridine was employed as both solvent and base (Scheme 5.6). Unfortunately, following purification over silica gel the isolated yield was only 23%.

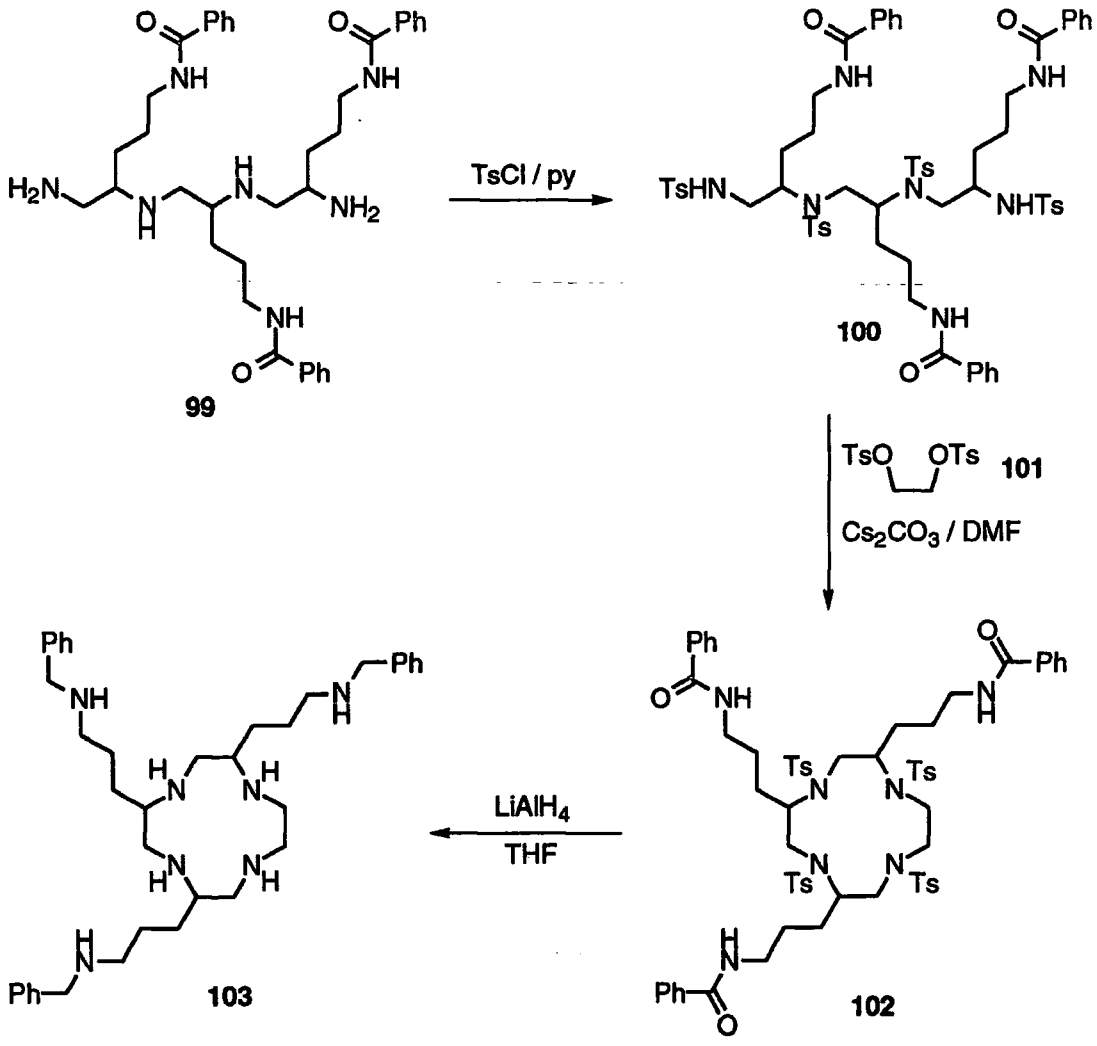

Scheme 5.6 The ring closure of trialkyl cyclen **103**, using the Richman-Atkins approach.

The standard conditions for the synthesis of cyclen were then employed. Ethylene glycol bis-ditosylate **101** was added to a solution of the tetratosylamide in *N,N*-dimethylformamide in the presence of caesium carbonate. After stirring overnight at room temperature, the reaction was heated at 70°C for 3 hours. The desired cyclised tetratosylamide derivative **102**, was obtained following column chromatography over silica gel, using 5% methanol in dichloromethane as the eluent. It proved difficult to obtained conclusive evidence for the presence of the product, as the compound is

difficult to ionise. This was eventually solved by MALDI-TOF mass spectrometry, the peak centred at 1280 and covering several mass units indicating that the cyclisation had indeed been successful.

The removal of the tosyl groups was undertaken following the methods reported by Garrity *et al.* using lithium aluminium hydride.[4] This would inevitably reduce the benzoyl amides to *N*-benzyl groups. However, this was not considered detrimental to the synthesis of the target compund, since the purpose of the substituents is to facilitate linkage to a macromolecular array. When the acetate substitutents are added to the ring nitrogens, they may also be added to the remote secondary amines. Only the DOTA framework is anticipated to form strongly associative complexes with lanthanide(III) ions, thus leaving the substituents free to be bound to the chosen macromolecules through the carboxylates.

Although the described route leads to the preparation of a key precursor to the desired complex, the overall sequence is rather too long to be commercially viable. Overall there are 13 steps, leading to the formation of **103** in 1% yield.

5.3. References

1 Edlin, C.D.; Faulkner, S.; Parker, D.; Wilkinson, M.P.; *J. Chem. Soc. Chem. Commun.*, (1996), **35**, 1249.

2 Cox, J.P.L.; Craig, A.S.; Helps, I.M.; Jankowski, K.J.; Parker, D.; Eaton, M.A.W.; Millican, A.T.; Millar, K.; Beely, N.R.A.; Boyce, B.A.; *J. Chem. Soc. Perkin. Trans. 1*, (1990), 2567.

3 Moi, M.K.; Meares, C.F.; DeNardo, S.J.; *J. Am. Chem. Soc.*, (1988), **110**, 6266.

4 Garrity, M.L.; Brown, G.M.; Elbert, J.E.; Sachleben, R.A.; *Tetrahedron Lett.*, (1993), 5531.

Chapter Six
Experimental

6.1. Experimental Methods

Reagents and Solvents

Reagents and solvents were purified using standard techniques.[1] Solvents were dried over an appropriate drying agent before use: dichloromethane, acetonitrile, pyridine, and triethylamine over calcium hydride; tetrahydrofuran and diethyl ether over sodium with benzophenone as an indicator; methanol and ethanol from the corresponding magnesium alkoxide. *N,N*-Dimethylformamide and dimethylsulfoxide were used directly from "sure-seal" bottles. "Water" and "H_2O" refer to high purity water with conductivity ≤ 0.04 μS cm^{-1}, obtained from the PURITE™ purification system. "Aristar" grade hydrochloric acid was used throughout.

All reactions were carried out in apparatus which had been washed with acid, rinsed twice with water then acetone before being oven dried.

Chromatography

Column chromatography was carried out using "gravity" silica (Merck Art 7734) or neutral alumina (Merck Art 1077) which had been pretreated with ethyl acetate. Cation exchange chromatography was performed using Dowex 50W strong ion exchange resin which had be pretreated with an aqueous solution of an appropriate salt or acid. Anion exchange chromatography was carried using Amberlite-IRA 400 strong anion exchange resin pretreated with an aqueous solution of the desired anion.

Spectroscopy

^1H NMR spectra were recorded at 65.15 MHz on a 1.53T magnet connected to a Varian VXR400 console, at 199.99 MHz on Varian Mercury-200, Gemini-200, and VXR200 spectrometers, at 250.13 MHz on a Brüker AC250, at 299.91 MHz on a Varian Unity-300, at 399.96 MHz on a Varian VXR400 and at 500.13 MHz on Brüker AMX500 or 499.79 MHz on a Varian Unity Inova-500 spectrometer. ^{13}C NMR spectra were recorded on the Varian Gemini-200 and Mercury-200 spectrometers operating at 50.29 MHz, the Brüker AC250 operating at 62.90 MHz, the Varian Unity-300 operating at 75.41 MHz and the Varian VXR400 operating at 100.58 MHz. ^{19}F NMR spectra were recorded on the Brüker AC250 operating at 235.34 MHz. ^{17}O NMR measurements were recorded on the JEOL EX90 operating at 12.00 MHz. Proton relaxation measurments were made on Stelar Spin-Master operating at 20MHz. NMRD

profiles were recorded by Dr Mauro Botta and Allesandro Barge on the Koenig-Brown field-cycling Relaxometer in Torino.

Infra-red spectra were recorded on a Perkin Elmer 1600 FTIR spectrometer. Samples were run on a "Golden Gate" apparatus as thin films or powdered solid samples, on NaCl discs as thin films or nujol mulls, or as KBr discs.

Mass spectra were recorded using a VG Platform II electrospray mass spectrometer with methanol, water or acetonitrile as a carrier solvent. VG 7070E and Micromass Autospec spectrometers were also used, operating in EI, CI (NH_3) and FAB ionisation modes, as stated. MALDI-TOF spectra were recorded on a Kratos Kompact 4 spectrometer, operated in linear detection mode to generate positively charged ions.

The luminescence measurements for europium and terbium complexes were made on a Perkin Elmer LS50B spectrophotometer. The luminescence of ytterbium complexes were measured by excitation with a YAG driven optical parametric oscillator and detection using a liquid nitrogen cooled germanium photodiode (North Coast) equipped with a 1055 nm interference filter and a 40nm bandpass.

Analysis

Melting points were determined on a Reichert Köfler Block and are uncorrected. Elemental analyses were determined on a Carlorba 1106.

Crystallographic Data Collection

Single crystal X-ray intensity data was collected by Janet Moloney, on a Siemens SMART automated 3-circle diffractometer equipped with a CCD (512 x 512 pixel) area detector. The Molybdenum target sealed tube generator settings were 50kV and 45mA. The structures were solved, also by Janet Moloney, using direct and Fourier methods. All non-hydrogen atoms were refined with anisotropic displacement parameters.

6.2. Chapter 2 Experimental

(S)-Diethyl malate **23**[2]

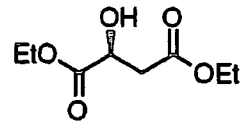

Malic acid **22** (2.5 g, 19 mmol) was dissolved in ethanol (80 ml) and conc. H_2SO_4 (1 ml) added. The mixture was boiled under reflux for 40 h until t.l.c. analysis showed the reaction to be complete. The solvents were removed under vacuum and the residue taken up into ethyl acetate (50 ml). The organic phase was washed with water (2 x 25 ml) and dried over K_2CO_3. The solvents were removed and the residue dried under vacuum to give a colourless oil (2.8 g, 99%).

δ_H ($CDCl_3$, 200 MHz): 1.20 (6H, t, $^3J_{H\text{-}H}$ = 6.7Hz, $CH_2C\underline{H}_3$), 2.73 (1H, d, $^3J_{H\text{-}H}$ = 5.9Hz, $CHC\underline{H}^aH^b$), 2.75 (1H, d, $^3J_{H\text{-}H}$ = 4.5Hz, $CHCH^a\underline{H}^b$), 3.36 (1H, s br, OH), 4.09 (2H, q, $^3J_{H\text{-}H}$ = 6.7Hz, $C\underline{H}_2CH_3$), 4.19 (2H, q, $^3J_{H\text{-}H}$ = 6.7Hz, $C\underline{H}_2CH_3$), 4.42 (1H, dd, $^3J_{H\text{-}H}$ = 5.9Hz $^3J_{H\text{-}H}$ = 4.5Hz, CH); δ_C ($CDCl_3$, 50 MHz): 12.4 (2 x $CH_2\underline{C}H_3$), 37.2 ($CHCH_2$), 59.2 ($\delta CO_2\underline{C}H_2CH_3$), 60.1 ($\alpha CO_2\underline{C}H_2CH_3$), 65.8 (CH), 168.9 (C=O), 171.7 (C=O); ν_{max} (Thin film)/cm^{-1}: 3491 (OH), 2984, 2948, 1736 (C=O), 1468, 1452, 1373, 1274, 1222, 1182, 1105, 1026, 956, 859; Data is consistent with that quoted in the literature.[2]

Diethyl-2-trifluoromethanesulfonatobutan-1,4-dioate **21**[3]

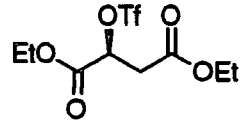

Diethyl malate **23**, (3.35 g, 17 mmol) and 2,6-lutidine (1.9 g, 17 mmol) were dissolved in dichloromethane (10 ml) under argon and the solution cooled to -78°C. A solution of trifluoromethanesulfonic anhydride (5.0g, 17 mmol) in dichloromethane (15 ml) cooled to -78°C was added *via* cannula transfer over 10 min. The reaction was left to stir for 1 h at -78°C before warming to room temperature and stirring for a further 3 h. The solvents were removed under vacuum. The pink residue was taken up into hexane (30 ml) and the salts removed by filtration. The solvents were removed under vacuum to give a pale pink viscous oil (3.5 g, 62%).

δ_H ($CDCl_3$, 200 MHz): 1.29 (3H, t, $^3J_{H-H}$ = 7.1Hz, $CH_2C\underline{H}_3$), 1.34 (3H, t, $^3J_{H-H}$ = 7.1Hz, $CH_2C\underline{H}_3$), 3.05 (2H, d, $^3J_{H-H}$ = 5.9 Hz, $CHC\underline{H}_2$), 4.22 (2H, q, $^3J_{H-H}$ = 7.1Hz, $C\underline{H}_2CH_3$), 4.33 (2H, q, $^3J_{H-H}$ = 7.1Hz, $C\underline{H}_2CH_3$), 5.49 (1H, t, $^3J_{H-H}$ = 5.9 Hz $^3J_{H-H}$ = 5.9 Hz, CH). Data is consistent with that quoted in the literature.[3]; δ_F ($CDCl_3$, 235 MHz) -75.0 (s, CF_3SO_3); ν_{max} (Thin film)/cm^{-1} 2987, 1745 (C=O), 1468, 1420, 1299, 1211, 1143, 1028, 937, 800, 619; $[\alpha]_D$ = -53.3° (c 3, dichloromethane).

1,4,7-tris[(3'ethoxycarbonyl)ethoxycarbonylpropyl]-1,4,7,10-tetraazacyclododecane **25**

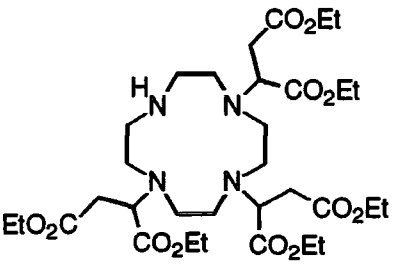

1,4,7,10-tetraazacyclododecane **5** (0.2 g, 1.2 mmol) and 2,6-lutidine (0.6 g, 5.9 mmol) were dissolved in dichloromethane (2 ml). A solution of the triflate of diethyl malate **21**, (1.9 g, 5.9 mmol) in dichloromethane (3 ml) was added under argon and the reaction was stirred at room temperature for 9 days. A second solution of the triflate (2.4 g, 7.4 mmol) was added to the reaction mixture and the reaction left for a further 14 days. The solvents were then removed and the residue purified by column chromatography over silica gel, eluting with 1% ammonia, 1% methanol and 30% dichloromethane in tetrahydrofuran. The solvents were removed to yield a colourless oil (180 mg, 25%).

R_f = 0.7 (5% NH_3, 5% methanol, 30% dichloromethane, 60% tetrahydrofuran); δ_H ($CDCl_3$, 200 MHz): 1.22 (18H, m, $CH_2C\underline{H}_3$), 2.75 (22H, m br, $C\underline{H}_2N$ and $CHC\underline{H}_2$), 4.10 (12H, m, $C\underline{H}_2CH_3$), 4.20 (3H, m, CH); δ_C ($CDCl_3$, 50 MHz): 14.1 ($CH_2\underline{C}H_3$), 29.5 - 38.7 (7 resonances, $CH\underline{C}H_2$), 46.0-51.5 (16 resonances, CH_2N), 56.6 - 61.8 (7 resonances, $\underline{C}HCH_2$), 60.5 ($\underline{C}H_2CH_3$), 171.0 - 171.7 (12 resonances, $\underline{C}O_2Et$); $^m/_z$ (Electrospray, ES+) = 689 (100%, M + H^+); Found 689.397 (CI+, NH_3), $C_{32}H_{56}N_4O_{12}$ requires 689.397; $[\alpha]_D$ = +1.6° (c 1, ethanol).

(±)-(R,R,R,R-)-1,4,7,10-Tetrakis-[(3'carboxy])-1'-carboxypropyl]-1,4,7,10-tetraazacyclododecane **26**

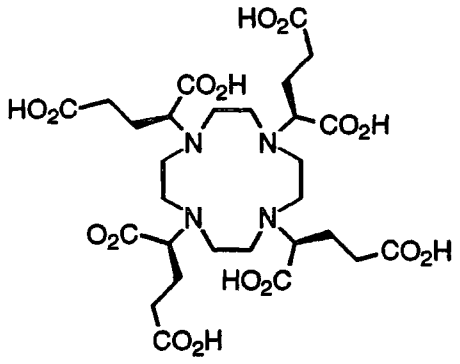

This sample was generously donated by Guerbet s.a., Paris, following fractional crystallisation of a stereoisomeric mixture from acidic aqueous solution.

δ_H (D_2O, 400 MHz): 1.81 (8H, m br, CHC<u>H</u>$_2$), 2.12 (8H, s br, C<u>H</u>$_2$CO$_2$H) 3.12 (16H, s br, C<u>H</u>$_2$N), 3.42 (4H, s br, CH); δ_C (D_2O, 100 MHz): 23.9 (CH<u>C</u>H$_2$), 34.4 (<u>C</u>H$_2$CO$_2$H), 47.4 (<u>C</u>H$_2$N), 64.1 (<u>C</u>H), 175.0 (C=O), 180.9 (C=O); ν_{max} (KBr Disc)/cm^{-1}: 3436 (OH), 2920, 1720 (δ-C=O), 1632 (α-C=O), 1460, 1402, 1366, 1314, 1222, 1088, 1032, 956, 826; $^m/_z$ (Electrospray, ES-) = 345 (100% M-2H$^+$) 691 (30% M-H$^+$).

(±)-(R,R,R,S-)-1,4,7,10-Tetrakis-[(3'carboxy])-1'-carboxypropyl]-1,4,7,10-tetraazacyclododecane **26**

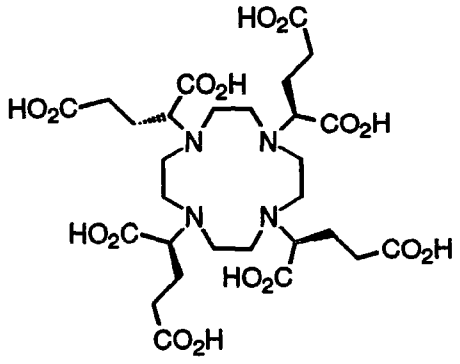

This sample was generously donated by Guerbet s.a., Paris, following fractional crystallisation of a stereoisomeric mixture from acidic aqueous solution.

δ_H (D_2O, 400MHz): 1.79 (8H, m br, CHC<u>H</u>$_2$), 2.41 (8H, m br, C<u>H</u>$_2$CO$_2$H) 3.13 (16H, m br, C<u>H</u>$_2$N), 3.63 (4H, m br, CH); δ_C (D_2O, 100 MHz): 20.4 (CH<u>C</u>H$_2$), 32.0 (<u>C</u>H$_2$CO$_2$H), 32.5 (<u>C</u>H$_2$CO$_2$H), 44.7 (<u>C</u>H$_2$N), 45.7 (<u>C</u>H$_2$N), 46.5 (<u>C</u>H$_2$N), 47.1 (<u>C</u>H$_2$N), 62.3 (<u>C</u>H), 63.5 (<u>C</u>H), 173.1 (C=O), 178.3 (C=O), 178.5

(C=O); ν_{max} (KBr Disc)/cm^{-1}: 3436 (OH), 2920, 1720 (δ-C=O), 1632 (α-C=O), 1460, 1402, 1366, 1314, 1222, 1088, 1032, 956, 826; $^{m}/_{z}$ (Electrospray, ES-) = 345 (100% M-2H$^+$), 691 (43% M-H$^+$); X-ray quality crystals were grown from aqueous solution acidified to pH 2 with hydrochloric acid. The crystallographic data are appended (Appendix II).

(R,S,R,S-)-1,4,7,10-Tetrakis-[(3'carboxy])-1'-carboxypropyl]-1,4,7,10-tetraazacyclododecane **26**

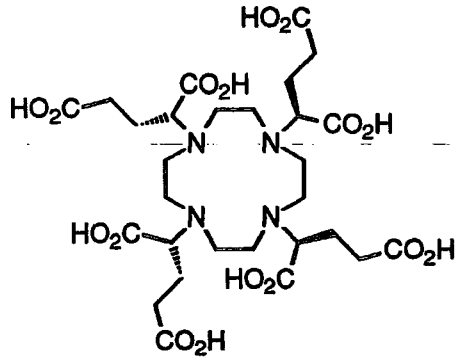

This sample was generously donated by Guerbet s.a., Paris, following fractional crystallisation of a stereoisomeric mixture from acidic aqueous solution.

δ_H (D_2O, 400 MHz): 1.3 - 2.8 (32H, m vbr, C$\underline{H}_2$N, C$\underline{H}_2$C$\underline{H}_2$$CO_2H$), 3.00 (4H, m br, C$\underline{H}$); δ_C (D_2O, 100 MHz): 19.1 (CH$\underline{C}H_2$), 27.4 (CH$\underline{C}H_2$), 34.9 ($\underline{C}H_2CO_2H$), 36.4 ($\underline{C}H_2CO_2H$), 44.8 ($\underline{C}H_2N$), 45.5 ($\underline{C}H_2N$), 46.2 ($\underline{C}H_2N$), 46.7 ($\underline{C}H_2N$), 63.0 ($\underline{C}H$), 64.6 ($\underline{C}H$), 178.7 (C=O), 180.9 (C=O), 182.5 (C=O), 183.1 (C=O); ν_{max} (KBr Disc)/cm^{-1}: 3436 (OH), 2920, 1720 (δ-C=O), 1632 (α-C=O), 1460, 1402, 1366, 1314, 1222, 1088, 1032, 956, 826; $^{m}/_{z}$ (Electrospray, ES-) = 345 (100% M-2H$^+$), 691 (35% M-H$^+$); X-ray quality crystals were grown from aqueous solution acidified to pH 2 with hydrochloric acid. The crystallographic data are appended (Appendix II).

(R,R,S,S-)-1,4,7,10-Tetrakis-[(3'carboxy])-1'-carboxypropyl]-1,4,7,10-tetraazacyclododecane **26**

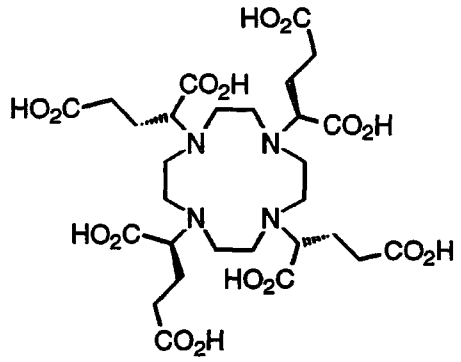

This sample was generously donated by Guerbet s.a., Paris, following fractional crystallisation of a stereoisomeric mixture from acidic aqueous solution.

δ_C (D_2O, 50 MHz): 24.1 (CH<u>C</u>H_2), 31.8 (CH<u>C</u>H_2), 39.5 (<u>C</u>H_2CO_2H), 40.9 (<u>C</u>H_2CO_2H), 48.7 (<u>C</u>H_2N), 49.3 (<u>C</u>H_2N), 50.6 (<u>C</u>H_2N), 51.8 (<u>C</u>H_2N), 67.8 (<u>C</u>H), 68.1 (<u>C</u>H), 68.4 (<u>C</u>H), 69.5 (<u>C</u>H), 185.1 (C=O), 188.9 (C=O); $^m/_z$ (Electrospray, ES-) = 345 (100% M-2H^+) 691 (40% M-H^+); X-ray quality crystals were grown from aqueous solution acidified to pH 2 with hydrochloric acid. The crystallographic data are appended (Appendix II).

General Method for the Synthesis of Europium(III) Complexes

A solution of europium(III) nitrate pentahydrate (31 mg, 73 μmol) in water (3 ml) was added to 1,4,7,10-tetrakis-[(3'carboxy)-1'-carboxypropyl]-1,4,7,10-tetraazacyclododecane **26** (50 mg, 73 μmol). The pH was raised to 5.5 by addition of sodium hydroxide solution, at which point the ligand slowly dissolved. The solution was heated at 90°C for 18 hours. The solvents were removed in *vacuo* and the complex recrystallised from water at pH 3, acidified with HCl.

Europium(III).(RRRR-) **26**

δ_H (D_2O, 200 MHz): 25 (4H, s, H^1_{ax}), 4 (4H, s, CHC<u>H</u>$^aH^b$), -0.5 (4H, s, C<u>H</u>$^aH^bCO_2H$), -1 (4H, s, CH^a<u>H</u>$^bCO_2H$), -2 (4H, s, CHCH^a<u>H</u>^{b}), -3 (4H, s, H^1_{eq}), -4 (4H, s, H^2_{ax}), -9 (4H, s, H^2_{eq}), -12 (4H, s, CH); ν_{max} (Thin film)/cm^{-1}: 3445 (OH), 2984, 2933, 1688 (br, C=O), 1598, 1451, 1410, 1315, 1219, 1097, 1076, 983, 920, 880; $^m/_z$ (Electrospray, ES-) = 419 (100% M-H^+), 839 (20% M^-) with correct isotope pattern; X-ray quality crystals were grown from aqueous

solution brought to pH 2 with hydrochloric acid. The crystallographic data are appended (Appendix II).

Europium(III).(RRRS-) **26**

δ_H (D_2O, 200 MHz): 48 (1H, s, H^1_{ax}), 46 (1H, s, H^1_{ax}), 45 (1H, s, H^1_{ax}), 40 (1H, s, H^1_{ax}), 27 (1/2H, s, H^1_{ax}), 24 (1/2H, s, H^1_{ax}), 22 (1/2H, s, H^1_{ax}), 21 (1/2H, s, H^1_{ax}), 8, 4, 3, 1, 0.5, 0.2, -2, -3, -6, -8, -9, -10, -11, -14, -16, -27 (1H, s, CH), -28 (2H, s, CH), -29 (1H, s, CH); ν_{max} (Thin film)/cm^{-1}: 3445 (OH), 2984, 2933, 1688 (br, C=O), 1598, 1451, 1410, 1315, 1097, 1076, 1000, 880; $^m/_z$ (Electrospray, ES-) = 419 (100% M-H^+), 839 (25% M^-) with the correct isotope pattern.

Europium(III).(RSRS-) **26**

δ_H (D_2O, 200 MHz): 50 (2H, s, 'H^1_{ax}), 39 (2H, s, H^1_{ax}), 7 (2H, s, H^1_{eq}), 0 (2H, s, 'H^1_{eq}), -1 (2H, s, '$C\underline{H}^aH^bCO_2H$), -3 (4H, s, $C\underline{H}_2CO_2H$), -4 (2H, s, '$CH^a\underline{H}^bCO_2H$), -5 (2H, s, 'H^2_{ax}), -6 (4H, s, $CHC\underline{H}_2$), -7 (2H, s, H^2_{ax}), -8 (2H, s, 'H^2_{eq}), -11 (2H, s, $CHC\underline{H}^aH^b$), -15 (2H, s, H^2_{eq}), -18 (2H, s, $CHCH^a\underline{H}^b$), 18.5 (2H, s, CH), -28 (2H, s, 'CH); ν_{max} (Thin film)/cm^{-1}: 3445 (OH), 2984, 2933, 1688 (br, C=O), 1598, 1451, 1410, 1315, 1174, 1097, 1076, 1000, 864, 737; $^m/_z$ (Electrospray, ES-) = 419 (100% M-H^+), 839 (33% M^-) with the correct statistical isotope pattern.

Europium(III).(RRSS-) **26**

δ_H (D_2O, 200 MHz): 51 (1H, s, H^1_{ax}), 46 (1H, s H^1_{ax}), 45 (1H, s, H^1_{ax}), 40 (1H, s, H^1_{ax}), 8, 4, 3, 2, -0.5, -2, -3, -4, -4.5, -5, -8, -9, -10, -11, -12, -13, -17, -18, -19, -26 (2H, s, CH), -29 (2H, s, CH); ν_{max} (Thin film)/cm^{-1}: 3445 (OH), 2984, 2933, 1688 (br, C=O), 1598, 1451, 1410, 1315, 1219, 1174, 1097, 1076, 1000, 880, 737; $^m/_z$ (Electrospray, ES-) = 419 (100% M-H^+), 839 (40% M^-) with correct isotope pattern.

General Method for the Synthesis of Gadolinium(III) Complexes

A solution of gadolinium(III) nitrate hexahydrate (34 mg, 73 μmol) in water (3 ml) was added to 1,4,7,10-tetrakis-[(3'carboxy)-1'-carboxypropyl]-1,4,7,10-tetraazacyclododecane **26** (50 mg, 73 μmol). The pH was raised to 5.5 with sodium hydroxide solution, at which point the ligand dissolved. The solution was heated at 90°C for 18 h. The solvents were removed in *vacuo*, and the complex crystallised from water acidified with HCl to pH 3.

Gadolinium(III).(RRRR-) **26**

ν_{max} (KBr disc)/cm^{-1}: 3446 (OH), 2934, 2869, 1717 (br, C=O), 1592, 1533, 1483, 1433, 1411, 1397, 1215, 1239, 1073, 1020, 794; $^{m}/_{z}$ (Electrospray, ES-) = 421 (100% M-H^+), 845 (38% M^-) with the correct isotope pattern; X-ray quality crystals were grown from aqueous solution by slow evaporation at pH 2. The crystallographic data is appended (Appendix II).

Gadolinium(III).(RRRS-) **26**

ν_{max} (KBr disc)/cm^{-1}: 3446 (OH), 2934, 2870, 1717 (br, C=O), 1592, 1533, 1483, 1446, 1411, 1397, 1215, 1171, 1239, 1073, 1003, 977, 794; $^{m}/_{z}$ (Electrospray, ES-) = 421 (100% M-H^+), 845 (42% M^-) with the correct isotope pattern.

Gadolinium(III).(RSRS-) **26**

ν_{max} (KBr disc)/cm^{-1}: 3447 (OH), 2935, 2869, 1717 (br, C=O), 1592, 1533, 1446, 1433, 1411, 1397, 1370, 1215, 1171, 1073, 1003, 927, 794; $^{m}/_{z}$ (Electrospray, ES-) = 421 (100% M-H^+), 845 (35% M^-) with the correct statistical isotope pattern.

General Method for Praseodymium(III) and Terbium(III) Complexes

A solution of terbium(III) nitrate (8 mg, 23 μmol) in water (3 ml) was added to the 1,4,7,10-tetrakis-[(3'carboxy)-1'-carboxypropyl]-1,4,7,10-tetraazacyclododecane **26** (15 mg, 22 μmol). The pH was raised to 5.5 with sodium hydroxide solution, upon which the ligand dissolved. The solution was heated at 90°C for 18 h. The complex was purified by ion exchange chromatography over Dowex 50W resin, eluting with aqueous ammonia, and the solvents removed in *vacuo.*

Praseodymium(III).(RRRR-) **26**

δ_H (D_2O, 200 MHz): 29 (4H, s, CH), 15, 14, 9, 8, 7, -3, -13 (4H, s, H^1_{eq}), -36 (4H, s, H^1_{ax}); $^{m}/_{z}$ (Electrospray, ES-) = 414 (55% M-H^+), 828 (100% M^-) with the correct isotope pattern.

Terbium(III).(RRRR-) **26**

δ_H (D_2O, 65 MHz): 359 (2.4H, s, CH^m), 336 (4H, s, CH^M), 153, 81, 73, 69, 63, 54, 48, 42, -93, -96, -106, -113, -410 (4H, s, H^M_{ax}), -476 (2.4H, s, H^m_{ax}); $^{m}/_{z}$ (Electrospray, ES-) = 848 (100% M-H^+) exhibiting correct isotope pattern; X-ray

quality crystals were grown from aqueous solution at pH 2. The crystallographic data are appended (Appendix II).

General Method for Neodymium(III) and Ytterbium(III) Complexes

Ytterbium oxide (6 mg, 15 μmol) and 1,4,7,10-tetrakis-[(3'carboxy)-1'-carboxypropyl]-1,4,7,10-tetraazacyclododecane **26** (20 mg, 29 μmol) were added to water (3 ml). The suspension was heated with stirring at 90°C for 3 days. The reaction was filtered through a plug of cotton wool and the solvents removed in *vacuo* and the complex crystallised from water acidified with hydrochloric acid.

Neodymium(III).(RRRR-) **26**

δ_H (D_2O, 200 MHz): 14 (4H, s, CH), 11, 9, 8, 7, 6, 5, 2 -14 (4H, s, H_{ax}); $^m/_z$ (Electrospray, ES-) = 832 (100%, M^-) with statistical isotope pattern.

Ytterbium(III) (RRRR-) **26**

δ_H (D_2O, 200 MHz): 100 (4H, s, H^1_{ax}), 18 (4H, s, H^1_{eq}), 12 (4H, s, H^2_{ax}), -10 (8H, s, $C\underline{H_2}CO_2H$), -13 (4H, s, $CHC\underline{H_2}$), -18 (4H, s, $CHC\underline{H_2}$), -38 (4H, s, H^2_{eq}), -75 (4H, s, CH); $^m/_z$ (Electrospray, ES-) = 430 (100% $M\text{-}H^+$), 861 (83% M^-) with the correct ytterbium isotope pattern.

Holmium(III).(RRRR-) **26**

A solution of holmium chloride (4 mg, 12 μmol) in water (3 ml) was added to the 1,4,7,10-tetrakis-[(3'carboxy)-1'-carboxypropyl]-1,4,7,10-tetraazacyclododecane **26** (8 mg, 12 μmol). The pH was raised to 5.5 with sodium hydroxide solution, upon which the ligand dissolved. The solution was heated at 90°C for 18 h then the solvents removed under reduced pressure.

δ_H (D_2O, 200 MHz): 85 (4H, s, CH), 50, 45, 37, 30, 25, 20, -40, -45, -90 (4H, s, H_{ax}); $^m/_z$ (Electrospray, ES-) = 425 (50% $M\text{-}H^+$), 853 (100% M^-) with a typical holmium isotope pattern;

Gadolinium(III) tetra(carboxamido-per-O-methyl-β-cyclodextrin ethyl)DOTA **35**

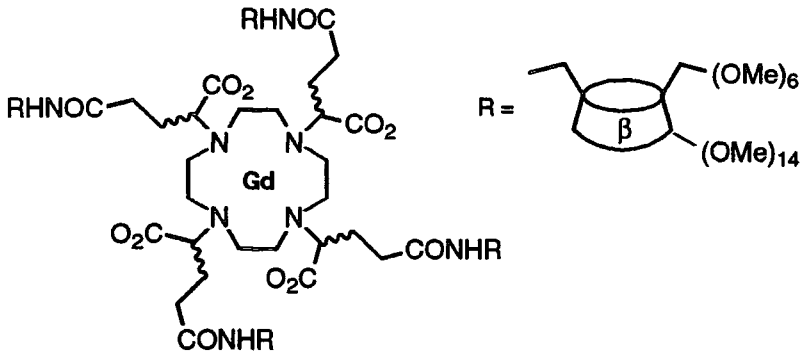

EDC (36 mg, 0.19 mmol) and *N*-hydroxysuccinimide (1 mg, 9 μmol) were added to a solution of Gadolinium(III) **26** (as a mixture of stereoisomers) (30 mg, 31 μmol) in water (2 ml). The solution was stirred at room temperature for 10 mins before addition of a solution of mono-amino-per-O-methyl β-cyclodextrin **34** (217 mg, 0.13 mmol) in water (2 ml). The reaction was left to stir at room temperature overnight. The reaction mixture was then transferred to a Sigma benzoylated dialysis membrane with a 2000 Dalton cutoff, which was placed in a beaker of water. The water was stirred continuously for 48 h and the water changed regularly. The reaction mixture was removed from the dialysis membrane and the solvents removed under reduced pressure to yield a colourless solid (120 mg, 59%).

ν_{max} (Thin film)/cm^{-1}: 2978, 2924, 2832, 1656 (C=O), 1624 (C=O), 1456, 1378, 1192, 1137, 1086, 1018, 969, 854, 503. Found C=49.8% H=7.5% N=2.1%, $C_{276}H_{476}N_8O_{148}GdNa.12H_2O$ requires C=49.7% H=7.6% N=1.7%.

General Method for the Epimerisation and Complexation of (±)-26 to (RRRR-)26

A suspension of ytterbium(III) oxide (4 mg, 11 μmol) and (±)-1,4,7,10-tetrakis-[(3'carboxy)-1'-carboxypropyl]-1,4,7,10-tetra-azacyclododecane **26** (15 mg, 22 μmol) in water (5 ml) was heated with stirring at 90°C for 3 days. The reaction mixture was then filtered through cotton wool and the solvents removed under reduced pressure. The colourless residue was then recrystallised from aqueous solution by slow evaporation of the solvent at 40°C. The small colourless crystals obtained gave identical data to that obtained for [Yb.(*RRRR*-)]**26**.

6.3. Chapter 3 Experimental

1,4,7-Tris[(3'methoxycarboxy)-1'-methoxycarboxypropyl]-1,4,7,10-tetraazacyclododecane **39**

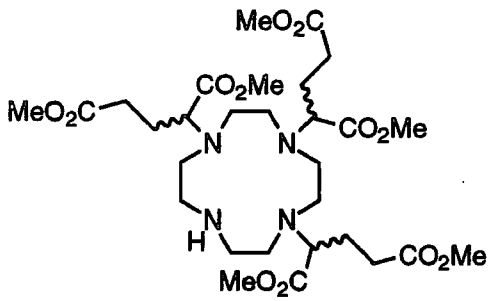

To a mixture of cyclen **5** (0.8 g, 4.6 mmol) and sodium hydrogen carbonate (1.2 g, 14 mmol) under argon in the presence of 4Å molecular sieves, was added dimethyl α-bromoglutarate **27** in acetonitrile (10 ml) by cannula transfer. The reaction was heated with stirring at 50°C under argon and followed by ESMS analysis. After 3 days the reaction mixture was filtered and the solvents removed under vacuo and the residue taken up into dichloromethane (20 ml). The organic layer was washed with HCl (pH 3), dried over K_2CO_3 and the solvents removed in *vacuo*. The residue was purified by column chromatography over silica gel. The column was eluted with dichloromethane, followed by 30% tetrahydrofuran in dichloromethane. The product was then obtained by elution with 5% ammonia, 5% methanol and 30% dichloromethane in tetrahydrofuran. The solvents were removed under vacuum to yield a pale yellow oil (0.48 g, 33%) which contained a mixture of the (*RRR-/SSS-*), (*RSR-/SRS-*) and (*RRS-/SSR-*) diastereoisomers.

R_f = 0.65 (5% NH_3, 5% methanol, 30% dichloromethane, 60% tetrahydrofuran, SiO_2); δ_H ($CDCl_3$, 300 MHz): 1.72-3.54 (28H, m, cyclen ring and 3 x CH_2CH_2), 3.62 (9H, s, $CH_2CO_2C\underline{H}_3$), 3.64 (6H, s, 2 x $CHCO_2C\underline{H}_3$), 3.70 (3H, s, $CHCO_2C\underline{H}_3$), 3.89 (2H, dd, $^3J_{H\text{-}H}$ = 6.0Hz, $^3J_{H\text{-}H}$ = 4.8Hz, 2 x CH), 4.31 (1H, dd overlapping, $^3J_{H\text{-}H}$ = 5.8Hz $^3J_{H\text{-}H}$ = 5.8Hz, CH); δ_C ($CDCl_3$, 50 MHz): 30.3 - 30.7 (6 resonances, $\underline{C}H_2CH_2CO_2H$), 44.5 - 64.4 (21 resonances, cyclen ring, $\underline{C}H$, $\underline{C}H_2CO_2H$), 51.7 (OCH_3), 172.1 - 173.4 (8 resonances, C=O); $^m/_z$ (Electrospray ES+) = 647 (100% $M+H^+$); ν_{max} (Thin film)/cm^{-1}: 3443 br (NH), 2953, 2847, 1730 (C=O), 1745 (C=O), 1453, 1253, 1209, 1169, 919, 732.

1,4,7,-Tris[(3'carboxy)-1'-carboxypropyl]-1,4,7,10-tetraazacyclododecane **40**

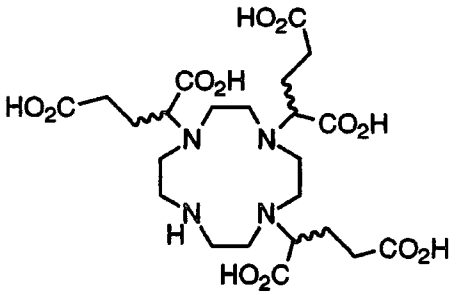

1,4,7-Tris[(3'methoxycarboxy)-1'-methoxycarboxypropyl]-1,4,7,10-tetraazacyclododecane **39** (63 mg, 97 μmol) was dissolved in a solution of lithium hydroxide (1M, 5 ml). The solution was heated to 80°C with stirring for 18 h. The solution was then eluted down a column of Dowex 50W cation ion exchange resin in strong acid form. The title compound was eluted with a 12% solution of aqueous ammonia. The solvents were removed under reduced pressure to yield the title compound as the hexaammonium salt (48 mg, 88%).

δ_H (D_2O, 300 MHz) 1.42 - 3.02 (28H, m, cyclen ring, C<u>H</u>$_2$C<u>H</u>$_2$), 3.08 (1H, m, C<u>H</u>), 3.14 (2H, m, C<u>H</u>); δ_C (D_2O, 75 MHz): 21.0 - 27.1 (7 resonances, <u>C</u>$H_2CH_2CO_2H$), 33.4 - 35.8 (4 resonances, CH_2<u>C</u>H_2CO_2H), 42.2 - 48.5 (12 resonances, cyclen ring), 62.7 - 64.2 (7 resonances, <u>C</u>H), 178.2 - 181.8 (7 resonances, C=O); ν_{max} (KBr disc)/cm^{-1}: 3600 - 3100 (NH, OH), 2868, 2812, 1628 (C=O), 1579, 1403, 1226, 1183, 1127, 1036, 1008, 666; Mp. > 250°C; $m/_z$ (Electrospray, ES+) = 563 (100% M+H^+);

1,4,7-Tris(tert-*butoxycarboxymethyl)-1,4,7,10-tetraazacyclododecane* **43**

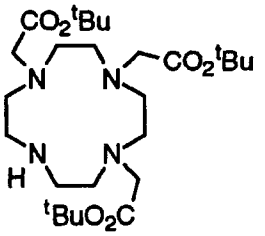

Sodium hydrogen carbonate (0.81 g, 9.6 mmol) and cyclen **5** (0.55 g, 3.2 mmol) were placed into a flask containing 4Å molecular sieves under argon. A solution of *tert*-butyl bromoacetate **42** (1.88 g, 9.6 mmol) in acetonitrile (15 ml) was added at room temperature under argon *via* cannula transfer. The reaction was left to stir for 18 h at room temperature. The inorganic material and molecular sieves were removed by filtration. The solvents were then removed under vacuo and the residue purified by column chromatography over silica gel. The column was first washed with dichloromethane, then 30%

tetrahydrofuran in dichloromethane before the title compound was eluted using 5% ammonia, 5% methanol, 30% dichloromethane, 60% tetrahydrofuran. The pale oil obtained was crystallised from acetonitrile and diethyl ether to give small colourless crystals (0.41 g, 25%).

R_f = 0.5 (5% NH_3, 5% methanol, 30% dichloromethane, 60% tetrahydrofuran, SiO_2); δ_H ($CDCl_3$, 200 MHz): 1.42 (27H, s, t-Bu), 2.95 (16H, m br, cyclen ring), 3.26 (2H, s, acetate CH_2), 3.34 (4H, s, 2 x acetate CH_2's); δ_C ($CDCl_3$, 50 MHz): 30.2 (9 x CH_3), 49.5 (CH_2 cyclen ring), 50.4 (acetate CH_2), 51.2 (acetate CH_2), 53.1 (CH_2 cyclen ring), 53.6 (CH_2 cyclen ring), 60.4 (CH_2 cyclen ring), 83.6 (2 x $\underline{C}(CH_3)_3$), 83.8 ($\underline{C}(CH_3)_3$), 171.4 (C=O), 172.2 (2 x C=O); ν_{max} (Golden Gate)/cm^{-1}: 1715 (C=O), 1367, 1254, 1152, 935, 848, 790, 752, 626; Mp. = 166 - 168 °C; $^m/_z$ (Electrospray, ES+) = 515 (100% $M+H^+$), 537 (5% $M+Na^+$); A suitable elemental analysis of this compound could not be obtained.

1,4,7-Tris(carboxymethyl)-1,4,7,10-tetraazacyclododecane 7[4]

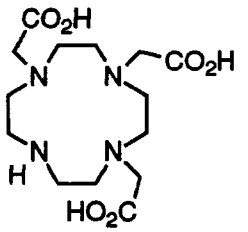

The *tert*-butyl ester of DO3A **43** (40 mg, 78 μmol) was dissolved in an 80% solution of trifluoroacetic acid in dichloromethane (4 ml) and stirred at room temperature for 1 h. The solvents were then removed under reduced pressure. Dichloromethane (2 x 10 ml) was added and removed under vacuum followed by diethyl ether (2 x 10 ml). The resulting white gum was taken up into water (5 ml) and the solvent removed on a freeze-drier to yield a colourless solid (27 mg, 99%).

δ_H (D_2O, 300 MHz): 2.64 - 3.53 (16H, m, cyclen ring), 3.36 (2H, s, $C\underline{H}_2CO_2H$), 3.95 (4H, s, $C\underline{H}_2CO_2H$); δ_C ($CDCl_3$, 50 MHz): 42.4 (CH_2N), 47.9 (CH_2N), 49.3 (CH_2N), 52.1 (CH_2N), 53.3 (CH_2CO_2H), 55.1 (CH_2CO_2H), 169.1 (C=O), 174.6 (C=O); ν_{max} (Golden gate)/cm^{-1}: 2978, 1731 (C=O), 1623 (C=O), 1558, 1472, 1349, 1181, 1139, 978, 876, 842, 699, 680; Mp. = 173-175°C; $^m/_z$ (Electrospray, ES+) = 347 (100% $M+H^+$). Data is consistent with that quoted in the literature.[4]

Molybdenum tricarbonyl-1,4,7,10-tetraazacyclododecane complex **44**[5]

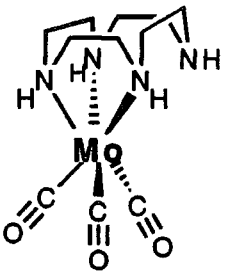

Molybdenum hexacarbonyl (1.64 g, 6.21 mmol) and cyclen **5** (1.07 g, 6.21 mmol) were placed in a flask under argon. Dibutyl ether (40 ml) was added and the mixture heated to 160°C with stirring for 2 h. The reaction was allowed to cool and the yellow preciptate was filtered from the reaction mixture under argon and dried in *vacuo*.

The yellow solid obtained was used directly without characterisation.

N-*Methyl-1,4,7,10-tetraazacyclododecane* **45**[6]

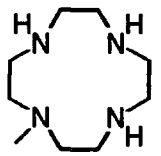

N,N-Dimethylformamide (5 ml) and triethylamine (53 mg, 0.5 mmol) were added to the cyclen molybdenum tricarbonyl complex **44** (184 mg, 0.5 mmol). At room temperature, methyl iodide (0.33 g, 2.3 mmol) was added and the reaction allowed to stir under argon for 4 h. The solvents were then removed under vacuo. The reaction was opened to the atmosphere, HCl (3M, 10 ml) added, and the solution stirred overnight. The solution was washed with dichloromethane (50 ml) before the pH was raised to 14 by addition of sodium hydroxide pellets. The solution was extracted into chloroform (3 x 300 ml). The organics extracts were combined and dried over K_2CO_3, the solvents were then removed in *vacuo* to yield a yellow solid, which was recrystallised from ethanol and water (74 mg, 76%).

δ_H (D_2O, 200 MHz): 2.32 (3H, s, NCH_3), 2.87 (16H, m, cyclen ring); δ_C (D_2O, 50 MHz): 46.3 (CH_2N), 46.6 (CH_2N), 47.4 (CH_2N), 48.0 (NCH_3), 56.8 (CH_2N); ν_{max} (Golden gate)/cm^{-1}: 3380 (NH), 2970, 2944, 2852, 1641 (NH), 1594, 1566, 1531, 1469, 1457, 1364, 1296, 1144, 1047, 1018, 987, 942, 857, 764, 747; Mp. = 15 -162 °C (lit[6]: 161-162°C); $^m/_z$ (Electrospray, ES+) = 187 (100% $M+H^+$); Data are consistent with that quoted in the literature.[6]

1-Methyl-4,7,10-tris(tert-*butoxycarboxymethyl*)*-1,4,7,10-tetraazacyclododecane* **46**

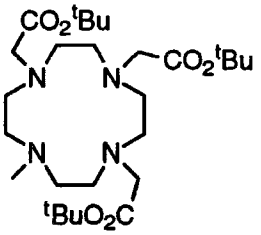

Mono-*N*-methyl-cyclen **45** (60 mg, 0.3 mmol) and caesium carbonate (0.32 g, 0.9 mmol) were added to acetonitrile (2 ml) under argon. A solution of *tert*-butyl bromoacetate **42** (0.19 g, 0.9 mmol) in acetonitrile (3 ml) was added at room temperature over 5 min by cannula transfer. The mixture was stirred under argon for 18 h. The solvents were removed under reduced pressure and the residue taken up into dichloromethane (15 ml). The inorganic residues were removed by filtration and the solvents removed under reduced pressure. The title compound was separated by column chromatography over silica gel. The column was washed with dichloromethane before elution with 30% tetrahydrofuran in dichloromethane. The solvents were removed under reduced pressure to afford a colourless oil (110 mg, 68%).

R_f = 0.6 (30% tetrahydrofuran in dichloromethane, SiO_2); δ_H ($CDCl_3$, 250 MHz): 1.39 (18H, s, CH_3), 1.43 (9H, s, CH_3), 2.21 (3H, s, NCH_3), 2.69 (16H, m br, cyclen ring), 3.03 (2H, s, NCH_2), 3.13 (4H, s, NCH_2); δ_C ($CDCl_3$, 50 MHz): 29.9 (CH_3), 30.1 (CH_3), 45.9 (NCH_3), 52.2 (CH_2N), 53.6 (CH_2N), 56.9 (CH_2N), 58.0 (CH_2N), 59.0 ($\underline{C}H_2CO$), 59.2 $\underline{C}H_2CO$), 83.9 ($\underline{C}(CH_3)_3$), 84.7 ($\underline{C}(CH_3)_3$), 174.8 ($\underline{C}O_2$t-Bu), 175.2 ($\underline{C}O_2$t-Bu); ν_{max} (Thin film)/cm^{-1}: 2976 br, 2832, 1725 (C=O), 1455, 1392, 1368, 1228, 1159, 919, 848, 730; $^m/_z$ (Electrospray, ES+) = 529 (30% $M+H^+$), 551 (100% $M+Na^+$).

1Methyl-4,7,10-tris-(*carboxymethyl*)*-1,4,7,10-tetraazacyclododecane* **41**

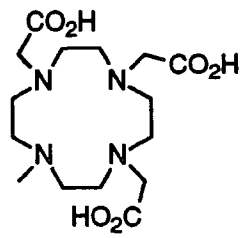

Tri-*tert*-butyl ester **43** (200 mg, 0.38 mmol) was dissolved in a 50% solution of trifluoroacetic acid in dichloromethane (10 ml) and stirred for 20 h. The solvents were removed under vacuum. Dichloromethane (3 x 30 ml) was added and removed under vacuum followed by diethyl ether (2 x 30 ml),

before water (20 ml) was added, washed with dichloromethane (30 ml) and removed under vacuum to yield a colourless solid (105mg, 77%)..

δ_H (D_2O, 300 MHz): 2.82 (3H, s, N-Me), 2.8-3.5 (22H, m br, cyclen ring, CH_2); δ_C (D_2O, 75 MHz): 43.2 (N-CH_3), 48.2 (CH_2N), 48.9 (CH_2N), 52.0 (CH_2N), 52.9 (CH_2N), 53.3 ($\underline{C}H_2CO_2H$ -N3 and 10), 55.2 ($\underline{C}H_2CO_2H$-N7), 168.9 (CO_2H), 174.7 (CO_2H); ν_{max} (Golden gate)/cm^{-1}: 3630 (OH), 1671 (C=O), 1560, 1461, 1179, 1127, 829, 801, 722, 666; Mp. = 105-108°C; $^m/_z$ (Electrospray, ES+) = 361 (100% M+H^+), 383 (5% M+Na^+).

1,4,7-Tris[(3'-methoxycarboxy)-1'methoxycarboxypropyl]-10-methoxycarbonyl methyl-1,4,7,10-tetraazacyclododecane **49**

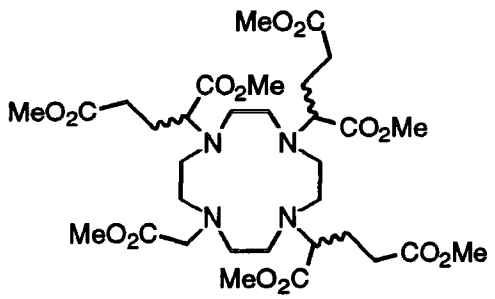

1,4,7,-Tris[(3'-methoxycarboxy)-1'-methoxycarboxypropyl]-1,4,7,10-tetra-azacyclododecane **39** (120 mg, 0.2mmol) and caesium carbonate (60 mg, 0.2 mmol) were dissolved in acetonitrile (1 ml) under argon. A solution of methyl bromoacetate (27 mg, 0.2 mmol) in acetonitrile (3 ml) was added at room temperature by cannula transfer. The solution was stirred under argon for 18 h. The solvents were removed under reduced pressure and the residue taken up into dichloromethane (10 ml). The inorganic material was removed by filtration and the solvents removed under reduced pressure. The title compound was purified by column chromatography over silica gel. The column was washed with dichloromethane before elution with 30% tetrahydrofuran in dichloromethane to obtain a colourless oil (29 mg, 22%).

R_f = 0.5 (5% methanol in dichloromethane, SiO_2); δ_H ($CDCl_3$, 300 MHz): 1.75-2.95 (16H, m, cyclen ring), 3.27 (5H, m, $C\underline{H}CO_2H$, $C\underline{H}_2CO_2H$), 3.60 (12H, s, α-OCH_3), 3.62 (9H, s, α-OCH_3); δ_C ($CDCl_3$, 75 MHz): 24.4-30.9 (10 resonances, $\underline{C}H_2\underline{C}H_2$), 50.3-53.7 (12, resonances, cyclen ring), 62.1 ($\underline{C}H_2CO_2H$), 63.4 ($\underline{C}HCO_2H$), 63.5 ($\underline{C}HCO_2H$), 71.8 ($\underline{C}HCO_2H$), 170.0-173.9 (7 resonances, C=O); ν_{max} (Thin film)/cm^{-1}: 2954, 2848, 1730 (C=O), 1676 (C=O), 1438, 1362, 1208, 1168, 986; $^m/_z$ (Electrospray, ES+) = 719 (100% M+H^+), 741 (20% M+Na^+);

1,4,7-Tris[(3'carboxy)-1'-carboxypropyl]-10-carboxyl methyl-1,4,7,10-tetraazacyclododecane **50**

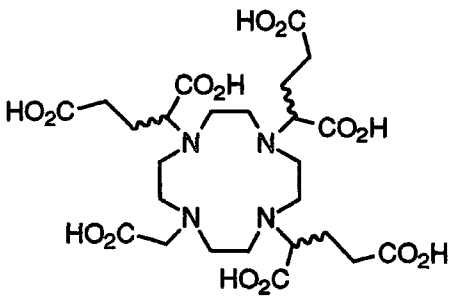

1,4,7-Tris[(3'methoxycarboxy)-1'-methoxycarboxypropyl]-10-methoxy carbonylmethyl-1,4,7,10-tetraazacyclododecane **49** (24 mg, 39 μmol) was dissolved in a solution of lithium hydroxide (1M, 5 ml). The solution was heated to 80°C with stirring for 18 h. The solution was then passed down a column of Dowex 50W cation ion exchange resin in strong acid form. The title compound was eluted with a 12% solution of aqueous ammonia. The solvents were removed under reduced pressure to yield the title compound as the corresponding ammonium salt (22 mg, 78%).

δ_H (D_2O, 200 MHz): 0.78 - 3.56 (33H, m, v br, cyclen ring, C<u>H</u>C<u>H</u>$_2$C<u>H</u>$_2$CO$_2$H); ν_{max} (KBr disc)/cm^{-1}: 3421 (OH), 2958, 2880, 1656 (C=O), 1590, 1407, 1346, 1178, 1154, 1091, 782, 636; Mp. > 250°C; $^m/_z$ (Electrospray, ES+) = 322 (100% $[M+H+Na]^{2+}$).

General Method for the Synthesis of Europium(III) Complexes

To a solution of 1,4,7-tris-[(3'carboxy)-1'-carboxypropyl]-10-carboxy methyl-1,4,7,10-tetraazacyclododecane **40** (40 mg, 71 μmol) in water (2 ml) was added a solution of europium(III) nitrate pentahydrate (31 mg, 71 μmol) in water (5 ml). The pH was raised to 5.5 by addition of sodium hydroxide solution and the solution was heated at 90°C for 8 h and the solvents removed under reduced pressure.

Direct preparation of Europium(III) **49** from **40**

A solution of europium triflate (19 mg, 31 μmol) in acetonitrile (2 ml) was added to a solution of the hexa ester (20 mg, 31 μmol) in acetontirile (1 ml) under argon. The solution was stirred for 6 hours before the addition of water (20 μl). The reaction was heated to 70°C for 18 h and the solvents removed under vacuo. The residue was taken up into water (3 ml) and heated at reflux

for 3 days until no ester was observed by ESMS analysis. The solvents were then removed under reduced pressure.

δ_H (D_2O, 200 MHz): 39, 35, 28, 26, 14-22 (br), 1, 0.5, -1, -2, -3, -4, -10, -11, -14, -18, -22; $^m/_z$ (Electrospray, ES-) = 710 (100% $M-H^+$) with correct isotope pattern.

Europium(III) **7**

δ_H (D_2O, 200 MHz): 25 (s), -2 (br), -3 (br), -5 (br), -6 (br), -8 (br), -13 (br); $^m/_z$ (Electrospray, ES+) = 519 (100% $M+Na^+$) with a typical europium isotope pattern.

Europium(III) **41**

The complex was purified by elution over alumina with 20% methanol in dicholoromethane to give a colourless solid.

δ_H (D_2O, 200 MHz): 40, 35, 28, 26, 20, 14 (br), 10 (br), -1, -2, -5, -6,-7, -10, -11, -12, -15 (br), -18, -23; $^m/_z$ (Electrospray, ES+) = 533 (100% $M+Na^+$) with the correct statistical isotope pattern.

Europium (III) **50**

δ_H (D_2O, 200 MHz): 50 (H_{ax}), 46 (H_{ax}), 45 (H_{ax}), 43 (H_{ax}), 42 (H_{ax}), 40 (H_{ax}), 36 (H_{ax}), 35 (H_{ax}), 34 (H_{ax}), 8, 7, -1, -2, -3, -4, -5, 6, -7, -8, -9, -10, -11, -12, -14, -15, -16, -17, -20 (CH), -22 (CH), -25 (CH), -26 (CH), -27 (CH); $^m/_z$ (Electrospray, ES+) = 768 (100% $M+H^+$) with correct isotope pattern.

6.4. Chapter 4 Experimental

m-*Nitrophenyl Glyoxal* **69**

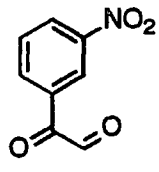

Selenium(IV) oxide (3.35g, 30.2 mmol) and *m*-nitroacetophenone (3.71g, 27.5 mmol) were dissolved in a 1,4-dioxane (18 ml) / water (2.4 ml) mixture. The solution was heated under reflux for 18 h and then allowed to cool to room temperature. The selenous salts were removed by filtration through celite and the solvents removed under vacuum. The brown residue was eluted over silica

gel with 20% tetrahydrofuran in dichloromethane. The solvents were removed under vacuo and the orange residue distilled twice by Kugelröhr (120°C, 0.5 mbar) to yield a bright yellow waxy solid (2.1g, 39%).

R_f = 0.3 (5% tetrahydrofuran in dichloromethane, SiO_2); δ_H ($CDCl_3$, 250 MHz): 7.75 (1H, t, $^3J_{H-H}$ = 8.0Hz, H-5), 8.52 (2H, m, H-4, H-6), 9.00 (1H, t, $^4J_{H-H}$ = 1.5Hz, H-2), 9.64 (1H, s, CHO); δ_C ($CDCl_3$, 50 MHz): 123.8 (d), 127.4 (d), 128.7 (s), 128.8 (d), 134.4 (d), 147.1 (s), 183.8 (s, ketone), 197.2 (d, aldehyde); ν_{max} (Thin film)/cm^{-1}: 3452 br (OH), 3089, 1705 br (C=O), 1614, 1531 (NO_2), 1480, 1439, 1351 (NO_2), 1086, 1000, 910, 811, 728; Mp. = 52.5-57°C; $^m/_z$ (EI+) = 104 (52%, $[M-NO_2-HCO]^+$), 122 (9% $[M-H(CO)_2]^+$), 133 (28%, $[M-NO_2]^+$), 150 (100%, $[M-HCO]^+$), 179 (6%, M^+); Found C=52.5% H=3.4% N=7.3%, $C_8H_5NO_4.0.2H_2O$ requires C=52.6% H=3.0% N=7.7%.

m-*Cyanophenyl Glyoxal* **70**

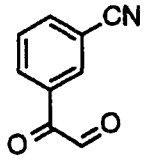

Selenium(IV) oxide (3.35g, 30.2 mmol) and *m*-acetylbenzonitrile (3.98g, 27.5 mmol) were dissolved in a 1,4-dioxane (18 ml) / water (2.4 ml) mixture. The solution was heated under reflux for 18 h and then allowed to cool to room temperature. The selenous salts were removed by filtration through celite and the solvents removed under vacuum. The brown residue was eluted over silica gel with 5% tetrahydrofuran in dichloromethane. The solvents were removed under vacuo and the orange residue distilled twice by Kugelröhr (140°C, 0.5 mbar) to yield a bright yellow waxy solid (3.32g, 76%).

R_f = 0.4 (5% tetrahydrofuran in dichloromethane, SiO_2); δ_H ($CDCl_3$, 300 MHz): 7.66 (1H, t, $^3J_{H-H}$ = 7.8Hz, H-5), 7.92 (1H, dt, $^3J_{H-H}$ = 7.8Hz $^4J_{H-H}$ = 1.5Hz, H-4), 8.43 (1H, dt, $^3J_{H-H}$ = 7.8Hz $^4J_{H-H}$ = 1.5Hz, H-6), 8.47 (1H, t, $^4J_{H-H}$ = 1.5Hz, H-2), 9.60 (1H, s, CHO); δ_C ($CDCl_3$, 75 MHz): 113.8 (CN), 117.7 (Ar-CN), 130.3 (C-5), 131.8 (C-1), 134.4 (C-4), 134.5 (C-6), 137.8 (C-2), 185.5 (ketone), 188.8 (aldehyde); ν_{max} (Thin film)/cm^{-1}: 3078, 2979, 2936, 2234 (CN), 1700 br (C=O), 1599, 1579, 1479, 1421, 1291, 1269, 1102, 1047, 984, 912, 786, 732, 678; Mp. = 65-73°C; $^m/_z$ (CI+) = 336 (100% $2M+NH_4^+$); Found C=66.7% H=3.4% N=8.6%, $C_9H_5NO_2$ $0.2H_2O$ requires C=66.7% H=3.3% N=8.6%.

2-(m-Cyanophenyl)-1,4,7,10-tretraazacyclododecane **71**

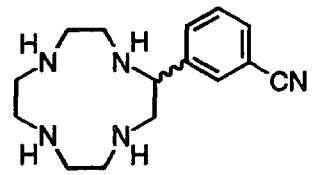

Iron(III) chloride hexahydrate (0.74 g, 2.7 mmol) was dissolved in methanol (20 ml) under argon. A solution of triethylenetetraamine **58** (0.40 g, 2.7 mmol) in methanol (10 ml) was added dropwise under argon over 30 min, resulting in the formation of an orange brown precipitate. *m*-Cyanophenyl glyoxal **70** (0.40 g 2.7 mmol) was dissolved in methanol (20 ml) and added to the triethylenetetraamine iron(III) complex. The reaction was left to stir at room temperature for 4 h under argon before $NaBH_4$ (3 x 0.4 g pellets, 32 mmol) was added over 30 min. The reaction was stirred for a further 2 h after which HCl (2M, ca. 10 ml) was added until a clear yellow solution was obtained. The volatile sovents were removed under vacuum and the remaining solution washed with dichloromethane (50 ml). The pH was then raised to 14 by addition of sodium hydroxide pellets and the solution extracted with chloroform (3 x 200 ml). The organic extracts were combined, dried over K_2CO_3 and the solvents removed under vacuum. The residue was purified by column chromatography over silica gel (10% ammonia, 10% methanol in tetrahydrofuran) to give a pale yellow oil (0.4g, 54%).

R_f = 0.2 (10% NH_3, 10% methanol in tetrahydrofuran, SiO_2); δ_H ($CDCl_3$, 250 MHz): 2.02-3.24 (14H, m , CH_2N), 2.37 (4H, s br, NH), 3.90 (1H, dd, CHN), 7.45 (1H, t, $^3J_{H\text{-}H}$ = 7.8Hz, H-5′), 7.56 (1H, d, $^3J_{H\text{-}H}$ = 7.8Hz, H-6′), 7.64 (1H, d, $^3J_{H\text{-}H}$ = 7.8Hz, H-4′), 7.73 (1H, s, H-2′); δ_C ($CDCl_3$, 50 MHz): 41.5 (CH_2N), 45.8 (CH_2N), 46.0 (CH_2N), 52.4 (CH_2N), 53.0 (CH_2N), 58.0 (CH_2N), 59.4 (CHN), 61.2 (CH_2N), 112.3 (CN), 118.7 (C-1′), 129.1 (C-6′), 130.7 (C-5′), 131.1 (C-2′), 131.6 (C-4′), 143.9 (C-3′); ν_{max} (Thin film)/cm^{-1}: 3540 (NH), 3018, 2844, 2236 (CN), 1434, 1202, 1136, 904, 837, 806, 718, 694; $^m/_z$ (Electrospray, ES+) = 274 (100% $M+H^+$).

2-(m-Cyanophenyl)-1,4,7,10-tetraazacyclododecane -N,N',N'',N'''*-1,4,7,10-tetra*-tert-*butylacetate* **MWC13**

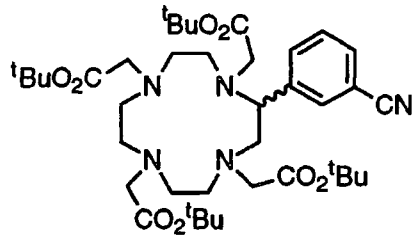

m-Cyanophenyl cyclen **71** (0.37 g, 1.3 mmol) and caesium carbonate (1.74 g, 5 mmol) were dissolved in acetonitrile (5 ml) under argon. *tert*-Butyl bromoacetate **42** (0.78 g, 4 mmol) was dissolved in acetonitrile (10 ml) under argon and added to the cyclen over 10 min by cannula transfer at room temperature. The reaction was left to stir for 4 h and followed by ESMS analysis. When no starting materials remained the solvents were removed in *vacuo*, and the residue taken up into dichloromethane (20 ml) and the inorganic material removed by filtration. The solvents were removed under vacuum and the residue purified by column chromatography over silica gel. The column was washed with dichloromethane before the title compound was eluted with 20% tetrahydrofuran in dichloromethane. Removal of the solvents under reduced pressure yielded a colourless oil (0.21 g, 22%).

R_f = 0.7 (20% tetrahydrofuran in dichloromethane, SiO_2); δ_H ($CDCl_3$, 200 MHz): 2.47 (36H, s, CH_3), 2.0-3.2 (16, m, CH_2N, $C\underline{H}_2CO_2H$), 3.42 (2H, s, $C\underline{H}_2CO_2H$), 3.51 (4H, s, $C\underline{H}_2CO_2H$), 3.74 (1H, dd , $^3J_{H\text{-}H}$ = 7.5Hz $^3J_{H\text{-}H}$ = 2.5Hz, CHN), 7.48 (1H, t, $^3J_{H\text{-}H}$ = 8.0Hz, H-5'), 7.63 (1H, d, $^3J_{H\text{-}H}$ = 8.0Hz, H-6'), 7.70 (1H, d, $^3J_{H\text{-}H}$ = 8.0Hz, H-4'), 7.77 (1H, s, H-2'); δ_C ($CDCl_3$, 50 MHz): 26.7 (CH_3), 50.1 (CH_2N), 50.7 (CH_2N), 51.7 (CH_2N), 51.9 (CH_2N), 54.8 (CH_2N), 55.1 (CH_2N), 55.3 (CH_2N), 60.5 ($\underline{C}H_2CO_2H$, CHN), 63.1 ($\underline{C}H_2CO_2H$), 79.3 ($\underline{C}(CH_3)_3$), 79.4 ($\underline{C}(CH_3)_3$), 79.5 ($\underline{C}(CH_3)_3$), 111.2 (CN), 117.3 (C-1'), 127.9 (C-6), 129.4 (C-5'), 130.3 (C-2'), 131.2 (C-4'), 141.3 (C-3'), 168.1 (C=O), 169.2 (C=O), 169.4 (C=O); ν_{max} (Thin film)/cm^{-1}: 2977, 2817, 2229 (CN), 1731 (C=O), 1479, 1455, 1392, 1367, 1156, 916, 851, 801, 735, 697; $^m/_z$ (Electrospray, ES+) = 730 (100% $M+H^+$), 752 (95% $M+Na^+$); Found C=60.6% H=8.2% N=9.0%, $C_{39}H_{63}N_5O_8.2H_2O$ requires C=61.1% H=8.7% N=9.2%.

2-m-Cyanophenyl-1,4,7,10-tetraazacyclododecane-N,N',N'',N'''-1,4,7,10-tetraacetic acid **73**

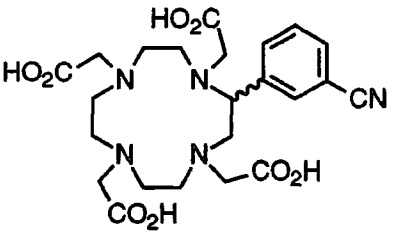

The tetra-*t*-butyl ester **71** (112 mg, 0.15 mmol) was dissolved in 50% trifluoroacetic acid in dichloromethane (5 ml) and stirred for 24 h. The solvents were then removed under vacuum and dichloromethane (2 x 5 ml) added and removed under vacuum. Methanol (5 ml) was added and removed under vacuum before the oily residue was titurated twice with diethyl ether. Upon decanting the solvents and drying under vacuum a colourless solid was obtained in quantitative yield.

δ_H (CD_3OD, 300 MHz): 2.50-3.37 (16H, m, CH_2N (ring), $C\underline{H}_2CO_2H$), 3.43 (4H, s, $C\underline{H}_2CO_2H$), 3.65 (2H, s, $C\underline{H}_2CO_2H$), 3.89 (1H, dd overlapping, $^3J_{H\text{-}H}$ = 8.2Hz $^3J_{H\text{-}H}$ = 7.9Hz, CHAr), 6.96 (1H, t, $^3J_{H\text{-}H}$ = 7.8Hz, H-5'), 7.08 (1H, d, $^3J_{H\text{-}H}$ = 7.8Hz, H-6'), 7.22 (1H, d, $^3J_{H\text{-}H}$ = 7.8Hz, H-4'), 7.31 (1H, s, H-2'); δ_C (D_2O, 75 MHz): 49.7 (CH_2N), 50.5 (CH_2N), 51.6 (CH_2N), 52.1 ($\underline{C}H_2CO_2H$), 52.5 (CH_2N), 52.7 (CH_2N), 53.9 (CH_2N), 54.0 ($\underline{C}H_2CO_2H$), 54.6 (CH_2N), 56.3 (CH_2N), 56.6 ($\underline{C}H_2CO_2H$), 112.3 (CN), 119.1 (C-1'), 128.6 (H-5'), 129.9, (H-6'), 130.5 (H-4'), 133.8 (H-2'), 136.6 (H-3') 172.0 (C=O), 172.8 (C=O), 173.9 (C=O), 174.1 (C=O); ν_{max} (Nujol mull)/cm^{-1}: 2234 (CN), 1718 (C=O), 1650 (C=O), 1304, 1202, 978, 966, 918, 834, 800, 720; $^m/_z$ (Electrospray, ES+) = 506 (100% $M+H^+$); Mp. = 119-122°C.

Europium(III) **73**

The complex was prepared according to the general method given Chapter 6.2, although it could not be crystallised from acidic aqueous solution.

δ_H ($CDCl_3$, 200 MHz): 16 (s, br), 6-10 (m, br), 2-3.5 (m), 1 (m), 0--8 (m, br), -10--14 (m, br); ν_{max} (KBr disc)/cm^{-1} 2244 (CN), 1690 (C=O), 1648 (C=O), 1386, 1214, 1142, 1090, 940, 838, 806, 640; $^m/_z$ (Electrospray, ES-) = 652 (100% M^-) with the expected europium isotope pattern.

1,3-Dithiolane-2-carboxylic acid **79**

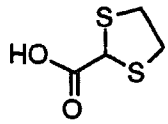

Ethyl 1,3-dithiolane-2-carboxylate **78** (15.5 g, 106 mmol) and lithium hydroxide (1M, 100 ml) were heated to 60°C with stirring for 4 h. The reaction was allowed to cool, then washed with dichloromethane (200 ml). The pH was lowered to <1 by addition of HCl (10M) before extraction with dichloromethane (3 x 300 ml). The organic layers were combined, dried over $MgSO_4$ and the solvents removed under vacuo to give a colourless solid (12.6 g, 96%).

δ_H ($CDCl_3$, 200 MHz): 3.40 (4H, m, AA'BB', CH_2CH_2), 4.83 (1H, s, CH), 9.9 (1H, s br, CO_2H); δ_C ($CDCl_3$, 50MHz): 40.9 (CH_2CH_2), 52.2 (CH), 179.3 (C=O); ν_{max} (Thin film)/cm^{-1}: 2966, 2932, 2844, 1691 (C=O), 1424, 1300, 1196, 915, 807, 770, 686, 654; Mp. = 78-80°C (lit[7]: 86-88°C); $^m/_z$ (Electrospray, ES-) = 149 (100% M-H^+); Found C=31.5% H=4.0%, $C_4H_6O_2S_2$ requires C=32.0% H=4.0%.

2-Piperidylcarbonyl-1,3-dithiolane **80**

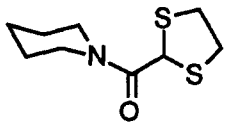

The 1,3-dithiolane-2-carboxylic acid **79** (12 g, 80 mmol) was dissolved in dichloromethane (50 ml). Piperidine (35 g, 418 mmol) was added followed by thionyl chloride (15 g, 125 mmol) added dropwise and the reaction mixture stirred for 1 h. The volatile materials were removed under reduced pressure and the residue taken up into dichloromethane (50 ml). The organic phase was washed with water (2 x 50 ml), dried over K_2CO_3 and the solvents removed under reduced pressure. The residue was dissolved in hot diethyl ether (800 ml) and filtered. The solvents were removed under reduced pressure to give a colourless solid (12.7g, 73%).

δ_H ($CDCl_3$, 200 MHz): 1.68 (6H, s br, $CH_2C\underline{H_2}C\underline{H_2}C\underline{H_2}CH_2$), 3.45 (8H, m, $C\underline{H_2}NC\underline{H_2}$ overlapping $SC\underline{H_2}C\underline{H_2}S$), 5.27 (1H, s, CH); δ_C ($CDCl_3$, 75 MHz): 25.6 (NCH_2), 29.9 ($NCH_2\underline{C}H_2$), 39.4 ($S\underline{C}H_2$), 44.1 ($NCH_2CH_2\underline{C}H_2$), 50.4 (CH), 168.1 (C=O); ν_{max} (Golden gate)/cm^{-1}: 2938, 2922, 2852, 1625 (C=O), 1437, 1292, 1271, 1218, 1121, 1011, 853, 788, 661; Mp. = 88-89°C; $^m/_z$ (EI+) = 185

(15% M^+), 112 (100% $[C_5H_{10}NCO]^+$) 84 (55% $C_5H_{10}N^+$); Found C=49.3% H=7.0% N=6.5%, $C_9H_{15}NOS_2$ requires C=49.7% H=7.0% N=6.4%.

3-Phenyl-1,1-dithiolane **81**

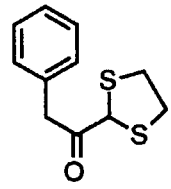

The piperidylamide **80** (4.5 g, 21 mmol) was dissolved in diethyl ether (150 ml) and added dropwise, under argon, to an ether solution of benzylmagnesium chloride (1M, 90 ml) by cannula transfer at room temperature over 1 h. The reaction was then heated under reflux for 4.5 h. The reaction was allowed to cool to room temperature before a saturated ammonium chloride solution (100 ml) was added and stirred for 30 min. The organic layer was separated and the aqueous phase washed with diethyl ether (3 x 50 ml). The organic layers were combined, dried over K_2CO_3 and the solvents removed under reduced pressure. The residue was purified by column chromatography over silica gel with dichloromethane to afford the title compound as a waxy colourless solid (4.4 g, 79%).

R_f = 0.8 (dichloromethane, SiO_2); δ_H ($CDCl_3$, 250 MHz): 3.32 (4H, s, CH_2CH_2), 3.95 (2H, s, Ph-$C\underline{H}_2$), 4.96 (1H, s, CH), 7.32 (5H, m, Ph); δ_C ($CDCl_3$, 63 MHz): 39.2 (CH_2CH_2), 45.7 (Ph-$\underline{C}H_2$), 57.2 (CH), 127.4 (C-4), 128.9 (C-3), 130.0 (C-2), 134.2 (C-1), 200.9 (C=O); ν_{max} (Thin film)/cm^{-1}: 3085, 3058, 3027, 2932, 2860, 1716 (C=O), 1636 (C=O), 1495, 1453, 1422, 1322, 1276, 1105, 1056, 846, 750, 699; Mp. = 43-47 °C; $^m/_z$ (GCMS, EI+) = 91 (26% $PhCH_2^+$), 105 (100% $PhCH_2CO^+$), 196 (5% $(M-C_2H_4)^+$), 224 (4% M^+); Found C=59.3% H=5.5%, $C_{11}H_{12}OS_2$ requires C=58.9% H=5.4%.

6.5. Chapter 5 Experimental

N'N''N'''N''''- *Tetra*-tert-*butylcarbamate-1,5,12,16 -tetraaminohexadeca-6,10-diamideamide.* **84**

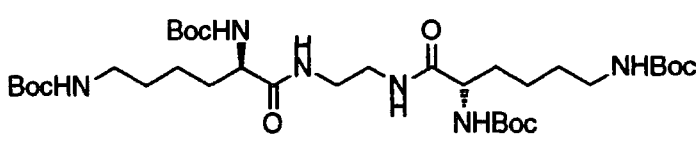

N_α, N_ε-Di-^{t}Boc Lysine-*N*-hydroxysuccinimide ester **82** (2.5 g, 5.6 mmol) was dissolved in dichloromethane (15 ml) under argon. A solution of

ethylenediamine (0.17 g, 2.8 mmol) in dichloromethane (5 ml) was added and the reaction left to stir at room temperature for 1 h. The reaction was filtered and washed with dichloromethane (50 ml) and aqueous sodium hydrogen carbonate solution (50 ml). The organic layer was separated and the solvents removed under vacuum to yield a colourless solid (3.9 g, 97%).

δ_H (DMSO, 200 MHz): 1.38 (44H, s overlapping m, CH_3, $C\underline{H}_2C\underline{H}_2CH_2NH$), 2.87 - 3.09 (12H, m, $C\underline{H}_2NH$, $CHC\underline{H}_2$), 3.81 (2H, dd, $^3J_{H\text{-}H}$ = Hz, CH), 6.78 (4H, s br, NHBoc), 7.87 (2H, s br, CONH); δ_C (DMSO, 50 MHz): 24.6 ($\underline{C}H_2CH_2NHBoc$), 30.0 ($CHCH_2\underline{C}H_2$), 30.1 (t-Bu), 31.0 ($CH\underline{C}H_2$), 33.5 ($CH_2\underline{C}H_2NHBoc$), 56.2 (CH), 81.0 ($\underline{C}(CH_3)_3$), 157.1 (carbamate), 157.4 (carbamate), 174.1 (amide); ν_{max} (Golden gate)/cm^{-1}: 3376 (NH), 3342 (NH), 3319 (NH), 2987, 2939, 1685 (carbamate), 1633 (amide), 1519, 1435, 1363, 1299, 1163, 998, 621; Mp. = 177.5-179°C; $^m/_z$ (Electrospray, ES+) = 717 (100% $M+H^+$), 739 (15% $M+Na^+$); Found C=54.3% H=8.7% N=11.3%, $C_{34}H_{64}N_6O_6.2H_2O$ requires C=54.3% H=9.0% N=11.2%; An $[\alpha]_D$ of this compound could not be obtained due to its poor solubility.

1,5,12,16-Tetraaminohexadeca-6,10-diamideamide tetra(trifluoroacetate). **85**

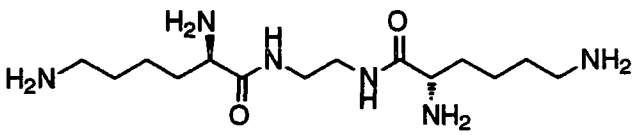

N'N''N'''N''''- Tetra-*tert*-butylcarbamate-1,5,12,16-tetraaminohexadeca-6,10-diamideamide **84** (3.86 g, 5.4 mmol) was dissolved in 80% trifluoroacetic acid in dichloromethane (20 ml) and allowed to stir for 15 min. The solvents were then removed under reduced pressure, dichloromethane (3 x 30 ml) was added and removed under vacuum, followed by diethyl ether (2 x 30 ml). The resulting residue was stirred with methanol (30 ml) for 5 min before addition of diethyl ether (20 ml). Filtration gave the title compound as a colourless solid (2.84 g, 92%).

δ_H (D_2O, 300 MHz): 1.32 (4H, m, $CHCH_2C\underline{H}_2$), 1.61 (8H, m, $CHC\underline{H}_2$ and $C\underline{H}_2CH_2NH_2$), 2.92 (4H, t, $^3J_{H\text{-}H}$ = 6.9Hz, $C\underline{H}_2NH_2$), 3.24 (4H, s, $C\underline{H}_2NHC{=}O$), 3.46 (2H, dd overlapping, $^3J_{H\text{-}H}$ = 7.4Hz $^3J_{H\text{-}H}$ = 5.9Hz, CH); δ_C (D_2O, 100 MHz): 22.0 ($CHCH_2\underline{C}H_2$), 29.5 ($\underline{C}H_2CH_2NH_2$), 33.8 ($CH\underline{C}H_2$), 38.3 (CH_2NH_2), 39.7 ($\underline{C}H_2NHC{=}O$), 54.4 (CH), 177.8 (C=O); ν_{max} (Golden gate)/cm^{-1}: 3250 (NH), 2970, 2936, 2872, 1669, (C=O), 1596, 1514, 1434, 1394, 1198, 1123, 838, 796, 721;

$^{m}/_{z}$ (Electrospray, ES+) = 339 (15% M+Na$^+$), 317 (100% M+H$^+$), 164 (40%, M+2H$^+$); $[\alpha]_D$ = +62° (c 1.6, methanol).

1,5,12,16-Tetraamino-7,11-diazahexadecane hexahydrochloride **86**

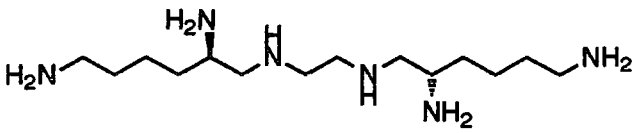

Lysine ethylenediamide **85** (1.3 g, 2.4 mmol) was dissolved in a solution of borane THF complex in tetrahydrofuran (1M, 100 ml) at room temperature, under argon. The solution was heated under reflux with stirring for 48 h. The reaction was allowed to cool to room temperature and the residual borane quenched by dropwise addition of methanol. The solvents were removed under reduced pressure before further addition of methanol (3 x 40 ml), which was successively removed under vacuum. This procedure was repeated on the residue. The resulting residue was taken up into HCl (2M, 30 ml) and heated to 100°C for 24 h. The solvents were then removed in *vacuo* and dried under vacuum to give a hygroscopic, colourless, sticky gum (1.00 g, 98%).

δ_H (CD_3OD, 200 MHz): 1.74 (12H, m br, $C\underline{H_2}CH_2C\underline{H_2}NH_2$), 3.00 (8H, m br,), 3.09 (8H, s, $NHC\underline{H_2}C\underline{H_2}NH$), 3.73 (2H, dd overlapping, $^3J_{H\text{-}H}$ = 6.6Hz $^3J_{H\text{-}H}$ = 8.2Hz, CH); δ_C (CD_3OD, 50 MHz): 21.8 ($CHCH_2\underline{C}H_2$), 26.1 ($\underline{C}H_2CH_2NH_2$), 30.7 ($CH\underline{C}H_2CH_2$), 37.9 ($\underline{C}H_2NH_2$), 48.9 ($CH\underline{C}H_2$), 50.4 ($\underline{C}H_2NHCH_2CH$), 60.0 (CH); ν_{max} (Thin film)/cm^{-1}: 3400 (br NH), 2938, 2862,1438, 1386, 1200, 1172, 1119, 976, 832, 798, 720, 668; $^{m}/_{z}$ (Electrospray, ES+) = 289 (40% M+H$^+$), 157 (45% M+2Na$^+$), 146 (15% M+2H$^+$), 128 (70% M+3Na$^+$), 98 (100% M+3H$^+$); $[\alpha]_D$ = +16° (c 2.5, methanol).

The free amine was obtained by elution of an aqueous solution of the hydrochloride salt over Amberlite-IRA 400 strong anion exchange resin pretreated with sodium hydroxide.

2-m-Nitrophenyl-5,12-(S),(S)-(4-aminobutyl)-1,4,7,10-cyclododecane **88**

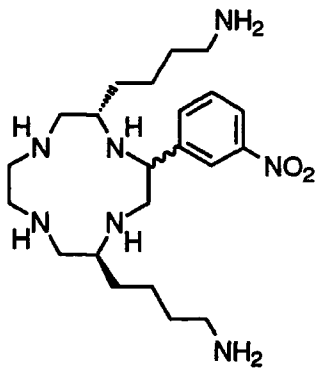

To a solution of iron(III) chloride (0.28 g, 1.0 mmol) in methanol (10 ml) under argon was added a solution of 1,5,12,16-tetraamino-7,11-diazahexadecane **86** (0.30 g, 1.0 mmol) in methanol (10 ml). An orange precipitate rapidly formed and the resultant suspension was stirred for 30 min. Di-*tert*-butyl dicarbonate (0.67 g, 3.1 mmol) was added and the reaction stirred overnight at room temperature under argon. *m*-Nitrophenyl glyoxal **69** (0.18 g, 1.0 mmol) was added and the reaction was left to stir at room temperature for 4 h under argon before $NaBH_4$ (3 x 0.4 g pellets, 32 mmol) was added over 30 min. The reaction was stirred for a further 2 h after which HCl (2M) was added until a clear yellow solution was obtained. The volatile solvents were removed under vacuum and the remaining solution washed with dichloromethane (50 ml). The pH was then raised to 14 by addition of sodium hydroxide pellets and the solution extracted with chloroform (3 x 200 ml). The organic extracts were combined, dried over K_2CO_3 and the solvents removed under vacuum. No further purification was undertaken and the title compound was not isolated in pure form.

δ_H (D_2O 300 MHz): 1.59 (12H, m, $CHC\underline{H_2}C\underline{H_2}C\underline{H_2}$), 2.40 - 4.00 (17H, m br, cyclen ring, $C\underline{H_2}NH_2$), 7.76 (1H, t, $^3J_{H\text{-}H}$ = 7.5 Hz, H-5′), 7.94 (1H, d, $^3J_{H\text{-}H}$ = 7.5 Hz, H-6′), 8.32 (1H, d, $^3J_{H\text{-}H}$ = 7.5 Hz, H-4′), 8.41 (1H, s, H-2′).

tert-*Butylcarbamate-glutamine amide* **91**

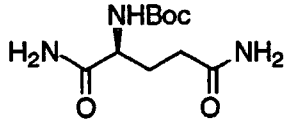

N-Boc-glutamine *para*nitrophenol ester **90** (13 g, 35 mmol) was dissolved in dichloromethane (100 ml) and ammonia (100 ml) condensed into the solution. The reaction rapidly turned bright yellow and was left to stir for 1 h then the ammonia was allowed to evaporate overnight. The precipitate was filtered and washed repeatedly with ether until the filtrate was colourless. The residue was taken up into water (70 ml) and washed with ether (300 ml). The water was removed under reduced pressure to yield a colourless solid (8.0 g, 93%).

δ_H (D_2O, 300 MHz): 1.28 (9H,s , t-Bu), 1.83 (2H,m , $CHC\underline{H}_2$), 2.24 (2H, t, $^3J_{H\text{-}H}$ = 7.2Hz, $C\underline{H}_2CONH_2$), (1H, dd overlaping, $^3J_{H\text{-}H}$ = 6.0Hz $^3J_{H\text{-}H}$ = 6.3Hz, CH); δ_C (D_2O, 50 MHz): 27.2 ($CH\underline{C}H_2$), 27.8 (CH_3), 31.4 ($\underline{C}H_2CONH_2$), 54.2 ($\underline{C}(CH_3)_3$), 81.8 (CH), 157.6 (γ-amide), 177.4 (α-amide), 178.1 (carbamate); ν_{max} (Golden gate)/cm^{-1}: 3387 (NH), 3327 (NH), 3182 (NH), 2932, 1686 (carbamate), 1657 (amide), 1270, 1250, 1165, 1059; Mp. = 118-119°C (lit[8]: 132-133°C); $^m/_z$ (Electrospray, ES+) = 268 (100% M+Na^+); Found C=48.8% H=7.9% N=17.0%, $C_{10}H_{19}N_3O_4$ requires C=48.9% H=7.8% N=17.1%; $[\alpha]_D$ = +2.8° (c 5, methanol).

Glutamine amide trifluoroacetate **92**

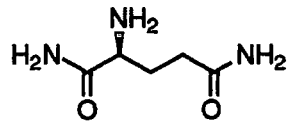

The *N*-t-Boc glutamine amide **91** (7.4 g, 30 mmol) was dissolved in 80% trifluoroacetic acid in dichloromethane (40 ml) and allowed to stir for 15 min. The solvents were then removed under reduced pressure, dichloromethane (3 x 30 ml) was added and removed under vacuum, followed by diethyl ether (2 x 30 ml). The resulting residue was stirred with methanol (50 ml) for 5 min before addition of diethyl ether (20 ml) and filtration gave the title compound as a colourless solid (7.24 g, 99%).

δ_H (D_2O, 200 MHz): 2.16 (2H, m, $CHC\underline{H}_2$), 2.48 (2H, t, $^3J_{H\text{-}H}$ = 7.1Hz, $C\underline{H}_2CONH_2$), 3.99 (1H, dd overlaping, $^3J_{H\text{-}H}$ = 6.0Hz $^3J_{H\text{-}H}$ = 6.3Hz, CH); δ_C (D_2O, 50 MHz): 29.9 ($CH\underline{C}H_2$), 33.5 ($\underline{C}H_2CONH_2$), 55.7 (CH), 174.1 (γ-amide), 179.0 (α-amide); ν_{max} (Golden gate)/cm^{-1}: 3336 (br, NH), 1657 (C=O), 1427, 1184, 1134, 972, 836, 723; $^m/_z$ (Electrospray, ES+) = 146 (100% M+H^+), 291 (10% M_2+H^+); $[\alpha]_D$ = +16° (c 1.2, trifluoroacetic acid).

tert-*Butylcarbamate-glutamine-glutamine amide* **93**

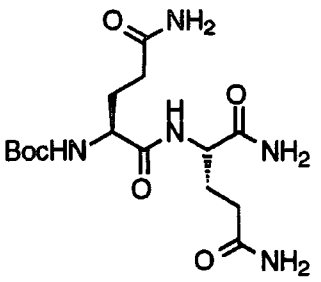

To a solution of glutamine amide **91** (7.2 g, 29.8 mmol) in tetrahydrofuran (100 ml) was added a solution of Boc glutamine *p*-nitrophenol ester **90** (10.9 g, 29.8 mmol) in tetrahydrofuran (100 ml) at room temperature. Triethylamine (3.0 g, 30 mmol) was added and the solution was left to stir for 6 h. The precipitate was filtered from the bright yellow solution and washed repeatedly with diethyl ether until the washings were colourless. The residue was taken up into water (50 ml) and washed with diethyl ether (200 ml). The solvents were removed under reduced pressure to give a colourless solid (9.5 g, 85%).

δ_H (D_2O, 300 MHz): 1.27 (9H, s, CH_3), 1.90 (4H, m, $CHC\underline{H}_2$), 2.23 (4H, t, $^3J_{H\text{-}H}$ = 6.9Hz, $C\underline{H}_2CONH_2$), 3.89 (1H, dd overlapping, $^3J_{H\text{-}H}$ = 7.5Hz $^3J_{H\text{-}H}$ = 5.4Hz, CH), 4.18 (1H, dd overlapping, $^3J_{H\text{-}H}$ = =7.2Hz $^3J_{H\text{-}H}$ = 5.5Hz, CH); δ_C (D_2O, 50 MHz): 25.3 ($CH\underline{C}H_2$), 26.1 (CH_3), 29.7 ($\underline{C}H_2CONH_2$), 51.3 (CH), 52.9 (CH), 80.2 ($\underline{C}(CH_3)_3$), 173.1 (amide), 174.2 (carbamate), 176.4 (amide); ν_{max} (Golden gate)/cm^{-1}: 3360 (NH), 3202 (NH), 2966, 2940, 1637 (br, C=O), 1516, 1417, 1366, 1336, 1250, 1168, 1049, 950, 867, 784; Mp. = 179-180°C; $^m/_z$ (Electrospray, ES+) = 396 (100% $M+Na^+$), 792 (10% $2M+2Na^+$); Found C=47.6% H=7.3% N=17.8%, $C_{15}H_{27}N_5O_6.0.5H_2O$ requires C=47.1% H=7.4% N=18.3%; $[\alpha]_D$ = -48° (c 1.25, water).

Glutamine-glutamine amide trifluoroacetate **94**

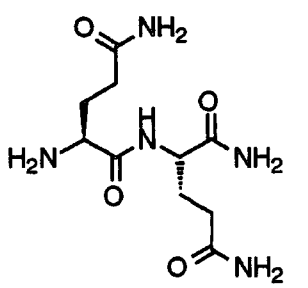

N-Boc-Gln-Gln-NH_2 **93** (8.8 g, 23.7 mmol) was dissolved in 80% trifluoroacetic acid in dichloromethane (50 ml) and allowed to stir for 15 min. The solvents were then removed under reduced pressure, dichloromethane (3 x 30 ml) was added and removed under vacuum, followed by diethyl ether (2 x 30 ml). The resulting residue was stirred with methanol (30 ml) for 5 min before addition of diethyl ether (20 ml) and filtration gave the title compound as a colourless solid (8.0 g, 99%).

δ_H (CD_3OD, 300 MHz): 2.12 (4H, m, $CHC\underline{H}_2$), 2.35 (2H, t, $^3J_{H\text{-}H}$ = 7.2 Hz, $C\underline{H}_2CO_2H$), 2.46 (2H, t, $^3J_{H\text{-}H}$ = 6.9 Hz, $C\underline{H}_2CO_2H$), 3.99 (1H, dd overlapped, $^3J_{H\text{-}H}$ = 6.0 Hz, $^3J_{H\text{-}H}$ = 6.0 Hz, CH), 4.42 (1H, dd overlapped, $^3J_{H\text{-}H}$ = 8.4 Hz, $^3J_{H\text{-}H}$ = 4.8 Hz, CH); δ_C (CD_3OD, 50 MHz): 28.1 ($CH\underline{C}H_2$), 29.0 ($CH\underline{C}H_2$), 31.5 ($\underline{C}H_2CO_2H$), 32.4 ($\underline{C}H_2CO_2H$), 53.8 (CH), 54.1 (CH), 169.9 (C=O), 175.7 (C=O), 177.2 (C=O), 177.7 (C=O); ν_{max} (Golden gate)/cm^{-1}: 3321 (NH) 2927, 2849, 1622 (C=O), 1568, 1536, 1448, 1435, 1309, 1242, 1185, 1087, 1045, 891, 640; Mp. = Decomposes at 150°C; $^m/_z$ (Electrospray, ES+) = 274 (100% $M+H^+$), 547 (5% $2M+H^+$); $[\alpha]_D$ = +8° (c 5, water).

tert-*Butylcarbamoyl-glutamine-glutamine-glutamine amide* **95**

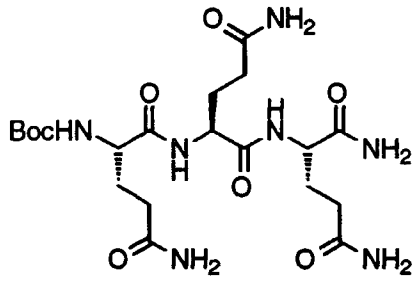

To a solution of Gln-Gln-NH_2 trifluoroacetate **94** (7.6 g, 22.1 mmol) in tetrahydrofuran (100 ml) was added a solution of Boc glutamine *p*-nitrophenol ester **90** (8.1 g, 22.1 mmol) in tetrahydrofuran (100 ml) at room temperature. Triethylamine (3.0 g, 30 mmol) was added and the solution was left to stir for 6 h. The precipitate was filtered from the bright yellow reaction and washed repeatedly with diethyl ether until the washings were colourless. The residue was then taken up into water (50 ml) and washed with diethyl ether (200 ml). The solvents were removed under reduced pressure to give a colourless solid (8.5 g, 76%).

δ_H (D_2O, 200 MHz): 1.29 (9H, s, t-Bu), 1.8 (6H, m, $CHC\underline{H}_2$), 2.26 (6H, t, $^3J_{H\text{-}H}$ = 7.1Hz, $C\underline{H}_2CONH_2$), 3.92 (1H, dd, $^3J_{H\text{-}H}$ = 5.7Hz, $^3J_{H\text{-}H}$ = 5.1Hz, CH), 4.17 (1H, dd overlapping, $^3J_{H\text{-}H}$ = 5.7Hz, $^3J_{H\text{-}H}$ = 4.3Hz, CH), 4.21 (1H, dd overlapping, $^3J_{H\text{-}H}$ = 7.1Hz, $^3J_{H\text{-}H}$ = 4.3Hz, CH); δ_C (D_2O, 50 MHz): 26.8

($CH\underline{C}H_2$), 27.1 ($CH\underline{C}H_2$), 27.7 (CH_3), 31.2 ($CH_2\underline{C}H_2CO_2H$), 31.3 ($CH_2\underline{C}H_2CO_2H$), 53.1 (CH), 53.3 (CH), 81.8 ($\underline{C}(CH_3)_3$), 173.3 (C=O), 175.9 (C=O), 178.0 (C=O); ν_{max} (Golden gate)/cm^{-1}: 3352 (NH), 3192 (NH), 2962, 1678 (carbamate), 1652 (amide), 1638 (amide), 1516, 1456, 1418, 1167, 646, 610; Mp. = 192-194°C; $^{m}/_{z}$ (Electrospray, ES+) = 524 (100% M+Na^+), 1025 (15% M_2+Na^+); Found C=46.2% H=6.8% N=18.3%, $C_{20}H_{35}N_7O_8.1.25H_2O$ requires C=45.9% H=6.7% N=18.7%; $[\alpha]_D$ = -17° (c 1.2, water).

Glutamine-glutamine-glutamine amide trifluoroacetate **96**

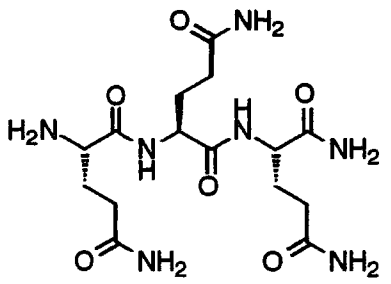

N-Boc-Gln-Gln-Gln-NH_2 **95** (4.1 g, 8.2 mmol) was dissolved in 80% trifluoroacetic acid in dichloromethane (30 ml) and allowed to stir for 15 min. The solvents were then removed under reduced pressure, dichloromethane (3 x 30 ml) was added and removed under vacuum, followed by diethyl ether (2 x 30 ml). The resulting residue was stirred in methanol (30 ml) for 5 min and then filtered, affording the title compound as a colourless solid (3.8 g, 90%).

δ_H (D_2O, 250 MHz): 2.25 (6H, m br, $CHC\underline{H}_2$), 2.59 (6H, 3 overlapping t, $^3J_{H\text{-}H}$ = 7.9Hz, $C\underline{H}_2CONH_2$), 4.31 (1H, overlapping dd, $^3J_{H\text{-}H}$ = 7.1Hz, CH), 4.51 (1H, overlaping dd, $^3J_{H\text{-}H}$ = 5.5Hz, CH) 4.61 (1H, overlapping dd, $^3J_{H\text{-}H}$ = 7.2Hz, CH); δ_C (D_2O, 63MHz) 28.9 ($CH\underline{C}H_2$), 29.2 ($CH\underline{C}H_2$), 29.3 ($CH\underline{C}H_2$), 32.4 ($\underline{C}H_2CONH_2$), 33.3 ($\underline{C}H_2CONH_2$), 33.5 ($\underline{C}H_2CONH_2$), 54.7 (CH), 55.4 (CH), 55.7 (CH), 171.7 (C=O), 175.2 (C=O), 177.9 (C=O), 179.2 (C=O), 180.1 (C=O), 180.3 (C=O); ν_{max} (Golden Gate)/cm^{-1}: 3298 (NH), 3204 (NH), 2928, 1656 (C=O), 1642 (C=O), 1536, 1416, 1200, 1180, 1128, 844, 720, 688, 620; Mp. = 107-109°C; $^{m}/_{z}$ (Electrospray, ES+) = 402 (100% M+H^+), 803 (5% M_2+H^+); Found C=38.0% H=5.4% N=18.4%, $C_{15}H_{27}N_7O_6.CF_3CO_2H.H_2O$ requires C=38.3% H=5.5% N=18.4%; $[\alpha]_D$ = +10° (c 2, water).

(1S,4S,7S)-2,5,8-Tris(3-propylamine)triethylenetetraamine heptahydrochloride **97**

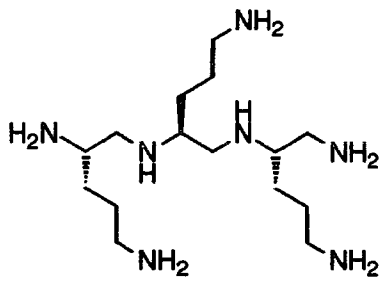

Gln-Gln-Gln-NH_2 trifluoroacetate **96** (3.8 g 7.4 mmol) was dissolved in a solution of borane THF complex in tetrahydrofuran (1M, 100 ml) at room temperature, under argon. The solution was heated under reflux with stirring for 48 h. The reaction was allowed to cool to room temperature and the residual borane quenched by dropwise addition of methanol. The solvents were then removed under reduced pressure before further addition of methanol (3 x 40 ml) which was also removed under vacuum. This procedure was repeated. The resulting residue was taken up into HCl (2M, 30 ml) and heated to 100°C for 24 h. The solvents were then removed in *vacuo* to give a hygroscopic, colourless, sticky gum (3.14 g, 74%).

δ_H (D_2O, 250 MHz): 2.2 (m br), 3.5 (m br), 5.8 (s br); δ_C (D_2O, 100 MHz, DEPT): 22.2 ($CH\underline{C}H_2CH_2$), 22.3 ($CH\underline{C}H_2CH_2$), 22.4 ($CH\underline{C}H_2CH_2$), 25.2 (CH_2), 25.5 (CH_2), 27.4 (CH_2), 27.6 (CH_2), 38.3 (CH_2), 43.8 (CH_2), 45.3 (CH_2), 46.9 (CH_2), 48.6 (CH), 56.4 (CH), 56.9 (CH), 61.3 (CH_2); ν_{max} (Thin film)/cm^{-1}: 3418 (NH), 2960, 1727 (NH), 1582, 1450, 1392, 1172, 1030, 824, 742, 666; $^m/_z$ (Electrospray, ES+) = 55 (100% $M+6H^+$), 160 (30% $M+2H^+$), 318 (30% $M+H^+$); $[\alpha]_D$ = +24° (c 2.5, water).

N-*Hydroxysuccinimide benzoate* **98**

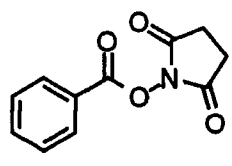

Benzoic acid (5 g, 42 mmol) and triethylamine (4.2 g, 42 mmol) were dissolved in dichloromethane (60 ml). At room temperature EDC (8 g, 42 mmol) was added and the reaction allowed to stir for 10 min before addition of *N*-hydroxysuccinimde (4.8 g, 42 mmol). The reaction was allowed to stir for 6 h before washing with water (2 x 50 ml) and drying over K_2CO_3. The solvents

were removed under vacuum to give a colourless solid which was recrystallised from diethyl ether to give large colourless prismatic crystals (7.4 g, 80%).

δ_H ($CDCl_3$, 250 MHz): 2.88 (4H, s, CH_2CH_2), 7.50 (2H, dd overlapping, $^3J_{H\text{-}H}$ = 7.8Hz, $^3J_{H\text{-}H}$ = 7.7Hz, H-3), 7.67 (1H, t, $^3J_{H\text{-}H}$ = 7.7Hz, H-4), 8.12 (2H, d, $^3J_{H\text{-}H}$ = 7.8Hz, H-2); δ_C ($CDCl_3$, 63 MHz): 20.6 (CH_2CH_2), 120.0 (C-1), 123.8 (C-3), 125.5 (C-2), 129.9 (C-4), 156.6 (ester), 164.2 (imide); ν_{max} (Golden gate)/cm^{-1}: 2970, 2944, 1731 (ester), 1694 (imide), 1644 (imide), 1526, 1452, 1360,1200, 1067, 994, 797, 701, 638; Mp. = 119-121°C (lit[9]: 139-140°C); $^m/_z$ (EI+) = 77 (47%, $(M\text{-}CO_2Su)^+$), 105 (100%, $(M\text{-}HCO)^+$), 219 (2%, M^+); Found C=60.0% H=4.1% N=6.4%, $C_{11}H_9NO_4$ requires C=60.3% H=4.1% N=6.4%.

(1S,4S,7S)-2,5,8-Tris(phenylcarbamoylpropyl)triethylenetetraamine **99**

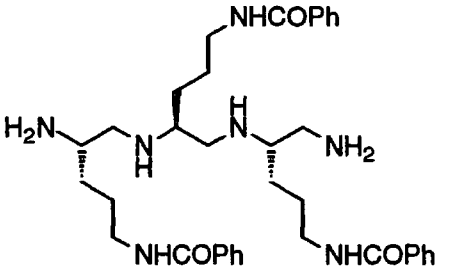

A solution of the heptaamine **97** (3.1g, 5.5 mmol) in water (40 ml) was neutralised by addition of sodium hydroxide solution. $Cu(CO_3)Cu(OH)_2$ (1.2g, 5.5 mmol) was added and a deep blue solution rapidly ensued. Excess copper was removed by filtration. The blue solution was then warmed to 40°C and a solution of *N*-hydroxysuccinimide benzoate **98** (4.8g, 22 mmol) in tetrahydrofuran (25 ml) was added over the period of 1 h. The pH was maintained at 7.5 by addition of sodium hydroxide solution (1M). The reaction was stirred for a further 4 h at 40°C and then overnight at room temperature. The volatile solvents were removed in *vacuo* and washed with diethyl ether (2 x 100 ml) before addition of a solution of ammonium hexafluorophosphate (0.5M, 40 ml). The supernatant liquid was decanted to leave a deep blue gum. The gum was washed with cold water (10 ml) and diethyl ether (20 ml) then taken up into acetonitrile (40 ml). Hydrogen sulfide was bubbled through the solution and the resulting black precipitate removed by filtration. The solvents were removed under vacuum and the yellow residue taken up into HCl (1M, 50 ml) and washed with dichloromethane (200 ml). The pH was then raised to 14 by addition of sodium hydroxide pellets. The solution was then exhaustively

extracted with dichloromethane, dried over K_2CO_3 and the solvents removed under reduced pressure to give a colourless solid (1.8g, 50%).

δ_H ($CDCl_3$, 250 MHz): 1.59 (18H, m br), 2.67 (12H, m br), 3.36 (6H, s br, NH), 7.35 (9H, m, H-3, H-4), 7.74 (6H, d $^3J_{H-H}$ = 7.3Hz, H-2); δ_C (CD_3OD, 100 MHz): 26.8 ($CH\underline{C}H_2CH_2$), 26.9 ($CH\underline{C}H_2CH_2$), 27.0 ($CH\underline{C}H_2CH_2$), 30.3 (CH_2N), 30.7 (CH_2N), 33.7 (CH_2N), 40.9 (CH_2N), 41.0 (CH_2N), 41.1 (CH_2N), 45.1 (CH_2N), 50.8 (CH_2N), 51.8 (CHN), 53.8 (CHN), 58.4 (CHN), 60.6 (CH_2), 128.2 (C-3), 129.5 (C-2), 132.5 (C-4), 135.7 (C-1), 170.1 (C=O); ν_{max} (Golden gate)/cm^{-1} 3282 (NH), 2940, 2858, 1659 (C=O), 1448, 1372, 1095, 927, 826, 694; Mp. Decomposes above 230°C; $^m/_z$ (Electrospray, ES+) = 630 (100% M_2+2H^+) 642 (80% M_2+Na^++H^+); $[\alpha]_D$ = -11° (c 1.8, methanol).

N,N',N'',N'''-*Tetrakistosyl-(1S,4S,7S)-2,5,8-tris(phenylcarbamoylpropyl)-triethylenetetraamine* **100**

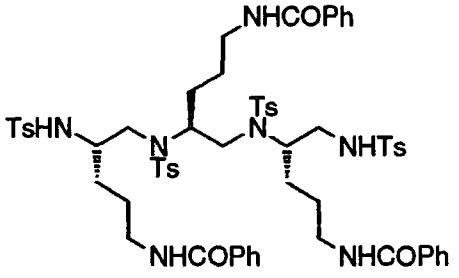

A solution of tosyl chloride (2.3 g, 12 mmol) in pyridine (50 ml) was added to tris(phenylcarbamoylpropyl)triethylenetetraamine **99** (1.5 g, 2.4 mmol), under argon, *via* a cannula. The reaction was stirred at 60°C for 3 days. The solvents were removed under vacuo and the residue taken up into dichloromethane (50 ml) and washed repeatedly with copper nitrate solution until the blue colour of the aqueous phase persisted. After drying over K_2CO_3 the solvents were removed under reduced pressure and the residue purified over silica gel. The column was washed with dichloromethane to remove excess tosyl chloride before eluting with 20% tetrahydrofuran in dichloromethane. The title compound was obtained as a pale yellow solid (0.7 g, 23%).

R_f = 0.4 (10% tetrahydrofuran in dichloromethane, SiO_2); δ_H ($CDCl_3$, 300 MHz): 1.25 (3H, s, Ph-$C\underline{H}_3$), 1.43 (9H, s, Ph-$C\underline{H}_3$), 1.95-4.0 (29H, m, CH_2N, CHN, N$\underline{H}$Ts), 5.83 (1H, t, $^3J_{H-H}$ = 6.2Hz, CONH), 6.18 (1H, t, $^3J_{H-H}$ = 7.5Hz, CONH), 6.78 (1H, t, $^3J_{H-H}$ = 7.0Hz, CONH), 7.15-7.90 (31H, m, overlapping Ts, Bz); δ_C ($CDCl_3$, 100 MHz): 21.1-66.7 15 resonances (CH_2's, CH's), 29.3 (Ph-$\underline{C}H_3$), 30.2 (Ph-$\underline{C}H_3$), 125.4-151.8 28 resonances (Ts, Bz), 167.2 (C=O), 167.8

(C=O), 168.0 (C=O); ν_{max} (Golden gate)/cm^{-1}: 2964, 2924, 2972, 1640 (C=O), 1602, 1542, 1432, 1326 (SO_2), 1294, 1154, (SO_2), 1122, 1088, 1024, 812, 716; Mp. = 112-114°C; $^m/_z$ (Electrospray, ES-) = 1244 (100% M-H^+); $[\alpha]_D$ = +15° (c 1.3, methanol).

N,N',N'',N'''-*Tetrakistosyl-(1S,4S,7S)-2,5,8-tris(phenylcarbamoylpropoyl)-1,4,7,10 tetraazacyclododecane* **102**

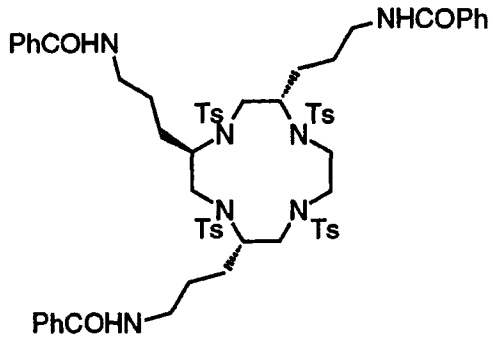

Caesium carbonate (54 mg, 0.17 mmol), tetratosyl-tris(phenyl-carbamoylpropyl)triethylenetetraamine **101** (207g, 0.17mmol) and ethyleneglycol ditosylate **102** (56 mg, 0.17 mmol) were placed in a schlenk tube under argon and dimethylformamide (5 ml) added. The reaction was allowed to stir at room temperature overnight before heating to 70°C for 3 h. The solvents were removed under reduced pressure and the residue taken up into an aqueous lithium chloride solution (10 ml) which was exhaustively extracted with dichloromethane. The combined organic extracts were dried over K_2CO_3 and the solvent removed under vacuum. The residue was purified over silica gel using 5% methanol in dichloromethane as an eluent. The solvents were removed under vacuum to yield a colourles solid (65 mg, 31%).

R_f = 0.5 (5% methanol in dichloromethane); δ_H (CD_3OD, 300 MHz): 0.86-2.47 (24H, m, CH_3, CH_2), 2.82-3.90 (19H, m br, CH_2N, CHN), 7.19-7.84 (31H, m, overlapping Ts, Bz); δ_C (CD_3OD, 75 MHz): 21.5, 21.6, 26.9, 27.2, 28.7, 30.4, 30.6, 33.1, 40.3, 40.7, 54.8, 67.9, 128.1 (Ar), 128.3 (Ar), 128.5 (Ar), 128.6 (Ar), 128.8 (Ar), 129.6 (Ar), 130.9 (Ar), 131.0 (Ar), 132.6 (Ar), 135.6 (Ar), 135.7 (Ar), 137.8 (Ar), 138.5 (Ar), 139.3 (Ar), 144.8 (Ar), 144.9 (Ar), 145.4 (Ar), 145.5 (Ar), 169.9 (C=O), 170.0 (C=O); ν_{max} (KBr disc)/cm^{-1}: 3321 (NH), 3061, 2955, 2871, 1643 (C=O), 1599, 1577, 1537, 1490, 1453, 1434, 1330, 1159, 1089, 1020, 815, 715, 664; Mp. = 166-170°C; $^m/_z$ (MOLDI-TOF+) = 1280 (100% M+H^+); $[\alpha]_D$ = -27° (c 3, dichloromethane).

(1S,4S,7S)-2,5,8-tris-(phenylcarbamoylpropyl)-1,4,7,10 tetraazacycloddodecane **103**

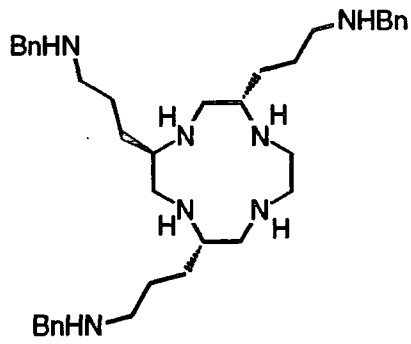

Lithium aluminium hydride (0.15 g, 3.8 mmol) was added to a solution of the tetratosyl cyclen **102** derivative (30 mg, 24 μmol) in tetrahydrofuran (10 ml) under argon at -78°C. The solution was stirred at -78°C for 2 h before warming to room temperature. The reaction was allowed to stir, under argon overnight at room temperature, and then heated under reflux for 2h. Excess lithium aluminium hydride was quenched by the cautious addition of saturated sodium sulfate solution (3 ml) and the inorganic residue removed by filtration. The solvents were then removed under reduced pressure and the residue dried under vacuum to yield a colourless solid (15 mg, 64%).

δ_H ($CDCl_3$, 300 MHz): 0.81-2.07 (12H, m v br), 2.18-2.88 (16H, m v br), 3.43-4.16 (9H, m, v br), 7.13-7.82 (15H, m, v br); δ_C ($CDCl_3$, 75 MHz): 21.4-35.3 (14 resonances), 60.1 (CH), 62.4 (CH), 62.7 ($PhC\underline{H}_2$), 126.1 (C-'1), 126.8 (C-'2), 129.6 (C-'4), 129.8 (C-'3); ν_{max} (Thin film)/cm^{-1}: 3386 (NH), 3063, 3029, 2950, 2968, 1649 (NH bend) 1599, 1577, 1550, 1453, 1398, 1328, 1233, 1185, 1160, 1124, 1092, 1036, 1012, 815, 736, 697; Mp. = Decomposes at 180°C; $^{m}/_{z}$ (Electrospray, ES+) = 366 (100% $M+2Na^+$); $[\alpha]_D$ = +14° (c 1.4, methanol).

6.6 References

1 Perrin, D.D.; Armarego, W.L.F.; Perrin, D.R.; *"Purification of Laboratory Chemicals"*, 2nd Ed, Pergamon Press, Oxford, (1980),

2 Cicchi, S.; Goti, A.; Brandi, A.; *J. Org. Chem.*, (1995), **60**, 4743.

3 Effenberger, F.; Burkard, U.; Willfart, J.; *Liebigs. Ann. Chem.*, (1986), 314.

4 Kumar, K.; Tweedle, M.F.; *Inorg. Chem.*, (1993), **32**, 4193.

5 Yaouanc, J.; le Bris, N.; le Gall, G. Clément,J-C.; Handel, H.; des Abbayes, H.; *J. Chem. Soc. Chem. Commun.*, (1991), 206.

6 Roignant, A.; Gardinier, I.; Bernard, H.; Yaounac, J-J.; Handel, H.; *J. Chem. Soc., Chem. Commun.*, (1995), 1233.

7 Salomon, C.J.; Mata, E.G.; Mascaretti, O.; *J. Org. Chem.*, (1994), **24**, 7259.

8 Poulos, C.; Stravropoulos, G.; Brown, J.R.; Jordan, C.C.; *J. Med. Chem.*, (1987), 1512.

9 Horner, L; Jordan, M.; *Justus Liebigs Ann. Chem.*; (1978), 1518.

Appendices

Appendix I : Best Fitting Parameters for NMRD Profile

Best Fitting Parameters for [Gd.(RRRR-)] (Figure 2.33)

Parameter	15°C	25°C	39°C
τ_{S0} (ps)	435	368	277
τ_V (ps)	35	13	5
τ_R (ps)	136	108	75
τ_M (ns)	195	70	19
q	1	1	1
r (Å)	2.90	2.90	2.90
A (Å)	3.8	3.8	3.8
D ($cm^{-1}s^{-1}$).10^5	1.65	2.40	3.15

Best Fitting Parameters for [Gd.(RRRS-)] (Figure 2.34)

Parameter	15°C	25°C	39°C
τ_{S0} (ps)	246	161	108
τ_V (ps)	11.4	13	7
τ_R (ps)	178	120	92.6
τ_M (ns)	720	255	66.6
q	1	1	1
r (Å)	2.90	2.90	2.90
A (Å)	3.8	3.8	3.8
D ($cm^{-1}s^{-1}$).10^5	1.65	2.40	3.15

Best Fitting Parameters for [Gd.(RSRS-)] (Figure 2.35)

Parameter	15°C	25°C	39°C
τ_{S0} (ps)	295	373	305
τ_V (ps)	17.3	11.1	6
τ_R (ps)	143	105	74
τ_M (ns)	240	119	48
q	1	1	1
r (Å)	2.90	2.90	2.90
A (Å)	3.8	3.8	3.8
D ($cm^{-1}s^{-1}$).10^5	1.65	2.40	3.15

Best Fitting Parameters for [Gd.35] (Figure 2.36)

Parameter	15°C
τ_{S0} (ps)	200
τ_V (ps)	47.5
τ_R (ps)	414
τ_M (ns)	97
q	1
r (Å)	2.94
A (Å)	4.0
D ($cm^{-1}s^{-1}$).10^5	1.6

*Best Fitting Parameters for [Gd.**DOTA**]$^-$ (Figure 1.3)*

Parameter	25°C
τ_{S0} (ps)	692
τ_V (ps)	7.2
τ_R (ps)	72.7
τ_M (ns)	244
q	1
r (Å)	3.12
A (Å)	3.60
D ($cm^{-1}s^{-1}$).10^5	2.4

Appendix II : Crystallographic Data

Crystallographic Data for (RRSS-)26.

Table 1. Crystal data and structure refinement for (*RRSS*-)**26**.

Empirical formula	$C_{28}H_{60}N_4O_{22}$	
Formula weight	804.80	
Temperature	150(2) K	
Wavelength	0.71073 Å	
Crystal system	Triclinic	
Space group	P(-1)	
Unit cell dimensions	a = 9.2517(2)Å	α = 97.19(2)°
	b = 9.7886(3)Å	β = 106.94(2)°
	c = 12.2960(4)Å	γ = 113.08(2)°
Volume, Z	942.99(5) $Å^3$, 1	
Density (calculated)	1.417 Mg/m^3	
Absorption coefficient	0.122 mm^{-1}	
F(000)	432	
Crystal size	0.25 x 0.20 x 0.10 mm	
θ range for data collection	1.80 to 25.00°	
Limiting indices	$-9 \le h \le 11, -12 \le k \le 9, -15 \le l \le 15$	
Reflections collected	6701	
Independent reflections	3321 [$R_{(int)}$ = 0.0943]	
Absorption correction	Integration	
Max. and min. transmission	0.977 and 0.636	
Refinement method	Full-matrix least-squares on F^2	
Data / restraints / parameters	3321 / 0 / 344	
Goodness-of-fit on F^2	1.044	
Final R indices [I>2σ(I)]	R_1 = 0.0790, wR_2 = 0.1683	
R indices (all data)	R_1 = 0.1720, wR_2 = 0.2287	
Extinction coefficient	not refined	
Largest diff. peak and hole	0.433 and -0.369 $eÅ^{-3}$	

Table 2. Atomic coordinates (x 10^5) and equivalent isotropic displacement parameters ($Å^2$ x 10^4) for (*RRSS*-)**26**. $U_{(eq)}$ is defined as one third of the trace of the orthogonalized U_{ij} tensor.

	x	y	z	$U_{(eq)}$
O(121)	45350(5)	-5270(5)	32780(4)	289(11)

O(122)	69670(5)	-900(5)	30500(4)	276(10)
O(151)	16280(5)	-34130(5)	51140(4)	336(11)
O(152)	39260(5)	-37980(5)	57260(4)	281(10)
O(221)	63900(5)	-17070(5)	690(3)	302(11)
O(222)	83800(5)	6660(5)	11740(4)	272(10)
O(251)	86570(6)	-47690(5)	12430(4)	439(13)
O(252)	77590(7)	-57970(6)	-6920(5)	436(14)
N(1)	77300(5)	-17340(5)	45990(4)	195(11)
N(2)	96220(5)	-6400(5)	29130(4)	177(11)
C(1)	80020(7)	-26720(7)	37190(5)	200(13)
C(2)	97250(7)	-17600(7)	36430(6)	193(13)
C(3)	113110(7)	7320(7)	31990(6)	206(14)
C(4)	82400(7)	-20170(7)	57580(5)	203(13)
C(11)	60080(7)	-18320(7)	42250(5)	201(13)
C(12)	59020(7)	-7400(7)	34530(5)	209(13)
C(13)	45400(7)	-34950(7)	36090(5)	211(13)
C(14)	28570(7)	-37240(8)	37260(5)	229(14)
C(15)	28840(7)	-36450(6)	49520(5)	212(13)
C(21)	87520(7)	-15230(7)	16050(5)	179(13)
C(22)	77560(7)	-7740(7)	9070(5)	199(13)
C(23)	99850(7)	-17290(7)	10560(5)	226(14)
C(24)	90820(8)	-30970(7)	-290(5)	222(14)
C(25)	84710(7)	-46450(7)	2500(6)	239(14)
O(1S)	63900(6)	15270(5)	-4120(4)	321(11)
O(2S)	57730(5)	-14500(5)	-21850(5)	285(11)
O(3S)	14610(7)	-32560(7)	72270(5)	397(13)
O(4S)	52020(19)	-48080(18)	7330(13)	1050(5)

Table 3. Bond lengths [Å] and angles [deg] for (*RRSS*-)**26**.

O(121)-C(12)	1.322(6)	O(121)-H(121)	0.90(7)
O(122)-C(12)	1.223(6)	O(151)-C(15)	1.331(6)
O(151)-H(151)	0.96(7)	O(152)-C(15)	1.214(6)
O(221)-C(22)	1.262(7)	O(222)-C(22)	1.251(7)
O(251)-C(25)	1.211(7)	O(252)-C(25)	1.302(8)
O(252)-H(252)	0.72(8)	N(1)-C(4)	1.462(7)
N(1)-C(1)	1.473(7)	N(1)-C(11)	1.484(6)
N(2)-C(3)	1.511(7)	N(2)-C(2)	1.515(7)
N(2)-C(21)	1.527(7)	N(2)-H(2)	1.01(7)
C(1)-C(2)	1.529(7)	C(1)-H(1A)	1.11(6)
C(1)-H(1B)	1.01(5)	C(2)-H(2A)	1.01(5)
C(2)-H(2B)	0.96(6)	C(3)-C(4)#1	1.509(8)
C(3)-H(3B)	1.06(5)	C(3)-H(3A)	0.79(5)
C(4)-C(3)#1	1.509(8)	C(4)-H(4B)	0.99(5)
C(4)-H(4A)	0.99(7)	C(11)-C(12)	1.528(7)
C(11)-C(13)	1.558(8)	C(11)-H(11)	1.09(5)
C(13)-C(14)	1.537(7)	C(13)-H(13A)	1.12(6)
C(13)-H(13B)	0.97(5)	C(14)-C(15)	1.492(8)
C(14)-H(14A)	1.12(7)	C(14)-H(14B)	0.92(5)
C(21)-C(22)	1.533(7)	C(21)-C(23)	1.547(7)
C(21)-H(21)	1.02(6)	C(23)-C(24)	1.515(8)
C(23)-H(23A)	0.89(5)	C(24)-H(24B)	0.88(5)
C(24)-H(24A)	1.09(5)	O(1S)-H(1SA)	0.74(5)
O(1S)-H(1SB)	0.89(7)	O(2S)-H(2SA)	0.87(8)
O(2S)-H(2SB)	0.86(6)	O(3S)-H(3SA)	0.65(8)
O(3S)-H(3SB)	0.80(11)	O(4S)-O(4S)#2	1.69(3)

C(12)-O(121)-H(121)	109(4)	C(15)-O(151)-H(151)	110(4)
C(25)-O(252)-H(252)	98(8)	C(4)-N(1)-C(1)	111.8(4)
C(4)-N(1)-C(11)	112.0(4)	C(1)-N(1)-C(11)	114.7(5)
C(3)-N(2)-C(2)	113.4(4)	C(3)-N(2)-C(21)	113.1(4)
C(2)-N(2)-C(21)	109.1(4)	C(3)-N(2)-H(2)	104(4)
C(2)-N(2)-H(2)	110(4)	C(21)-N(2)-H(2)	107(4)
N(1)-C(1)-C(2)	110.5(5)	N(1)-C(1)-H(1A)	118(3)
C(2)-C(1)-H(1A)	103(3)	N(1)-C(1)-H(1B)	110(3)
C(2)-C(1)-H(1B)	109(3)	H(1A)-C(1)-H(1B)	107(4)
N(2)-C(2)-C(1)	109.9(4)	N(2)-C(2)-H(2A)	108(3)
C(1)-C(2)-H(2A)	113(3)	N(2)-C(2)-H(2B)	105(3)
C(1)-C(2)-H(2B)	111(3)	H(2A)-C(2)-H(2B)	110(4)
C(4)#1-C(3)-N(2)	113.3(4)	C(4)#1-C(3)-H(3B)	116(3)
N(2)-C(3)-H(3B)	103(3)	C(4)#1-C(3)-H(3A)	111(4)
N(2)-C(3)-H(3A)	105(4)	H(3B)-C(3)-H(3A)	107(5)
N(1)-C(4)-C(3)#1	115.8(5)	N(1)-C(4)-H(4B)	106(3)
C(3)#1-C(4)-H(4B)	115(3)	N(1)-C(4)-H(4A)	113(4)
C(3)#1-C(4)-H(4A)	105(4)	H(4B)-C(4)-H(4A)	102(5)
N(1)-C(11)-C(12)	109.4(4)	N(1)-C(11)-H(11)	105(3)
C(12)-C(11)-H(11)	106(3)	C(13)-C(11)-H(11)	110(3)
O(122)-C(12)-O(121)	122.3(5)	O(122)-C(12)-C(11)	124.8(5)
O(121)-C(12)-C(11)	112.9(4)	C(14)-C(13)-C(11)	114.1(5)
C(14)-C(13)-H(13A)	103(3)	C(11)-C(13)-H(13A)	116(3)
C(14)-C(13)-H(13B)	106(3)	C(11)-C(13)-H(13B)	109(3)
H(13A)-C(13)-H(13B)	108(4)	C(15)-C(14)-C(13)	114.0(5)
C(15)-C(14)-H(14A)	110(3)	C(13)-C(14)-H(14A)	108(3)
C(15)-C(14)-H(14B)	115(3)	C(13)-C(14)-H(14B)	110(3)
H(14A)-C(14)-H(14B)	99(5)	O(152)-C(15)-O(151)	122.8(5)
O(152)-C(15)-C(14)	123.9(5)	O(151)-C(15)-C(14)	113.3(5)
N(2)-C(21)-C(22)	110.7(4)	N(2)-C(21)-C(23)	113.1(4)
C(22)-C(21)-C(23)	111.8(4)	N(2)-C(21)-H(21)	110(3)
C(22)-C(21)-H(21)	105(3)	C(23)-C(21)-H(21)	106(3)
O(222)-C(22)-O(221)	126.4(5)	O(222)-C(22)-C(21)	118.6(5)
O(221)-C(22)-C(21)	115.0(5)	C(24)-C(23)-C(21)	112.1(5)
C(24)-C(23)-H(23A)	110(4)	C(21)-C(23)-H(23A)	107(3)
C(24)-C(23)-H(23B)	110(3)	C(21)-C(23)-H(23B)	111(3)
H(23A)-C(23)-H(23B)	107(5)	C(23)-C(24)-C(25)	113.5(5)
C(23)-C(24)-H(24B)	110(3)	C(25)-C(24)-H(24B)	113(4)
C(23)-C(24)-H(24A)	113(3)	C(25)-C(24)-H(24A)	110(3)
H(24B)-C(24)-H(24A)	97(4)	O(251)-C(25)-O(252)	124.8(6)
O(251)-C(25)-C(24)	123.0(6)	O(252)-C(25)-C(24)	112.2(6)
O(251)-C(25)-H(252)	98(3)	O(252)-C(25)-H(252)	27(3)
C(24)-C(25)-H(252)	139(3)	H(1SA)-O(1S)-H(1SB)	77(5)
H(2SA)-O(2S)-H(2SB)	125(6)	H(3SA)-O(3S)-H(3SB)	77(8)

Table 4. Anisotropic displacement parameters ($Å^2$ x 10^4) for (*RRSS*-)**26**. The anisotropic displacement factor exponent takes the form: $-2\,(\,2\,[h^2.a^{*2}.U_{11} + ... + 2hk.a^*.b^*.U_{12}]$

	U_{11}	U_{22}	U_{33}	U_{23}	U_{13}	U_{12}
O(121)	180(2)	380(3)	460(3)	280(2)	190(2)	180(2)
O(122)	220(2)	310(3)	470(3)	260(2)	250(2)	150(2)
O(151)	260(2)	430(3)	460(3)	230(2)	230(2)	200(2)
O(152)	250(2)	280(3)	360(3)	150(2)	130(2)	140(2)

O(221)	170(2)	300(3)	310(2)	0(2)	-30(2)	90(2)
O(222)	190(2)	260(3)	380(3)	160(2)	120(2)	80(2)
O(251)	670(3)	260(3)	370(3)	140(2)	230(3)	150(3)
O(252)	550(3)	260(3)	400(3)	110(3)	150(3)	90(3)
N(1)	130(2)	180(3)	320(3)	110(2)	120(2)	80(2)
N(2)	120(2)	180(3)	260(3)	110(2)	100(2)	50(2)
C(1)	160(3)	190(3)	270(3)	100(3)	110(3)	60(3)
C(2)	120(3)	260(4)	240(3)	150(3)	90(3)	90(3)
C(3)	180(3)	200(4)	210(4)	90(3)	110(3)	20(3)
C(4)	150(3)	180(3)	340(4)	150(3)	130(3)	80(3)
C(11)	120(3)	250(4)	270(3)	120(3)	100(3)	80(3)
C(12)	150(3)	200(3)	250(3)	40(3)	50(3)	80(3)
C(13)	60(3)	170(3)	300(4)	60(3)	50(2)	-20(3)
C(14)	120(3)	230(4)	350(4)	150(3)	100(3)	60(3)
C(15)	130(3)	70(3)	320(4)	20(3)	50(3)	-30(3)
C(21)	120(3)	150(3)	270(3)	100(3)	90(3)	30(3)
C(22)	140(3)	270(4)	230(3)	90(3)	130(3)	80(3)
C(23)	160(3)	220(4)	270(4)	60(3)	80(3)	70(3)
C(24)	250(3)	180(3)	280(4)	110(3)	140(3)	100(3)
C(25)	220(3)	160(4)	310(4)	60(3)	90(3)	70(3)

Table 5. Hydrogen coordinates ($x10^3$) and isotropic displacement parameters ($Å^2 \times 10^3$) for (*RRSS*-)**26**.

	x	y	z	$U_{(eq)}$
H(121)	432(9)	-19(9)	263(7)	55(23)
H(151)	172(9)	-336(8)	592(7)	54(22)
H(252)	755(11)	-642(11)	-41(8)	74(35)
H(2)	889(10)	-17(8)	310(6)	68(24)
H(1A)	804(8)	-375(7)	387(5)	36(16)
H(1B)	708(6)	-298(6)	292(5)	13(13)
H(2A)	1013(7)	-244(6)	326(5)	21(15)
H(2B)	1056(8)	-113(7)	441(5)	26(16)
H(3B)	1215(7)	23(6)	328(4)	23(15)
H(3A)	1123(6)	101(6)	262(5)	7(15)
H(4B)	914(7)	-234(6)	580(4)	16(14)
H(4A)	735(9)	-294(8)	583(6)	54(21)
H(11)	591(7)	-135(6)	504(5)	24
H(13A)	418(7)	-391(6)	263(5)	22(14)
H(13B)	485(7)	-422(6)	397(5)	19(14)
H(14A)	184(9)	-487(9)	312(6)	52(20)
H(14B)	248(6)	-310(6)	336(5)	15(14)
H(21)	786(8)	-261(7)	150(5)	30(16)
H(23A)	1073(7)	-188(6)	161(5)	18(15)
H(23B)	1070(8)	-67(8)	84(5)	42(18)
H(24B)	827(7)	-300(6)	-55(5)	12(14)
H(24A)	983(7)	-307(6)	-58(5)	25(15)
H(1SA)	597(6)	164(5)	-1(4)	3(13)
H(1SB)	693(9)	134(8)	23(6)	48(20)
H(2SA)	520(9)	-229(9)	-277(7)	51(21)
H(2SB)	598(7)	-142(7)	-146(6)	34(17)
H(3SA)	194(10)	-343(10)	762(8)	56(26)
H(3SB)	186(13)	-254(12)	780(9)	98(35)

Crystallographic Data for (RRRS-)*26.*

Identification code: 97srv131 (*RRRS*-)isomer.

Empirical formula	C29 H54.50 N4 O20.25	
Formula weight	783.27	
Temperature	150(2) K	
Wavelength	0.71073 Å	
Crystal system	Monoclinic	
Space group	$P2_1/c$	
Unit cell dimensions	a = 16.70420(10) Å	α= 90°.
	b = 10.72220(10) Å	β= 102.7460(10)°.
	c = 21.1538(2) Å	γ = 90°.
Volume	3695.40(5) $Å^3$	
Z	4	
Density (calculated)	1.408 Mg/m^3	
Absorption coefficient	0.120 mm^{-1}	
Absorption correction	None	
Data corrections	SADABS, SORTAV & BAYES	
F(000)	1674	
Crystal size	0.20 x 0.20 x 0.20 mm^3	
Theta range for data collection	1.97 to 27.47°.	
Index ranges	-21<=h<=21, 0<=k<=13, 0<=l<=27	
Reflections collected	Total	25267
	Unique	8402
	Observed	3199 Fo > 4σ(Fo)
Independent reflections	8402 [R(int) = 0.0772]	
Completeness to theta = 27.47°	99.4 %	
Refinement method	Full-matrix least-squares on F^2	
Data / restraints / parameters	8402 / 0 / 496	
Goodness-of-fit on F^2	0.954	
Final R indices [I>2sigma(I)]	R1 = 0.0830, wR2 = 0.2103	
R indices (all data)	R1 = 0.1580, wR2 = 0.2700	
Largest diff. peak and hole	0.949 and -0.567 $e.Å^{-3}$	

Table 2. Atomic co-ordinates (x 10^4) and equivelent isotropic displacement parameters ($Å^2$ x 10^3) for 97srv131. U(eq) is defined as one third of the trace of the orthogonalised U^{ij} tensor.

	x	y	z	U(eq)
O(12B)	-6375(2)	6280(4)	-167(2)	61(1)
O(12A)	-5094(2)	6669(5)	-274(2)	89(2)
O(22B)	-8082(2)	8106(3)	-343(1)	42(1)
O(22A)	-8049(2)	7190(3)	620(1)	51(1)
O(25A)	-7187(6)	3367(10)	1070(4)	47(2)
O(251)	-7026(8)	3893(12)	950(6)	51(3)
O(252)	-7373(10)	2859(16)	1080(7)	53(4)
O(25B)	-7731(2)	3071(3)	19(2)	60(1)
O(32B)	-10776(2)	9387(3)	-2082(1)	40(1)
O(32A)	-10789(2)	9234(3)	-1026(1)	44(1)
O(35B)	-9916(2)	12087(3)	-13(1)	43(1)
O(35A)	-10046(2)	12352(3)	-1072(1)	51(1)
O(42B)	-6476(2)	8580(3)	-1067(2)	57(1)
O(42A)	-6963(8)	10576(8)	-1044(4)	83(4)
O(421)	-6396(7)	10520(10)	-1181(5)	72(3)
O(45B)	-7729(2)	13333(3)	-2679(1)	46(1)
O(45A)	-8401(2)	11502(3)	-2849(1)	42(1)
N(1)	-6963(2)	5845(3)	-1446(2)	35(1)
N(2)	-8540(2)	5938(3)	-1015(1)	28(1)
N(3)	-9193(2)	8177(3)	-1783(1)	28(1)
N(4)	-7678(2)	8199(3)	-2187(1)	29(1)
C(1)	-7369(3)	4693(4)	-1245(2)	35(1)
C(2)	-8293(3)	4820(4)	-1324(2)	32(1)
C(3)	-9428(2)	6164(4)	-1250(2)	31(1)
C(4)	-9609(2)	6921(3)	-1870(2)	29(1)
C(5)	-9167(2)	8747(4)	-2435(2)	29(1)
C(6)	-8453(2)	8217(4)	-2689(2)	30(1)
C(7)	-7075(2)	7359(4)	-2380(2)	33(1)
C(8)	-7194(3)	6017(4)	-2177(2)	35(1)
C(11)	-6034(3)	5844(5)	-1189(2)	49(1)
C(12)	-5813(4)	6313(6)	-482(3)	63(2)
C(13)	-5665(3)	4557(6)	-1270(2)	57(2)

C(14A)	-4704(8)	4996(14)	-1266(6)	38(3)
C(15A)	-4347(8)	3828(12)	-1466(6)	40(2)
O(15A)	-4583(6)	3441(10)	-2048(4)	52(3)
O(15B)	-3812(5)	3164(9)	-1059(4)	45(2)
C(14B)	-4760(5)	4392(9)	-1231(4)	48(2)
C(15B)	-4491(5)	3122(8)	-1341(3)	40(2)
O(151)	-4712(4)	2574(7)	-1873(3)	71(2)
O(152)	-4038(3)	2530(6)	-857(3)	53(2)
C(21)	-8295(3)	5873(4)	-299(2)	36(1)
C(22)	-8141(3)	7186(4)	-18(2)	35(1)
C(23)	-8864(3)	5075(4)	24(2)	40(1)
C(24)	-8416(3)	4432(5)	644(2)	47(1)
C(25)	-7770(3)	3574(5)	526(2)	48(1)
C(31)	-9507(3)	9017(4)	-1310(2)	30(1)
C(32)	-10428(3)	9228(4)	-1495(2)	34(1)
C(33)	-9009(3)	10219(4)	-1179(2)	41(1)
C(34)	-9066(3)	10828(4)	-539(2)	35(1)
C(35)	-9725(3)	11796(4)	-582(2)	35(1)
C(41)	-7354(3)	9475(4)	-2021(2)	36(1)
C(42)	-6780(4)	9452(5)	-1353(2)	55(1)
C(43)	-6921(3)	10093(4)	-2518(2)	40(1)
C(44)	-6919(3)	11525(5)	-2489(2)	50(1)
C(45)	-7759(3)	12086(4)	-2690(2)	39(1)
O(1SA)	-2171(4)	697(6)	-1205(3)	60
O(1SB)	-2410(11)	392(16)	-1043(8)	60
O(2S)	-4104(5)	-2254(7)	-833(3)	62(2)
C(1S)	-4389(9)	-627(15)	-2102(7)	84(4)
O(3S)	-4197(5)	272(7)	-1991(3)	58(2)
C(2S)	-4987(6)	-1614(9)	-1962(4)	47(2)
O(4SA)	-4994(7)	-640(11)	249(5)	52(3)
O(4SB)	-4411(5)	-920(8)	17(4)	48(2)
O(4SC)	-5113(8)	-1259(13)	577(6)	57(3)
O(5SA)	-3429(6)	-350(11)	-258(5)	52(3)
O(5SB)	-3268(6)	323(9)	-411(4)	59(2)
O(5SC)	-3448(8)	-813(13)	-956(6)	58(3)
O(6S)	-5075(9)	1181(14)	-1872(7)	59(4)

Table 3. Bond lengths [Å] and angles [°] for 97srv131.

O(12B)-C(12)	1.265(7)	N(4)-C(7)	1.477(5)
O(12A)-C(12)	1.245(6)	N(4)-C(6)	1.482(5)
O(22B)-C(22)	1.218(5)	N(4)-C(41)	1.485(5)
O(22A)-C(22)	1.325(5)	C(1)-C(2)	1.521(6)
O(22A)-H(22A)	0.8400	C(1)-H(1A)	0.9900
O(25A)-O(252)	0.630(16)	C(1)-H(1B)	0.9900
O(25A)-O(251)	0.696(13)	C(2)-H(2A)	0.9900
O(25A)-C(25)	1.352(9)	C(2)-H(2B)	0.9900
O(251)-O(252)	1.31(2)	C(3)-C(4)	1.515(5)
O(251)-C(25)	1.405(13)	C(3)-H(3A)	0.9900
O(252)-C(25)	1.434(16)	C(3)-H(3B)	0.9900
O(25B)-C(25)	1.214(5)	C(4)-H(4A)	0.9900
O(32B)-C(32)	1.261(4)	C(4)-H(4B)	0.9900
O(32A)-C(32)	1.269(5)	C(5)-C(6)	1.521(5)
O(35B)-C(35)	1.348(5)	C(5)-H(5A)	0.9900
O(35B)-H(35A)	0.8400	C(5)-H(5B)	0.9900
O(35A)-C(35)	1.213(5)	C(6)-H(6A)	0.9900
O(42B)-C(42)	1.168(6)	C(6)-H(6B)	0.9900
O(42A)-O(421)	1.051(13)	C(7)-C(8)	1.527(6)
O(42A)-C(42)	1.436(11)	C(7)-H(7A)	0.9900
O(421)-C(42)	1.324(10)	C(7)-H(7B)	0.9900
O(45B)-C(45)	1.338(5)	C(8)-H(8A)	0.9900
O(45B)-H(45A)	0.8400	C(8)-H(8B)	0.9900
O(45A)-C(45)	1.223(5)	C(11)-C(13)	1.536(7)
N(1)-C(1)	1.515(5)	C(11)-C(12)	1.544(7)
N(1)-C(8)	1.521(5)	C(11)-H(11A)	1.0000
N(1)-C(11)	1.527(5)	C(13)-C(14B)	1.505(9)
N(1)-H(1)	0.9300	C(13)-C(14A)	1.670(14)
N(2)-C(2)	1.468(5)	C(13)-H(13A)	0.9900
N(2)-C(3)	1.477(5)	C(13)-H(13B)	0.9900
N(2)-C(21)	1.480(5)	C(14A)-C(15A)	1.488(18)
N(3)-C(4)	1.508(5)	C(14A)-H(14A)	0.9900
N(3)-C(5)	1.518(4)	C(14A)-H(14B)	0.9900
N(3)-C(31)	1.523(5)	C(15A)-O(15A)	1.276(14)
N(3)-H(3)	0.9300	C(15A)-O(15B)	1.307(15)

C(14B)-C(15B)	1.469(11)	O(4SA)-O(4SB)	1.221(12)
C(14B)-H(14C)	0.9900	O(4SA)-O(4SA)#1	1.73(2)
C(14B)-H(14D)	0.9900	O(5SA)-O(5SB)	0.858(12)
C(15B)-O(151)	1.250(9)	O(5SA)-O(5SC)	1.552(16)
C(15B)-O(152)	1.297(9)	O(5SB)-O(5SC)	1.659(16)
C(21)-C(22)	1.527(6)		
C(21)-C(23)	1.546(6)	C(22)-O(22A)-H(22A)	109.5
C(21)-H(21A)	1.0000	O(252)-O(25A)-O(251)	161(3)
C(23)-C(24)	1.524(6)	O(252)-O(25A)-C(25)	84.3(19)
C(23)-H(23A)	0.9900	O(251)-O(25A)-C(25)	79.6(14)
C(23)-H(23B)	0.9900	O(25A)-O(251)-O(252)	9.1(14)
C(24)-C(25)	1.481(7)	O(25A)-O(251)-C(25)	71.2(14)
C(24)-H(24A)	0.9900	O(252)-O(251)-C(25)	63.7(8)
C(24)-H(24B)	0.9900	O(25A)-O(252)-O(251)	10.0(15)
C(31)-C(32)	1.519(6)	O(25A)-O(252)-C(25)	69.8(18)
C(31)-C(33)	1.524(6)	O(251)-O(252)-C(25)	61.4(8)
C(31)-H(31A)	1.0000	C(35)-O(35B)-H(35A)	109.5
C(33)-C(34)	1.525(5)	O(421)-O(42A)-C(42)	62.1(9)
C(33)-H(33A)	0.9900	O(42A)-O(421)-C(42)	73.4(8)
C(33)-H(33B)	0.9900	C(45)-O(45B)-H(45A)	109.5
C(34)-C(35)	1.500(6)	C(1)-N(1)-C(8)	110.9(3)
C(34)-H(34A)	0.9900	C(1)-N(1)-C(11)	112.5(3)
C(34)-H(34B)	0.9900	C(8)-N(1)-C(11)	111.8(3)
C(41)-C(42)	1.522(6)	C(1)-N(1)-H(1)	107.1
C(41)-C(43)	1.549(6)	C(8)-N(1)-H(1)	107.1
C(41)-H(41A)	1.0000	C(11)-N(1)-H(1)	107.1
C(43)-C(44)	1.538(6)	C(2)-N(2)-C(3)	110.2(3)
C(43)-H(43A)	0.9900	C(2)-N(2)-C(21)	112.1(3)
C(43)-H(43B)	0.9900	C(3)-N(2)-C(21)	112.5(3)
C(44)-C(45)	1.499(7)	C(4)-N(3)-C(5)	110.8(3)
C(44)-H(44A)	0.9900	C(4)-N(3)-C(31)	113.1(3)
C(44)-H(44B)	0.9900	C(5)-N(3)-C(31)	116.3(3)
O(1SA)-O(1SB)	0.666(18)	C(4)-N(3)-H(3)	105.2
C(1S)-O(3S)	1.026(15)	C(5)-N(3)-H(3)	105.2
C(1S)-C(2S)	1.530(17)	C(31)-N(3)-H(3)	105.2
O(4SA)-O(4SC)	1.011(14)	C(7)-N(4)-C(6)	110.5(3)

C(7)-N(4)-C(41)	113.0(3)	C(5)-C(6)-H(6B)	109.1
C(6)-N(4)-C(41)	111.9(3)	H(6A)-C(6)-H(6B)	107.9
N(1)-C(1)-C(2)	113.7(3)	N(4)-C(7)-C(8)	111.0(3)
N(1)-C(1)-H(1A)	108.8	N(4)-C(7)-H(7A)	109.4
C(2)-C(1)-H(1A)	108.8	C(8)-C(7)-H(7A)	109.4
N(1)-C(1)-H(1B)	108.8	N(4)-C(7)-H(7B)	109.4
C(2)-C(1)-H(1B)	108.8	C(8)-C(7)-H(7B)	109.5
H(1A)-C(1)-H(1B)	107.7	H(7A)-C(7)-H(7B)	108.0
N(2)-C(2)-C(1)	113.7(3)	N(1)-C(8)-C(7)	112.4(3)
N(2)-C(2)-H(2A)	108.8	N(1)-C(8)-H(8A)	109.1
C(1)-C(2)-H(2A)	108.8	C(7)-C(8)-H(8A)	109.1
N(2)-C(2)-H(2B)	108.8	N(1)-C(8)-H(8B)	109.1
C(1)-C(2)-H(2B)	108.8	C(7)-C(8)-H(8B)	109.1
H(2A)-C(2)-H(2B)	107.7	H(8A)-C(8)-H(8B)	107.8
N(2)-C(3)-C(4)	111.9(3)	N(1)-C(11)-C(13)	111.3(4)
N(2)-C(3)-H(3A)	109.2	N(1)-C(11)-C(12)	110.5(4)
C(4)-C(3)-H(3A)	109.2	C(13)-C(11)-C(12)	112.6(4)
N(2)-C(3)-H(3B)	109.2	N(1)-C(11)-H(11A)	107.4
C(4)-C(3)-H(3B)	109.2	C(13)-C(11)-H(11A)	107.4
H(3A)-C(3)-H(3B)	107.9	C(12)-C(11)-H(11A)	107.4
N(3)-C(4)-C(3)	112.0(3)	O(12A)-C(12)-O(12B)	126.3(5)
N(3)-C(4)-H(4A)	109.2	O(12A)-C(12)-C(11)	116.7(6)
C(3)-C(4)-H(4A)	109.2	O(12B)-C(12)-C(11)	117.0(4)
N(3)-C(4)-H(4B)	109.2	C(14B)-C(13)-C(11)	121.5(6)
C(3)-C(4)-H(4B)	109.2	C(14B)-C(13)-C(14A)	23.3(5)
H(4A)-C(4)-H(4B)	107.9	C(11)-C(13)-C(14A)	99.0(6)
N(3)-C(5)-C(6)	110.6(3)	C(14B)-C(13)-H(13A)	104.5
N(3)-C(5)-H(5A)	109.5	C(11)-C(13)-H(13A)	112.0
C(6)-C(5)-H(5A)	109.5	C(14A)-C(13)-H(13A)	111.9
N(3)-C(5)-H(5B)	109.5	C(14B)-C(13)-H(13B)	95.8
C(6)-C(5)-H(5B)	109.5	C(11)-C(13)-H(13B)	112.0
H(5A)-C(5)-H(5B)	108.1	C(14A)-C(13)-H(13B)	112.0
N(4)-C(6)-C(5)	112.4(3)	H(13A)-C(13)-H(13B)	109.7
N(4)-C(6)-H(6A)	109.1	C(15A)-C(14A)-C(13)	101.9(9)
C(5)-C(6)-H(6A)	109.1	C(15A)-C(14A)-H(14A)	111.4
N(4)-C(6)-H(6B)	109.1	C(13)-C(14A)-H(14A)	111.4

C(15A)-C(14A)-H(14B)	111.4	O(25B)-C(25)-O(25A)	120.6(6)
C(13)-C(14A)-H(14B)	111.4	O(25B)-C(25)-O(251)	117.4(7)
H(14A)-C(14A)-H(14B)	109.3	O(25A)-C(25)-O(251)	29.2(5)
O(15A)-C(15A)-O(15B)	118.6(12)	O(25B)-C(25)-O(252)	112.2(8)
O(15A)-C(15A)-C(14A)	119.4(11)	O(25A)-C(25)-O(252)	25.9(7)
O(15B)-C(15A)-C(14A)	122.0(11)	O(251)-C(25)-O(252)	54.9(8)
C(15B)-C(14B)-C(13)	116.1(7)	O(25B)-C(25)-C(24)	127.5(4)
C(15B)-C(14B)-H(14C)	108.3	O(25A)-C(25)-C(24)	111.9(5)
C(13)-C(14B)-H(14C)	108.2	O(251)-C(25)-C(24)	108.4(6)
C(15B)-C(14B)-H(14D)	108.3	O(252)-C(25)-C(24)	114.6(7)
C(13)-C(14B)-H(14D)	108.3	C(32)-C(31)-C(33)	113.7(3)
H(14C)-C(14B)-H(14D)	107.4	C(32)-C(31)-N(3)	113.2(3)
O(151)-C(15B)-O(152)	119.1(7)	C(33)-C(31)-N(3)	111.5(3)
O(151)-C(15B)-C(14B)	122.5(7)	C(32)-C(31)-H(31A)	105.9
O(152)-C(15B)-C(14B)	118.3(7)	C(33)-C(31)-H(31A)	105.9
N(2)-C(21)-C(22)	109.8(3)	N(3)-C(31)-H(31A)	105.9
N(2)-C(21)-C(23)	114.8(3)	O(32B)-C(32)-O(32A)	125.0(4)
C(22)-C(21)-C(23)	113.9(3)	O(32B)-C(32)-C(31)	119.7(4)
N(2)-C(21)-H(21A)	105.8	O(32A)-C(32)-C(31)	115.3(3)
C(22)-C(21)-H(21A)	105.8	C(31)-C(33)-C(34)	112.6(3)
C(23)-C(21)-H(21A)	105.8	C(31)-C(33)-H(33A)	109.1
O(22B)-C(22)-O(22A)	124.5(4)	C(34)-C(33)-H(33A)	109.1
O(22B)-C(22)-C(21)	123.7(3)	C(31)-C(33)-H(33B)	109.1
O(22A)-C(22)-C(21)	111.8(4)	C(34)-C(33)-H(33B)	109.1
C(24)-C(23)-C(21)	113.5(4)	H(33A)-C(33)-H(33B)	107.8
C(24)-C(23)-H(23A)	108.9	C(35)-C(34)-C(33)	115.5(4)
C(21)-C(23)-H(23A)	108.9	C(35)-C(34)-H(34A)	108.4
C(24)-C(23)-H(23B)	108.9	C(33)-C(34)-H(34A)	108.4
C(21)-C(23)-H(23B)	108.9	C(35)-C(34)-H(34B)	108.4
H(23A)-C(23)-H(23B)	107.7	C(33)-C(34)-H(34B)	108.4
C(25)-C(24)-C(23)	111.9(4)	H(34A)-C(34)-H(34B)	107.5
C(25)-C(24)-H(24A)	109.2	O(35A)-C(35)-O(35B)	120.1(4)
C(23)-C(24)-H(24A)	109.2	O(35A)-C(35)-C(34)	124.9(4)
C(25)-C(24)-H(24B)	109.2	O(35B)-C(35)-C(34)	114.9(3)
C(23)-C(24)-H(24B)	109.2	N(4)-C(41)-C(42)	109.0(3)
H(24A)-C(24)-H(24B)	107.9	N(4)-C(41)-C(43)	115.8(3)

C(42)-C(41)-C(43)	110.2(4)	C(45)-C(44)-C(43)	113.3(4)
N(4)-C(41)-H(41A)	107.2	C(45)-C(44)-H(44A)	108.9
C(42)-C(41)-H(41A)	107.2	C(43)-C(44)-H(44A)	108.9
C(43)-C(41)-H(41A)	107.2	C(45)-C(44)-H(44B)	108.9
O(42B)-C(42)-O(421)	114.9(6)	C(43)-C(44)-H(44B)	108.9
O(42B)-C(42)-O(42A)	123.2(5)	H(44A)-C(44)-H(44B)	107.7
O(421)-C(42)-O(42A)	44.5(5)	O(45A)-C(45)-O(45B)	122.9(4)
O(42B)-C(42)-C(41)	127.4(4)	O(45A)-C(45)-C(44)	125.5(4)
O(421)-C(42)-C(41)	114.1(6)	O(45B)-C(45)-C(44)	111.5(4)
O(42A)-C(42)-C(41)	104.8(5)	O(3S)-C(1S)-C(2S)	142.2(14)
C(44)-C(43)-C(41)	113.3(4)	O(4SC)-O(4SA)-O(4SB)	114.1(13)
C(44)-C(43)-H(43A)	108.9	O(4SC)-O(4SA)-O(4SA)#1	164.3(16)
C(41)-C(43)-H(43A)	108.9	O(4SB)-O(4SA)-O(4SA)#1	81.6(9)
C(44)-C(43)-H(43B)	108.9	O(5SB)-O(5SA)-O(5SC)	81.6(12)
C(41)-C(43)-H(43B)	108.9	O(5SA)-O(5SB)-O(5SC)	67.7(11)
H(43A)-C(43)-H(43B)	107.7	O(5SA)-O(5SC)-O(5SB)	30.8(5)

Table 4. Anisotropic displacement parameters ($Å^2 x\ 10^3$) for 97srv131. The anisotropic displacement factor exponent takes the form: $-2\pi^2[\ h^2\ a^{*2}U^{11} + ... + 2\ h\ k\ a^*\ b^*\ U^{12}\ ]$

	U^{11}	U^{22}	U^{33}	U^{23}	U^{13}	U^{12}
O(12B)	55(2)	79(3)	40(2)	-24(2)	-11(2)	17(2)
O(12A)	60(3)	106(4)	78(3)	-37(3)	-34(2)	3(2)
O(22B)	45(2)	35(2)	45(2)	-7(1)	9(1)	-5(2)
O(22A)	69(2)	48(2)	30(2)	-12(1)	0(2)	3(2)
O(25B)	87(3)	39(2)	48(2)	-7(2)	3(2)	9(2)
O(32B)	55(2)	37(2)	28(1)	4(1)	8(1)	15(2)
O(32A)	54(2)	51(2)	30(2)	4(1)	17(1)	19(2)
O(35B)	52(2)	46(2)	33(1)	7(1)	16(1)	19(2)
O(35A)	67(2)	48(2)	36(2)	13(2)	7(2)	13(2)
O(42B)	68(2)	52(2)	40(2)	-8(2)	-7(2)	2(2)
O(42A)	159(11)	29(4)	36(4)	-9(3)	-35(6)	-6(6)

O(421)	102(8)	49(5)	50(5)	1(4)	-19(5)	-37(6)
O(45B)	55(2)	32(2)	44(2)	1(1)	-3(2)	-17(2)
O(45A)	42(2)	38(2)	41(2)	-1(1)	1(1)	-14(2)
N(1)	32(2)	40(2)	28(2)	-9(2)	-2(1)	2(2)
N(2)	33(2)	29(2)	22(2)	-4(1)	5(1)	2(2)
N(3)	35(2)	25(2)	26(2)	-1(1)	9(1)	-1(1)
N(4)	34(2)	30(2)	23(2)	-7(1)	4(1)	-5(2)
C(1)	40(2)	31(2)	29(2)	-5(2)	0(2)	7(2)
C(2)	38(2)	26(2)	29(2)	-3(2)	2(2)	2(2)
C(3)	35(2)	26(2)	33(2)	1(2)	11(2)	2(2)
C(4)	32(2)	25(2)	28(2)	0(2)	6(2)	1(2)
C(5)	42(2)	25(2)	21(2)	-1(2)	8(2)	2(2)
C(6)	35(2)	34(2)	23(2)	-5(2)	10(2)	-6(2)
C(7)	28(2)	40(2)	30(2)	-8(2)	6(2)	-6(2)
C(8)	36(2)	40(2)	24(2)	-8(2)	0(2)	-1(2)
C(11)	33(2)	64(3)	42(2)	-13(2)	-8(2)	0(2)
C(12)	52(3)	69(4)	53(3)	-23(3)	-24(3)	8(3)
C(13)	32(2)	93(4)	40(2)	-9(3)	-4(2)	17(3)
C(21)	49(3)	30(2)	28(2)	-4(2)	8(2)	0(2)
C(22)	34(2)	39(2)	30(2)	-9(2)	1(2)	1(2)
C(23)	54(3)	39(2)	27(2)	3(2)	10(2)	-4(2)
C(24)	61(3)	45(3)	34(2)	-1(2)	8(2)	-1(2)
C(25)	52(3)	57(3)	31(2)	5(2)	2(2)	1(3)
C(31)	45(2)	24(2)	23(2)	-2(2)	11(2)	0(2)
C(32)	51(3)	25(2)	24(2)	-1(2)	5(2)	11(2)
C(33)	68(3)	30(2)	29(2)	-6(2)	20(2)	-5(2)
C(34)	47(3)	26(2)	32(2)	-2(2)	12(2)	5(2)
C(35)	41(2)	35(2)	28(2)	-2(2)	8(2)	-2(2)
C(41)	53(3)	30(2)	24(2)	-5(2)	7(2)	-12(2)
C(42)	95(4)	31(3)	31(2)	-2(2)	-3(2)	-21(3)
C(43)	38(2)	41(3)	36(2)	5(2)	-2(2)	-13(2)
C(44)	50(3)	47(3)	46(3)	14(2)	-6(2)	-22(2)
C(45)	48(3)	38(2)	28(2)	-1(2)	-1(2)	-16(2)

Table 5. Hydrogen coordinates (x 10^4) and isotropic displacement parameters ($Å^2$x 10^3) for 97srv131.

	x	y	z	U(eq)
H(22A)	-7971	7924	759	76
H(35A)	-9656	11617	279	64
H(45A)	-8209	13621	-2755	69
H(1)	-7170	6528	-1262	41(13)
H(3)	-8649	8011	-1586	38(12)
H(1A)	-7120	4507	-785	41
H(1B)	-7256	3976	-1507	41
H(2A)	-8553	4842	-1792	38
H(2B)	-8502	4074	-1137	38
H(3A)	-9640	6614	-912	37
H(3B)	-9718	5354	-1327	37
H(4A)	-9421	6453	-2213	34
H(4B)	-10210	7041	-2012	34
H(5A)	-9106	9663	-2390	35
H(5B)	-9688	8571	-2749	35
H(6A)	-8589	7356	-2845	36
H(6B)	-8374	8724	-3061	36
H(7A)	-6513	7639	-2176	39
H(7B)	-7137	7395	-2856	39
H(8A)	-7775	5777	-2338	41
H(8B)	-6853	5456	-2381	41
H(11A)	-5796	6448	-1458	59
H(13A)	-5933	4155	-1683	68
H(13B)	-5690	3994	-904	68
H(14A)	-4693	5679	-1579	46
H(14B)	-4410	5265	-829	46
H(14C)	-4599	4952	-1554	58
H(14D)	-4459	4669	-797	58
H(21A)	-7749	5446	-199	43
H(23A)	-9299	5616	125	48
H(23B)	-9133	4433	-288	48

H(24A)	-8163	5071	964	57
H(24B)	-8817	3957	830	57
H(31A)	-9400	8556	-888	37
H(33A)	-9210	10813	-1537	49
H(33B)	-8427	10033	-1172	49
H(34A)	-9160	10167	-237	41
H(34B)	-8531	11221	-349	41
H(41A)	-7831	10017	-1990	43
H(43A)	-6346	9793	-2437	48
H(43B)	-7199	9825	-2960	48
H(44A)	-6671	11792	-2040	60
H(44B)	-6571	11851	-2775	60

Table 6. Selected torsion angles [°]for 97srv131.

-52.10 (0.43)	N1 - C1 - C2 - N2
-59.61 (0.41)	N2 - C3 - C4 - N3
-46.73 (0.43)	N3 - C5 - C6 - N4
-69.02 (0.42)	N4 - C7 - C8 - N1
19.51 (0.70)	N1 - C11 - C12 - O12B
-12.58 (0.58)	N2 - C21 - C22 - O22B
140.37 (0.35)	N3 - C31 - C32 - O32A
-40.06 (0.50)	N3 - C31 - C32 - O32B
16.91 (0.79)	N4 - C41 - C42 - O42B

Crystallographic Data for [Eu.(RRRR-)/(SSSS-)]26.

Table 1. Crystal data and structure refinement for [**Eu.**(*RRRR*-)].

Empirical formula	$C_{28}H_{49}N_4O_{20.25}Eu$	
Formula weight	917.67	
Temperature	150(2) K	
Wavelength	0.71073 Å	
Crystal system	Triclinic	
Space group	$P_{(-1)}$	
Unit cell dimensions	a = 9.637(2) Å	α = 102.47(2)°.
	b = 12.690(4) Å	β = 101.28(2)°.
	c = 16.186(5) Å	γ = 110.42(2)°.
Volume, Z	1729.84(3) $Å^3$, 2	
Density (calculated)	1.762 Mg/m^3	
Absorption coefficient	1.906 mm^{-1}	
F(000)	940	
Crystal size	0.16 x 0.16 x 0.10 mm	
θ range for data collection	1.35 to 27.45°.	
Limiting indices	$-11 \le h \le 12, -15 \le k \le 16, -20 \le l \le 20$	
Number of reflexions used	Calculation of cell:	512
	Total:	13944
	Unique:	7826
	Obs. [$F_o > 4.\sigma(F_o)$]	7242
Independent reflections	7826 [$R_{(int)}$ = 0.0310]	
Absorption correction	Integration	
Max. and min. transmission	0.835 and 0.713	
Refinement method	Full-matrix least-squares on F^2	
Data / restraints / parameters	7797 / 0 / 627	
Goodness-of-fit on F^2	1.094	
Final R indices [$I>2\sigma(I)$]	R_1 = 0.0305, wR_2 = 0.0670	
R indices (all data)	R_1 = 0.0364, wR_2 = 0.0747	
Extinction coefficient	not refined	
Largest diff. peak and hole	0.979 and -0.950 $e.Å^{-3}$	

Table 2. Atomic coordinates (x 10^5) and equivalent isotropic displacement parameters (Å^2 x 10^4) for [Eu.(*RRRR*-)]. $U_{(eq)}$ is defined as one third of the trace of the orthogonalized U_{ij} tensor.

	x	y	z	$U_{(eq)}$
Eu(1)	41789(2)	27646(1)	26636(1)	122(1)
O(5)	19580(4)	31180(3)	29600(3)	290(6)
O(12A)	66450(7)	60990(5)	49560(3)	181(10)
O(12B)	71640(10)	58850(7)	50620(5)	160(2)
O(12C)	63250(16)	63370(12)	47320(9)	240(3)
O(122)	50370(3)	43900(2)	39850(2)	219(5)
O(151)	108540(3)	90800(2)	39290(2)	249(5)
O(152)	108130(3)	92160(2)	53160(2)	275(6)
O(221)	35390(3)	7950(2)	46340(2)	254(5)
O(222)	32400(3)	16070(2)	35527(15)	174(5)
O(251)	76820(3)	44670(2)	64610(2)	321(6)
O(252)	61390(3)	38060(2)	72750(2)	284(6)
O(321)	7190(4)	-4610(2)	4450(2)	283(6)
O(322)	19510(3)	13110(2)	14699(15)	167(4)
O(351)	3860(4)	-43770(3)	13930(3)	549(10)
O(352)	22090(4)	-37730(3)	7450(2)	358(7)
O(421)	29910(3)	44140(2)	6160(2)	289(6)
O(422)	37800(3)	40920(2)	18919(15)	180(5)
O(451)	26920(4)	8130(3)	-12690(2)	413(8)
O(452)	11800(4)	12940(3)	-21990(2)	509(10)
O(1SA)	100450(5)	91300(4)	68170(3)	522(10)
O(1SB)	104570(19)	89600(14)	70000(11)	460(4)
O(2SA)	1390(12)	35800(9)	19200(7)	370(2)
O(2SB)	-2150(13)	31990(10)	8020(7)	710(3)
O(3SB)	-10010(10)	16660(8)	14520(6)	720(2)
O(3SA)	-9680(11)	18720(8)	18810(7)	480(2)
O(3SC)	-16310(15)	12840(11)	8820(9)	500(3)
N(1)	70010(3)	44470(2)	29550(2)	175(6)
N(2)	63870(3)	25430(2)	38350(2)	174(5)
N(3)	43690(3)	7050(2)	20750(2)	140(5)
N(4)	49980(3)	25940(2)	11750(2)	144(5)
C(1)	82150(4)	41110(3)	33970(2)	230(7)
C(2)	78750(4)	36260(3)	41490(2)	240(7)
C(3)	66820(4)	15050(3)	34220(2)	209(7)
C(4)	52360(4)	4380(3)	28220(2)	171(6)
C(5)	52290(4)	7660(3)	14080(2)	161(6)
C(6)	47700(4)	13500(3)	7410(2)	162(6)
C(7)	66780(4)	33750(3)	13880(2)	173(6)
C(8)	72140(4)	45660(3)	20800(2)	191(7)
C(11)	70530(4)	55760(3)	35070(2)	209(7)
C(12)	62330(5)	53220(3)	42070(2)	306(9)
C(13)	86610(4)	66160(3)	38950(3)	249(7)
C(14)	85550(4)	78160(3)	41110(3)	296(8)
C(15)	101780(4)	87820(3)	45150(2)	229(7)
C(21)	57560(4)	23910(3)	46030(2)	162(6)
C(22)	40430(4)	15160(3)	42400(2)	171(6)
C(23)	67240(4)	20940(3)	53140(2)	187(6)
C(24)	63990(4)	23620(3)	62050(2)	202(7)
C(25)	68250(4)	36560(3)	66470(2)	216(7)

C(31)	27350(4)	-2260(3)	17050(2)	161(6)
C(32)	17350(4)	2560(3)	11680(2)	158(6)
C(33)	25770(4)	-14660(3)	12370(2)	200(7)
C(34)	10920(4)	-24490(3)	12410(3)	281(8)
C(35)	11730(4)	-36400(3)	11340(2)	236(7)
C(41)	39670(4)	29270(3)	5580(2)	156(6)
C(42)	35620(4)	39060(3)	10540(2)	175(6)
C(43)	45370(4)	31900(3)	-2310(2)	190(6)
C(44)	32430(5)	28680(3)	-10740(2)	247(7)
C(45)	23490(5)	15530(3)	-15140(2)	258(8)

Table 3. Selected torsion angles [deg] for [**Eu.**(*RRRR*-)].

59.52 (0.40)	N1 - C1 - C2 - N2
58.43 (0.36)	N2 - C3 - C4 - N3
58.67 (0.36)	N3 - C5 - C6 - N4
60.86 (0.37)	N4 - C7 - C8 - N1
-38.52 (0.50)	N1 - C11 - C12 - O122
-39.69 (0.38)	N2 - C21 - C22 - O222
-40.62 (0.38)	N3 - C31 - C32 - O322
-17.50 (0.40)	N4 - C41 - C42 - O422

Table 4. Bond lengths [Å] and angles [deg] for [**Eu.**(*RRRR*-)].

Eu(1)-O(222)	2.354(2)	Eu(1)-O(422)	2.391(2)
Eu(1)-O(122)	2.393(2)	Eu(1)-O(322)	2.412(2)
Eu(1)-O(5)	2.447(3)	Eu(1)-N(3)	2.664(3)
Eu(1)-N(4)	2.667(3)	Eu(1)-N(1)	2.681(3)
Eu(1)-N(2)	2.696(3)	Eu(1)-H(5D)	2.81(6)
O(5)-H(5D)	0.64(6)	O(5)-H(5C)	0.76(9)
O(12A)-O(12B)	0.660(8)	O(12A)-O(12C)	0.622(13)
O(12A)-C(12)	1.274(6)	O(12B)-O(12C)	1.25(2)
O(12B)-C(12)	1.367(9)	O(12C)-C(12)	1.343(14)
O(122)-C(12)	1.249(4)	O(151)-C(15)	1.300(4)
O(151)-H(151)	0.91(6)	O(152)-C(15)	1.227(4)
O(221)-C(22)	1.242(4)	O(222)-C(22)	1.277(4)
O(251)-C(25)	1.213(4)	O(252)-C(25)	1.331(4)
O(252)-H(252)	0.85(6)	O(321)-C(32)	1.275(4)
O(321)-H(321)	0.56(7)	O(322)-C(32)	1.248(4)
O(351)-C(35)	1.193(5)	O(352)-C(35)	1.319(4)
O(352)-H(352)	0.91(6)	O(421)-C(42)	1.230(4)
O(422)-C(42)	1.287(4)	O(451)-C(45)	1.214(5)
O(452)-C(45)	1.304(5)	O(452)-H(452)	0.77(9)
O(1SA)-O(1SB)	0.58(2)	O(2SA)-O(2SB)	1.70(2)
O(3SB)-O(3SA)	0.677(11)	O(3SB)-O(3SC)	0.915(12)
O(3SA)-O(3SC)	1.52(2)	N(1)-C(1)	1.488(5)
N(1)-C(11)	1.494(4)	N(1)-C(8)	1.501(4)
N(2)-C(3)	1.489(4)	N(2)-C(2)	1.497(4)
N(2)-C(21)	1.507(4)	N(3)-C(5)	1.483(4)
N(3)-C(4)	1.501(4)	N(3)-C(31)	1.503(4)
N(4)-C(7)	1.496(4)	N(4)-C(41)	1.500(4)
N(4)-C(6)	1.501(4)	C(1)-C(2)	1.520(5)

C(1)-H(1A)	0.99	C(1)-H(1B)	0.99
C(2)-H(2A)	0.96(4)	C(2)-H(2B)	1.01(5)
C(3)-C(4)	1.518(5)	C(3)-H(3B)	0.99
C(3)-H(3A)	0.99	C(4)-H(4B)	1.00(4)
C(4)-H(4A)	0.99(4)	C(5)-C(6)	1.516(4)
C(5)-H(5B)	0.97(4)	C(5)-H(5A)	0.93(4)
C(6)-H(6A)	1.03(4)	C(6)-H(6B)	0.93(3)
C(7)-C(8)	1.518(5)	C(7)-H(7B)	0.99(4)
C(7)-H(7A)	1.00(4)	C(8)-H(8B)	0.96(4)
C(8)-H(8A)	1.00(4)	C(11)-C(12)	1.530(5)
C(11)-C(13)	1.540(5)	C(11)-H(11)	1.00
C(13)-C(14)	1.531(5)	C(13)-H(13B)	1.00(4)
C(13)-H(13A)	0.98(4)	C(14)-C(15)	1.514(5)
C(14)-H(14B)	0.99	C(14)-H(14A)	0.99
C(21)-C(23)	1.532(5)	C(21)-C(22)	1.537(4)
C(21)-H(21)	0.98(4)	C(23)-C(24)	1.527(5)
C(23)-H(23B)	0.98(4)	C(23)-H(23A)	0.94(4)
C(24)-C(25)	1.511(5)	C(24)-H(24B)	0.93(4)
C(24)-H(24A)	0.93(4)	C(31)-C(33)	1.532(4)
C(31)-C(32)	1.539(4)	C(31)-H(31A)	0.93(4)
C(33)-C(34)	1.539(5)	C(33)-H(33B)	0.99(4)
C(33)-H(33A)	1.02(4)	C(34)-C(35)	1.515(5)
C(34)-H(34A)	0.95(5)	C(34)-H(34B)	0.96(6)
C(41)-C(42)	1.540(4)	C(41)-C(43)	1.542(4)
C(41)-H(41)	0.98(4)	C(43)-C(44)	1.523(5)
C(43)-H(43B)	0.96(4)	C(43)-H(43A)	0.95(4)
C(44)-C(45)	1.510(5)	C(44)-H(44A)	0.98(5)
C(44)-H(44B)	0.98(4)		

O(222)-Eu(1)-O(422)	145.19(8)	O(222)-Eu(1)-O(122)	84.31(8)
O(422)-Eu(1)-O(122)	85.84(8)	O(222)-Eu(1)-O(322)	85.83(8)
O(422)-Eu(1)-O(322)	83.23(8)	O(122)-Eu(1)-O(322)	144.73(8)
O(222)-Eu(1)-O(5)	72.73(9)	O(422)-Eu(1)-O(5)	72.52(9)
O(122)-Eu(1)-O(5)	70.15(11)	O(322)-Eu(1)-O(5)	74.58(10)
O(222)-Eu(1)-N(3)	72.75(8)	O(422)-Eu(1)-N(3)	130.35(8)
O(122)-Eu(1)-N(3)	140.88(9)	O(322)-Eu(1)-N(3)	65.85(8)
O(5)-Eu(1)-N(3)	128.46(9)	O(222)-Eu(1)-N(4)	140.90(8)
O(422)-Eu(1)-N(4)	65.16(8)	O(122)-Eu(1)-N(4)	131.41(8)
22)-Eu(1)-N(4)	72.43(8)	O(5)-Eu(1)-N(4)	128.38(11)
N(3)-Eu(1)-N(4)	68.80(8)	O(222)-Eu(1)-N(1)	129.88(8)
O(422)-Eu(1)-N(1)	74.11(8)	O(122)-Eu(1)-N(1)	65.34(8)
O(322)-Eu(1)-N(1)	141.10(8)	O(5)-Eu(1)-N(1)	125.29(10)
N(3)-Eu(1)-N(1)	106.20(8)	N(4)-Eu(1)-N(1)	69.47(8)
O(222)-Eu(1)-N(2)	65.39(8)	O(422)-Eu(1)-N(2)	141.58(8)
O(122)-Eu(1)-N(2)	73.13(9)	O(322)-Eu(1)-N(2)	131.54(8)
O(5)-Eu(1)-N(2)	125.97(11)	N(3)-Eu(1)-N(2)	68.63(8)
N(4)-Eu(1)-N(2)	105.62(8)	N(1)-Eu(1)-N(2)	67.98(9)
O(222)-Eu(1)-H(5D)	75.7(12)	O(422)-Eu(1)-H(5D)	69.9(12)
O(122)-Eu(1)-H(5D)	81.2(12)	O(322)-Eu(1)-H(5D)	63.5(12)
O(5)-Eu(1)-H(5D)	11.4(11)	N(3)-Eu(1)-H(5D)	121.2(12)
N(4)-Eu(1)-H(5D)	119.2(11)	N(1)-Eu(1)-H(5D)	132.0(12)
N(2)-Eu(1)-H(5D)	134.8(11)	Eu(1)-O(5)-H(5D)	119(5)
Eu(1)-O(5)-H(5C)	119(7)	H(5D)-O(5)-H(5C)	98(8)
O(12B)-O(12A)-O(12C)	154(2)	O(12B)-O(12A)-C(12)	83.6(9)
O(12C)-O(12A)-C(12)	82.5(14)	O(12A)-O(12B)-O(12C)	12.9(9)
O(12A)-O(12B)-C(12)	67.8(8)	O(12C)-O(12B)-C(12)	61.6(7)
O(12A)-O(12C)-O(12B)	13.7(10)	O(12A)-O(12C)-C(12)	70.1(14)
O(12B)-O(12C)-C(12)	63.6(8)	C(12)-O(122)-Eu(1)	125.7(2)

C(15)-O(151)-H(151)	111(3)	C(22)-O(222)-Eu(1)	126.7(2)
C(25)-O(252)-H(252)	113(4)	C(32)-O(321)-H(321)	120(9)
C(32)-O(322)-Eu(1)	124.1(2)	C(35)-O(352)-H(352)	113(4)
C(42)-O(422)-Eu(1)	124.6(2)	C(45)-O(452)-H(452)	108(7)
O(3SA)-O(3SB)-O(3SC)	146(2)	O(3SB)-O(3SA)-O(3SC)	19.6(11)
O(3SB)-O(3SC)-O(3SA)	14.4(8)	C(1)-N(1)-C(11)	112.3(3)
C(1)-N(1)-C(8)	109.0(3)	C(11)-N(1)-C(8)	109.8(3)
C(1)-N(1)-Eu(1)	110.0(2)	C(11)-N(1)-Eu(1)	107.1(2)
C(8)-N(1)-Eu(1)	108.7(2)	C(3)-N(2)-C(2)	108.8(3)
C(3)-N(2)-C(21)	111.8(3)	C(2)-N(2)-C(21)	109.4(2)
C(3)-N(2)-Eu(1)	110.2(2)	C(2)-N(2)-Eu(1)	111.4(2)
C(21)-N(2)-Eu(1)	105.2(2)	C(5)-N(3)-C(4)	107.8(2)
C(5)-N(3)-C(31)	112.9(2)	C(4)-N(3)-C(31)	109.3(2)
C(5)-N(3)-Eu(1)	109.7(2)	C(4)-N(3)-Eu(1)	110.4(2)
C(31)-N(3)-Eu(1)	106.8(2)	C(7)-N(4)-C(41)	112.6(2)
C(7)-N(4)-C(6)	107.9(2)	C(41)-N(4)-C(6)	108.6(2)
C(7)-N(4)-Eu(1)	109.4(2)	C(41)-N(4)-Eu(1)	107.4(2)
C(6)-N(4)-Eu(1)	110.9(2)	N(1)-C(1)-C(2)	114.2(3)
N(1)-C(1)-H(1A)	108.7(2)	C(2)-C(1)-H(1A)	108.7(2)
N(1)-C(1)-H(1B)	108.7(2)	C(2)-C(1)-H(1B)	108.7(2)
H(1A)-C(1)-H(1B)	107.6	N(2)-C(2)-C(1)	111.5(3)
N(2)-C(2)-H(2A)	110(3)	C(1)-C(2)-H(2A)	111(3)
N(2)-C(2)-H(2B)	109(3)	C(1)-C(2)-H(2B)	107(3)
H(2A)-C(2)-H(2B)	108(4)	N(2)-C(3)-C(4)	114.3(3)
N(2)-C(3)-H(3B)	108.7(2)	C(4)-C(3)-H(3B)	108.7(2)
N(2)-C(3)-H(3A)	108.7(2)	C(4)-C(3)-H(3A)	108.7(2)
H(3B)-C(3)-H(3A)	107.6	N(3)-C(4)-C(3)	112.7(3)
N(3)-C(4)-H(4B)	112(2)	C(3)-C(4)-H(4B)	105(2)
N(3)-C(4)-H(4A)	111(2)	C(3)-C(4)-H(4A)	112(2)
H(4B)-C(4)-H(4A)	105(3)	N(3)-C(5)-C(6)	114.3(3)
N(3)-C(5)-H(5B)	112(2)	C(6)-C(5)-H(5B)	107(2)
N(3)-C(5)-H(5A)	111(2)	C(6)-C(5)-H(5A)	107(2)
H(5B)-C(5)-H(5A)	105(3)	N(4)-C(6)-C(5)	112.3(3)
N(4)-C(6)-H(6A)	111(2)	C(5)-C(6)-H(6A)	108(2)
N(4)-C(6)-H(6B)	111(2)	C(5)-C(6)-H(6B)	111(2)
H(6A)-C(6)-H(6B)	104(3)	N(4)-C(7)-C(8)	114.6(3)
N(4)-C(7)-H(7B)	105(2)	C(8)-C(7)-H(7B)	110(2)
N(4)-C(7)-H(7A)	112(2)	C(8)-C(7)-H(7A)	109(2)
H(7B)-C(7)-H(7A)	107(3)	N(1)-C(8)-C(7)	112.3(3)
N(1)-C(8)-H(8B)	110(2)	C(7)-C(8)-H(8B)	107(2)
N(1)-C(8)-H(8A)	108(2)	C(7)-C(8)-H(8A)	107(2)
H(8B)-C(8)-H(8A)	112(3)	N(1)-C(11)-C(12)	109.2(3)
N(1)-C(11)-C(13)	115.9(3)	C(12)-C(11)-C(13)	113.1(3)
N(1)-C(11)-H(11)	105.9(2)	C(12)-C(11)-H(11)	105.9(2)
C(13)-C(11)-H(11)	105.9(2)	O(122)-C(12)-O(12A)	120.7(4)
O(122)-C(12)-O(12B)	123.2(4)	O(12A)-C(12)-O(12B)	28.6(3)
O(122)-C(12)-O(12C)	120.9(6)	O(12A)-C(12)-O(12C)	27.3(6)
O(12B)-C(12)-O(12C)	54.8(7)	O(122)-C(12)-C(11)	117.9(3)
O(12A)-C(12)-C(11)	120.9(4)	O(12B)-C(12)-C(11)	114.3(4)
O(12C)-C(12)-C(11)	109.9(7)	C(14)-C(13)-C(11)	112.3(3)
C(14)-C(13)-H(13B)	112(3)	C(11)-C(13)-H(13B)	109(3)
C(14)-C(13)-H(13A)	109(2)	C(11)-C(13)-H(13A)	108(2)
H(13B)-C(13)-H(13A)	106(3)	C(15)-C(14)-C(13)	108.8(3)
C(15)-C(14)-H(14B)	109.9(2)	C(13)-C(14)-H(14B)	109.9(2)
C(15)-C(14)-H(14A)	109.9(2)	C(13)-C(14)-H(14A)	109.9(2)
H(14B)-C(14)-H(14A)	108.3	O(152)-C(15)-O(151)	123.2(3)
O(152)-C(15)-C(14)	123.3(3)	O(151)-C(15)-C(14)	113.4(3)
N(2)-C(21)-C(23)	115.0(3)	N(2)-C(21)-C(22)	108.7(2)

C(23)-C(21)-C(22)	113.7(3)	N(2)-C(21)-H(21)	104(2)
C(23)-C(21)-H(21)	108(2)	C(22)-C(21)-H(21)	107(2)
O(221)-C(22)-O(222)	125.1(3)	O(221)-C(22)-C(21)	118.6(3)
O(222)-C(22)-C(21)	116.3(3)	C(24)-C(23)-C(21)	113.3(3)
C(24)-C(23)-H(23B)	108(2)	C(21)-C(23)-H(23B)	110(2)
C(24)-C(23)-H(23A)	107(2)	C(21)-C(23)-H(23A)	112(2)
H(23B)-C(23)-H(23A)	107(3)	C(25)-C(24)-C(23)	114.5(3)
C(25)-C(24)-H(24B)	106(3)	C(23)-C(24)-H(24B)	110(3)
C(25)-C(24)-H(24A)	109(3)	C(23)-C(24)-H(24A)	111(3)
H(24B)-C(24)-H(24A)	106(4)	O(251)-C(25)-O(252)	123.5(3)
O(251)-C(25)-C(24)	124.9(3)	O(252)-C(25)-C(24)	111.7(3)
N(3)-C(31)-C(33)	115.1(3)	N(3)-C(31)-C(32)	108.4(2)
C(33)-C(31)-C(32)	115.6(3)	N(3)-C(31)-H(31A)	108(2)
C(33)-C(31)-H(31A)	104(2)	C(32)-C(31)-H(31A)	105(2)
O(322)-C(32)-O(321)	124.2(3)	O(322)-C(32)-C(31)	118.3(3)
O(321)-C(32)-C(31)	117.4(3)	C(31)-C(33)-C(34)	112.7(3)
C(31)-C(33)-H(33B)	109(2)	C(34)-C(33)-H(33B)	114(2)
C(31)-C(33)-H(33A)	108(2)	C(34)-C(33)-H(33A)	107(2)
H(33B)-C(33)-H(33A)	106(3)	C(35)-C(34)-C(33)	114.3(3)
C(35)-C(34)-H(34A)	107(3)	C(33)-C(34)-H(34A)	112(3)
C(35)-C(34)-H(34B)	107(3)	C(33)-C(34)-H(34B)	111(3)
H(34A)-C(34)-H(34B)	104(4)	O(351)-C(35)-O(352)	123.5(4)
O(351)-C(35)-C(34)	122.7(3)	O(352)-C(35)-C(34)	113.8(3)
N(4)-C(41)-C(42)	112.2(3)	N(4)-C(41)-C(43)	114.3(3)
C(42)-C(41)-C(43)	112.7(3)	N(4)-C(41)-H(41)	107(2)
C(42)-C(41)-H(41)	104(2)	C(43)-C(41)-H(41)	106(2)
O(421)-C(42)-O(422)	124.9(3)	O(421)-C(42)-C(41)	117.8(3)
O(422)-C(42)-C(41)	117.2(3)	C(44)-C(43)-C(41)	114.3(3)
C(44)-C(43)-H(43B)	106(2)	C(41)-C(43)-H(43B)	110(2)
C(44)-C(43)-H(43A)	112(3)	C(41)-C(43)-H(43A)	107(3)
H(43B)-C(43)-H(43A)	108(4)	C(45)-C(44)-C(43)	113.6(3)
C(45)-C(44)-H(44A)	110(3)	C(43)-C(44)-H(44A)	110(3)
C(45)-C(44)-H(44B)	108(3)	(43)-C(44)-H(44B)	108(3)
H(44A)-C(44)-H(44B)	108(4)	O(451)-C(45)-O(452)	123.4(4)
O(451)-C(45)-C(44)	123.9(3)	O(452)-C(45)-C(44)	112.8(3)

Table 5. Anisotropic displacement parameters ($Å^2$ x 10^4) for [Eu.(*RRRR*-)]. The anisotropic displacement factor exponent takes the form: $-2\pi^2$ [$h^2.a^{*2}.U_{11}$ + ... + 2hk.a*.b*.U_{12}]

	U_{11}	U_{22}	U_{33}	U_{23}	U_{13}	U_{12}
Eu(1)	122(1)	105(1)	125(1)	17(1)	48(1)	35(1)
O(5)	240(2)	172(14)	480(2)	62(13)	180(2)	94(12)
O(122)	219(12)	156(11)	211(12)	-7(9)	125(10)	-1(9)
O(151)	199(12)	242(13)	199(12)	24(10)	30(10)	7(10)
O(152)	273(13)	265(13)	266(14)	77(11)	70(11)	93(11)
O(221)	186(12)	250(13)	264(13)	135(11)	44(10)	-2(10)
O(222)	156(11)	199(11)	154(11)	59(9)	50(9)	51(9)
O(251)	400(2)	221(13)	302(14)	83(11)	117(12)	70(12)
O(252)	339(15)	211(13)	293(14)	16(11)	128(12)	120(12)
O(321)	287(15)	171(12)	249(14)	8(10)	-103(11)	62(11)

O(322)	154(11)	138(10)	194(11)	28(9)	33(9)	67(9)
O(351)	580(2)	310(2)	1060(3)	380(2)	590(2)	240(2)
O(352)	470(2)	227(14)	580(2)	201(13)	340(2)	226(13)
O(421)	450(2)	286(14)	284(14)	138(11)	152(12)	276(13)
O(422)	243(12)	142(11)	180(11)	43(9)	87(9)	99(9)
O(451)	550(2)	262(15)	350(2)	42(12)	-30(14)	191(14)
O(452)	530(2)	480(2)	360(2)	-80(2)	-160(2)	310(2)
N(1)	158(13)	144(13)	165(13)	8(10)	71(11)	7(10)
N(2)	141(13)	200(14)	150(13)	47(11)	49(10)	35(11)
N(3)	136(12)	124(12)	152(13)	36(10)	31(10)	55(10)
N(4)	152(13)	132(12)	151(12)	46(10)	55(10)	54(10)
C(1)	170(2)	220(2)	230(2)	41(14)	67(13)	18(13)
C(2)	170(2)	280(2)	190(2)	53(14)	40(13)	18(14)
C(3)	180(2)	270(2)	160(2)	56(13)	35(13)	88(14)
C(4)	190(2)	190(2)	180(2)	74(13)	56(13)	119(13)
C(5)	170(2)	155(15)	180(2)	43(12)	78(13)	76(13)
C(6)	210(2)	147(15)	145(15)	31(12)	66(13)	97(13)
C(7)	170(2)	200(2)	170(2)	62(13)	77(13)	81(13)
C(8)	170(2)	170(2)	210(2)	69(13)	97(13)	19(13)
C(11)	190(2)	160(2)	200(2)	13(13)	80(13)	10(13)
C(12)	340(2)	220(2)	240(2)	-34(15)	200(2)	-20(2)
C(13)	190(2)	180(2)	310(2)	43(15)	70(2)	16(14)
C(14)	230(2)	200(2)	380(2)	20(2)	80(2)	46(15)
C(15)	210(2)	160(2)	280(2)	24(14)	49(14)	72(13)
C(21)	138(14)	170(2)	152(15)	37(12)	54(12)	39(12)
C(22)	159(15)	166(15)	153(15)	18(12)	54(12)	40(12)
C(23)	190(2)	220(2)	180(2)	59(13)	54(13)	112(14)
C(24)	240(2)	200(2)	180(2)	68(13)	55(14)	100(14)
C(25)	240(2)	210(2)	160(2)	41(13)	11(13)	81(14)
C(31)	160(15)	131(14)	180(2)	44(12)	39(12)	57(12)
C(32)	131(14)	156(15)	180(2)	46(12)	40(12)	61(12)
C(33)	210(2)	119(15)	280(2)	52(13)	95(14)	76(13)
C(34)	230(2)	130(2)	490(2)	80(2)	170(2)	47(14)
C(35)	220(2)	190(2)	280(2)	52(14)	87(14)	60(14)
C(41)	190(2)	131(14)	151(15)	34(12)	55(12)	80(12)
C(42)	180(2)	132(14)	210(2)	47(12)	67(13)	60(12)
C(43)	220(2)	190(2)	190(2)	76(13)	99(13)	94(14)
C(44)	370(2)	270(2)	190(2)	111(15)	120(2)	190(2)
C(45)	350(2)	300(2)	170(2)	65(14)	80(15)	190(2)

Table 6. Hydrogen coordinates (x 10^3) and isotropic displacement parameters (Å^2 x 10^3) for **[Eu.(*RRRR*-)]**.

	x	y	z	$U_{(eq)}$
H(5D)	131(7)	287(5)	266(4)	39(19)
H(5C)	202(10)	375(8)	308(6)	117(33)
H(151)	1178(7)	971(5)	419(4)	56(16)
H(252)	632(7)	453(5)	750(4)	55(16)
H(321)	32(10)	-31(8)	25(6)	103(34)
H(352)	229(7)	-447(6)	71(4)	68(18)
H(452)	75(11)	61(8)	-238(6)	125(36)

H(1A)	922(1)	481(1)	363(1)	28
H(1B)	833(1)	351(1)	295(1)	28
H(2A)	784(5)	421(4)	462(3)	28(11)
H(2B)	876(5)	342(4)	439(3)	34(12)
H(3B)	720(1)	127(1)	390(1)	25
H(3A)	741(1)	175(1)	307(1)	25
H(4B)	561(4)	-17(3)	260(2)	12(9)
H(4A)	454(5)	9(3)	316(3)	18(9)
H(5B)	510(4)	-2(3)	107(2)	12(9)
H(5A)	629(4)	117(3)	168(2)	7(8)
H(6A)	543(4)	134(3)	31(2)	16(9)
H(6B)	376(4)	90(3)	38(2)	5(8)
H(7B)	723(4)	292(3)	160(2)	12(9)
H(7A)	697(4)	351(3)	85(2)	14(9)
H(8B)	829(5)	500(3)	215(3)	19(10)
H(8A)	656(5)	496(4)	186(3)	24(10)
H(11)	640(1)	583(1)	310(1)	25
H(13B)	926(5)	650(4)	442(3)	28(11)
H(13A)	923(5)	657(4)	346(3)	22(10)
H(14B)	803(1)	786(1)	453(1)	36
H(21)	579(5)	317(4)	487(3)	20(10)
H(23B)	783(5)	254(3)	541(2)	16(9)
H(23A)	653(4)	128(4)	514(3)	18(10)
H(24B)	698(5)	213(4)	660(3)	21(10)
H(24A)	536(5)	193(4)	615(3)	24(10)
H(31A)	234(4)	-32(3)	218(3)	14(9)
H(33B)	268(5)	-150(4)	64(3)	22(10)
H(33A)	350(5)	-159(4)	157(3)	28(11)
H(34A)	81(6)	-226(4)	177(3)	45(14)
H(34B)	21(7)	-257(5)	78(4)	57(16)
H(41)	297(5)	224(3)	30(3)	17(9)
H(43B)	512(5)	274(4)	-38(3)	22(10)
H(43A)	522(5)	400(4)	-4(3)	28(11)
H(44A)	253(5)	323(4)	-95(3)	34(12)
H(44B)	372(5)	320(4)	-149(3)	30(11)

Crystallographic Data for [Gd.(SSSS-)/(RRRR-)]26.

Table 1. Crystal data and structure refinement for [**Gd.**(*SSSS*-)].

Empirical formula	$C_{28}H_{49}N_4O_{20}Gd$	
Formula weight	918.96	
Temperature	150(2) K	
Wavelength	0.71073 Å	
Crystal system	Triclinic	
Space group	$P_{(-1)}$	
Unit cell dimensions	a = 9.6460(5) Å	α = 102.652(4)°.
	b = 12.6915(7) Å	β = 101.192(4)°.
	c = 16.2000(11) Å	γ = 110.446(3)°.
Volume, Z	1731.9(2) $Å^3$, 2	
Density (calculated)	1.762 Mg/m^3	
Absorption coefficient	2.007 mm^{-1}	
F(000)	938	
Crystal size	0.34 x 0.32 x 0.18 mm	
θ range for data collection	1.35 to 27.50°.	
Limiting indices	$-12 \le h \le 12, -16 \le k \le 16, -13 \le l \le 21$	
Reflections collected	14872	
Independent reflections	7843 [$R_{(int)}$ = 0.0251]	
Absorption correction	Multiscan - SADABS	
Max. and min. transmission	0.610200 and 0.490919	
Refinement method	Full-matrix least-squares on F^2	
Data / restraints / parameters	7843 / 0 / 651	
Goodness-of-fit on F^2	1.046	
Final R indices [I>2σ(I)]	R_1 = 0.0211, wR_2 = 0.0511	
Extinction coefficient	none	
Largest diff. peak and hole	0.656 and -0.714 e.$Å^{-3}$	

Table 2. Atomic coordinates (x 10^5) and equivalent isotropic displacement parameters ($Å^2$ x 10^4) for [**Gd.**(*SSSS*-)]. $U_{(eq)}$ is defined as one third of the trace of the orthogonalized U_{ij} tensor.

	x	y	z	$U_{(eq)}$
Gd(1)	8058(1)	-77649(1)	23351(1)	114(1)
O(5)	30170(2)	-81090(2)	20447(15)	276(4)
O(121)	19910(2)	-94210(2)	43678(11)	281(4)
O(122)	12050(2)	-90916(13)	30974(10)	182(3)

O(151)	23170(3)	-58150(2)	62682(13)	395(5)
O(152)	38020(3)	-63100(2)	72009(14)	483(6)
O(22A)	-16360(5)	-110990(3)	400(2)	191(7)
O(22B)	-21570(6)	-109010(4)	-600(3)	136(10)
O(22C)	-13260(11)	-113260(8)	2430(6)	240(2)
O(222)	-450(2)	-93819(14)	10147(10)	217(3)
O(251)	-58170(2)	-142210(2)	-3151(11)	248(3)
O(252)	-58550(2)	-140760(2)	10729(11)	250(4)
O(321)	14600(2)	-57930(2)	3754(11)	248(4)
O(322)	17530(2)	-66073(14)	14538(10)	164(3)
O(352)	-11320(2)	-88100(2)	-22646(12)	293(4)
O(351)	-26780(2)	-94710(2)	-14537(12)	328(4)
O(421)	42840(2)	-45482(15)	45552(11)	272(4)
O(422)	30280(2)	-63190(13)	35241(10)	164(3)
O(452)	27650(2)	-12380(2)	42371(15)	368(5)
O(451)	46330(3)	-6120(2)	36260(2)	578(7)
N(1)	-50(2)	-75930(2)	38222(11)	142(3)
N(2)	-20070(2)	-94450(2)	20429(12)	167(4)
N(3)	-13900(2)	-75470(2)	11666(12)	160(3)
N(4)	6250(2)	-57080(2)	29230(11)	133(3)
C(1)	-16880(2)	-83730(2)	36067(14)	164(4)
C(2)	-22210(3)	-95710(2)	29143(15)	182(4)
C(3)	-32280(2)	-91120(2)	16048(15)	197(4)
C(4)	-28780(3)	-86310(2)	8540(2)	216(5)
C(5)	-16930(3)	-65070(2)	15829(15)	189(4)
C(6)	-2440(3)	-54380(2)	21848(14)	168(4)
C(7)	-2380(2)	-57690(2)	35937(14)	157(4)
C(8)	2270(3)	-63520(2)	42576(14)	158(4)
C(11)	10240(2)	-79300(2)	44351(14)	149(4)
C(12)	14210(2)	-89080(2)	39316(14)	165(4)
C(13)	4560(3)	-81950(2)	52215(15)	191(4)
C(14)	17510(3)	-78750(2)	60650(2)	246(5)
C(15)	26440(3)	-65590(2)	65120(2)	252(5)
C(21)	-20600(3)	-105780(2)	14866(15)	197(4)
C(22)	-12320(3)	-103220(2)	7910(2)	305(6)
C(23)	-36620(3)	-116140(2)	11010(2)	230(5)
C(24)	-35580(3)	-128180(2)	8820(2)	284(5)
C(25)	-51750(3)	-137860(2)	4840(2)	214(4)
C(31)	-7600(2)	-73910(2)	4035(14)	154(4)
C(32)	9540(2)	-65150(2)	7690(14)	159(4)
C(33)	-17190(3)	-70910(2)	-3063(15)	189(4)
C(34)	-13940(3)	-73610(2)	-11971(15)	200(4)
C(35)	-18260(3)	-86570(2)	-16423(15)	214(4)
C(41)	22640(2)	-47780(2)	32973(14)	159(4)
C(42)	32540(2)	-52630(2)	38317(14)	162(4)
C(43)	24260(3)	-35360(2)	37670(2)	205(4)
C(44)	39050(3)	-25520(2)	37550(2)	308(6)
C(45)	38170(3)	-13630(2)	38660(2)	250(5)
O(1WA)	50100(4)	-41530(3)	81970(2)	303(7)
O(1WB)	46570(7)	-40220(6)	80580(4)	204(13)
O(2WA)	-40050(7)	-66850(5)	35170(5)	304(12)
O(2WB)	-34210(9)	-63030(7)	40710(5)	420(2)
O(2WC)	-40510(6)	-68770(5)	31330(4)	267(11)
O(3WA)	51470(9)	-14210(7)	69220(5)	900(2)
O(3WB)	47970(8)	-17840(6)	57910(4)	760(2)

Table 3. Selected torsion angles for [Gd.(*SSSS*-)].

-61.45 (0.24)	N1 - C1 - C2 - N2
-59.59 (0.26)	N2 - C3 - C4 - N3
-58.06 (0.23)	N3 - C5 - C6 - N4
-58.94 (0.23)	N4 - C7 - C8 - N1
17.49 (0.26)	N1 - C11 - C12 - O122
37.58 (0.33)	N2 - C21 - C22 - O222
39.45 (0.24)	N3 - C31 - C32 - O322
40.61 (0.24)	N4 - C41 - C42 - O422

Table 4. Bond lengths [Å] and angles [deg] for [Gd.(*SSSS*-)].

Gd(1)-O(322)	2.349(2)	Gd(1)-O(222)	2.383(2)
Gd(1)-O(122)	2.385(2)	Gd(1)-O(422)	2.403(2)
Gd(1)-O(5)	2.432(2)	Gd(1)-N(4)	2.655(2)
Gd(1)-N(1)	2.662(2)	Gd(1)-N(2)	2.674(2)
Gd(1)-N(3)	2.689(2)	O(5)-H(5D)	0.75(6)
O(5)-H(5C)	0.68(5)	O(121)-C(12)	1.235(3)
O(122)-C(12)	1.282(3)	O(151)-C(15)	1.213(3)
O(152)-C(15)	1.307(3)	O(152)-H(152)	1.03(7)
O(22A)-O(22C)	0.587(9)	O(22A)-O(22B)	0.645(5)
O(22A)-C(22)	1.275(4)	O(22B)-O(22C)	1.199(11)
O(22B)-C(22)	1.363(6)	O(22C)-C(22)	1.346(9)
O(222)-C(22)	1.250(3)	O(251)-C(25)	1.225(3)
O(252)-C(25)	1.305(3)	O(252)-H(252)	0.86(4)
O(321)-C(32)	1.244(3)	O(322)-C(32)	1.275(3)
O(352)-C(35)	1.330(3)	O(352)-H(352)	0.83(5)
O(351)-C(35)	1.216(3)	O(421)-C(42)	1.280(3)
O(422)-C(42)	1.246(3)	O(452)-C(45)	1.313(3)
O(452)-H(452)	0.98(5)	O(451)-C(45)	1.198(3)
N(1)-C(8)	1.495(3)	N(1)-C(1)	1.497(3)
N(1)-C(11)	1.501(3)	N(2)-C(3)	1.492(3)
N(2)-C(21)	1.498(3)	N(2)-C(2)	1.500(3)
N(3)-C(5)	1.496(3)	N(3)-C(4)	1.498(3)
N(3)-C(31)	1.500(3)	N(4)-C(7)	1.491(3)
N(4)-C(6)	1.497(3)	N(4)-C(41)	1.507(3)
C(1)-C(2)	1.522(3)	C(1)-H(1B)	0.95(3)
C(1)-H(1A)	0.95(2)	C(2)-H(2B)	1.00(3)
C(2)-H(2A)	1.00(3)	C(3)-C(4)	1.520(3)
C(3)-H(3A)	0.94(3)	C(3)-H(3B)	0.95(3)
C(4)-H(4B)	0.93(3)	C(4)-H(4A)	1.00(3)
C(5)-C(6)	1.520(3)	C(5)-H(5B)	0.95(3)
C(5)-H(5A)	1.05(3)	C(6)-H(6B)	0.98(3)
C(6)-H(6A)	0.99(3)	C(7)-C(8)	1.516(3)
C(7)-H(7A)	0.98(2)	C(7)-H(7B)	0.99(3)
C(8)-H(8A)	1.01(3)	C(8)-H(8B)	1.02(3)
C(11)-C(12)	1.538(3)	C(11)-C(13)	1.538(3)
C(11)-H(11)	0.98(3)	C(13)-C(14)	1.527(3)
C(13)-H(13A)	0.99(3)	C(13)-H(13B)	1.02(3)
C(14)-C(15)	1.510(4)	C(14)-H(14A)	1.04(3)
C(14)-H(14B)	0.97(3)	C(21)-C(22)	1.529(3)
C(21)-C(23)	1.534(3)	C(21)-H(21)	0.95(2)
C(23)-C(24)	1.535(3)	C(23)-H(23A)	0.99(3)
C(23)-H(23B)	0.98(3)	C(24)-C(25)	1.511(3)

C(24)-H(24A)	0.97(2)	C(24)-H(24B)	0.98(3)
C(31)-C(33)	1.532(3)	C(31)-C(32)	1.539(3)
C(31)-H(31)	0.97(3)	C(33)-C(34)	1.528(3)
C(33)-H(33B)	0.95(3)	C(33)-H(33A)	0.94(3)
C(34)-C(35)	1.512(3)	C(34)-H(34A)	0.95(3)
C(34)-H(34B)	0.93(3)	C(41)-C(43)	1.531(3)
C(41)-C(42)	1.538(3)	C(41)-H(41)	0.99(3)
C(43)-C(44)	1.540(3)	C(43)-H(43B)	1.02(3)
C(43)-H(43A)	0.99(3)	C(44)-C(45)	1.515(3)
C(44)-H(42B)	1.01(4)	C(44)-H(42A)	0.92(4)
O(2WA)-O(2WC)	0.604(6)	O(2WA)-O(2WB)	0.883(8)
O(2WB)-O(2WC)	1.434(9)	O(3WA)-O(3WB)	1.722(9)

O(322)-Gd(1)-O(222)	84.22(5)	O(322)-Gd(1)-O(122)	144.86(5)
O(222)-Gd(1)-O(122)	85.82(6)	O(322)-Gd(1)-O(422)	85.68(5)
O(222)-Gd(1)-O(422)	144.47(5)	O(122)-Gd(1)-O(422)	83.14(5)
O(322)-Gd(1)-O(5)	72.57(6)	O(222)-Gd(1)-O(5)	70.33(7)
O(122)-Gd(1)-O(5)	72.34(6)	O(422)-Gd(1)-O(5)	74.14(6)
O(322)-Gd(1)-N(4)	72.59(5)	O(222)-Gd(1)-N(4)	140.73(6)
O(122)-Gd(1)-N(4)	130.66(5)	O(422)-Gd(1)-N(4)	66.02(5)
O(5)-Gd(1)-N(4)	128.11(6)	O(322)-Gd(1)-N(1)	140.92(5)
O(222)-Gd(1)-N(1)	131.61(5)	O(122)-Gd(1)-N(1)	65.28(5)
O(422)-Gd(1)-N(1)	72.43(5)	O(5)-Gd(1)-N(1)	128.11(6)
N(4)-Gd(1)-N(1)	69.03(5)	O(322)-Gd(1)-N(2)	130.09(5)
O(222)-Gd(1)-N(2)	65.47(5)	O(122)-Gd(1)-N(2)	74.17(6)
O(422)-Gd(1)-N(2)	141.16(5)	O(5)-Gd(1)-N(2)	125.48(6)
N(4)-Gd(1)-N(2)	106.36(5)	N(1)-Gd(1)-N(2)	69.56(5)
O(322)-Gd(1)-N(3)	65.51(5)	O(222)-Gd(1)-N(3)	72.95(6)
O(122)-Gd(1)-N(3)	141.63(5)	O(422)-Gd(1)-N(3)	131.78(5)
O(5)-Gd(1)-N(3)	125.97(6)	N(4)-Gd(1)-N(3)	68.72(5)
N(1)-Gd(1)-N(3)	105.89(5)	N(2)-Gd(1)-N(3)	68.03(5)
Gd(1)-O(5)-H(5D)	122(4)	Gd(1)-O(5)-H(5C)	118(4)
H(5D)-O(5)-H(5C)	102(5)	C(12)-O(122)-Gd(1)	124.52(13)
C(15)-O(152)-H(152)	107(4)	O(22C)-O(22A)-O(22B)	153.7(13)
O(22C)-O(22A)-C(22)	83.9(10)	O(22B)-O(22A)-C(22)	83.6(6)
O(22A)-O(22B)-O(22C)	12.5(6)	O(22A)-O(22B)-C(22)	68.4(6)
O(22C)-O(22B)-C(22)	63.0(5)	O(22A)-O(22C)-O(22B)	13.8(7)
O(22A)-O(22C)-C(22)	70.4(10)	O(22B)-O(22C)-C(22)	64.5(5)
C(22)-O(222)-Gd(1)	125.88(14)	C(25)-O(252)-H(252)	115(2)
C(32)-O(322)-Gd(1)	126.64(13)	C(35)-O(352)-H(352)	110(3)
C(42)-O(422)-Gd(1)	124.31(13)	C(45)-O(452)-H(452)	113(3)
C(8)-N(1)-C(1)	107.9(2)	C(8)-N(1)-C(11)	108.7(2)
C(1)-N(1)-C(11)	112.8(2)	C(8)-N(1)-Gd(1)	110.87(12)
C(1)-N(1)-Gd(1)	109.20(12)	C(11)-N(1)-Gd(1)	107.41(11)
C(3)-N(2)-C(21)	112.2(2)	C(3)-N(2)-C(2)	108.8(2)
C(21)-N(2)-C(2)	109.5(2)	C(3)-N(2)-Gd(1)	110.29(12)
C(21)-N(2)-Gd(1)	107.13(12)	C(2)-N(2)-Gd(1)	108.81(12)
C(5)-N(3)-C(4)	108.4(2)	C(5)-N(3)-C(31)	111.8(2)
C(4)-N(3)-C(31)	109.8(2)	C(5)-N(3)-Gd(1)	110.20(12)
C(4)-N(3)-Gd(1)	111.33(13)	C(31)-N(3)-Gd(1)	105.36(12)
C(7)-N(4)-C(6)	107.5(2)	C(7)-N(4)-C(41)	112.7(2)
C(6)-N(4)-C(41)	109.7(2)	C(7)-N(4)-Gd(1)	109.45(12)
C(6)-N(4)-Gd(1)	110.83(12)	C(41)-N(4)-Gd(1)	106.69(11)
N(1)-C(1)-C(2)	114.5(2)	N(1)-C(1)-H(1B)	106(2)
C(2)-C(1)-H(1B)	110(2)	N(1)-C(1)-H(1A)	111(2)
C(2)-C(1)-H(1A)	109(2)	H(1B)-C(1)-H(1A)	106(2)
N(2)-C(2)-C(1)	111.8(2)	N(2)-C(2)-H(2B)	109(2)
C(1)-C(2)-H(2B)	108(2)	N(2)-C(2)-H(2A)	110.9(14)

C(1)-C(2)-H(2A)	107(2)	H(2B)-C(2)-H(2A)	110(2)
N(2)-C(3)-C(4)	113.4(2)	N(2)-C(3)-H(3A)	110(2)
C(4)-C(3)-H(3A)	110(2)	N(2)-C(3)-H(3B)	108(2)
C(4)-C(3)-H(3B)	109(2)	H(3A)-C(3)-H(3B)	106(2)
N(3)-C(4)-C(3)	111.8(2)	N(3)-C(4)-H(4B)	109(2)
C(3)-C(4)-H(4B)	112(2)	N(3)-C(4)-H(4A)	110(2)
C(3)-C(4)-H(4A)	109.3(14)	H(4B)-C(4)-H(4A)	105(2)
N(3)-C(5)-C(6)	114.0(2)	N(3)-C(5)-H(5B)	112(2)
C(6)-C(5)-H(5B)	107(2)	N(3)-C(5)-H(5A)	109(2)
C(6)-C(5)-H(5A)	111(2)	H(5B)-C(5)-H(5A)	103(2)
N(4)-C(6)-C(5)	112.7(2)	N(4)-C(6)-H(6B)	112(2)
C(5)-C(6)-H(6B)	107(2)	N(4)-C(6)-H(6A)	107(2)
C(5)-C(6)-H(6A)	112(2)	H(6B)-C(6)-H(6A)	106(2)
N(4)-C(7)-C(8)	114.1(2)	N(4)-C(7)-H(7A)	107.7(14)
C(8)-C(7)-H(7A)	108.3(14)	N(4)-C(7)-H(7B)	113(2)
C(8)-C(7)-H(7B)	110(2)	H(7A)-C(7)-H(7B)	103(2)
N(1)-C(8)-C(7)	112.3(2)	N(1)-C(8)-H(8A)	110(2)
C(7)-C(8)-H(8A)	110(2)	N(1)-C(8)-H(8B)	110(2)
C(7)-C(8)-H(8B)	107(2)	H(8A)-C(8)-H(8B)	108(2)
N(1)-C(11)-C(12)	112.0(2)	N(1)-C(11)-C(13)	114.4(2)
C(12)-C(11)-C(13)	112.9(2)	N(1)-C(11)-H(11)	105(2)
C(12)-C(11)-H(11)	104.0(14)	C(13)-C(11)-H(11)	107.8(14)
O(121)-C(12)-O(122)	124.8(2)	O(121)-C(12)-C(11)	117.5(2)
O(122)-C(12)-C(11)	117.5(2)	C(14)-C(13)-C(11)	114.3(2)
C(14)-C(13)-H(13A)	107(2)	C(11)-C(13)-H(13A)	109(2)
C(14)-C(13)-H(13B)	109(2)	C(11)-C(13)-H(13B)	110(2)
H(13A)-C(13)-H(13B)	107(2)	C(15)-C(14)-C(13)	113.7(2)
C(15)-C(14)-H(14A)	110(2)	C(13)-C(14)-H(14A)	110(2)
C(15)-C(14)-H(14B)	108(2)	C(13)-C(14)-H(14B)	109(2)
H(14A)-C(14)-H(14B)	105(3)	O(151)-C(15)-O(152)	123.6(3)
O(151)-C(15)-C(14)	124.0(2)	O(152)-C(15)-C(14)	112.4(2)
N(2)-C(21)-C(22)	109.2(2)	N(2)-C(21)-C(23)	115.8(2)
C(22)-C(21)-C(23)	113.5(2)	N(2)-C(21)-H(21)	105.3(14)
C(22)-C(21)-H(21)	105.5(13)	C(23)-C(21)-H(21)	106.6(14)
O(222)-C(22)-O(22A)	120.6(2)	O(222)-C(22)-O(22C)	120.8(4)
O(22A)-C(22)-O(22C)	25.7(4)	O(222)-C(22)-O(22B)	123.6(3)
O(22A)-C(22)-O(22B)	28.0(2)	O(22C)-C(22)-O(22B)	52.6(5)
O(222)-C(22)-C(21)	117.9(2)	O(22A)-C(22)-C(21)	121.1(2)
O(22C)-C(22)-C(21)	111.3(4)	O(22B)-C(22)-C(21)	113.9(3)
C(21)-C(23)-C(24)	112.2(2)	C(21)-C(23)-H(23A)	111(2)
C(24)-C(23)-H(23A)	110(2)	C(21)-C(23)-H(23B)	107(2)
C(24)-C(23)-H(23B)	108(2)	H(23A)-C(23)-H(23B)	108(3)
C(25)-C(24)-C(23)	108.9(2)	C(25)-C(24)-H(24A)	109.0(14)
C(23)-C(24)-H(24A)	113.4(14)	C(25)-C(24)-H(24B)	108(2)
C(23)-C(24)-H(24B)	113(2)	H(24A)-C(24)-H(24B)	104(2)
O(251)-C(25)-O(252)	123.0(2)	O(251)-C(25)-C(24)	123.3(2)
O(252)-C(25)-C(24)	113.6(2)	N(3)-C(31)-C(33)	115.4(2)
N(3)-C(31)-C(32)	108.8(2)	C(33)-C(31)-C(32)	113.5(2)
N(3)-C(31)-H(31)	105(2)	C(33)-C(31)-H(31)	107(2)
C(32)-C(31)-H(31)	106(2)	O(321)-C(32)-O(322)	125.2(2)
O(321)-C(32)-C(31)	118.5(2)	O(322)-C(32)-C(31)	116.3(2)
C(34)-C(33)-C(31)	113.4(2)	C(34)-C(33)-H(33B)	108(2)
C(31)-C(33)-H(33B)	110(2)	C(34)-C(33)-H(33A)	108(2)
C(31)-C(33)-H(33A)	106(2)	H(33B)-C(33)-H(33A)	111(2)
C(35)-C(34)-C(33)	114.5(2)	C(35)-C(34)-H(34A)	105(2)
C(33)-C(34)-H(34A)	111(2)	C(35)-C(34)-H(34B)	107(2)
C(33)-C(34)-H(34B)	112(2)	H(34A)-C(34)-H(34B)	107(3)
O(351)-C(35)-O(352)	123.3(2)	O(351)-C(35)-C(34)	125.0(2)

O(352)-C(35)-C(34)	111.7(2)		N(4)-C(41)-C(43)	115.0(2)
N(4)-C(41)-C(42)	108.5(2)		C(43)-C(41)-C(42)	115.6(2)
N(4)-C(41)-H(41)	109(2)		C(43)-C(41)-H(41)	103(2)
C(42)-C(41)-H(41)	105(2)		O(422)-C(42)-O(421)	124.1(2)
O(422)-C(42)-C(41)	118.1(2)		O(421)-C(42)-C(41)	117.8(2)
C(41)-C(43)-C(44)	112.8(2)		C(41)-C(43)-H(43B)	108(2)
C(44)-C(43)-H(43B)	107(2)		C(41)-C(43)-H(43A)	109(2)
C(44)-C(43)-H(43A)	112(2)		H(43B)-C(43)-H(43A)	107(2)
C(45)-C(44)-C(43)	114.1(2)		C(45)-C(44)-H(42B)	107(2)
C(43)-C(44)-H(42B)	111(2)		C(45)-C(44)-H(42A)	109(2)
C(43)-C(44)-H(42A)	112(3)		H(42B)-C(44)-H(42A)	102(3)
O(451)-C(45)-O(452)	123.5(2)		O(451)-C(45)-C(44)	122.4(2)
O(452)-C(45)-C(44)	114.2(2)			
O(2WC)-O(2WA)-O(2WB)		148.9(12)		
O(2WA)-O(2WB)-O(2WC)		12.6(5)		
O(2WA)-O(2WC)-O(2WB)		18.6(8)		

Table 5. Anisotropic displacement parameters ($Å^2 \times 10^4$) for [**Gd**.(*SSSS*-)]. The anisotropic displacement factor exponent takes the form: $-2\pi^2 [h^2.a^{*2}.U_{11} + ... + 2hk.a^*.b^*.U_{12}]$

	U_{11}	U_{22}	U_{33}	U_{23}	U_{13}	U_{12}
Gd(1)	114(1)	98(1)	121(1)	20(1)	47(1)	35(1)
O(5)	239(9)	177(9)	449(12)	69(8)	188(9)	100(8)
O(121)	444(11)	281(9)	265(9)	131(7)	141(8)	269(9)
O(122)	248(8)	150(7)	176(7)	46(6)	92(6)	102(6)
O(151)	523(12)	254(10)	332(10)	47(8)	-47(9)	193(9)
O(152)	516(13)	444(14)	347(11)	-59(10)	-149(10)	289(11)
O(222)	213(8)	160(8)	212(8)	-3(6)	121(7)	8(6)
O(251)	243(8)	248(9)	241(9)	70(7)	58(7)	97(7)
O(252)	202(8)	250(9)	207(8)	32(7)	35(7)	29(7)
O(321)	206(8)	248(9)	238(8)	133(7)	38(7)	14(7)
O(322)	134(7)	184(8)	166(7)	62(6)	48(6)	48(6)
O(352)	336(10)	227(10)	307(10)	21(8)	138(8)	121(8)
O(351)	390(10)	229(9)	314(10)	83(8)	130(8)	56(8)
O(421)	266(9)	159(8)	248(9)	-8(7)	-86(7)	55(7)
O(422)	141(7)	126(7)	211(8)	39(6)	30(6)	58(6)
O(452)	482(12)	235(10)	582(13)	194(9)	341(10)	231(9)
O(451)	580(15)	311(12)	1140(2)	387(13)	600(2)	236(11)
N(1)	166(8)	120(8)	142(8)	31(7)	50(7)	66(7)
N(2)	168(8)	151(9)	151(8)	22(7)	69(7)	34(7)
N(3)	121(8)	180(9)	152(8)	42(7)	53(7)	31(7)
N(4)	122(8)	127(8)	146(8)	39(7)	29(6)	55(7)
C(1)	150(10)	178(10)	165(10)	44(8)	73(8)	59(8)
C(2)	180(10)	156(10)	186(10)	50(8)	89(8)	27(8)
C(3)	125(10)	215(11)	197(11)	52(9)	47(8)	15(8)
C(4)	136(10)	248(12)	174(11)	45(9)	25(8)	2(9)
C(5)	162(10)	250(12)	169(10)	58(9)	39(8)	110(9)
C(6)	201(10)	181(11)	163(10)	71(8)	65(8)	109(9)
C(7)	181(10)	139(10)	164(10)	28(8)	64(8)	85(8)
C(8)	201(10)	132(10)	140(10)	19(8)	53(8)	81(8)

C(11)	181(10)	144(10)	145(9)	51(8)	58(8)	84(8)
C(12)	167(10)	109(9)	224(11)	51(8)	79(8)	50(8)
C(13)	235(11)	188(11)	186(10)	83(9)	98(9)	95(9)
C(14)	356(13)	265(13)	188(11)	105(10)	85(10)	182(11)
C(15)	329(13)	299(13)	176(11)	61(9)	77(10)	190(11)
C(21)	189(10)	145(10)	206(11)	11(8)	95(9)	16(8)
C(22)	366(14)	192(12)	263(12)	-19(10)	205(11)	2(10)
C(23)	165(10)	168(11)	281(12)	39(9)	67(9)	0(9)
C(24)	197(11)	197(12)	368(14)	15(10)	70(11)	28(9)
C(25)	201(11)	165(11)	270(12)	43(9)	64(9)	85(9)
C(31)	144(9)	167(10)	136(9)	44(8)	43(8)	45(8)
C(32)	152(9)	151(10)	161(10)	35(8)	55(8)	51(8)
C(33)	186(10)	199(11)	171(10)	52(9)	39(8)	76(9)
C(34)	235(11)	195(11)	164(10)	67(9)	52(9)	77(9)
C(35)	225(11)	223(12)	166(10)	62(9)	11(9)	83(9)
C(41)	137(9)	125(10)	196(10)	40(8)	28(8)	51(8)
C(42)	132(9)	150(10)	189(10)	46(8)	33(8)	51(8)
C(43)	206(11)	121(10)	280(12)	31(9)	83(9)	69(8)
C(44)	237(12)	152(12)	550(2)	84(11)	185(12)	70(10)
C(45)	227(11)	190(11)	303(13)	53(10)	95(10)	56(9)

Table 6. Hydrogen coordinates (x 10^3) and isotropic displacement parameters ($Å^2$ x 10^3) for [Gd.(*SSSS*-)].

	x	y	z	$U_{(eq)}$
H(5D)	381(6)	-779(5)	237(3)	85(18)
H(5C)	295(6)	-868(5)	192(3)	78(17)
H(152)	426(8)	-541(6)	750(4)	144(24)
H(252)	-676(5)	-1465(4)	86(2)	54(11)
H(352)	-134(5)	-952(4)	-248(3)	76(14)
H(452)	253(6)	-56(5)	417(3)	101(17)
H(1B)	-223(3)	-794(2)	341(2)	18(6)
H(1A)	-195(3)	-850(2)	412(2)	14(6)
H(2B)	-159(3)	-999(3)	313(2)	23(7)
H(2A)	-334(3)	-1002(2)	285(2)	14(6)
H(3A)	-419(3)	-976(3)	140(2)	20(7)
H(3B)	-331(3)	-853(2)	204(2)	14(6)
H(4B)	-283(3)	-919(3)	40(2)	30(8)
H(4A)	-375(3)	-845(2)	58(2)	17(6)
H(5B)	-219(3)	-625(3)	116(2)	24(7)
H(5A)	-251(3)	-677(3)	192(2)	22(7)
H(6B)	-58(3)	-481(2)	241(2)	17(6)
H(6A)	49(3)	-512(2)	186(2)	18(6)
H(7A)	-134(3)	-623(2)	328(2)	9(5)
H(7B)	-19(3)	-499(3)	391(2)	20(7)
H(8A)	135(3)	-586(3)	463(2)	22(7)
H(8B)	-44(3)	-635(3)	467(2)	22(7)
H(11)	201(3)	-723(2)	467(2)	14(6)
H(13A)	-16(3)	-774(3)	537(2)	29(7)
H(13B)	-26(3)	-907(3)	505(2)	25(7)
H(14A)	251(4)	-826(3)	593(2)	37(8)

H(14B)	131(4)	-822(3)	648(2)	35(8)
H(21)	-144(3)	-1081(2)	187(2)	4(5)
H(23A)	-428(4)	-1155(3)	57(2)	33(8)
H(23B)	-420(4)	-1158(3)	155(2)	38(8)
H(24A)	-303(3)	-1296(2)	139(2)	3(5)
H(24B)	-296(4)	-1291(3)	46(2)	43(9)
H(31)	-77(3)	-815(3)	13(2)	21(7)
H(33B)	-152(3)	-627(3)	-12(2)	17(6)
H(33A)	-277(4)	-757(3)	-39(2)	29(7)
H(34A)	-197(4)	-712(3)	-161(2)	30(8)
H(34B)	-36(3)	-696(3)	-115(2)	22(7)
H(41)	271(3)	-466(3)	281(2)	24(7)
H(43B)	150(3)	-342(2)	344(2)	20(7)
H(43A)	236(4)	-350(3)	438(2)	34(8)
H(42B)	484(5)	-243(4)	424(3)	59(11)
H(42A)	418(4)	-276(4)	325(3)	56(11)

Crystallographic Data for [Tb.(SSSS-)/(RRRR-)]26.

Identification code	98srv123	
Empirical formula	$(C28\ H42\ N4\ O20\ Tb)^{-}.(H30)^{+}.2(H20)$	
Formula weight	920.63	
Temperature	150(2) K	
Wavelength	0.71073 Å	
Crystal system	Triclinic	
Space group	P-1	
Unit cell dimensions	a = 9.62890(10) Å	α= 102.7389(8)°.
	b = 12.6877(2) Å	β= 101.2348(9)°.
	c = 16.2170(2) Å	γ = 110.5812(4)°.
Volume	1726.76(4) $Å^3$	
Z	2	
Density (calculated)	1.771 g/cm^3	
Absorption coefficient	2.141 mm^{-1}	
Absorption correction	Semi-empirical - Sadabs	
Max. and min. transmission	0.677155 and 0.419893	
F(000)	940	
Crystal size	0.10 x 0.20 x 0.25 mm^3	
Experimental device	Siemens SMART-CCD	
Experimental methods	ω scans	
θ range for data collection	1.35 to 27.53°.	
Index ranges	-11<=h<=12, -16<=k<=16, -21<=l<=20	
Reflections collected	Total	13969
	Observed	6646 [I > 2σ(I)]
	Unique	7856
	Calculation of cell	481
Independent reflections	7856 [R(int) = 0.0381]	
Completeness to θ = 27.53°	98.5 %	
Refinement method	Full-matrix least-squares on F^2	
Data / restraints / parameters	7856 / 0 / 610	
Goodness-of-fit on F^2	1.085	
Final R indices [I>2σ(I)]	R1 = 0.0442, wR2 = 0.1057	
R indices (all data)	R1 = 0.0601, wR2 = 0.1177	
Largest diff. peak and hole	2.683 and -2.362 $e.Å^{-3}$	

Table 2. Atomic coordinates (x 10^4) and equivalent isotropic displacement parameters ($Å^2$x 10^3) for 98srv123. U(eq) is defined as one third of the trace of the orthogonalized U^{ij} tensor.

	x	y	z	U(eq)
Tb(1)	795(1)	-7763(1)	2339(1)	16(1)
O(5)	3017(5)	-8097(4)	2060(3)	32(1)
O(121)	1981(5)	-9419(4)	4361(3)	31(1)
O(122)	1200(4)	-9082(3)	3090(2)	22(1)
O(151)	2335(6)	-5805(4)	6262(3)	43(1)
O(152)	3797(7)	-6313(5)	7196(3)	56(2)
O(22A)	-1634(11)	-11104(7)	37(5)	21(2)
O(22B)	-2130(16)	-10915(11)	-49(8)	20(3)
O(22C)	-1310(20)	-11349(16)	269(12)	19(4)
O(222)	-36(4)	-9377(3)	1027(2)	25(1)
O(251)	-5832(5)	-14229(4)	-315(3)	31(1)
O(252)	-5846(5)	-14073(4)	1073(2)	28(1)
O(321)	1463(4)	-5803(3)	382(2)	27(1)
O(322)	1746(4)	-6615(3)	1465(2)	20(1)
O(352)	-1141(5)	-8818(4)	-2266(3)	32(1)
O(351)	-2684(5)	-9483(4)	-1460(3)	36(1)
O(421)	4283(5)	-4547(3)	4560(3)	31(1)
O(422)	3010(4)	-6323(3)	3524(2)	19(1)
O(451)	4625(7)	-607(4)	3621(5)	63(2)
O(452)	2777(6)	-1231(4)	4249(4)	44(1)
N(1)	-17(5)	-7595(3)	3820(3)	17(1)
N(2)	-2013(5)	-9452(4)	2044(3)	21(1)
N(3)	-1403(5)	-7554(4)	1166(3)	19(1)
N(4)	609(5)	-5714(3)	2922(3)	15(1)
C(1)	-1700(6)	-8374(4)	3604(3)	20(1)
C(2)	-2239(6)	-9573(4)	2918(3)	21(1)
C(3)	-3233(6)	-9127(5)	1600(4)	24(1)
C(4)	-2904(6)	-8642(5)	852(4)	25(1)
C(5)	-1710(6)	-6522(5)	1582(3)	24(1)
C(6)	-255(6)	-5446(4)	2178(3)	19(1)
C(7)	-247(6)	-5768(4)	3590(3)	19(1)

C(8)	206(6)	-6345(4)	4252(3)	21(1)
C(11)	1026(6)	-7922(4)	4438(3)	18(1)
C(12)	1413(6)	-8896(4)	3932(3)	20(1)
C(13)	447(6)	-8186(5)	5226(3)	22(1)
C(14)	1748(7)	-7873(5)	6062(4)	26(1)
C(15)	2653(7)	-6556(5)	6508(4)	30(1)
C(21)	-2067(7)	-10584(4)	1487(4)	26(1)
C(22)	-1232(7)	-10316(5)	799(4)	34(1)
C(23)	-3652(7)	-11620(5)	1098(4)	29(1)
C(24)	-3555(7)	-12824(5)	887(5)	34(1)
C(25)	-5179(7)	-13794(5)	488(4)	28(1)
C(31)	-762(6)	-7399(4)	411(3)	20(1)
C(32)	956(6)	-6523(4)	775(3)	20(1)
C(33)	-1724(7)	-7099(5)	-308(3)	22(1)
C(34)	-1399(7)	-7370(5)	-1199(3)	23(1)
C(35)	-1834(6)	-8670(5)	-1641(3)	23(1)
C(41)	2251(6)	-4775(4)	3300(3)	20(1)
C(42)	3238(6)	-5266(4)	3835(3)	20(1)
C(43)	2408(6)	-3537(4)	3764(4)	24(1)
C(44)	3904(7)	-2550(5)	3760(5)	34(1)
C(45)	3823(7)	-1346(5)	3870(4)	30(1)
O(1WA)	5015(10)	-4154(7)	8200(5)	33(2)
O(1WB)	4690(17)	-4024(12)	8075(9)	28(3)
O(2WA)	-4004(14)	-6656(11)	3559(10)	39(3)
O(2WB)	-3420(30)	-6280(20)	4075(16)	46(5)
O(2WC)	-4072(16)	-6864(12)	3173(10)	32(3)
O(3WA)	5130(20)	-1426(18)	6927(13)	120(6)
O(3WB)	4800(20)	-1782(16)	5790(12)	108(5)

Table 3. Bond lengths [Å] and angles [°] for 98srv123

Tb(1)-O(322)	2.335(3)	O(452)-C(45)	1.312(7)
Tb(1)-O(122)	2.368(4)	O(452)-H(452)	0.68(9)
Tb(1)-O(222)	2.371(3)	N(1)-C(1)	1.492(6)
Tb(1)-O(422)	2.386(3)	N(1)-C(8)	1.505(6)
Tb(1)-O(5)	2.427(4)	N(1)-C(11)	1.507(6)
Tb(1)-N(4)	2.644(4)	N(2)-C(3)	1.487(7)
Tb(1)-N(1)	2.654(4)	N(2)-C(21)	1.495(6)
Tb(1)-N(2)	2.665(4)	N(2)-C(2)	1.508(6)
Tb(1)-N(3)	2.686(4)	N(3)-C(5)	1.490(7)
O(5)-H(5D)	0.64(9)	N(3)-C(31)	1.496(6)
O(5)-H(5C)	0.61(8)	N(3)-C(4)	1.501(6)
O(121)-C(12)	1.238(6)	N(4)-C(7)	1.483(6)
O(122)-C(12)	1.296(6)	N(4)-C(6)	1.500(6)
O(151)-C(15)	1.218(7)	N(4)-C(41)	1.507(6)
O(152)-C(15)	1.298(7)	C(1)-C(2)	1.516(7)
O(152)-H(152)	0.94(10)	C(1)-H(1A)	1.03(6)
O(22A)-O(22B)	0.611(12)	C(1)-H(1B)	0.90(6)
O(22A)-O(22C)	0.638(18)	C(2)-H(2A)	1.05(6)
O(22A)-C(22)	1.292(9)	C(2)-H(2B)	1.05(6)
O(22B)-O(22C)	1.21(2)	C(3)-C(4)	1.515(8)
O(22B)-C(22)	1.353(14)	C(3)-H(3A)	0.99(7)
O(22C)-C(22)	1.366(18)	C(3)-H(3B)	0.84(7)
O(222)-C(22)	1.249(7)	C(4)-H(4A)	0.75(7)
O(251)-C(25)	1.231(7)	C(4)-H(4B)	0.98(7)
O(252)-C(25)	1.289(7)	C(5)-C(6)	1.518(7)
O(252)-H(252)	0.92(8)	C(5)-H(5A)	0.85(7)
O(321)-C(32)	1.242(6)	C(5)-H(5B)	1.08(6)
O(322)-C(32)	1.276(6)	C(6)-H(6A)	0.91(6)
O(352)-C(35)	1.331(7)	C(6)-H(6B)	0.98(6)
O(352)-H(352)	0.71(8)	C(7)-C(8)	1.506(7)
O(351)-C(35)	1.207(7)	C(7)-H(7A)	0.98(6)
O(421)-C(42)	1.284(6)	C(7)-H(7B)	0.97(6)
O(422)-C(42)	1.247(6)	C(8)-H(8A)	1.07(6)
O(451)-C(45)	1.191(7)	C(8)-H(8B)	0.98(6)

C(11)-C(12)	1.529(6)	C(45)-H(452)	1.50(10)
C(11)-C(13)	1.546(7)	O(2WA)-O(2WC)	0.604(15)
C(11)-H(11)	1.04(6)	O(2WA)-O(2WB)	0.83(2)
C(13)-C(14)	1.522(7)	O(2WB)-O(2WC)	1.39(3)
C(13)-H(13A)	0.98(6)	O(3WA)-O(3WB)	1.73(3)
C(13)-H(13B)	1.09(6)		
C(14)-C(15)	1.507(8)	O(322)-Tb(1)-O(122)	144.33(12)
C(14)-H(14A)	1.09(7)	O(322)-Tb(1)-O(222)	84.08(12)
C(14)-H(14B)	1.00(7)	O(122)-Tb(1)-O(222)	85.38(13)
C(21)-C(23)	1.518(7)	O(322)-Tb(1)-O(422)	85.78(12)
C(21)-C(22)	1.527(7)	O(122)-Tb(1)-O(422)	83.04(12)
C(21)-H(21)	1.01(7)	O(222)-Tb(1)-O(422)	144.00(12)
C(23)-C(24)	1.531(8)	O(322)-Tb(1)-O(5)	72.46(14)
C(23)-H(23A)	1.14(7)	O(122)-Tb(1)-O(5)	71.91(14)
C(23)-H(23B)	1.02(7)	O(222)-Tb(1)-O(5)	70.16(14)
C(24)-C(25)	1.510(8)	O(422)-Tb(1)-O(5)	73.84(14)
C(24)-H(24A)	0.97(8)	O(322)-Tb(1)-N(4)	72.76(12)
C(24)-H(24B)	1.02(8)	O(122)-Tb(1)-N(4)	131.03(12)
C(31)-C(32)	1.536(7)	O(222)-Tb(1)-N(4)	140.94(13)
C(31)-C(33)	1.545(7)	O(422)-Tb(1)-N(4)	66.25(12)
C(31)-H(31)	0.77(6)	O(5)-Tb(1)-N(4)	128.06(13)
C(33)-C(34)	1.528(7)	O(322)-Tb(1)-N(1)	141.17(12)
C(33)-H(33A)	0.93(7)	O(122)-Tb(1)-N(1)	65.54(12)
C(33)-H(33B)	0.95(7)	O(222)-Tb(1)-N(1)	131.71(12)
C(34)-C(35)	1.511(7)	O(422)-Tb(1)-N(1)	72.40(12)
C(34)-H(34A)	0.91(7)	O(5)-Tb(1)-N(1)	127.81(15)
C(34)-H(34B)	0.90(7)	N(4)-Tb(1)-N(1)	69.15(12)
C(41)-C(43)	1.524(7)	O(322)-Tb(1)-N(2)	130.28(12)
C(41)-C(42)	1.542(7)	O(122)-Tb(1)-N(2)	74.10(13)
C(41)-H(41)	0.99(6)	O(222)-Tb(1)-N(2)	65.65(12)
C(43)-C(44)	1.543(8)	O(422)-Tb(1)-N(2)	141.07(12)
C(43)-H(43A)	1.06(6)	O(5)-Tb(1)-N(2)	125.39(14)
C(43)-H(43B)	1.05(6)	N(4)-Tb(1)-N(2)	106.51(13)
C(44)-C(45)	1.530(8)	N(1)-Tb(1)-N(2)	69.57(12)
C(44)-H(44A)	0.98(8)	O(322)-Tb(1)-N(3)	65.60(12)
C(44)-H(44B)	0.92(8)	O(122)-Tb(1)-N(3)	141.70(13)

O(222)-Tb(1)-N(3)	73.21(13)	C(21)-N(2)-Tb(1)	107.4(3)
O(422)-Tb(1)-N(3)	131.99(12)	C(2)-N(2)-Tb(1)	109.0(3)
O(5)-Tb(1)-N(3)	126.09(15)	C(5)-N(3)-C(31)	112.2(4)
N(4)-Tb(1)-N(3)	68.71(12)	C(5)-N(3)-C(4)	108.0(4)
N(1)-Tb(1)-N(3)	106.07(13)	C(31)-N(3)-C(4)	110.1(4)
N(2)-Tb(1)-N(3)	68.24(13)	C(5)-N(3)-Tb(1)	110.0(3)
Tb(1)-O(5)-H(5D)	117(8)	C(31)-N(3)-Tb(1)	105.0(3)
Tb(1)-O(5)-H(5C)	129(8)	C(4)-N(3)-Tb(1)	111.5(3)
H(5D)-O(5)-H(5C)	103(10)	C(7)-N(4)-C(6)	107.8(4)
C(12)-O(122)-Tb(1)	124.2(3)	C(7)-N(4)-C(41)	112.3(4)
C(15)-O(152)-H(152)	111(6)	C(6)-N(4)-C(41)	109.3(4)
O(22B)-O(22A)-O(22C)	150(3)	C(7)-N(4)-Tb(1)	109.7(3)
O(22B)-O(22A)-C(22)	82.2(15)	C(6)-N(4)-Tb(1)	110.8(3)
O(22C)-O(22A)-C(22)	82.7(19)	C(41)-N(4)-Tb(1)	106.9(3)
O(22A)-O(22B)-O(22C)	15.2(14)	N(1)-C(1)-C(2)	114.5(4)
O(22A)-O(22B)-C(22)	71.2(15)	N(1)-C(1)-H(1A)	107(3)
O(22C)-O(22B)-C(22)	64.2(10)	C(2)-C(1)-H(1A)	107(3)
O(22A)-O(22C)-O(22B)	14.5(14)	N(1)-C(1)-H(1B)	110(4)
O(22A)-O(22C)-C(22)	69.7(18)	C(2)-C(1)-H(1B)	108(4)
O(22B)-O(22C)-C(22)	63.0(10)	H(1A)-C(1)-H(1B)	111(5)
C(22)-O(222)-Tb(1)	125.6(3)	N(2)-C(2)-C(1)	111.6(4)
C(25)-O(252)-H(252)	106(4)	N(2)-C(2)-H(2A)	106(3)
C(32)-O(322)-Tb(1)	127.0(3)	C(1)-C(2)-H(2A)	111(3)
C(35)-O(352)-H(352)	116(7)	N(2)-C(2)-H(2B)	106(3)
C(42)-O(422)-Tb(1)	124.3(3)	C(1)-C(2)-H(2B)	107(3)
C(45)-O(452)-H(452)	92(8)	H(2A)-C(2)-H(2B)	115(5)
C(1)-N(1)-C(8)	107.4(4)	N(2)-C(3)-C(4)	114.6(4)
C(1)-N(1)-C(11)	113.2(4)	N(2)-C(3)-H(3A)	111(4)
C(8)-N(1)-C(11)	108.9(4)	C(4)-C(3)-H(3A)	112(4)
C(1)-N(1)-Tb(1)	109.4(3)	N(2)-C(3)-H(3B)	107(4)
C(8)-N(1)-Tb(1)	110.7(3)	C(4)-C(3)-H(3B)	109(4)
C(11)-N(1)-Tb(1)	107.5(3)	H(3A)-C(3)-H(3B)	102(6)
C(3)-N(2)-C(21)	111.8(4)	N(3)-C(4)-C(3)	111.5(4)
C(3)-N(2)-C(2)	108.7(4)	N(3)-C(4)-H(4A)	105(5)
C(21)-N(2)-C(2)	109.9(4)	C(3)-C(4)-H(4A)	111(5)
C(3)-N(2)-Tb(1)	110.0(3)	N(3)-C(4)-H(4B)	111(4)

C(3)-C(4)-H(4B)	114(4)	C(14)-C(13)-H(13A)	106(4)
H(4A)-C(4)-H(4B)	104(6)	C(11)-C(13)-H(13A)	112(4)
N(3)-C(5)-C(6)	113.8(4)	C(14)-C(13)-H(13B)	108(3)
N(3)-C(5)-H(5A)	105(4)	C(11)-C(13)-H(13B)	109(3)
C(6)-C(5)-H(5A)	117(4)	H(13A)-C(13)-H(13B)	108(5)
N(3)-C(5)-H(5B)	113(3)	C(15)-C(14)-C(13)	113.3(4)
C(6)-C(5)-H(5B)	109(3)	C(15)-C(14)-H(14A)	107(4)
H(5A)-C(5)-H(5B)	98(5)	C(13)-C(14)-H(14A)	110(3)
N(4)-C(6)-C(5)	112.2(4)	C(15)-C(14)-H(14B)	106(4)
N(4)-C(6)-H(6A)	110(4)	C(13)-C(14)-H(14B)	102(4)
C(5)-C(6)-H(6A)	103(4)	H(14A)-C(14)-H(14B)	118(5)
N(4)-C(6)-H(6B)	111(3)	O(151)-C(15)-O(152)	123.8(6)
C(5)-C(6)-H(6B)	108(3)	O(151)-C(15)-C(14)	124.1(5)
H(6A)-C(6)-H(6B)	112(5)	O(152)-C(15)-C(14)	112.0(5)
N(4)-C(7)-C(8)	114.5(4)	N(2)-C(21)-C(23)	116.3(4)
N(4)-C(7)-H(7A)	112(3)	N(2)-C(21)-C(22)	108.8(4)
C(8)-C(7)-H(7A)	114(4)	C(23)-C(21)-C(22)	113.5(5)
N(4)-C(7)-H(7B)	109(3)	N(2)-C(21)-H(21)	104(4)
C(8)-C(7)-H(7B)	110(3)	C(23)-C(21)-H(21)	111(4)
H(7A)-C(7)-H(7B)	96(5)	C(22)-C(21)-H(21)	102(4)
N(1)-C(8)-C(7)	112.5(4)	O(222)-C(22)-O(22A)	120.4(6)
N(1)-C(8)-H(8A)	116(3)	O(222)-C(22)-O(22B)	124.1(7)
C(7)-C(8)-H(8A)	105(3)	O(22A)-C(22)-O(22B)	26.6(5)
N(1)-C(8)-H(8B)	110(4)	O(222)-C(22)-O(22C)	120.9(9)
C(7)-C(8)-H(8B)	111(4)	O(22A)-C(22)-O(22C)	27.6(7)
H(8A)-C(8)-H(8B)	102(5)	O(22B)-C(22)-O(22C)	52.7(10)
N(1)-C(11)-C(12)	111.4(4)	O(222)-C(22)-C(21)	118.2(5)
N(1)-C(11)-C(13)	114.0(4)	O(22A)-C(22)-C(21)	120.9(6)
C(12)-C(11)-C(13)	113.3(4)	O(22B)-C(22)-C(21)	114.1(7)
N(1)-C(11)-H(11)	106(3)	O(22C)-C(22)-C(21)	109.3(9)
C(12)-C(11)-H(11)	103(3)	C(21)-C(23)-C(24)	112.9(5)
C(13)-C(11)-H(11)	108(3)	C(21)-C(23)-H(23A)	116(3)
O(121)-C(12)-O(122)	124.0(4)	C(24)-C(23)-H(23A)	110(3)
O(121)-C(12)-C(11)	117.9(4)	C(21)-C(23)-H(23B)	108(4)
O(122)-C(12)-C(11)	118.0(4)	C(24)-C(23)-H(23B)	110(4)
C(14)-C(13)-C(11)	113.8(4)	H(23A)-C(23)-H(23B)	100(5)

C(25)-C(24)-C(23)	109.0(5)	O(352)-C(35)-C(34)	111.2(5)
C(25)-C(24)-H(24A)	113(4)	N(4)-C(41)-C(43)	115.2(4)
C(23)-C(24)-H(24A)	111(4)	N(4)-C(41)-C(42)	107.9(4)
C(25)-C(24)-H(24B)	113(4)	C(43)-C(41)-C(42)	116.1(4)
C(23)-C(24)-H(24B)	114(4)	N(4)-C(41)-H(41)	113(4)
H(24A)-C(24)-H(24B)	96(6)	C(43)-C(41)-H(41)	101(3)
O(251)-C(25)-O(252)	123.3(5)	C(42)-C(41)-H(41)	103(3)
O(251)-C(25)-C(24)	123.3(6)	O(422)-C(42)-O(421)	123.9(5)
O(252)-C(25)-C(24)	113.3(5)	O(422)-C(42)-C(41)	118.2(4)
N(3)-C(31)-C(32)	109.3(4)	O(421)-C(42)-C(41)	117.8(4)
N(3)-C(31)-C(33)	115.3(4)	C(41)-C(43)-C(44)	112.5(4)
C(32)-C(31)-C(33)	113.3(4)	C(41)-C(43)-H(43A)	114(3)
N(3)-C(31)-H(31)	108(5)	C(44)-C(43)-H(43A)	107(4)
C(32)-C(31)-H(31)	105(5)	C(41)-C(43)-H(43B)	110(3)
C(33)-C(31)-H(31)	106(5)	C(44)-C(43)-H(43B)	111(4)
O(321)-C(32)-O(322)	125.7(5)	H(43A)-C(43)-H(43B)	102(5)
O(321)-C(32)-C(31)	118.5(4)	C(45)-C(44)-C(43)	114.1(5)
O(322)-C(32)-C(31)	115.8(4)	C(45)-C(44)-H(44A)	106(4)
C(34)-C(33)-C(31)	113.8(4)	C(43)-C(44)-H(44A)	113(4)
C(34)-C(33)-H(33A)	107(4)	C(45)-C(44)-H(44B)	99(5)
C(31)-C(33)-H(33A)	113(4)	C(43)-C(44)-H(44B)	115(5)
C(34)-C(33)-H(33B)	107(4)	H(44A)-C(44)-H(44B)	109(6)
C(31)-C(33)-H(33B)	106(4)	O(451)-C(45)-O(452)	124.4(5)
H(33A)-C(33)-H(33B)	111(5)	O(451)-C(45)-C(44)	122.4(6)
C(35)-C(34)-C(33)	114.3(4)	O(452)-C(45)-C(44)	113.1(5)
C(35)-C(34)-H(34A)	108(4)	O(451)-C(45)-H(452)	98(4)
C(33)-C(34)-H(34A)	106(4)	O(452)-C(45)-H(452)	27(4)
C(35)-C(34)-H(34B)	109(4)	C(44)-C(45)-H(452)	138(4)
C(33)-C(34)-H(34B)	112(4)	O(2WC)-O(2WA)-O(2WB)	148(3)
H(34A)-C(34)-H(34B)	109(6)	O(2WA)-O(2WB)-O(2WC)	13.2(13)
O(351)-C(35)-O(352)	123.3(5)	O(2WA)-O(2WC)-O(2WB)	18.4(18)
O(351)-C(35)-C(34)	125.5(5)		

Table 4. Anisotropic displacement parameters ($Å^2 x\ 10^3$) for 98srv123. The anisotropic displacement factor exponent takes the form: $-2\pi^2[\ h^2\ a^{*2}U^{11} + \ldots + 2\ h\ k\ a^*\ b^*\ U^{12}\ ]$

	U^{11}	U^{22}	U^{33}	U^{23}	U^{13}	U^{12}
Tb(1)	18(1)	11(1)	14(1)	1(1)	5(1)	3(1)
O(5)	32(2)	18(2)	48(3)	6(2)	18(2)	11(2)
O(121)	46(3)	30(2)	32(2)	15(2)	15(2)	26(2)
O(122)	31(2)	15(2)	22(2)	3(1)	13(2)	11(2)
O(151)	55(3)	25(2)	36(2)	2(2)	-7(2)	16(2)
O(152)	70(4)	43(3)	38(3)	-8(2)	-18(3)	33(3)
O(222)	27(2)	15(2)	25(2)	-2(1)	14(2)	0(2)
O(251)	34(2)	30(2)	27(2)	8(2)	8(2)	14(2)
O(252)	28(2)	27(2)	18(2)	2(2)	0(2)	5(2)
O(321)	24(2)	25(2)	24(2)	12(2)	3(2)	0(2)
O(322)	17(2)	21(2)	18(2)	6(1)	4(1)	5(1)
O(352)	39(2)	22(2)	31(2)	-3(2)	14(2)	12(2)
O(351)	45(3)	23(2)	31(2)	6(2)	11(2)	6(2)
O(421)	31(2)	16(2)	28(2)	-2(2)	-9(2)	3(2)
O(422)	19(2)	15(2)	22(2)	5(1)	2(1)	7(1)
O(451)	63(4)	33(3)	119(5)	39(3)	60(4)	25(3)
O(452)	60(3)	25(2)	69(3)	23(2)	40(3)	25(2)
N(1)	23(2)	12(2)	14(2)	3(2)	7(2)	6(2)
N(2)	26(2)	18(2)	16(2)	2(2)	9(2)	5(2)
N(3)	16(2)	21(2)	14(2)	2(2)	3(2)	3(2)
N(4)	16(2)	12(2)	15(2)	3(2)	2(2)	4(2)
C(1)	22(3)	20(2)	20(2)	4(2)	10(2)	9(2)
C(2)	25(3)	16(2)	17(2)	2(2)	7(2)	3(2)
C(3)	18(3)	24(3)	22(3)	4(2)	5(2)	2(2)
C(4)	20(3)	25(3)	17(2)	0(2)	1(2)	-1(2)
C(5)	20(3)	33(3)	16(2)	4(2)	1(2)	13(2)
C(6)	25(3)	19(2)	16(2)	6(2)	4(2)	14(2)
C(7)	23(3)	16(2)	19(2)	5(2)	6(2)	9(2)
C(8)	28(3)	19(2)	16(2)	5(2)	8(2)	10(2)
C(11)	24(3)	13(2)	16(2)	4(2)	9(2)	8(2)
C(12)	22(3)	14(2)	25(3)	7(2)	7(2)	7(2)

C(13)	27(3)	22(2)	19(2)	8(2)	8(2)	10(2)
C(14)	36(3)	23(3)	21(3)	8(2)	5(2)	17(2)
C(15)	43(3)	32(3)	20(3)	7(2)	8(2)	21(3)
C(21)	27(3)	16(2)	26(3)	-2(2)	13(2)	2(2)
C(22)	41(3)	20(3)	26(3)	-4(2)	19(3)	-1(2)
C(23)	24(3)	22(3)	33(3)	3(2)	10(2)	5(2)
C(24)	30(3)	22(3)	43(4)	2(2)	12(3)	5(2)
C(25)	33(3)	17(2)	29(3)	4(2)	6(2)	9(2)
C(31)	23(3)	16(2)	17(2)	3(2)	5(2)	6(2)
C(32)	21(2)	17(2)	18(2)	3(2)	5(2)	5(2)
C(33)	27(3)	21(2)	17(2)	7(2)	6(2)	8(2)
C(34)	26(3)	22(2)	18(2)	5(2)	5(2)	8(2)
C(35)	24(3)	22(2)	17(2)	3(2)	-2(2)	7(2)
C(41)	21(2)	13(2)	23(2)	7(2)	5(2)	5(2)
C(42)	18(2)	14(2)	23(2)	7(2)	4(2)	4(2)
C(43)	25(3)	13(2)	31(3)	4(2)	8(2)	7(2)
C(44)	28(3)	19(3)	54(4)	6(3)	17(3)	10(2)
C(45)	29(3)	19(2)	35(3)	5(2)	9(2)	6(2)

Table 5. Hydrogen coordinates (x 10^4) and isotropic displacement parameters ($Å^2$x 10^3) for 98srv123.

	x	y	z	U(eq)
H(5D)	3670(100)	-7820(80)	2370(60)	48
H(5C)	3050(100)	-8560(80)	1880(60)	48
H(152)	4160(110)	-5530(90)	7570(60)	84
H(252)	-6850(90)	-14610(70)	760(50)	42
H(352)	-1360(100)	-9410(70)	-2520(50)	48
H(452)	2780(110)	-770(80)	4100(60)	67
H(1A)	-2320(70)	-7940(50)	3350(40)	24
H(1B)	-1920(70)	-8500(50)	4100(40)	24
H(2A)	-1600(70)	-10040(50)	3110(40)	25
H(2B)	-3440(70)	-10010(50)	2800(40)	25
H(3A)	-4280(80)	-9790(60)	1410(40)	29
H(3B)	-3320(70)	-8610(60)	1990(40)	29
H(4A)	-2800(80)	-9080(60)	510(40)	30
H(4B)	-3760(80)	-8500(60)	530(40)	30
H(5A)	-2270(80)	-6430(60)	1150(40)	29
H(5B)	-2550(70)	-6740(50)	1940(40)	29
H(6A)	-630(70)	-4920(50)	2400(40)	23
H(6B)	400(70)	-5160(50)	1810(40)	23
H(7A)	-1370(70)	-6070(50)	3310(40)	23
H(7B)	-110(70)	-4970(50)	3890(40)	23
H(8A)	1360(70)	-5740(50)	4650(40)	25
H(8B)	-370(70)	-6330(50)	4690(40)	25
H(11)	2100(70)	-7190(50)	4690(40)	21
H(13A)	-160(70)	-7740(60)	5390(40)	29
H(13B)	-300(70)	-9130(60)	5040(40)	29
H(14A)	2580(80)	-8230(60)	5900(40)	33
H(14B)	1160(80)	-8170(60)	6470(40)	33
H(21)	-1330(80)	-10770(60)	1900(40)	31
H(23A)	-4470(80)	-11590(60)	500(40)	37
H(23B)	-4260(80)	-11570(60)	1540(40)	37

H(24A)	-2890(90)	-12860(70)	510(50)	44
H(24B)	-2900(90)	-12940(70)	1410(50)	44
H(31)	-750(70)	-8000(60)	170(40)	23
H(33A)	-1560(70)	-6310(60)	-140(40)	29
H(33B)	-2780(80)	-7600(60)	-410(40)	29
H(34A)	-2000(80)	-7140(60)	-1560(40)	29
H(34B)	-390(80)	-6960(60)	-1150(40)	29
H(41)	2770(70)	-4610(50)	2840(40)	23
H(43A)	1460(70)	-3350(60)	3490(40)	31
H(43B)	2350(70)	-3470(60)	4410(40)	31
H(44A)	4820(90)	-2400(60)	4230(50)	44
H(44B)	4130(90)	-2660(70)	3230(50)	44

Table 6. Selected torsion angles [°] for 98srv123

N(1)-C(1)-C(2)-N(2)	-61.1(6)
N(2)-C(3)-C(4)-N(3)	-58.7(6)
N(3)-C(5)-C(6)-N(4)	-59.0(6)
N(4)-C(7)-C(8)-N(1)	-58.1(6)
N(1)-C(11)-C(12)-O(122)	18.2(6)
N(2)-C(21)-C(22)-O(222)	38.1(8)
N(3)-C(31)-C(32)-O(322)	39.2(6)
N(4)-C(41)-C(42)-O(422)	40.6(6)

NB.

For the crystallographic data for (*RSRS*-)**26** the reader is refered to the PhD. Thesis of Janet Moloney, University of Durham, 1999.

Appendix III

A sample of DOTA was prepared by the methods of Tweedle *et al.* according to Scheme 1.

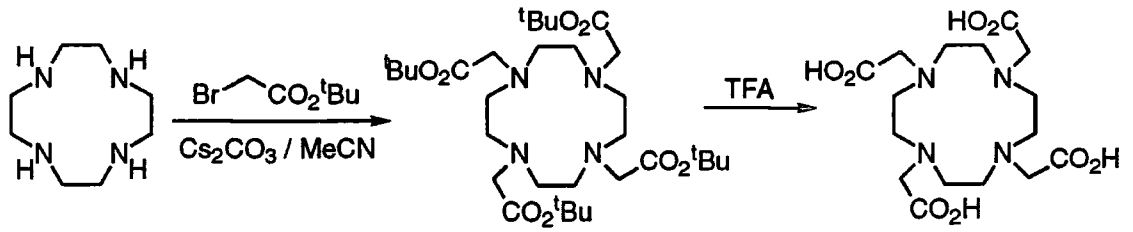

Scheme 1 The Synthesis of DOTA.

X-ray quality crystals were obtained from an aqueous solution of DOTA acidifies to below pH 1 with hydrochloric acid, by slow evaporation of the solvents at room temperature.

Large, square crystals of the dihydrochloride salt of DOTA were obtained. Structure was obtained from data collected on a Rigaku and solved by direct methods.

Crystallographic Data for DOTA 2

Identification code	99srv036 - dota	
Empirical formula	$[C_{16}H_{29}Cl_{12}N_4O_8].(4.H_2O).(H_3O)^+$	
Formula weight	567.42	
Temperature	150(2) K	
Wavelength	1.54178 Å	
Crystal system	Monoclinic	
Space group	$P2_1/n$	
Unit cell dimensions	a = 11.018(2) Å	α = 90 °.
	b = 20.019(4) Å	β = 91.30(3) °.
	c = 11.822(2) Å	γ = 90 °.
Volume, Z	2606.9(9) $Å^3$, 4	
Density (calculated)	1.446 $g.cm^3$	
Absorption coefficient	2.852 mm^{-1}	
F(000)	1208	
Crystal size	0.750 x 0.675 x 0.375 mm	
θ range for data collection	4.34 to 74.98 °.	
Limiting indices	0<=h<=13, 0<=k<=24, -14<=l<=14	
Reflections collected	Total 5021	
	Observed 4382 Fo > 4.σ(Fo)	
Experimental device	Rigaku AFC6S	
Experimental methods	ω scans	
Independent reflections	4801 [R_{int} = 0.0355]	
Absorption correction	Not applied	
Refinement method	Full-matrix least-squares on F^2	
Data / restraints / parameters	4801 / 0 / 315	
Goodness-of-fit on F^2	1.097	
Final R indices [I>2σ(I)]	R_1 = 0.0819, wR_2 = 0.2297	
R indices (all data)	R_1 = 0.0893, wR_2 = 0.2509	
Extinction coefficient	not refined	
Largest diff. peak and hole	0.831 and -0.990 $e.Å^{-3}$	

Table 2. Atomic coordinates (x 10^5) and equivalent isotropic displacement parameters (Å 2 x 10^4) for 1. U_{eq} is defined as one third of the trace of the orthogonalized U_{ij} tensor.

	x	y	z	U_{eq}
O(1)	47990(3)	25880(2)	110610(3)	384(8)
O(2)	34990(3)	30134(14)	97870(2)	302(6)
O(3)	4150(2)	28408(14)	131470(2)	269(6)
O(4)	19570(2)	25763(13)	120160(2)	247(6)
O(5)	75660(2)	29642(14)	120260(2)	280(6)
O(6)	61320(2)	26671(14)	132510(2)	252(6)
O(7)	31520(3)	25803(13)	143250(2)	284(6)
O(8)	44890(2)	30132(13)	155720(2)	255(6)
N(1)	21090(2)	13028(15)	128040(2)	178(6)
N(2)	37630(3)	13400(15)	109230(2)	169(6)
N(3)	59750(2)	13980(2)	123680(2)	167(6)
N(4)	43110(2)	13642(15)	142890(2)	162(6)
C(1)	17640(3)	10120(2)	116620(3)	203(7)
C(2)	28750(3)	7930(2)	110110(3)	202(7)
C(3)	49460(3)	10860(2)	105470(3)	187(7)
C(4)	57280(3)	8450(2)	115360(3)	178(7)
C(5)	63380(3)	11300(2)	135150(3)	182(7)
C(6)	52580(3)	8560(2)	141570(3)	179(7)
C(7)	31740(3)	10520(2)	146440(3)	194(7)
C(8)	24490(3)	7680(2)	136440(3)	181(7)
C(11)	11170(3)	17400(2)	132210(3)	203(7)
C(12)	12190(3)	24320(2)	127080(3)	197(7)
C(21)	33290(3)	18650(2)	101550(3)	208(7)
C(22)	39610(3)	25150(2)	103950(3)	224(8)
C(31)	69270(3)	18630(2)	119550(3)	206(7)
C(32)	68150(3)	25450(2)	124990(3)	207(7)
C(41)	47030(3)	18720(2)	151190(3)	188(7)
C(42)	40660(3)	25250(2)	149790(3)	223(8)
Cl(1A)	42940(3)	-7006(13)	126160(2)	210(7)
Cl(1B)	45390(2)	-7110(12)	125730(2)	186(7)
Cl(2A)	41430(3)	48170(2)	79510(4)	227(6)
Cl(2B)	40840(3)	49470(2)	83270(3)	331(8)
Cl(2C)	40110(3)	46940(2)	75980(3)	261(8)
O(1SA)	22320(4)	58560(3)	70980(4)	284(12)
O(1SB)	19520(16)	58640(9)	72250(14)	230(4)
O(2SA)	99460(6)	10320(4)	-15060(6)	470(2)
O(2SB)	84190(11)	11340(6)	-24200(9)	370(3)
0(2SC)	88140(18)	12980(10)	-24350(14)	380(4)
O(3SA)	75510(5)	11560(3)	-8260(5)	327(12)
O(3SB)	84280(5)	8710(3)	-890(5)	368(13)
O(4SA)	100000	0	0	630(3)
O(4SB)	95570(16)	160(9)	2200(14)	820(4)
O(5SA)	47450(6)	40960(4)	102900(5)	519(14)
O(5SB)	40420(10)	42540(5)	101780(9)	580(2)

Table 3. Selected torsion angles [°] for 1.

4.21 (0.45)	N1 - C11 - C12 - O4
6.47(0.53)	N2 – C21 – C22 - O1
7.39 (0.47)	N3 – C31 – C32 - O6
10.72 (0.47)	N4 – C41 – C42 - O7
-53.61 (0.37)	N1 - C1 - C2 - N2
-59.76 (0.36)	N2 - C3 - C4 - N3
-57.12 (0.36)	N3 - C5 - C6 - N4
-60.36 (0.37)	N4 - C7 - C8 - N1

Table 4. Bond lengths [Å] and angles [°] for 1.

O(1)-C(22)	1.208(5)	C(6)-H(6A)	0.99
O(2)-C(22)	1.325(4)	C(6)-H(6B)	0.99
O(2)-H(2)	0.84	C(7)-C(8)	1.523(4)
O(3)-C(12)	1.320(4)	C(7)-H(7A)	0.99
O(3)-H(3A)	0.84	C(7)-H(7B)	0.99
O(4)-C(12)	1.202(4)	C(8)-H(8A)	0.99
O(5)-C(32)	1.312(4)	C(8)-H(8B)	0.99
O(5)-H(5)	0.84	C(11)-C(12)	1.519(5)
O(6)-C(32)	1.202(4)	C(11)-H(11A)	0.99
O(7)-C(42)	1.261(5)	C(11)-H(11B)	0.99
O(8)-C(42)	1.284(4)	C(21)-C(22)	1.499(5)
N(1)-C(11)	1.492(4)	C(21)-H(21A)	0.99
N(1)-C(8)	1.502(4)	C(21)-H(21B)	0.99
N(1)-C(1)	1.510(4)	C(31)-C(32)	1.516(5)
N(1)-H(1)	0.93	C(31)-H(31A)	0.99
N(2)-C(21)	1.463(4)	C(31)-H(31B)	0.99
N(2)-C(2)	1.475(5)	C(41)-C(42)	1.491(5)
N(2)-C(3)	1.476(4)	C(41)-H(41A)	0.99
N(3)-C(31)	1.493(4)	C(41)-H(41B)	0.99
N(3)-C(4)	1.502(4)	Cl(2A)-Cl(2C)	0.503(4)
N(3)-C(5)	1.503(4)	Cl(2A)-Cl(2B)	0.522(4)
N(3)-H(3)	0.93	Cl(2B)-Cl(2C)	1.002(5)
N(4)-C(6)	1.468(4)	O(2SA)-0(2SC)	1.73(2)
N(4)-C(7)	1.470(4)	O(2SB)-0(2SC)	0.55(2)
N(4)-C(41)	1.471(4)	O(3SA)-O(3SB)	1.406(8)
C(1)-C(2)	1.525(5)	O(4SA)-O(4SB)#1	0.56(2)
C(1)-H(1A)	0.99	O(4SA)-O(4SB)	0.56(2)
C(1)-H(1B)	0.99	O(4SB)-O(4SB)#1	1.12(4)
C(2)-H(2A)	0.99	O(5SA)-O(5SB)	0.845(11)
C(2)-H(2B)	0.99		
C(3)-C(4)	1.515(4)	C(22)-O(2)-H(2)	109.5(2)
C(3)-H(3A)	0.99	C(12)-O(3)-H(3A)	109.5(2)
C(3)-H(3B)	0.99	C(32)-O(5)-H(5)	109.5(2)
C(4)-H(4A)	0.99	C(11)-N(1)-C(8)	111.9(3)
C(4)-H(4B)	0.99	C(11)-N(1)-C(1)	110.5(2)
C(5)-C(6)	1.528(5)	C(8)-N(1)-C(1)	111.7(3)
C(5)-H(5A)	0.99	C(11)-N(1)-H(1)	107.5(2)
C(5)-H(5B)	0.99	C(8)-N(1)-H(1)	107.5(2)

C(1)-N(1)-H(1)	107.5(2)
C(21)-N(2)-C(2)	111.7(3)
C(21)-N(2)-C(3)	109.9(3)
C(2)-N(2)-C(3)	110.9(3)
C(31)-N(3)-C(4)	111.3(2)
C(31)-N(3)-C(5)	110.1(2)
C(4)-N(3)-C(5)	111.6(3)
C(31)-N(3)-H(3)	107.9(2)
C(4)-N(3)-H(3)	107.9(2)
C(5)-N(3)-H(3)	107.9(2)
C(6)-N(4)-C(7)	110.4(3)
C(6)-N(4)-C(41)	110.6(2)
C(7)-N(4)-C(41)	110.0(3)
N(1)-C(1)-C(2)	111.9(3)
N(1)-C(1)-H(1A)	109.2(2)
C(2)-C(1)-H(1A)	109.2(2)
N(1)-C(1)-H(1B)	109.2(2)
C(2)-C(1)-H(1B)	109.2(2)
H(1A)-C(1)-H(1B)	107.9
N(2)-C(2)-C(1)	111.3(3)
N(2)-C(2)-H(2A)	109.4(2)
C(1)-C(2)-H(2A)	109.4(2)
N(2)-C(2)-H(2B)	109.4(2)
C(1)-C(2)-H(2B)	109.4(2)
H(2A)-C(2)-H(2B)	108.0
N(2)-C(3)-C(4)	111.6(3)
N(2)-C(3)-H(3A)	109.3(2)
C(4)-C(3)-H(3A)	109.3(2)
N(2)-C(3)-H(3B)	109.3(2)
C(4)-C(3)-H(3B)	109.3(2)
H(3A)-C(3)-H(3B)	108.0
N(3)-C(4)-C(3)	111.3(3)
N(3)-C(4)-H(4A)	109.4(2)
C(3)-C(4)-H(4A)	109.4(2)
N(3)-C(4)-H(4B)	109.4(2)
C(3)-C(4)-H(4B)	109.4(2)
H(4A)-C(4)-H(4B)	108.0
N(3)-C(5)-C(6)	112.4(3)
N(3)-C(5)-H(5A)	109.1(2)
C(6)-C(5)-H(5A)	109.1(2)
N(3)-C(5)-H(5B)	109.1(2)
C(6)-C(5)-H(5B)	109.1(2)
H(5A)-C(5)-H(5B)	107.9
N(4)-C(6)-C(5)	111.6(3)
N(4)-C(6)-H(6A)	109.3(2)
C(5)-C(6)-H(6A)	109.3(2)
N(4)-C(6)-H(6B)	109.3(2)
C(5)-C(6)-H(6B)	109.3(2)
H(6A)-C(6)-H(6B)	108.0
N(4)-C(7)-C(8)	111.9(3)
N(4)-C(7)-H(7A)	109.2(2)
C(8)-C(7)-H(7A)	109.2(2)
N(4)-C(7)-H(7B)	109.2(2)
C(8)-C(7)-H(7B)	109.2(2)
H(7A)-C(7)-H(7B)	107.9
N(1)-C(8)-C(7)	111.5(3)
N(1)-C(8)-H(8A)	109.3(2)
C(7)-C(8)-H(8A)	109.3(2)
N(1)-C(8)-H(8B)	109.3(2)
C(7)-C(8)-H(8B)	109.3(2)
H(8A)-C(8)-H(8B)	108.0
N(1)-C(11)-C(12)	110.0(3)
N(1)-C(11)-H(11A)	109.7(2)
C(12)-C(11)-H(11A)	109.7(2)
N(1)-C(11)-H(11B)	109.7(2)
C(12)-C(11)-H(11B)	109.7(2)
H(11A)-C(11)-H(11B)	108.2
O(4)-C(12)-O(3)	126.1(3)
O(4)-C(12)-C(11)	123.3(3)
O(3)-C(12)-C(11)	110.6(3)
N(2)-C(21)-C(22)	111.2(3)
N(2)-C(21)-H(21A)	109.4(2)
C(22)-C(21)-H(21A)	109.4(2)
N(2)-C(21)-H(21B)	109.4(2)
C(22)-C(21)-H(21B)	109.4(2)
H(21A)-C(21)-H(21B)	108.0
O(1)-C(22)-O(2)	122.7(4)
O(1)-C(22)-C(21)	125.0(3)
O(2)-C(22)-C(21)	112.3(3)
N(3)-C(31)-C(32)	111.0(3)
N(3)-C(31)-H(31A)	109.4(2)
C(32)-C(31)-H(31A)	109.4(2)
N(3)-C(31)-H(31B)	109.4(2)
C(32)-C(31)-H(31B)	109.4(2)
H(31A)-C(31)-H(31B)	108.0
O(6)-C(32)-O(5)	126.6(4)
O(6)-C(32)-C(31)	123.7(3)
O(5)-C(32)-C(31)	109.7(3)
N(4)-C(41)-C(42)	113.7(3)
N(4)-C(41)-H(41A)	108.8(2)
C(42)-C(41)-H(41A)	108.8(2)
N(4)-C(41)-H(41B)	108.8(2)
C(42)-C(41)-H(41B)	108.8(2)
H(41A)-C(41)-H(41B)	107.7
O(7)-C(42)-O(8)	123.0(4)
O(7)-C(42)-C(41)	120.8(3)
O(8)-C(42)-C(41)	116.3(3)
Cl(2C)-Cl(2A)-Cl(2B)	156.0(10)
Cl(2A)-Cl(2B)-Cl(2C)	11.8(5)
Cl(2A)-Cl(2C)-Cl(2B)	12.2(5)
O(2SB)-0(2SC)-O(2SA)	111(3)
O(4SB)#1-O(4SA)-O(4SB)	179.994(11)
O(4SA)-O(4SB)-O(4SB)#1	0.003(5)

Symmetry transformations used to generate equivalent atoms: #1 -x+2,-y,-z

Table 5. Anisotropic displacement parameters (Å ^{2} x 10 ^{4}) for 1. The anisotropic displacement factor exponent takes the form: $-2\pi^2 [h^2 a^{*2} U_{11} + ... + 2 h k a^* b^* U_{12}]$

	U_{11}	U_{22}	U_{33}	U_{23}	U_{13}	U_{12}
O(1)	400(2)	250(2)	490(2)	-20(13)	-234(14)	-9(13)
O(2)	356(14)	179(14)	367(14)	86(11)	-102(11)	-28(11)
O(3)	338(14)	166(14)	306(13)	41(11)	65(11)	73(11)
O(4)	301(13)	203(14)	237(12)	9(10)	23(10)	-3(11)
O(5)	321(14)	194(15)	327(14)	-19(11)	69(11)	-82(11)
O(6)	309(13)	201(14)	247(12)	-24(10)	33(10)	-19(11)
O(7)	334(14)	163(14)	349(14)	1(11)	-138(11)	18(11)
O(8)	277(13)	169(14)	318(13)	-76(11)	-53(10)	-19(10)
N(1)	143(12)	170(2)	218(13)	-10(11)	-17(10)	0(11)
N(2)	229(13)	142(15)	135(12)	7(11)	-24(10)	7(11)
N(3)	160(13)	160(2)	183(13)	29(11)	3(10)	-5(10)
N(4)	214(13)	144(15)	126(12)	-11(10)	-25(10)	-10(11)
C(1)	210(2)	180(2)	210(2)	-16(13)	-66(12)	-18(13)
C(2)	250(2)	150(2)	200(2)	-8(13)	-9(12)	-9(14)
C(3)	250(2)	140(2)	168(15)	14(13)	9(12)	15(13)
C(4)	240(2)	90(2)	200(2)	-7(13)	6(12)	-3(13)
C(5)	198(15)	140(2)	200(2)	-6(13)	-41(12)	24(13)
C(6)	240(2)	150(2)	146(14)	0(12)	-32(12)	11(13)
C(7)	220(2)	190(2)	171(15)	15(13)	4(12)	-10(13)
C(8)	215(15)	130(2)	200(2)	32(13)	-18(12)	-13(13)
C(11)	173(15)	180(2)	260(2)	16(14)	10(12)	16(13)
C(12)	210(2)	190(2)	187(15)	16(13)	-44(12)	18(13)
C(21)	250(2)	210(2)	156(14)	32(13)	-48(12)	1(14)
C(22)	260(2)	180(2)	230(2)	19(14)	-24(13)	17(14)
C(31)	188(15)	200(2)	230(2)	-34(14)	31(12)	-39(13)
C(32)	190(2)	240(2)	190(2)	23(14)	-34(12)	-34(13)
C(41)	230(2)	170(2)	165(14)	-44(13)	-37(12)	-25(13)
C(42)	280(2)	170(2)	230(2)	25(14)	37(13)	-9(14)

Table 6. Hydrogen coordinates (x 10 ^{3}) and isotropic displacement parameters (Å 2 x 10 ^{3}) for 1.

	x	y	z	U(eq)
H(2)	388(1)	337(1)	995(1)	45
H(3A)	48(1)	322(1)	1286(1)	40
H(5)	750(1)	334(1)	1233(1)	42
H(1)	279(1)	157(1)	1271(1)	21
H(3)	526(1)	164(1)	1245(1)	20
H(1A)	131(1)	135(1)	1121(1)	24
H(1B)	122(1)	62(1)	1177(1)	24
H(2A)	326(1)	41(1)	1140(1)	24
H(2B)	262(1)	65(1)	1024(1)	24
H(3A)	538(1)	145(1)	1015(1)	22
H(3B)	481(1)	71(1)	1001(1)	22

H(4A)	531(1)	47(1)	1192(1)	21
H(4B)	651(1)	67(1)	1125(1)	21
H(5A)	673(1)	149(1)	1397(1)	22
H(5B)	694(1)	77(1)	1342(1)	22
H(6A)	491(1)	47(1)	1374(1)	21
H(6B)	554(1)	70(1)	1491(1)	21
H(7A)	268(1)	139(1)	1504(1)	23
H(7B)	336(1)	69(1)	1519(1)	23
H(8A)	294(1)	42(1)	1327(1)	22
H(8B)	170(1)	55(1)	1392(1)	22
H(11A)	118(1)	177(1)	1406(1)	24
H(11B)	32(1)	154(1)	1301(1)	24
H(21A)	244(1)	192(1)	1024(1)	25
H(21B)	347(1)	173(1)	936(1)	25
H(31A)	684(1)	191(1)	1112(1)	25
H(31B)	774(1)	168(1)	1213(1)	25
H(41A)	559(1)	195(1)	1505(1)	23
H(41B)	456(1)	170(1)	1589(1)	23

Appendix IV

Research Colloqia, Seminars and Lectures

Postgraduate lecture courses attended

NMR Spectroscopy - Dr A.M. Kenwright
Mass Spectroscopy - Dr M. Jones and Dr. C. Woodward
Organometallic Chemistry - Prof. D. Parker

Departmental Colloqia

The following colloquia, organised by the Department of Chemistry, were attended by the author (October 1995 - September 1998).

1995

October 13	Prof. R. Schmutzler, Univ Braunschweig, FRG. Calixarene-Phosphorus Chemistry
October 18	Prof. A. Alexakis, Univ. Pierre et Marie Curie, Paris, Synthetic and Analytical Uses of Chiral Diamines
October 25	Dr.D. Martin Davies, University of Northumbria Chemical reactions in organised systems.
November 1	Prof. W. Motherwell, UCL London New Reactions for Organic Synthesis
November 3	Dr B. Langlois, University Claude Bernard-Lyon Radical Anionic and Psuedo Cationic Trifluoromethylation
November 8	Dr. D. Craig, Imperial College, London New Stategies for the Assembly of Heterocyclic Systems
November 15	Dr Andrea Sella, UCL, London Chemistry of Lanthanides with Polypyrazoylborate Ligands
December 8	Professor M.T. Reetz, Max Planck Institut, Mulheim Perkin Regional Meeting

1996

January 10	Dr Bill Henderson, Waikato University, NZ

Electrospray Mass Spectrometry - a new sporting technique

January 17 Prof. J. W. Emsley , Southampton University
Liquid Crystals: More than Meets the Eye

January 24 Dr Alan Armstrong, Nottingham Univesity
Alkene Oxidation and Natural Product Synthesis

January 31 Dr J. Penfold, Rutherford Appleton Laboratory,
Soft Soap and Surfaces

February 7 Dr R.B. Moody, Exeter University
Nitrosations, Nitrations and Oxidations with Nitrous Acid

February 12 Dr Paul Pringle, University of Bristol
Catalytic Self-Replication of Phosphines on Platinum(O)

February 14 Dr J. Rohr, Univ Gottingen, FRG
Goals and Aspects of Biosynthetic Studies on Low Molecular Weight Natural Products

February 21 Dr C R Pulham , Univ. Edinburgh
Heavy Metal Hydrides - an exploration of the chemistry of stannanes and plumbanes

February 28 Prof. E. W. Randall, Queen Mary & Westfield College
New Perspectives in NMR Imaging

March 7 Dr D.S. Wright, University of Cambridge
Synthetic Applications of Me_2N-p-Block Metal Reagents

March 12 RSC Endowed Lecture - Prof. V. Balzani, Univ of Bologna
Supramolecular Photochemistry

November 6 Dr Melinda Duer, Chemistry Department, Cambridge
Solid-state NMR Studies of Organic Solid to Liquid-crystalline Phase Transitions

November 13 Dr G. Resnati, Milan
Perfluorinated Oxaziridines: Mild Yet Powerful Oxidising Agents

November 18 Professor G. A. Olah, University of Southern California, USA

Crossing Conventional Lines in my Chemistry of the Elements

November 19 Professor R. E. Grigg, University of Leeds
Assembly of Complex Molecules by Palladium-Catalysed Queueing Processes

November 20 Professor J. Earnshaw, Deptartment of Physics, Belfast
Surface Light Scattering: Ripples and Relaxation

November 27 Dr Richard Templer, Imperial College, London
Molecular Tubes and Sponges

December 3 Professor D. Phillips, Imperial College, London
"A Little Light Relief" -

December 4 Professor K. Muller-Dethlefs, York University
Chemical Applications of Very High Resolution ZEKE Photoelectron Spectroscopy

December 11 Dr Chris Richards, Cardiff University
Sterochemical Games with Metallocenes

1997

January 15 Dr V. K. Aggarwal, University of Sheffield
Sulfur Mediated Asymmetric Synthesis

February 18 Professor Sir James Black, Foundation/King's College London
My Dialogues with Medicinal Chemists

March 4 Professor C. W. Rees, Imperial College
Some Very Heterocyclic Chemistry

March 5 Dr J. Staunton FRS, Cambridge University
Tinkering with biosynthesis: towards a new generation of antibiotics

October 8 Prof. E. Atkins, Department of Physics, University of Bristol
Advances in the control of architecture for polyamides: from nylons to genetically engineered silks to monodisperse oligoamides

October 15 Dr. R. Mark Ormerod, Department of Chemistry, Keele University
Studying catalysts in action

October 21 Prof. A. F. Johnson, IRC, Leeds
Reactive processing of polymers: science and technology

October 22 Prof. R.J. Puddephatt (RSC Endowed Lecture), University of Western Ontario
Organoplatinum chemistry and catalysis

October 23 Prof. M.R. Bryce, University of Durham, Inaugural Lecture
New Tetrathiafulvalene Derivatives in Molecular, Supramolecular and Macromolecular; Chemistry: controlling the electronic properties of organic solids

October 29 Prof. Bob Peacock, University of Glasgow
Probing chirality with circular dichroism

October 28 Prof. A P de Silva, The Queen's University, Belfast
Luminescent signalling systems"

November 5 Dr Mimi Hii, Oxford University
Studies of the Heck reaction

November 11 Prof. V Gibson, Imperial College, London
Metallocene polymerisation

November 19 Dr Gareth Morris, Dept of Chemistry, Manchester Univ.
Pulsed field gradient NMR techniques: Good news for the Lazy and DOSY

November 20 Dr Leone Spiccia, Monash University, Melbourne, Australia
Polynuclear metal complexes

November 25 Dr R. Withnall, University of Greenwich
Illuminated molecules and manuscripts

December 3 Prof. A.P. Davis, Department. of Chemistry, Trinity College Dublin.
Steroid-based frameworks for supramolecular chemistry

1998

January 14	Prof. David Andrews, University of East Anglia Energy transfer and optical harmonics in molecular systems
January 20	Prof. J. Brooke, University of Lancaster What's in a formula? Some chemical controversies of the 19th century
January 21	Prof. David Cardin, University of Reading Apects of metal and carbon cluster chemistry
February 18	Prof. Gus Hancock, Oxford University Surprises in the photochemistry of tropospheric ozone
February 24	Prof. R. Ramage, University of Edinburgh The synthesis and folding of proteins

Conferences attended

Stereochemistry at Sheffield University of Sheffield	18th December 1995
RSC UK Macrocycles Group University of Sheffield	4-5th January 1996
COST D1 Working Group on MRI Contrast Agents Den Haag, The Netherlands	17-19th October 1996
RSC Dalton Meeting University of Edinburgh	5th February 1997
COST D1 Working Group on MRI Contrast Agents* Bergen, Norway	9-10th September 1997
RSC UK Macrocyclic and Supramolecular Group University of Nottingham	5-6th January 1998

* Oral Presentation

Publications

"Structure and dynamics of all of the stereoisomers of europium complexes of tetra(carboxyethyl) derivatives of DOTA: ring inversion is decoupled from co-operative arm rotation in the RRRR *and* RRRS *isomers."*

Howard, J.A.K.; Kenwright, A.M.; Moloney, J.M.; Parker, D.; Port, M.; Navet, M.; Rousseau, O.; Woods, M.; *J. Chem. Soc. Chem. Commun.*, (1998), **38**, 1381.